Behavior of Fresh and Aged Catalysts In Response to Rapid Engine Control Perturbations

By

Chad A. Smutzer

B.S., Mechanical Engineering
Clarkson University, 2000

Submitted to the Department of Mechanical Engineering in Partial Fulfillment of the Requirements for the Degree of

Master of Science in Mechanical Engineering

at the

Massachusetts Institute of Technology

January 2002

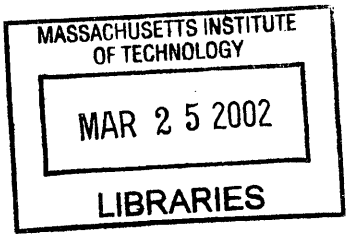

Signature of Author _____
Department of Mechanical Engineering
January 18, 2001

Certified by _____
John B. Heywood
Sun Jae Professor of Mechanical Engineering
Thesis Advisor

Certified by _____
Wai K. Cheng
Professor, Department of Mechanical Engineering
Thesis Advisor

Accepted by _____
Ain A. Sonin
Professor, Department of Mechanical Engineering
Chairman, Department Graduate Committee

Behavior of Fresh and Aged Catalysts In Response to Rapid Engine Control Perturbations

By

Chad A. Smutzer

Submitted to the Department of Mechanical Engineering
January 2002 in Partial Fulfillment of the Requirements for the Degree of
Master of Science in Mechanical Engineering

ABSTRACT

Continuously decreasing emissions standards and environmental concern have caused much research to be undertaken on the topic of catalytic converters and how to optimize their performance. The steady state performance of the Three Way Catalyst is excellent. As emissions standards become stricter, however, emphasis must be given to what happens during transients, what happens when there are substantial air fuel excursions, and the effects of the catalyst aging. The objective of this work is to take a systems approach to the engine/catalyst setup to quantify catalyst behavior as the catalyst ages.

To accomplish this objective, three sets of experiments were carried out: 1. Steady-state air/fuel ratio sweeps of catalyst NOx and HC removal efficiency, 2. Transient throttle perturbations, and 3. Oxygen storage tests. The goals of the steady-state efficiency testing and the oxygen storage tests were to quantify the effects of aging on the catalyst and separate the effects of active material degeneration from oxygen storage capacity. The goal of the throttle perturbations was to cause breakthrough in the catalyst and be able to quantify the amount of breakthrough that occurred. Three different dyno-aged catalysts on a production spark-ignition engine were the test bed for the three sets of experiments.

For the catalysts tested, there was not a substantial reduction in the hydrocarbon conversion efficiency as the catalyst aged, but there was approximately a 50% reduction in NOx conversion efficiency. The middle-aged catalyst was found to have a NOx conversion efficiency between that of the oldest catalyst and the newest catalyst. However, with respect to oxygen storage capacity, there was a 17% reduction between the newest catalyst and the middle-aged catalyst, but essentially no change between the oxygen storage capacity of the middle-aged catalyst and the oldest catalyst. This implies that the difference in conversion efficiency is not due to loss of oxygen storage, but rather to active material degeneration. The transient tests documented two types of breakthrough: a primary breakthrough that occurred when the throttle transient occurred, and a secondary breakthrough that occurred after the engine was at full load. The magnitude of both levels of breakthrough was found to increase rapidly with catalyst age. These breakthroughs are potentially of concern for aggressive driving under strict Tier 2 emissions regulations.

ACKNOWLEDGEMENTS

Under the guidance of Professors Cheng and Heywood, I have learned much about engines and the research process. Their experience in engine research guided this project in a direction that yielded interesting results and challenged me to continually think of the problem from a different angle.

I have also benefited from speaking with the members of the MIT Engine and Fuels Research Consortium. Their practical input helped to steer the research in an applicable direction. Frank Zhao (DaimlerChrysler), Chris Thomas (DaimlerChrysler), Arthur Frelund (GM), Walt Weissman (Exxon Mobil), Yeong Kwon (Exxon Mobil), Tim Coatesworth (DaimlerChrysler), Dave Radke (GM), Thomas Asmus (DaimlerChrysler), and Ron Herrin (GM) all spoke to me during the Consortium meetings to give helpful pointers. A special thanks belongs to Yeong Kwon for the testing of the sulfur level of the oil that I used during my experiments.

Richard Perdichizzi (MIT) was very helpful when I was trying to calibrate the hot wire anemometer (which we ended up not using). Dr. Mark Peckham (Cambustion) gave prompt, helpful replies to any queries I had regarding the fast NO meter. Thane Dewitt (MIT) receives thanks for lending a helping hand in the laboratory. Karla Stryker and Susan Lutin made the administrative procedures easy. Leslie Regan's organization and knowledge made all of the required paperwork seem very easy to complete.

I also would like to acknowledge my friends at MIT. Vinod, Ed Tully, and Tanaka-san often had their office invaded by me for social visits, and their humorous views through this project was invaluable. Brian (another resident of that office), my Waltham neighbor, provided many words of advice about the operation of the laboratory, life in general, and stereos. Sephir, who I keep following, was always helpful and a great encouragement. The other members of the Sloan Automotive Laboratory have also been friendly and supportive: Przemak, Yianni, Dan, Yong, Jim, Halim, Adam, Michael, Tony, Liang, Ertan, Ferran, and Jennifer.

Finally, I would like to thank my friends outside of MIT who have been supportive of my efforts and who think that I can fix their car after my experience here. I am not going to list everyone's name, as they probably will not read my thesis, but they know who they are. I am indebted to my parents, who have backed every decision that I have made. Without their help, I would not have made it this far.

Many people have had a hand, indirectly or directly, in this project. It is nice to see the compilation of the efforts of so many people.

Chad Smutzer
January 18, 2002

TABLE OF CONTENTS

Abstract 3
Acknowledgements 5
Table of Contents 7
List of Tables 9
List of Figures 11
Nomenclature 15
Chapter 1: Introduction and Background 17
1.1: Issues With Emissions 17
1.2: Emissions Standards 17
1.3: Technical Background 19
1.3.1: Engine Emissions 19
1.3.2: Normal Catalyst Function 20
1.3.3: Catalyst Deterioration 22
1.4: Objective 23
Chapter 2: Experimental Setup 25
2.1: Introduction 25
2.2: Experimental Setup 25
2.2.1: Engine and Dynamometer Control 25
2.2.2 Catalytic Converters 27
2.2.3: Fuel Used 27
2.2.4: Oil Used 28
2.3 Diagnostics 28
2.3.1 Data Acquisition 28
2.3.2 Air/Fuel Ratio Measurement and Theory 28
2.3.3 Hydrocarbon Measurement and Theory 30
2.3.4 NO Measurement and Theory 30
2.3.5: Carbon Monoxide Measurement and Theory 31
2.3.6: Temperature Measurement 32
2.3.7: Locations of Sampling Probes 32
Chapter 3: Steady State Results and Discussion 37
3.1 Introduction 37
3.2 Steady State Emissions and Catalyst Efficiency 38
3.2.1 Steady State Hydrocarbon Results 38
3.2.2 Steady State Oxide of Nitrogen Results 39
3.2.3 Steady State Catalyst Temperature Trends 40
3.2.4 Steady State Carbon Monoxide Results 41
3.2.5 Differences in Pre- and Post-Catalyst Oxygen Sensors 42
3.2.6: Engine Volumetric Efficiency 44
3.3 Steady State Conclusions 45
Chapter 4: Rapid Transients Results and Discussion 53
4.1 Introduction 53
4.2 Transient Tests 53
4.2.1 Description of Transient Tests 53

4.2.2: Definition of Terminology 54
4.2.3 Transients with 4K Catalyst 55
4.2.3.1: Slow Transient with the 4K Catalyst 55
4.2.3.2: Fast Throttle Transient with the 4K Catalyst 56
4.2.3.3: Multiple Steps Throttle Transients with the 4K Catalyst 57
4.3 Transients with the Aged Catalysts 57
4.4 Conclusions From Transient Tests 58
Chapter 5: Oxygen Storage Tests 85
5.1: Introduction 85
5.2 Oxygen Storage Calculation Methodology 85
5.2: Oxygen Storage Test Results 87
5.2.1: Determination of Rich Starting Point 87
5.2.2: Rich to Lean Transitions 88
5.2.2.1:Temperature Rise Phenomenon 89
5.3: Conclusions From Oxygen Storage Tests 90
Chapter 6: Conclusions and Further Research Directions 127
6.1: Conclusions 127
6.2: Further Research Directions 128
Appendix A: Step Motor Program Code 129
Appendix B: Fuel Properties [15] 131
Appendix C: Steady State Matlab Code 133
Appendix D: Water Content In Spark Ignition Exhaust [4] 135
Appendix E: Tables of Steady State Emissions Measurements and Efficiency 137
Appendix F: MATLAB Code Used To Evaluate Transients 139
Appendix H: MATLAB Code Used to Evaluate Oxygen Storage 145
Appendix I: Air/Fuel Modulation and Oxygen Supplied to the Catalyst 149
Appendix J: Calculation of HC Contribution to Temperature Rise 151
References 153

LIST OF TABLES

Table 2.1: Engine Specifications 25
Table 2.2: Dynamometer controller specifications 26
Table 2.3: Catalyst Ages and Aging Time 27
Table 2.4: PCI-6025E Specifications 28
Table 2.5: Horiba MEXA-110λ specifications 29
Table 2.6: Cambustion HFR400 Fast FID specifications 30
Table 2.7: Cambustion fNOx400 Fast CLD Specifications 31
Table 2.9: Axial Locations of Upstream Sensors 33
Table 2.10: Axial Locations of Downstream Sensors 33
Table 2.11 Axial Locations of Thermocouple Probes 33
Table 3.1: Data Recorded for Each of the Three Experiments 37
Table 3.2 Differences in Pre- and Post- Catalyst UEGO Readings @ 1600 RPM 43
Table 3.3: Differences in Pre- and Post-Catalyst UEGO Readings @ 2000 RPM 44
Table 3.4: Volumetric Efficiency Map 45
Table 4.1: Programmed Throttle Opening and Closing Times for Transient Tests 54
Table 5.1: Summary of Oxygen Depletion Times 88
Table 5.2: Oxygen Storage Test Matrix 88

LIST OF FIGURES

Figure 1.1: History of NOx Emissions 18
Figure 2.1: Schematic of λ Control 34
Figure 2.2: Schematic of Engine/Catalyst Setup 35
Figure 3.1: Pre-Catalyst HC Emissions as a Function of Upstream λ, 0.5 Bar MAP 46
Figure 3.2: Post-Catalyst HC Emissions as a Function of Upstream λ, 0.5 Bar MAP ... 46
Figure 3.3: Steady State HC Efficiency vs. Upstream λ @ 1600 RPM, 0.5 Bar MAP .. 47
Figure 3.4: Steady-State HC Efficiency vs. Upstream λ @ 2000 RPM, 0.5 Bar MAP .. 47
Figure 3.5: Pre-Catalyst NOx Emissions as a Function of Upstream λ, 0.5 Bar MAP .. 48
Figure 3.6: Post-Catalyst NOx Emissions as a Function of Upstream λ, 0.5 Bar MAP. 48
Figure 3.7: Steady State NOx Efficiency vs. Upstream λ @ 1600 RPM, 0.5 Bar MAP Efficiency values = 0 for λ >= 1.05 in this experimental run 49
Figure 3.8: Steady State NOx Efficiency vs. Upstream λ @ 2000 RPM, 0.5 Bar MAP Efficiency values = 0 for λ >= 1.05 in this experimental run 49
Figure 3.9: Steady State Brick Temperature vs. Upstream λ, 0.5 Bar MAP 50
Figure 3.10: Steady State Mid-Catalyst Temperature vs. Upstream λ, 0.5 Bar MAP 50
Figure 3.11: Steady State Pre-Catalyst CO vs. Upstream λ, 0.5 Bar MAP 51
Figure 3.12: Downstream λ vs. Upstream λ @ 1600 RPM, 0.5 Bar MAP 51
Figure 3.13: Downstream λ vs. Upstream λ @ 1600 RPM, 0.5 Bar MAP 52
Figure 3.14: Volumetric Efficiency Map 52
Figure 4.1: Definition of Some Chapter 4 Terminology 60
Figure 4.2: Slow Transient Pre- and Post-Catalyst (4K) λ 60
Figure 4.3: Slow Transient Pre- and Post-Catalyst (4K) HC 61
Figure 4.4: Slow Transient Pre- and Post-Catalyst (4K) NOx 61
Figure 4.5: Slow Transient Catalyst Brick and Mid-Catalyst (4K) Temperature 62
Figure 4.6: Fast Transient Pre- and Post-Catalyst (4K) λ 62
Figure 4.7: Fast Transient Pre- and Post-Catalyst (4K) HC 63
Figure 4.8: Fast Transient Expanded Pre- and Post-Catalyst (4K) HC 63
Figure 4.9: Fast Transient Pre- and Post-Catalyst (4K) NOx 64
Figure 4.10: Fast Transient Catalyst Brick and Mid-Catalyst (4K) Temperature 64
Figure 4.11: Multiple Steps Transient Pre- and Post-Catalyst (4K) λ 65
Figure 4.12: Multiple Steps Transient Pre- and Post-Catalyst (4K) HC 65
Figure 4.13: Multiple Steps Transient Expanded Pre- and Post-Catalyst (4K) HC 66
Figure 4.14: Multiple Steps Transient Pre- and Post-Catalyst (4K) NOx 66
Figure 4.15: Multiple Steps Transient Catalyst Brick and Mid-Catalyst (4K) Temperature 67
Figure 4.16: Slow Transient Pre- and Post-Catalyst (50K) λ 67
Figure 4.17: Slow Transient Pre- and Post-Catalyst (50K) HC 68
Figure 4.18: Slow Transient Pre- and Post-Catalyst (50K) NOx 68
Figure 4.19: Slow Transient Catalyst Brick and Mid-Catalyst (50K) Temperature 69
Figure 4.20: Fast Transient Pre- and Post-Catalyst (50K) λ 69
Figure 4.21: Fast Transient Pre- and Post-Catalyst (50K) HC 70
Figure 4.22: Fast Transient Expanded Pre- and Post-Catalyst (50K) HC 70
Figure 4.23: Fast Transient Pre- and Post-Catalyst (50K) NOx 71

Figure 4.24: Fast Transient Catalyst Brick and Mid-Catalyst (50K) Temperature 71
Figure 4.25: Multiple Steps Transient Pre- and Post-Catalyst (50K) λ 72
Figure 4.26: Multiple Steps Transient Pre- and Post-Catalyst (50K) HC 72
Figure 4.27: Multiple Steps Transient Expanded Pre- and Post-Catalyst (50K) HC 73
Figure 4.28: Multiple Steps Transient Pre- and Post-Catalyst (50K) NOx 73
Figure 4.29: Multiple Steps Transient Catalyst Brick and Mid-Catalyst (50K) Temperature 74
Figure 4.30: Slow Transient Pre- and Post-Catalyst (150K) λ 74
Figure 4.31: Slow Transient Pre- and Post-Catalyst (150K) HC 75
Figure 4.32: Slow Transient Pre- and Post-Catalyst (150K) NOx 75
Figure 4.33: Slow Transient Catalyst Brick and Mid-Catalyst (150K) Temperature 76
Figure 4.34: Fast Transient Pre- and Post-Catalyst (150K) λ 76
Figure 4.35: Fast Transient Pre- and Post-Catalyst (150K) HC 77
Figure 4.36: Fast Transient Expanded Pre- and Post-Catalyst (150K) HC 77
Figure 4.37: Fast Transient Pre- and Post-Catalyst (150K) NOx 78
Figure 4.38: Fast Transient Catalyst Brick and Mid-Catalyst (150K) Temperature 78
Figure 4.39: Multiple Steps Transient Pre- and Post-Catalyst (150K) λ 79
Figure 4.40: Multiple Steps Transient Pre- and Post-Catalyst (150K) HC 79
Figure 4.41: Multiple Steps Transient Expanded Pre- and Post-Catalyst (150K) HC 80
Figure 4.42: Multiple Steps Transient Pre- and Post-Catalyst (150K) NOx 80
Figure 4.43: Multiple Steps Transient Catalyst Brick and Mid-Catalyst (150K) Temperature 81
Figure 4.44: Slow Transient Primary Peak NOx Breakthrough 81
Figure 4.45: Slow Transient Secondary Peak NOx Breakthrough 82
Figure 4.46: Fast Transient Primary Peak NOx Breakthrough 82
Figure 4.47: Fast Transient Secondary Peak NOx Breakthrough 83
Figure 4.48: Multiple Steps Transient Primary Peak NOx Breakthrough: Values are Averaged Over 4 Cycles 83
Figure 4.49: Multiple Step Transient Secondary Peak NOx Breakthrough: Values are Averaged Over 4 Cycles 84
Figure 4.50: Fast Transient Expansion of Pre- and Post-Catalyst λ 84
Figure 5.1: Definition of Oxygen Storage Terminology 92
Figure 5.2: Comparison of Rich Starting Points 93
Figure 5.3: Oxygen Flush Times: 1600 RPM 4K Catalyst 94
Figure 5.4: 0.95→1.05 Step HC 1600 RPM 4K Catalyst 94
Figure 5.5: 0.95→1.05 Step NOx 1600 RPM 4K Catalyst 95
Figure 5.6: 0.95→1.05 Step Catalyst Brick and Mid-Catalyst Temperatures 1600 RPM 4K Catalyst 95
Figure 5.7: 0.95→1.1 Step HC 1600 RPM 4K Catalyst 96
Figure 5.8: 0.95→1.1 Step NOx 1600 RPM 4K Catalyst 96
Figure 5.9: 0.95→1.1 Step Catalyst Brick and Mid-Catalyst Temperatures 1600 RPM 4K Catalyst 97
Figure 5.10: 0.95→1.2 Step HC 1600 RPM 4K Catalyst 97
Figure 5.11: 0.95→1.2 Step NOx 1600 RPM 4K Catalyst 98
Figure 5.12: 0.95→1.2 Step Catalyst Brick and Mid-Catalyst Temperatures 1600 RPM 4K Catalyst 98

Figure 5.13: 0.95→1.05 Step HC 1600 RPM 50K Catalyst 99
Figure 5.14: 0.95→1.05 Step NOx 1600 RPM 50K Catalyst 99
Figure 5.15: 0.95→1.05 Step Catalyst Brick and Mid-Catalyst Temperatures 1600 RPM 50K Catalyst 100
Figure 5.16: 0.95→1.1 Step HC 1600 RPM 50K Catalyst 100
Figure 5.17: 0.95→1.1 Step NOx 1600 RPM 50K Catalyst 101
Figure 5.18: 0.95→1.1 Step Catalyst Brick and Mid-Catalyst Temperatures 1600 RPM 50K Catalyst 101
Figure 5.19: 0.95→1.2 Step HC 1600 RPM 50K Catalyst 102
Figure 5.20: 0.95→1.2 Step NOx 1600 RPM 50K Catalyst 102
Figure 5.21: 0.95→1.2 Step Catalyst Brick and Mid-Catalyst Temperatures 1600 RPM 50K Catalyst 103
Figure 5.22: 0.95→1.05 Step HC 1600 RPM 150K Catalyst 103
Figure 5.23: 0.95→1.05 Step NOx 1600 RPM 150K Catalyst 104
Figure 5.24: 0.95→1.05 Step Catalyst Brick and Mid-Catalyst Temperatures 1600 RPM 150K Catalyst 104
Figure 5.25: 0.95→1.1 Step HC 1600 RPM 150K Catalyst 105
Figure 5.26: 0.95→1.1 Step NOx 1600 RPM 150K Catalyst 105
Figure 5.27: 0.95→1.1 Step Catalyst Brick and Mid-Catalyst Temperatures 1600 RPM 150K Catalyst 106
Figure 5.28: 0.95→1.2 Step HC 1600 RPM 150K Catalyst 106
Figure 5.29: 0.95→1.2 Step NOx 1600 RPM 150K Catalyst 107
Figure 5.30: 0.95→1.2 Step Catalyst Brick and Mid-Catalyst Temperatures 1600 RPM 150K Catalyst 107
Figure 5.31: 0.95→1.05 Step HC 2000 RPM 4K Catalyst 108
Figure 5.32: 0.95→1.05 Step NOx 2000 RPM 4K Catalyst 108
Figure 5.33: 0.95→1.05 Step Catalyst Brick and Mid-Catalyst Temperatures 2000 RPM 4K Catalyst 109
Figure 5.34: 0.95→1.1 Step HC 2000 RPM 4K Catalyst 109
Figure 5.35: 0.95→1.1 Step NOx 2000 RPM 4K Catalyst 110
Figure 5.36: 0.95→1.1 Step Catalyst Brick and Mid-Catalyst Temperatures 2000 RPM 4K Catalyst 110
Figure 5.37: 0.95→1.2 Step HC 2000 RPM 4K Catalyst 111
Figure 5.38: 0.95→1.2 Step NOx 2000 RPM 4K Catalyst 111
Figure 5.39: 0.95→1.2 Step Catalyst Brick and Mid-Catalyst Temperatures 2000 RPM 4K Catalyst 112
Figure 5.40: 0.95→1.05 Step HC 2000 RPM 50K Catalyst 112
Figure 5.41: 0.95→1.05 Step NOx 2000 RPM 50K Catalyst 113
Figure 5.42: 0.95→1.05 Step Catalyst Brick and Mid-Catalyst Temperatures 2000 RPM 50K Catalyst 113
Figure 5.43: 0.95→1.1 Step HC 2000 RPM 50K Catalyst 114
Figure 5.44: 0.95→1.1 Step NOx 2000 RPM 50K Catalyst 114
Figure 5.45: 0.95→1.1 Step Catalyst Brick and Mid-Catalyst Temperatures 2000 RPM 50K Catalyst 115
Figure 5.46: 0.95→1.2 Step HC 2000 RPM 50K Catalyst 115
Figure 5.47: 0.95→1.2 Step NOx 2000 RPM 50K Catalyst 116

Figure 5.48: 0.95→1.2 Step Catalyst Brick and Mid-Catalyst Temperatures 2000 RPM 50K Catalyst 116
Figure 5.49: 0.95→1.05 Step HC 2000 RPM 150K Catalyst 117
Figure 5.50: 0.95→1.05 Step NOx 2000 RPM 150K Catalyst 117
Figure 5.51: 0.95→1.05 Step Catalyst Brick and Mid-Catalyst Temperatures 2000 RPM 150K Catalyst 118
Figure 5.52: 0.95→1.1 Step HC 2000 RPM 150K Catalyst 118
Figure 5.53: 0.95→1.1 Step NOx 2000 RPM 150K Catalyst 119
Figure 5.54: 0.95→1.1 Step Catalyst Brick and Mid-Catalyst Temperatures 2000 RPM 150K Catalyst 119
Figure 5.55: 0.95→1.2 Step HC 2000 RPM 150K Catalyst 120
Figure 5.56: 0.95→1.2 Step NOx 2000 RPM 150K Catalyst 120
Figure 5.57: 0.95→1.2 Step Catalyst Brick and Mid-Catalyst Temperatures 2000 RPM 150K Catalyst 121
Figure 5.58: 0.95→1.2 Step Catalyst Extended Brick and Mid-Catalyst Temperatures 2000 RPM 150K Catalyst 121
Figure 5.59: 0.95→1.1 Step λ Comparison of 4K, 50K, and 150K catalysts 122
Figure 5.60: 0.95→1.1 Step HC Breakthrough Comparison of 4K, 50K, and 150K catalysts 122
Figure 5.61: 0.95→1.1 Step Mid-Catalyst Temperature Comparison of 4K, 50K, and 150K catalysts 123
Figure 5.62: 0.95→1.1 Step NOx Breakthrough Comparison of 4K, 50K, and 150K catalysts 123
Figure 5.63: Oxygen Storage of 4K, 50K, 150K Catalyst as a Function of the Lean Step 124
Figure 5.64: Oxygen Storage of 4K, 50K, 150K Catalyst as a Function of the Catalyst Age 124
Figure 5.65: Oxygen Storage of 4K, 50K, 150K Catalyst as a Function of the Maximum Catalyst Brick Temperature 125

NOMENCLATURE

Acronyms/ Abbreviations	Meaning	First Occurrence (Chapter)
4K	4,000	3
50K	50,000	3
150K	150,000	3
CAA	Clean Air Act	1
C_aH_b	Fuel with *a* carbon molecules and *b* hydrogen molecules	1
CLD	Chemiluminescence Detector	2
CmHn	Hydrocarbon molecule with *m* carbon and *n* hydrogen atoms	1
CO	Carbon Monoxide	1
CO_2	Carbon dioxide	1
ECU	Engine Control Unit [or Computer]	2
FID	Flame Ionization Detector	2
FTP	Federal Test Procedure	1
H_2	Nitrogen	1
H_2O	Water	1
HC	Hydrocarbon	1
MAP	Manifold Absolute Pressure	4
NDIR	Non Dispersive Infra Red	2
NO	Nitric Oxide	1
NO_2	Nitrogen Dioxide	1
NOx	Oxides of nitrogen	1
O_2	Oxygen	1
O_3	Ozone	2
RHS	Right Hand Side	5
RPM	Revolutions Per Minute	3
Stoich	stoichiometric	2
TWC	Three-Way Catalyst	1
UEGO	Universal Exhaust Gas Oxygen sensor	2
WOT	Wide Open Throttle	4

Symbol	Meaning	First Occurrence (Chapter)
$\overline{MW}_i$	Average molecular weight of *i*	5
D_i	Diffusion coefficient of $_i$	2
F	Faraday constant=96485.3415(39) C mol^{-1}	2
h_i	Enthalpy of stream i	5
χ_i	Mole fraction of component i	1

$\dot{m}_i$	Mass flow rate of *i*	2
Ip	Pumping current of oxygen sensor	2
L	Length of gas diffusion path	2
m_i	Mass of *i*	3
$M_{O2stored}$	Mass of O2 stored	
N	Engine speed, rev/s	3
P'	Partial pressure	2
Q_{chem}	Chemical heat release	5
R	Univeral Gas Constant (8.314 J/mol-K) /molecular weight	2
S	Cross section of gas diffusion path	2
T	Temperature	2
V_d	Displaced volume	3
V_o	Oxygen sensor voltage output	2
y_i	Mass fraction of *i*	5
η_v	Volumetric efficiency	3
λ	Relative ratio of air/fuel to a stoichiometric mixture	1
ρ_{ai}	Air density at engine intake	3

CHAPTER 1: INTRODUCTION AND BACKGROUND

1.1: ISSUES WITH EMISSIONS

It is hard to imagine a world without the automobile, as the automobile has grown (especially in the Western world) to be a symbol of personal freedom. However, there is a downside having many people with this personal freedom: the increase in pollutants due to the increase in automobiles on the road. The three main pollutants of concern to health and the environment emitted from internal combustion engines are hydrocarbons (HC), oxides of nitrogen (NOx), and carbon monoxide (CO).

Lower level atmospheric ozone is formed by the reactions of NOx and volatile organic compounds when exposed to sunlight. Ozone, when in the lower atmosphere, is the main ingredient in smog, which is present in many urban areas. Short-term (1-3 hours) exposure to ozone has been linked to increased respiratory problems. Prolonged exposure to ozone can cause lung inflammation and permanently change the lung structure, leading to chronic respiratory illness. Ozone also affects crop health, can damage trees and plants, and chemically attacks elastomers [1].

In addition to being an ozone precursor, NOx also has detrimental health effects. The oxides of nitrogen irritate the lungs and lower the body's resistance to respiratory infection. NOx is a precursor to acid rain, and also may affect local ecosystems by altering growth patterns and changing the balance of species [1].

Carbon monoxide affects the human body negatively by reducing the delivery of oxygen to the body's organs and tissues. Long term exposure to CO is associated with impairment of visual perception, work and learning ability, and the ability to perform complex tasks [1].

1.2: EMISSIONS STANDARDS

Even though internal combustion engines have been in existence since the 1860s, it is only in the past half-century that emissions regulations have become a large design factor. The United State's Clean Air Act (CAA) passed in 1970 was the first step in legislative regulation of engine emissions. In response to the health risks and the

increasing vehicle population, the EPA has continually been lowering the emissions standards. The latest set of national standards, Tier 2, will limit the amount of NOx produced by new passenger vehicles to 0.07 grams/mile by the year 2007. CO emissions standards will be required to be 4.2 g/mile by 2007. The non-methane organic compounds must be less than 0.09 g/mile. These standards are sales-weighted fleet averages, and there is a proposed system in place for manufacturers to receive credit if their fleet average is less than the Tier 2 standard and be able to bank this extra credit in case the next model years do not meet the standards. Phase-in steps are in place so that the emissions standards are gradually reduced to the Tier 2 levels from the current levels [2].

Figure 1.1 shows the history of emissions standards for NOx and how the standards have seen a 98% reduction in allowable NOx emissions levels [3]. The allowable levels of HC and CO follow similar trends.

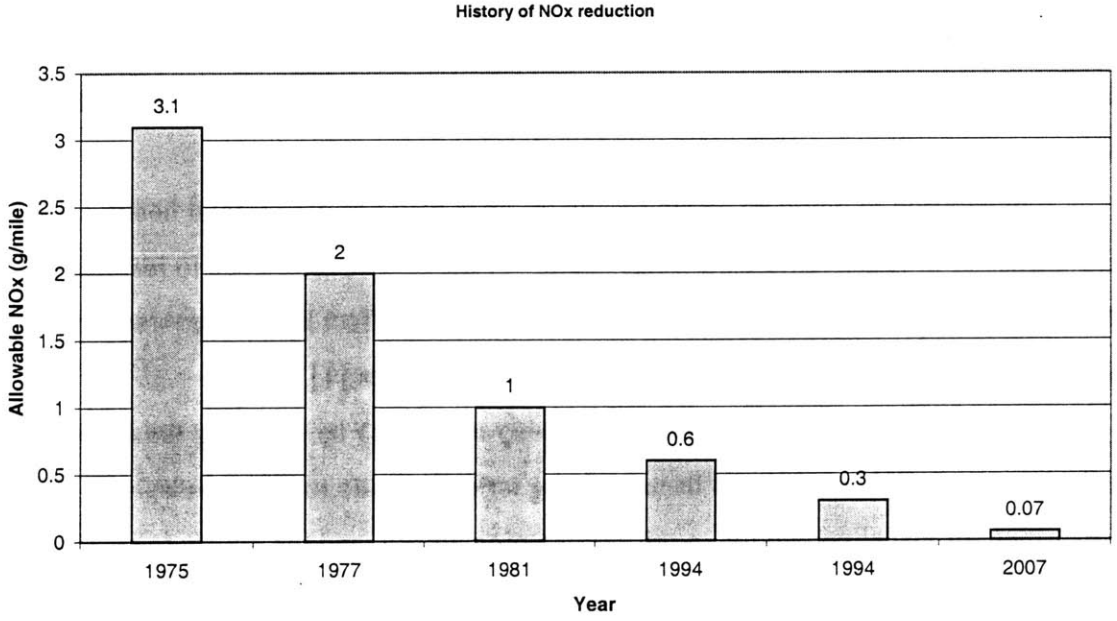

Figure 1.1: History of NOx Emissions [1]

From Figure 1.1, it is obviously important that steps be taken to reduce emissions to meet the EPA standards. Modern engine designers must design the engine in such a way that it produces low emissions, but even the emissions from advanced engine designs

are not at low enough levels to pass legal requirements. An additional measure must be added to the engine to complete the emissions-reducing task.

Introduced in the late 1970s, the catalytic converter (or catalyst) treats the engine exhaust to reduce the pollutants by approximately a factor of ten. This treatment is effective, provided that the engine is run with a near stoichiometric air/fuel ratio. Located between the exhaust port and the muffler in the exhaust system of a spark ignition engine, a fresh catalyst removes 96-98% of the pollutants that it encounters. However, as the car is driven over its life cycle, the catalyst efficiency deteriorates. The effects from this aging are important to quantify, as the effect of aging affects the manufacturer's ability to meet the strict emissions requirements. To meet these requirements, researchers are interested in quantifying as well as understanding qualitatively the effects of aging of the catalyst.

1.3: TECHNICAL BACKGROUND

1.3.1: Engine Emissions

As mentioned earlier, the three main pollutants emitted from spark-ignition engines are: carbon monoxide (CO), oxides of nitrogen (NOx), and hydrocarbon particles (HC). If theoretical chemistry held, the following equation would hold and no pollutants would be formed from the combustion process [4]:

$$C_aH_b + \left(a + \frac{b}{4}\right)(O_2 + 3.773N_2) \rightarrow aCO_2 + \frac{b}{2}H_2O + 3.773\left(a + \frac{b}{4}\right)N_2 \qquad 1.1$$

However, actual combustion resembles more of the following equation [4]:

$$C_aH_b + \left(a + \frac{b}{4}\right)(O_2 + 3.773N_2) \rightarrow \chi_{CmHn}CmHn + \chi_{CO}CO + \qquad 1.2$$

$$\chi_{CO_2}CO_2 + \chi_{H_2O}H_2O + \chi_{N2}3.773\left(a + \frac{b}{4}\right)N_2 + \chi_{H_2}H_2 + \chi_{O_2}O_2 +$$

$$\chi_{NO}NO + \chi_{NO_2}NO_2$$

As may be seen from equation 1.2. pollutants are formed in addition to the fully oxidized fuel products of equation 1.1. The reasons of the three pollutants of concern form will be discussed next.

Carbon monoxide formation is mainly a function of the air/fuel ratio; a fuel rich mixture leads to more CO formation. The spark-ignition engine is typically run near stoichiometric (meaning there is the exact amount of air present to completely oxidize the fuel), but at full load, the engine is run fuel rich (there is less air present than is needed to completely oxidize the fuel) to ensure appropriate engine response to driver input. From the stoichiometric point to a λ of 0.8, CO increases from approximately 0.5 volume percent to 8 volume percent. CO emissions are not considered important in compression ignition engines because these engines are typically run lean, and thus are not in the CO formation regime [4].

The oxides of nitrogen in a spark ignition engine are typically NO and NO_2, although the amount of NO_2 formed is typically negligible compared to the amount of NO formed. NO_2 forms at lower temperatures than are present during combustion events in a typical engine. NO formation is primarily a temperature driven phenomenon, with higher in-cylinder temperature leading to a higher concentration of NO. Engine variables that affect NO formation are spark timing, amount of dilution in the charge, and air-fuel ratio. NO emissions peak around an air/fuel ratio of 16.5, and decrease as the mixture is leaned or enriched [4].

Hydrocarbons are the result of partially oxidized fuel particles. Current understanding on the presence of hydrocarbons in the exhaust is that they result from four main contributions. The first contribution is the crevices in the combustion chamber; during high-pressure compression in the cycle, the fuel molecules are pushed into the crevice regions and therefore cannot be fully burned. Absorption/desorption from the hydrocarbon components of the engine oil also occurs. The third cause is incomplete combustion, and the fourth cause is engine deposits. These all factor into the presence of hydrocarbons in the exhaust [4].

1.3.2: Normal Catalyst Function

Along with hydrocarbons, NOx, and CO, the engine exhaust exiting the manifold also contains water (H_2O), carbon dioxide (CO_2), hydrogen (H_2), and oxygen (O_2). The modern three-way catalyst simultaneously oxidizes the CO and HC, and reduces the NOx. The oxidation reactions are [5]:

$$C_yH_n + (1+n/4)O_2 \rightarrow yCO_2 + n/2\ H_2O \quad 1.3$$

$$CO + \tfrac{1}{2}\ O_2 \rightarrow CO_2 \quad 1.4$$

$$CO + H_2O \rightarrow CO_2 + H_2 \quad 1.5$$

The reduction reactions that occur are [5]:

$$NO + CO \rightarrow \tfrac{1}{2}\ N_2 + CO_2 \quad 1.6$$

$$NO + H_2 \rightarrow \tfrac{1}{2}\ N_2 + H_2O \quad 1.7$$

$$(2 + n/2)\ NO + C_yH_n \rightarrow (1+ n/4)\ N_2 + yCO_2 + n/2\ H_2O \quad 1.8$$

The reason that the TWC performs best when run near stoichiometric may be seen from the reactions; the catalyst needs the three pollutants present in order to react with each other and form the desired species.

Another function that has been added into modern catalysts is the capability of oxygen storage. The oxygen storage is achieved with the addition of ceria (CeO_2), which has the additional benefit of strengthening the structure of the catalyst. A concentration of 30 % was found to maximize aged catalyst performance [6]. The ceria reactions are performed as follows [5]:

During fuel-rich conditions:

$$CeO_2 + CO \rightarrow Ce_2O_3 + CO_2 \quad 1.9$$

During fuel lean conditions:

$$Ce_2O_3 + \tfrac{1}{2}\ O_2 \rightarrow CeO_2 \quad 1.10$$

Thus, when the engine is running in a slightly lean condition, the catalyst can store oxygen on the ceria, and then use this oxygen during the rich conditions to oxidize the CO and HC. Ceria also has another benefit: it is a steam-reforming catalyst. Ceria promotes the reactions of CO and HC with H_2O to form H_2. The H_2 formed from this reaction then reduces a portion of the NOx to N_2 [5].

Engine controllers take advantage of the oxygen storage of the catalyst by using closed-loop feedback control. Typically oxygen sensors are mounted upstream and downstream of the catalyst. The upstream oxygen sensor is used for the engine feedback. This sensor determines whether the engine is running rich or lean and communicates this back to the engine control computer. The engine control computer then uses closed loop control to adjust the fueling to the proper levels. In practice, the A/F value is modulated

around stoichiometric to take advantage of the oxygen storage capacity of the catalyst. Then the conversion efficiency window for the three pollutants becomes wider with respect to the mean value of the A/F modulation. This larger control window allows the performance of the catalytic converter to be less susceptible to control errors and allows for efficient use of the precious metal. Perturbations of ± 0.5 A/F and a frequency of approximately 1.5 Hz yield the best use of the precious metal loading and lead to a higher catalyst efficiency [4,7,8].

1.3.3: Catalyst Deterioration

As the catalytic converter ages, its conversion efficiency decreases. The three main sources of deactivation are: thermal deactivation, catalyst poisoning, and less frequently, wash coat loss. Thermal deactivation occurs with sintering of the noble metal sites where the reactions actually take place. Sintering reduces the number of active sites, thus physically reducing the exposed catalyst area. Catalyst poisoning refers to the chemical deactivation of the sites by chemicals present in the exhaust. Poisons that affect the catalyst include sulfur, phosphorus, halogenides, and metals (such as zinc). It is also reported that the poisoning effect is accelerated by sintering [9].

Fuel sulfur causes SO_2 to form during stoichiometric and rich combustion. The SO_2 bonds to the precious metal sites in the catalyst and blocks reactions from occurring at that site. The orders of sensitivity of the precious metals used in the catalyst are palladium, platinum, and rhodium, listed in order of decreasing sensitivity. Under stoichiometric and lean conditions, sulfur decreases the oxygen storage of the catalyst by reacting with the ceria and forming $Ce_2(SO_4)_3$, thus effectively blocking the ceria from being used for oxygen storage. The reversibility of sulfur poisoning is something that depends on catalyst formulation, and must be done at high temperature (> 700 ^{o}C) with varying rich/lean excursions to decompose sulfur from the catalyst surface [10]. Most of the sulfur effects are reversible, but some are irreversible. Studies have found that an 18 to 96 % reversibility of the sulfur effects, depending on the driving cycle used and the pollutant considered for comparison [11].

1.4: OBJECTIVE

The objective of this work is to understand the engine and catalyst system behavior. It is desired to comprehend what governs the effectiveness of the catalyst when there are substantial A/F excursions such as imperfectly compensated throttle transients. Also desired is to examine in depth what happens to the catalyst as it ages and how the engine control may be changed to improve catalyst efficiency. This study endeavors to take a systems approach to the engine and catalyst combination, seeing ways that the two interact with one another. Fast-response emissions diagnostics allow further insight so that rapid step changes used to perturb the system can be tracked through the engine/catalyst system.

CHAPTER 2: EXPERIMENTAL SETUP

2.1: INTRODUCTION

The setup used an Original Equipment Manufacturer (OEM) engine with as few modifications as possible, making the experiment applicable to vehicles currently in production. A production 1998 DaimlerChrysler minivan engine was used, with 2001 model year (MY) catalysts attached to the exhaust system. Fast response instruments were used to measure HC and NOx, and dual oxygen sensors were located upstream and downstream of the catalyst to determine A/F ratio and measure oxygen storage. Fast response thermocouples located in the catalytic converter provided a measure of temperature profiles.

2.2: EXPERIMENTAL SETUP

2.2.1: Engine and Dynamometer Control

The engine used for this set of experiments is a 4-cylinder DaimlerChrysler engine commercially used in the Voyager or Caravan minivan. The engine control computer is as provided in these vehicles, with no modifications. Table 2.1 shows other pertinent specifications of the engine [12].

Type	In-Line Overhead Valve Dual Overhead Cam
Displacement	2.4L
Valves per Cylinder	4
Bore	87.5 mm (3.445 in)
Stroke	101 mm (3.976 in)
Compression Ratio	9.4:1
Firing Order	1,3,4,2
Intake Valve Close	51 ° ABDC
Intake Valve Open	1 ° BTDC
Exhaust Valve Close	8 ° ATDC
Exhaust Valve Open	52 ° BBDC

Table 2.1: Engine Specifications

This engine represents a typical modern spark-ignition engine, as it has a centrally located spark plug in a pent-roof shaped combustion chamber.

To give control over the air/fuel ratio, a breakout box was installed in the fuel injection wiring. The schematic for this is shown in Figure 2.1. As may be seen in Figure 2.1, the breakout box intercepts the signal from the engine control computer (ECU) to the injectors. The breakout box used a 555 chip to trigger its own voltage signal. The pulse width of this signal is dependant on the input of a potentiometer. Reducing the voltage supplied to the breakout box caused the engine to run lean, as the pulse width was shortened, and increasing the voltage caused the pulse width to be lengthened, leading to rich operation. When the breakout box was being used, the engine was run open loop, meaning that the upstream OEM lambda sensor was disconnected from the engine; i.e.: there is no modulation in the air/fuel ratio.

For the λ transitions (discussed in Chapter 5), two potentiometers were used with a switch that toggled control between the two. The air/fuel ratio was adjusted by using the potentiometers to obtain the desired reading on the pre-catalyst λ sensor. When the desired ratio was reached, the switch was used to cause the transition from one air/fuel ratio to the other.

The dynamometer used with this engine is the absorbing only type; the engine is started as it would be in actual use with a starter motor connected to a 12-volt battery. The dynamometer is from Froude Consine Limited, model AG80, capable of absorbing 107 BHP. Controlling this dynamometer is a Digalog Series 1000A Controller, the specifications of which are located in Table 2.2 [13]:

RPM Regulation	+/- 5 from 100 to 10,000 RPM
RPM Response	Engine response time
Load/Current Regulation	0.1 %
Load/Current Response	Instantaneous

Table 2.2: Dynamometer controller specifications

The dynamometer can be used to hold the engine at a constant speed or at a constant load. For the experiments detailed in the following pages, the engine was held at a constant RPM level and adjusting the intake pressure of the engine varied the load.

Intake pressure control is achieved by using a Pacific Scientific Powermax II stepper motor coupled to a Pacific Scientific 5240 Stepper Motor Indexer/Driver. The Indexer/Driver accepts commands from a 486 computer running MSDOS via a serial cable. Appendix A shows the computer code used in the various experiments. Computer control allowed precision programming of the controller, giving repeatability to the transient throttle experiments.

2.2.2 Catalytic Converters

The catalysts used in this experiment were 2001 model year catalysts provided by DaimlerChrysler Corporation. They fit the category of Ultra Low Emissions Vehicle (ULEV), which the EPA classifies as emitting less than 2.1 grams/mile of CO, 0.3 grams/mile of NOx, and 0.011 grams/mile of HCHO for a 10 year old/100,000 mile passenger car [14]. Corning makes the substrate of the catalyst, Johnson-Mathey applies the wash coat, and finally Arvin packages the catalyst in the final state. The catalysts contain two bricks, each having a volume of 1.23 liters. The front brick has a palladium wash coat, and the rear brick has a platinum/rhodium wash coat. Three catalysts of varying ages were used in the test matrix for these experiments, as shown in Table 2.3.

Equivalent Catalyst Age (miles)	Aging Time (hours)
4,000	14
50,000	178
150,000	534

Table 2.3: Catalyst Ages and Aging Time

The catalysts were dyno-aged using a fuel sulfur level of 30 ppm. The aging process used was a DaimlerChrysler proprietary accelerated aging process that DaimlerChrysler asserts will give equivalent numbers to the actual on-vehicle catalyst aging process.

2.2.3: Fuel Used

The fuel used throughout these experiments is California P-II Certification Fuel. Some pertinent properties of the fuel are 28.2 ppm sulfur, a research octane number of 96.5 and a motor octane number of 87.8. A complete listing of the specifications may be found in Appendix B [15].

2.2.4: Oil Used

The oil used in these experiments is an additional consideration, as some of the sulfur content in the oil will find its way into the exhausted gaseous mixture. Testing of the oil at ExxonMobil revealed the oil to contain 3500 ppm sulfur.

2.3 DIAGNOSTICS

2.3.1 Data Acquisition

Data was acquired using a Labview PCI-6025E internal multifunction input/output board, a National Instruments BNC-2090 connector board, and a custom written Labview data acquisition program. The specifications of the PCI-6025E are shown below in Table 2.4.

Analog Inputs	16 single ended/ 8 differential
Resolution	12 bits
Maximum sampling rate	200 Kb/s
Input Range	+/- 10 V
Analog Outputs	2
Analog Output Rate	10 Kb/s
Analog Output Range	+/- 10 V
Digital I/O	32
Counter/Timers	2,24 bit

Table 2.4: PCI-6025E Specifications

2.3.2 Air/Fuel Ratio Measurement and Theory

The relative air/fuel ratio, λ, is defined as:

$$\lambda = \left(\frac{\dot{m}_a}{\dot{m}_f} \right) \Bigg/ \left(\frac{\dot{m}_a}{\dot{m}_f} \right)_{stoich} \tag{2.1}$$

This is a useful measure to track the composition of the gas stream. The ratio tracks where the gas stream is in reference to the stoichiometric air/fuel ratio. There are two types of sensors used to measure this ratio: the switching type and the Universal Exhaust Gas Oxygen Sensor (UEGO). The switching sensor is comprised of a solid electrolyte through which current is carried by oxygen ions. One side of the sensor is exposed to the exhaust stream having oxygen partial pressure p', and the other side of the sensor is

exposed to the atmosphere having oxygen partial pressure p". The voltage output from this sensor is obtained through the Nernst equation:

$$V_o = \frac{RT}{4F}\ln\left(\frac{p''}{p'}\right) \qquad 2.2$$

This type of sensor is referred to as the switching type of sensor because the partial pressure of oxygen switches from the order of 10^{-10} when rich to 10^{3} Pascals when lean [4].

The UEGO, on the other hand, is composed of three solid zirconia substrates, the first cell being a pumping cell, the second being the galvanic cell, and the third being the oxygen reference cavity. A small constant pumping current is supplied, pumping oxygen from the pumping cell to the sampling cell. In lean environments, the output of the sensor is [16]:

$$Ip = \frac{4FDS}{RTL}(p'-p) \qquad 2.3$$

In rich environments, however, the oxygen supplied by the pumping cell is the oxygen required to oxidize the CO, H_2, and hydrocarbons present in the exhaust stream. The pumping current is then [16]:

$$Ip = \frac{2FS}{RTL}(D_{H2}P_{H2} + D_{CO}P_{CO} + D_{HC}P_{HC}) \qquad 2.4$$

The sensors used in this experiment were a Horiba MEXA-110λ and a NTK MO-1000. Both are the UEGO type. The specifications for the Horiba are shown below in Table 2.5.

Measurement range	A/F: 10.00-30.00 A/F λ: 0.50-2.00 O_2: 0-25% O_2
Accuracy	± 0.3 A/F when 12.5 A/F ± 0.1 A/F when 14.7 A/F ± 0.5 A/F when 23.0 A/F
Recorder Output	0-1 V DC
Exhaust Gas Temp	-7→900 °C

Table 2.5: Horiba MEXA-110λ specifications

2.3.3 Hydrocarbon Measurement and Theory

Typically, hydrocarbons have the structure of C_mH_n, and result from partially oxidized fuel or lubricant sources (as discussed in Section 1.3.1). The industry standard for measuring hydrocarbons is Flame Ionization Detection (FID). In this process, an exhaust sample is drawn into a sample chamber via a vacuum pump. The sample stream is held at a constant flow rate by the use of a constant differential pressure chamber. A hydrogen flame is used to combust a sample stream, which produces ionic hydrocarbons as shown in the following reaction scheme:

$$\begin{aligned} CH + O &\rightarrow CHO^+ + e^- \\ CHO^+ + H_2O &\rightarrow H_3O^+ + CO \\ H_3O^+ + e^- &\rightarrow 2H + OH \end{aligned} \qquad 2.5$$

The second two equations listed above are formed because of the large amount of water present in the sample stream. All of these electron charges are then gathered to an electrode held at 150-200 volts negatively biased to the burner, and a current is produced which is proportional to the hydrocarbon concentration [17].

The FID used for the experimental results presented later is a Cambustion HFR400 Fast FID. This piece of research equipment has a very small response time when compared to typical FIDs, as the hydrogen flame is contained in the sampling head, whereas with typical FIDs, the sample has to travel through a long sample tube before reaching the hydrogen flame. The specifications for the equipment are shown below in Table 2.6 [18]:

Number of channels	2
Measurement ranges	0-2000 to 0-1,000,000 ppm C1
Response Time	< 4 ms
Drift	< ± 2% Fullscale/hour
Linearity	< ± 2% Fullscale (@ 150,000 ppm C1)
Output	0-10 Volts

Table 2.6: Cambustion HFR400 Fast FID specifications

2.3.4 NO Measurement and Theory

For the measurement of NO in the exhaust stream, a Cambustion fNOx400 Fast CLD was used. This instrument uses the process of Chemiluminescence detection, which is the industry standard for the measurement of NO. In this method of measurement, a

sample of the exhaust stream is first drawn into the sampling chamber. A stream of ozone is then introduced into the reaction chamber, causing the following reaction:

$$NO + O_3 \rightarrow NO_2^* + O_2 \quad (2.6)$$

NO_2^* represents the NO_2 that is in an excited state. This molecule then reverts back to the ground state, emitting radiation in the wavelength range to 600 to 3000 nm. This light is then recorded by a photo-detector, the light emission being proportional to the NO concentration [19].

The Cambustion equipment used in this experiment uses the same sampling methodology as the Fast FID; the measurement takes place in the head of the instrument directly behind the sampling probe, resulting in a low response time. As with the fast FID, a constant pressure chamber is used to keep the sample independent of the exhaust stream flow rate. The specifications for the fast NO meter are shown below in Table 2.7 [20]:

Number of channels	2
Measurement ranges	0-10,000 ppm
Response Time	< 4 ms
Repeatability	< ± 1 % Fullscale
Zero Drift	< ± 1 % Fullscale/hour
Span Drift	< ± 1 % Fullscale/hour
Linearity	< ± 1% Fullscale to 5,000 ppm, < ± 2% Fullscale to 10,000 ppm
Output	0-10 Volts, 47 Ohms

Table 2.7: Cambustion fNOx400 Fast CLD Specifications

2.3.5: Carbon Monoxide Measurement and Theory

The industry standard method for the measurement of CO is Non Dispersive InfraRed (NDIR). This measurement method involves a hot glow bar that emits infrared radiation simultaneously through a cell filled with N_2 and a cell filled with the sample gas (a chopper wheel is used between the glow bar and the cells). To eliminate the IR emission of the hot gases, the sample gas is passed through a heat exchanger before going into the sample cell. Opposite the glow bar in line to receive the radiation passed through the two sample cells are two detection cells separated by a diaphragm. The IR that passed through the N_2 cell had no interference, as N_2 does not absorb any IR radiation, while the sample gas containing CO absorbs radiation. The two detection cells are filled

with CO gas, and the radiation that passes through the sample cell causes an increase in temperature in the one CO cell. This temperature differential causes a pressure difference in the two cells, and a radio frequency detector converts the deflection of the diaphragm into a voltage output [21].

The NDIR instrument used in this series of experiments was a Rosemount Analytical Model 880A. The sampling requirements of this instrument requires that the sample gas be moisture free, so the exhaust gas was run through a desiccant before entering the sample chamber. The specifications for the 880A are shown below in Table 2.8 [22].

Operating Temperature	0 to 45 °C
Measurement ranges	0-10% CO
Response Time	30 seconds (measured)
Repeatability	1 % Fullscale
Noise	1 % Fullscale
Zero Drift	< ± 1 % Fullscale/ 24 hours
Span Drift	< ± 1 % Fullscale/ 24 hours
Sample Pressure	Max 10 psig
Sensitivity	10 ppm fullscale CO

Table 2.8: Rosemount Analytical Model 880A specifications

2.3.6: Temperature Measurement

The catalytic converters were provided from DaimlerChrysler with two additional ports for sampling: one which fell in the middle of the front palladium brick, and the other which fell between the two bricks. These ports were used to sample temperature, which was measured using Omega Type K exposed junction thermocouples.

2.3.7: Locations of Sampling Probes

Figure 2.2 shows a schematic of the engine/catalytic converter setup (not to scale). One difference between the experimental setup and a production engine is that a short extender was inserted between the exhaust flange and the catalyst so that pre-cat measurements could be made. On the schematic is labeled where the various measurement probes were located. Table 2.9 shows the axial location of the pre-catalyst sensors measured from the exhaust flange to the centerline of the sampling probe or instrument.

Description	Axial Distance From Exhaust Manifold Flange (cm)
Upstream Fast FID	7.62
Upstream Fast NOx meter	2.54
Upstream UEGO	5.08

Table 2.9: Axial Locations of Upstream Sensors

For the downstream sensor measurements, the axial distance of the sensor placement is presented as the distance from the catalyst flange, located immediately at the catalyst exit (see Figure 2.2). The distance is shown in Table 2.10:

Description	Axial Distance From Catalytic Converter Flange (cm)
Downstream Fast FID	11.43
Downstream Fast NOx meter	5.08
Downstream UEGO	9.53

Table 2.10: Axial Locations of Downstream Sensors

Finally, the thermocouple probe locations are shown in Table 2.11, measured from the exhaust manifold flange:

Description	Axial Distance From Exhaust Manifold Flange (cm)
Mid-Brick Catalyst Temperature	19.69
Between Brick Catalyst Temperature	31.12

Table 2.11 Axial Locations of Thermocouple Probes

For the radial position of the probes, the fast FID and fast NOx probes were put in the center of the exhaust plumbing to minimize wall effects and provide a true average measure of the turbulent exhaust flow. The UEGOs were inserted using a standard flange mounting application, and so protruded ~1.5 cm into the exhaust stream.

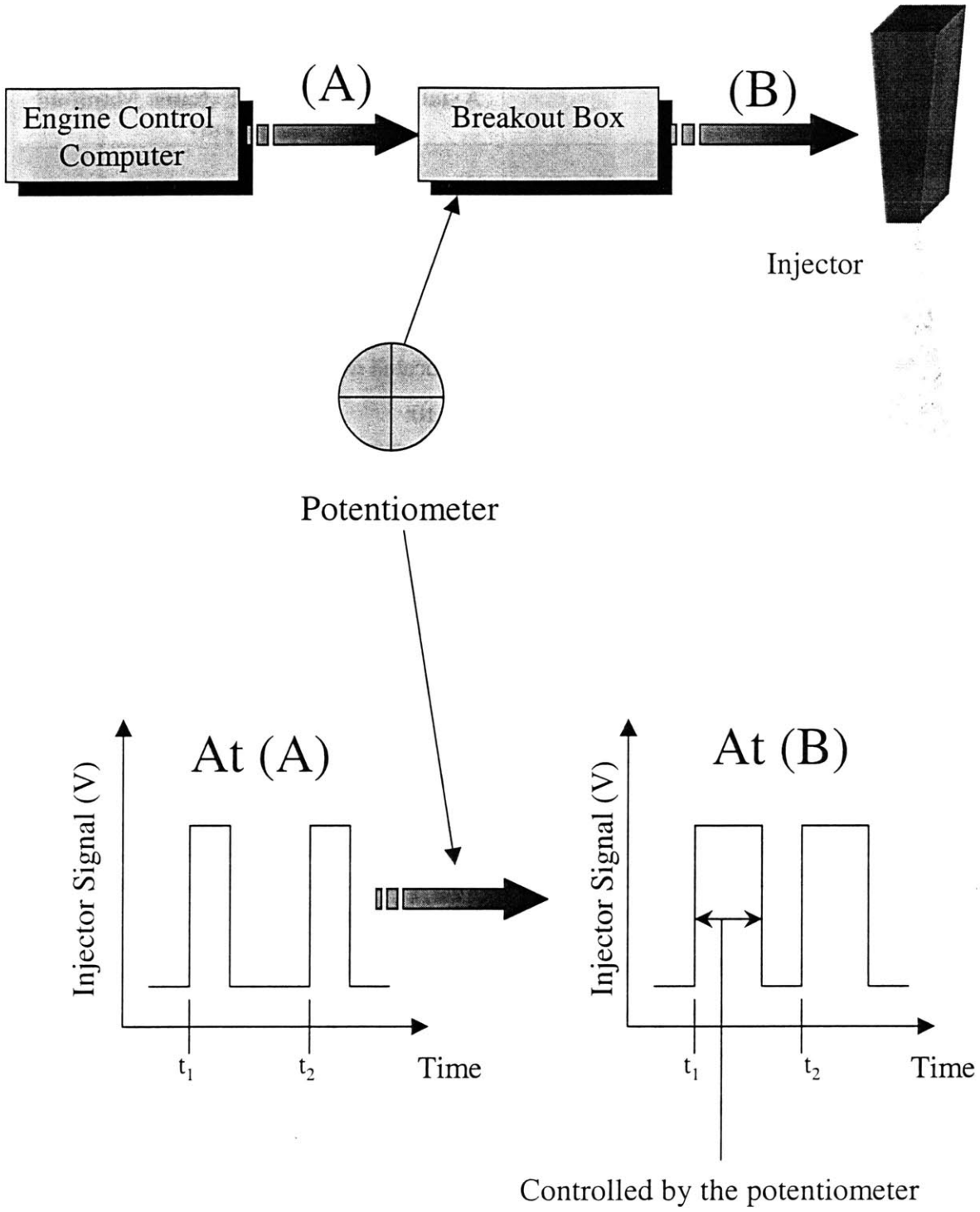

Figure 2.1: Schematic of λ Control

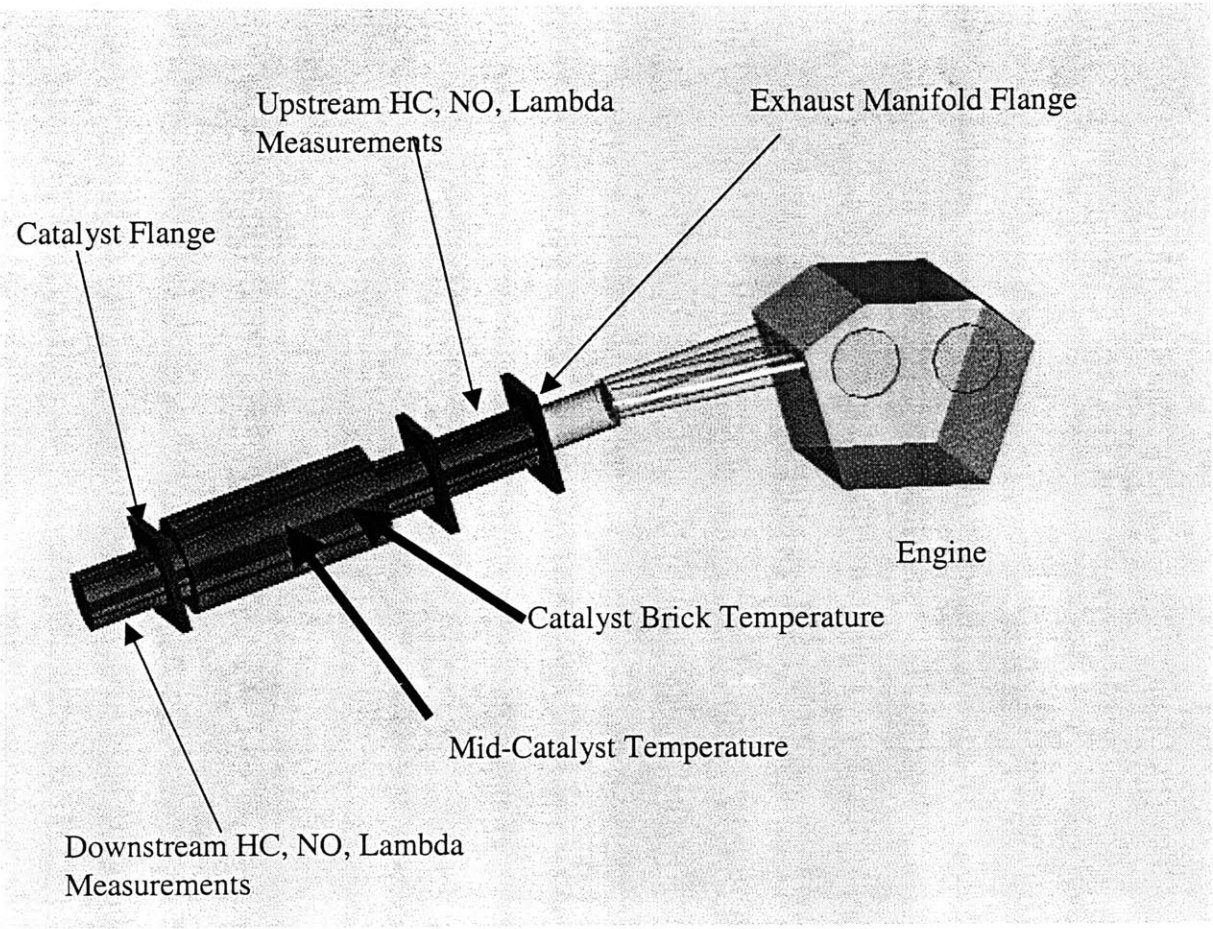

Figure 2.2: Schematic of Engine/Catalyst Setup

CHAPTER 3: STEADY STATE RESULTS AND DISCUSSION

3.1 INTRODUCTION

The experimental results presented in this chapter provide a framework for the results included in the following two chapters. First, the steady state catalyst efficiency with respect to HC and NOx are presented. These steady state values provide a reference for comparison with the transient performance of the catalytic converters. Also to be presented in this section are the values used for calculating the mass flow rate of the exhaust, which is later used in the calculation of oxygen storage.

The table below lists the three sets of experiments and what data were recorded for each of the experiments. This Chapter deals with the steady state measurements, Chapter 4 the transient tests, and Chapter 5 the oxygen storage tests.

Experiment	Data Recorded
Transient tests	Pre-catalyst λ, Post-catalyst λ, Intake Pressure, Pre- and Post-Catalyst Hydrocarbon and NOx concentrations, Catalyst front brick temperature, Catalyst between brick temperature
Oxygen Storage Tests	Pre-catalyst λ, Post-catalyst λ, Pre- and Post-Catalyst Hydrocarbon and NOx concentrations, Catalyst front brick temperature, Catalyst between brick temperature
Steady State Catalyst Efficiency Measurements	Pre-catalyst λ, Post-catalyst λ, Pre- and Post-Catalyst Hydrocarbon, CO, and NOx concentrations, Catalyst front brick temperature, Catalyst between brick temperature

Table 3.1: Data Recorded for Each of the Three Experiments

3.2 STEADY STATE EMISSIONS AND CATALYST EFFICIENCY

3.2.1 Steady State Hydrocarbon Results

Using the fast FID, HC emissions were simultaneously measured before and after the catalytic converter. This set of tests was done with no engine air/fuel modulation; the engine was held at a constant air/fuel ratio. The air/fuel ratio was controlled using the control system described in Section 2.2.1. The value of the upstream UEGO was used to set the air/fuel ratio. During the experiments, the output of the fast FID and the pre- and post catalyst λ values were averaged over a time period of 20 seconds. The MATLAB code used to convert the fast FID signal to the emissions level is included in Appendix C. The calibration was done using a zero gas of N_2 and span gases of 100 ppm propane, 700 ppm propane, and 1500 ppm propane before any data were recorded.

Figure 3.1 shows the pre-catalyst values of HC. As may be seen there is a variation of ~2500 ppm between runs. It would be expected that there would be little difference between the various runs in the engine out emissions. However, this data was taken over a period of several days, and the instrumentation was recalibrated differently for each run. The fast FID is a sensitive instrument, and there were many fluctuations even at steady state operation. The efficiency values will still be representative, as they were taken simultaneously, thus eliminating the calibration and daily operating parameter differences.

The shape of the curve, however, is very consistent, being the highest at the richest value. At rich values, there is more fuel injected into each cylinder than is necessary for combustion, and this excess fuel is not completely oxidized. The HC emissions decrease as the mixture becomes progressively leaner. At stoichiometric and leaner, the curve is fairly flat, as these are the hydrocarbons that are trapped in the crevices of the cylinder, absorbed/desorbed in the oil, and detached cylinder deposits. These variables are constant through the varying air/fuel ratio.

Figure 3.2 shows the post-catalyst HC as a function of upstream lambda. Shown on this plot are the different catalyst values. The oldest catalyst (150K) is represented as squares, and shows the highest levels of breakthrough, as one would expect for the oldest catalyst. The 2000 RPM values, shown with the dotted line, are slightly less, most likely

due to the higher catalyst temperature that exists at the higher mass flow rate. The middle-aged (50K) catalyst (represented as circles) HC breakthrough is lower than that of the 150K catalyst, with the same relationship between the lower and higher RPM values. The fresh catalyst (4K) has the lowest emissions. The 4K catalyst 2000 RPM and 1600 RPM curves are reversed from the order of the other catalyst ages, but these hydrocarbon values are in the low range of the fast FID's sensitivity and so the error in this region would explain the switch in the curves.

Figure 3.3 shows the catalyst efficiency with respect to HC at a speed of 1600 RPM. The efficiencies all follow the same trend; richer engine values have a lower efficiency due to the large amount of hydrocarbons produced and the lack of oxygen to oxidize them. The 150K catalyst, shown with the white bars, ranges from 3% lower efficiency at stoichiometric to 33% lower efficiency at λ=0.85 that that of the 4K catalyst (shown in the bars with the brick pattern). The 50K catalyst efficiency (the bars containing the diagonal pattern) falls between the 4K and 150K catalyst.

Figure 3.4 shows the hydrocarbon efficiency curves for the different catalysts at 2000 RPM. All of the HC efficiencies for this operating point are higher due to the increased temperature (the temperature curves will be shown later). The catalysts are represented as before with the same patterns indicating the same aged catalyst as in the plot for 1600 RPM.

3.2.2 Steady State Oxide of Nitrogen Results

The oxides of nitrogen were measured in the same manner as the hydrocarbons. The fast NOx meter was used, sampling for a time period of 20 seconds, converting the voltage output to NOx concentration, and then averaging the pre- and post-catalyst values. For calibration, 100 ppm NOx, 1000 ppm NOx, and 3000 ppm NOx gases were used, along with nitrogen as a zero gas. The MATLAB code used is included in Appendix C (HC, NOx, and catalyst temperature were all measured simultaneously, so the same code was used to analyze the data).

Figure 3.5 shows the variation in the upstream NOx measurements as a function of the upstream UEGO sensor value. These values are less spread out than the engine out hydrocarbons, only ranging a maximum of 250 ppm over the set of experiments. This

variation is simply due to the small variations in the engine operating conditions. The shape of the curve has the NOx peaking at a stoichiometric. NOx formation, as mentioned in Section 1.3.1, is a function of temperature, with higher temperature leading to more NOx being formed. The highest combustion temperature occurs at stoichiometric, as this is where the most energy release occurs. As the mixture is enriched or leaned out, the NOx formation drops due to the temperature drop that occurs in both directions.

A comparison of the post catalyst values is shown in Figure 3.6. At rich values of air/fuel ratio, the NOx breakthrough is essentially zero, as the CO produced during rich combustion is abundant enough to react with the majority of the NOx in the catalytic converter. The values of the NOx being so low in the rich regime make the measurement a difficult one, as there is uncertainty in the NOx meter at very low values of NOx (< 30 ppm). The NOx breakthrough may not be truly zero as shown here, but instead a very low number. At values of air/fuel ratio greater than stoichiometric, the post-catalyst NOx curve follows the pre-catalyst NOx curve, as the reduction of NOx in a lean environment is not possible under these circumstances. At stoichiometric, the 150K catalyst (represented using the squares) shows ~50% more breakthrough than that of the 50K catalyst (shown by the circles), and the 4K catalyst has no breakthrough.

The efficiencies of the catalysts are compared in Figure 3.7. It may be seen that the 150K catalyst shows an efficiency decrease even in the rich points of the spectrum, even though there is not much NOx produced in the combustion process. This implies that there is a decrease in the active catalytic material, as at those rich points more CO is present than is necessary to reduce the NOx. The lean points again show that under these conditions the NOx cannot be reduced, with the efficiency dropping to zero independent of the catalyst age. Figure 3.8 shows similar results for 2000 RPM.

3.2.3 Steady State Catalyst Temperature Trends

The temperature of the catalytic converter is an excellent measure of the catalytic activity that is occurring inside. The brick temperature reflects the heat release produced by the chemical activities caused by the interaction of the exhaust gas stream with the

catalytic precious metal. The temperature of the catalyst between the bricks is a measure of the reaction progress along the catalyst.

Figure 3.9 shows the catalyst brick temperature (measured in the center of the front palladium brick of the catalyst—see Figure 2.2) as a function of air/fuel ratio at varying engine speeds. The 2000 RPM curves (dashed lines) are clearly separated from the ones taken at 1600 RPM (solid lines), showing a trend that the higher mass flow rate leads to a higher temperature. The curves for each engine speed appear to be tightly grouped, even though the 150K catalyst curves (the square data points) appear to be the highest temperature curves. The shape of the curve is such that the point taken at stoichiometric is the highest temperature, as this is the point which has the potential for the highest oxidation, and hence the most chemical energy release.

Figure 3.10 shows the mid-catalyst temperature, which was measured in the volume between the two catalyst bricks (see Figure 2.2). This is a measure of the exhaust stream temperature after the palladium has decreased the activation energy of the chemistry detailed in Section 1.3.2. As with Figure 3.9, there is a clear distinction between the two different engine speeds. Also, it is interesting to note that the mid-catalyst temperature is on the order of 50 °C lower than that of the brick temperature (where the chemical reactions are occurring). Again, at stoichiometric, the temperature is observed to be the highest.

3.2.4 Steady State Carbon Monoxide Results

Carbon monoxide plays a large role in the catalyst and the reactions that occur inside of it. It was desired to find the efficiency of the catalytic converter with respect to this variable, but the Rosemount instrumentation was not sensitive enough to measure the post catalyst values (which would be on the order of tenths to hundredths of a percent). However, it was possible to measure the pre-catalyst values of CO using the instrumentation, and these will be useful for putting the tests to be shown in Chapters 4 and 5 in the proper framework and understanding what the catalyst sees in the feed gas.

The CO was measured on a dry basis, because the water present in the exhaust stream would interfere with the NDIR measurements. However, for proper comparison,

this dry value must be converted back into a wet value. This is done using the following relationship [4]:

$$\chi = (1 - \chi_{H2O})\chi^* \qquad 3.1$$

X* represents the dry mole fraction, and x the wet mole fraction. Since the mole fraction of water (x_{H2O}) was not measured during this experiment, previous data was used from Heywood [4]. The curve for the mole fraction of water used is included as Appendix D. Applying equation 3.1 to the dry mole fractions of pre-catalyst CO, Figure 3.11 results.

Figure 3.11 shows both 1600 RPM and 2000 RPM results for the CO mole fraction. They follow closely due to CO formation being a function of how rich the engine is run, and not of temperature (as NOx formation is).

Appendix E includes the CO, NOx, and HC results in tabular form.

3.2.5 Differences in Pre- and Post-Catalyst Oxygen Sensors

As discussed in Section 2.3.2, the UEGO is an excellent tool for determining how rich or how lean the exhaust gas stream is. However, because the sensor uses diffusion to measure the composition of the exhaust, there arises a problem when different species are diffusing through the membrane. By definition, the air/fuel ratio should not change across the catalyst, as conservation of moles has to apply to a control volume around the catalyst. However, it has been observed in previous work that the value that the oxygen sensor reports is different between pre- and post converter oxygen sensors even for a steady state stream. Buglass, et. al performed a study in which exhaust gas was simulated and sent through a catalyst, and the pre- and post catalyst oxygen sensor values were recorded. These researchers could vary the gas composition, and used these gas compositions to test the sensors' responses. The result of their research showed the presence of H_2 caused a lean lambda shift in the exhaust reading due to the diffusion rate difference of H_2 compared to oxygen and CO. Hydrogen has a higher rate of diffusion than O_2 and CO (which have similar mass and therefore similar diffusion rates), so this is what causes the lean shift. When large hydrocarbons such as toluene were present, the sensor is rich shifted because large molecules take a relatively long time to diffuse when compared to oxygen. This causes the sensor to report that there is a stoichiometric

balance only when many large HC are present, and hence a rich shift. The study also found that the sensor deception is enhanced at higher temperatures [23].

Germann, et al. also reported similar results, pegging the diffusion time difference as the reason for the sensor error. They also reported that as the catalyst aged, the sensor error decreases, as the catalyst changes the composition less as it deteriorates [24].

The results obtained here agree well with the literature. As a method of determining the error, the post-catalyst value was plotted versus the pre-converter value. For perfect agreement, the results should be a line at 45° with a slope of 1, but the results show that there is an increasing rich shift in the richer regimes and a constant rich shift in the lean regime. Figure 3.12 shows the differences between the two sensors at 1600 RPM and a MAP of 0.5 Bar. As may be seen from the curve fit recorded on the graph, the 150K has the lowest slope of the three curves (and hence the lowest sensor error due the deterioration of the catalyst), followed by the 50K and then the 4K catalyst. It may be seen from Table 3.2 that the UEGO reading for the 150K catalyst actually reads higher than the upstream catalyst, but it must be remembered that this difference is in the error range given for the oxygen sensors in Section 2.3.2. At 2000 RPM (shown in Figure 3.13), the downstream sensor is shown to be more sensitive to changes in composition than the 1600 RPM curves, but the same trend is seen in the relationship between the slopes of the 1600 and 2000 RPM curves. The increased sensitivity seen in the 2000 RPM plots may be due to the increased temperature experienced at the higher flow rate. The results are tabulated in Table 3.2 for 1600 RPM and Table 3.3 for 2000 RPM, which are averaged over a time period of 20 seconds.

4K Catalyst		50K Catalyst		150 K Catalyst	
Upstream λ	Downstream λ	Upstream λ	Downstream λ	Upstream λ	Downstream λ
0.852	0.828	0.853	0.861	0.854	0.862
0.902	0.883	0.903	0.902	0.901	0.913
0.963	0.950	0.953	0.944	0.952	0.959
1.006	0.996	1.001	0.997	1.014	1.017
1.055	1.050	1.054	1.050	1.054	1.050
1.099	1.093	1.098	1.090	1.105	1.096
1.155	1.145	1.158	1.146	1.155	1.144
1.211	1.196	1.230	1.212	1.209	1.192

Table 3.2 Differences in Pre- and Post- Catalyst UEGO Readings @ 1600 RPM

4K Catalyst		50K Catalyst		150 K Catalyst	
Upstream λ	Downstream λ	Upstream λ	Downstream λ	Upstream λ	Downstream λ
0.853	0.843	0.845	0.842	0.859	0.865
0.910	0.922	0.922	0.941	0.906	0.923
0.955	0.968	0.958	0.975	0.955	0.973
1.008	1.011	1.005	1.003	1.007	1.003
1.053	1.048	1.069	1.063	1.055	1.049
1.110	1.101	1.105	1.097	1.109	1.099
1.161	1.147	1.168	1.153	1.150	1.137
1.205	1.186	1.205	1.186	1.211	1.190

Table 3.3: Differences in Pre- and Post-Catalyst UEGO Readings @ 2000 RPM

3.2.6: Engine Volumetric Efficiency

As a way of determining the flow rate at the different speeds and intake conditions, volumetric efficiency was measured for the engine. Volumetric efficiency is defined as [4]:

$$\eta_v = \frac{2\dot{m}_{air}}{\rho_{ai} V_d N} = \frac{m_{air}}{\rho_{ai} V_d} \qquad (3.2)$$

Volumetric efficiency is a measure of how efficiently the engine uses the air it inducts. To measure the volumetric efficiency of the experimental engine, an injector was removed from the engine and a measured amount of fuel pulses were sprayed into a graduated cylinder that was in an ice bath. The graduated cylinder was then weighed, and using the known density of the fuel, the fuel volume was converted to the mass of fuel injected. From the calibration of the injector, which was done at varying fuel pulse widths, how much fuel is injected during engine operation may be recorded using the injection duration. This mass of fuel injected may be related to the air mass by the air/fuel ratio recorded from the upstream UEGO. From this data, the volumetric efficiency may be calculated. The results of this are shown in Table 3.4 and graphically in Figure 3.14.

	Speed (RPM)						
Intake Pres. (Bar)	1600	1700	1800	1900	2000	2100	2200
0.3	57.90%	56.14%	58.88%	61.20%	59.44%	59.71%	56.23%
0.5	66.17%	68.52%	69.87%	73.52%	73.22%	73.75%	68.19%
0.7	69.95%	71.42%	74.28%	75.74%	75.05%	75.51%	73.62%
0.99	77.88%	77.41%	78.05%	79.31%	79.58%	80.47%	79.08%

Table 3.4: Volumetric Efficiency Map

3.3 STEADY STATE CONCLUSIONS

From this portion of the research, it was seen that the catalyst efficiency (with respect to HC) did not decrease noticeably when comparing the 4K catalyst to the 150K catalyst (at a stoichiometric operating point). With the NOx, however, there was almost a 50% reduction in conversion efficiency. If CO efficiency were to be measured, it would be expected to find a similar decrease, as CO and NOx are linked to each other.

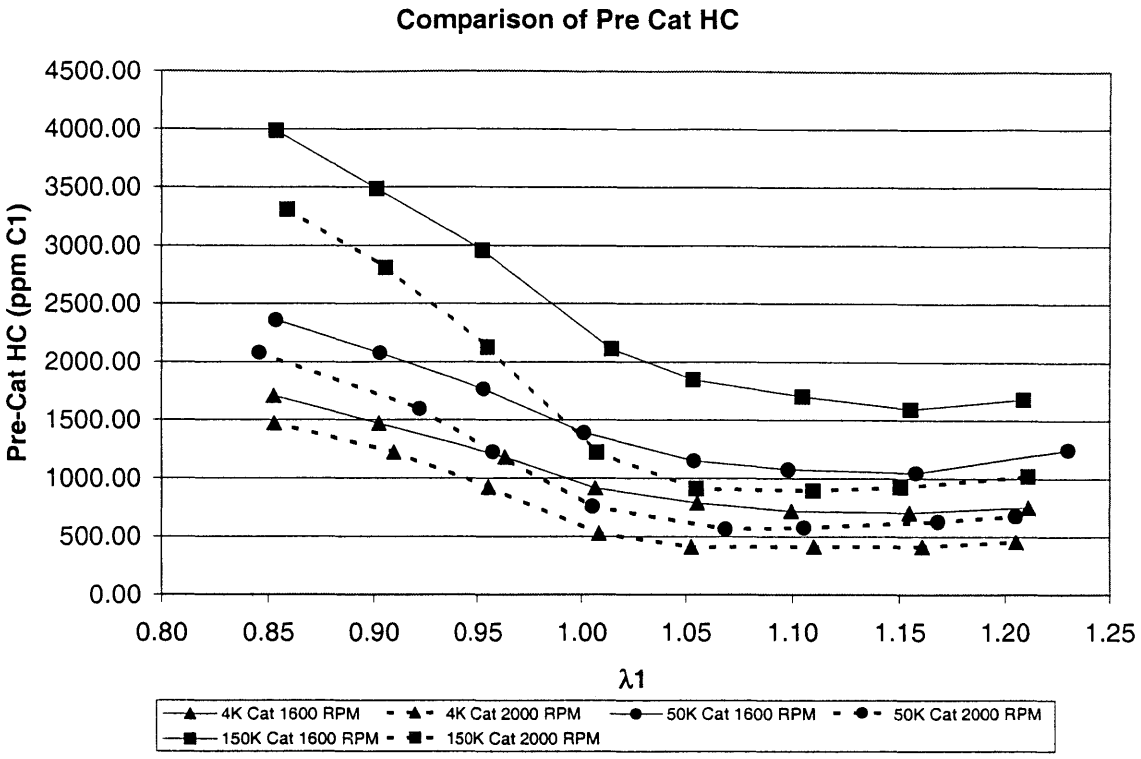

Figure 3.1: Pre-Catalyst HC Emissions as a Function of Upstream λ, 0.5 Bar MAP

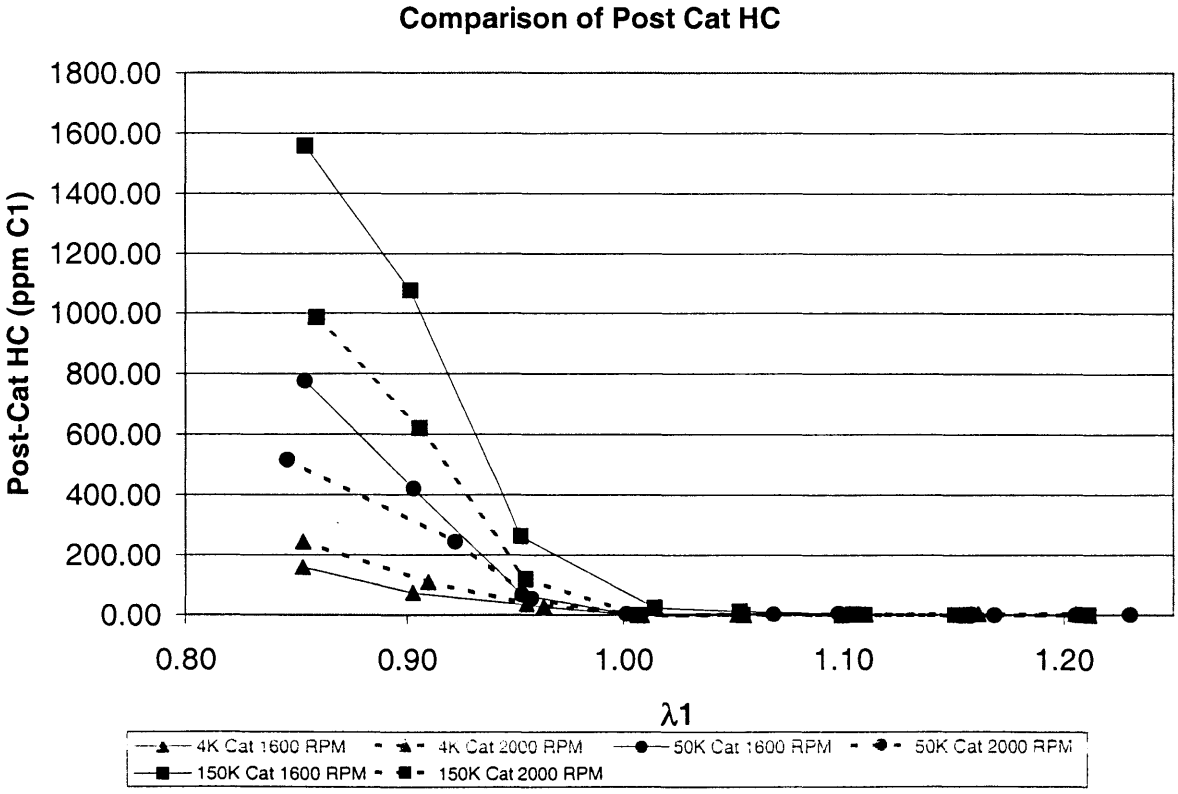

Figure 3.2: Post-Catalyst HC Emissions as a Function of Upstream λ , 0.5 Bar MAP

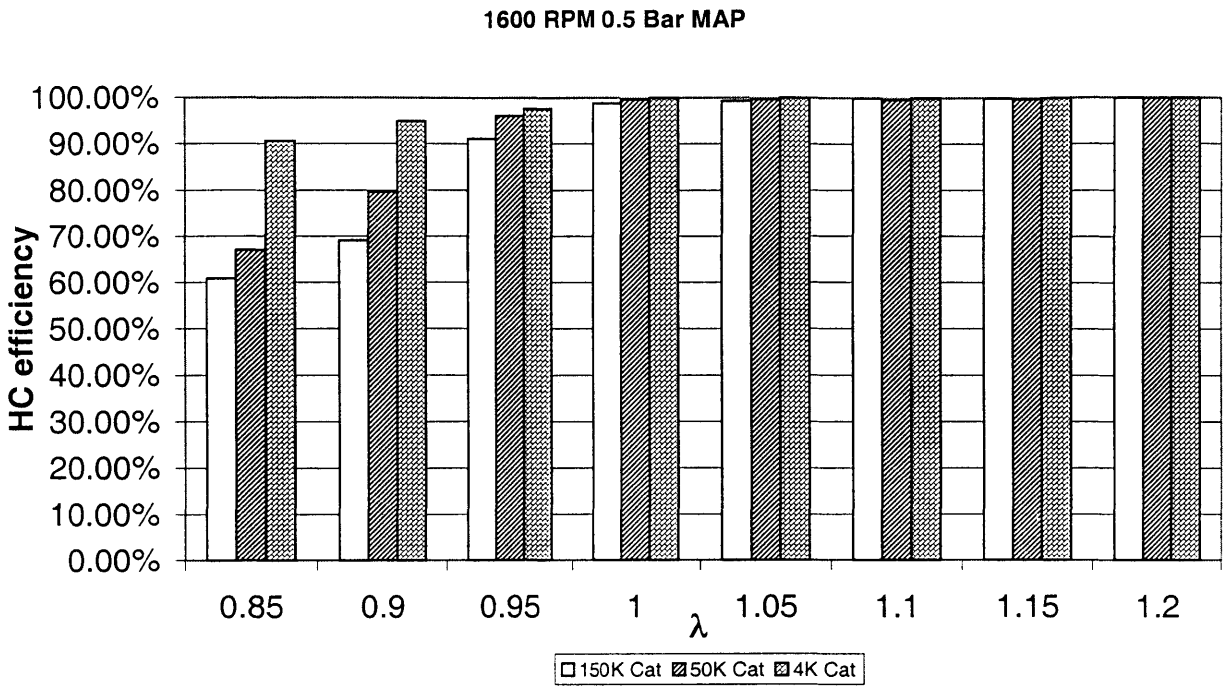

Figure 3.3: Steady State HC Efficiency vs. Upstream λ @ 1600 RPM, 0.5 Bar MAP

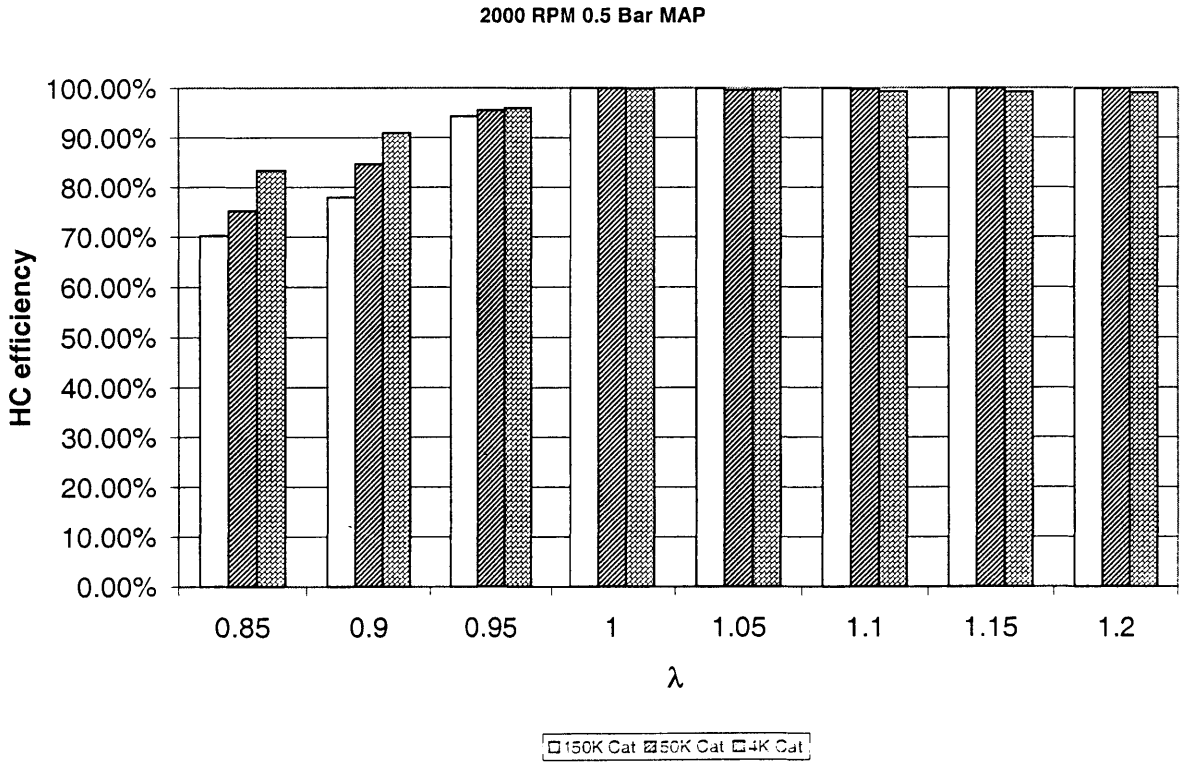

Figure 3.4: Steady State HC Efficiency vs. Upstream λ @ 2000 RPM, 0.5 Bar MAP

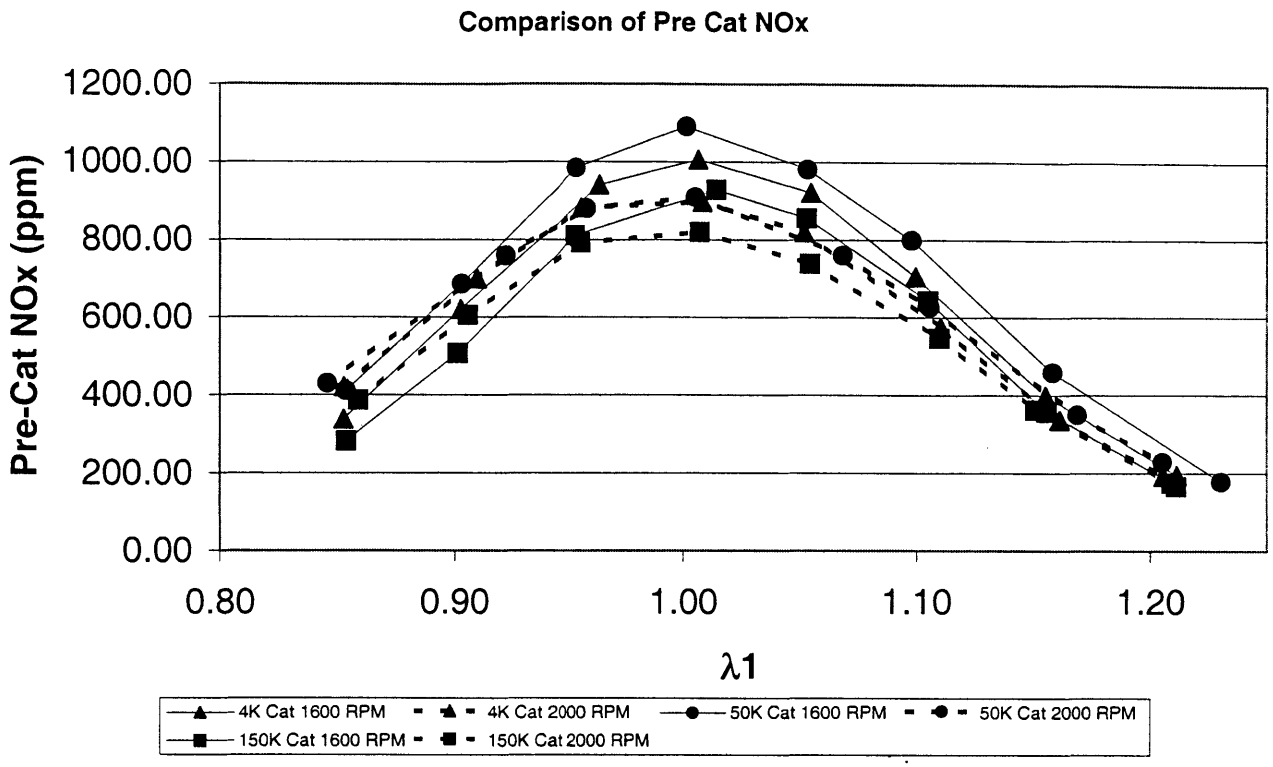

Figure 3.5: Pre-Catalyst NOx Emissions as a Function of Upstream λ, 0.5 Bar MAP

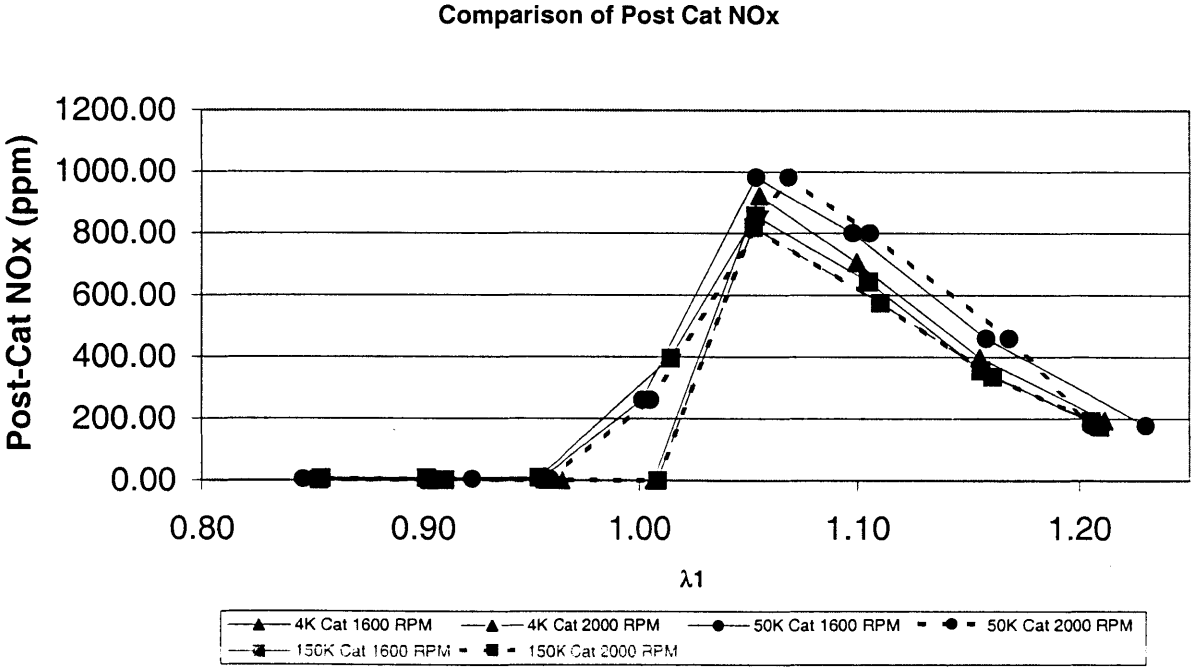

Figure 3.6: Post-Catalyst NOx Emissions as a Function of Upstream λ , 0.5 Bar MAP

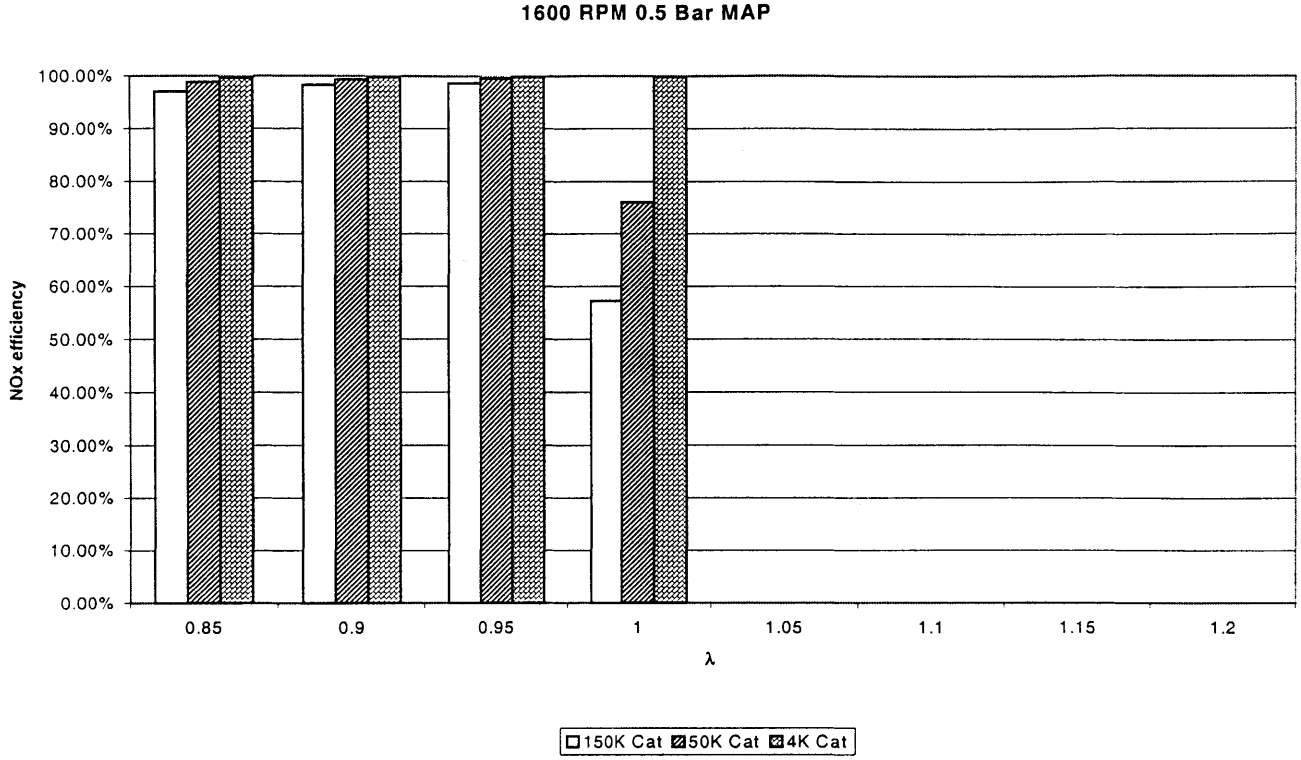

Figure 3.7: Steady State NOx Efficiency vs Upstream λ @ 1600 RPM, 0.5 Bar MAP. Efficiency Values = 0 @ λ >=1.05 in this experimental run

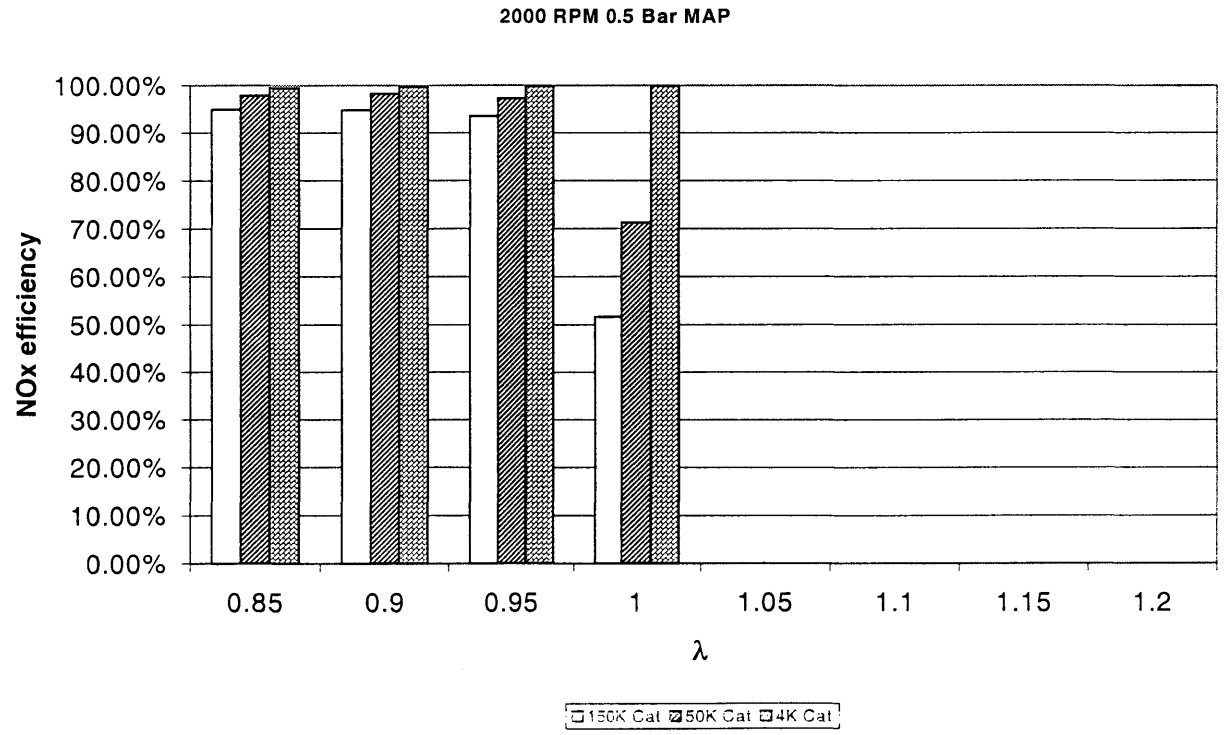

Figure 3.8: Steady State NOx Efficiency vs Upstream λ @ 2000 RPM, 0.5 Bar MAP. Efficiency Values = 0 @ λ >=1.05 in this experimental run

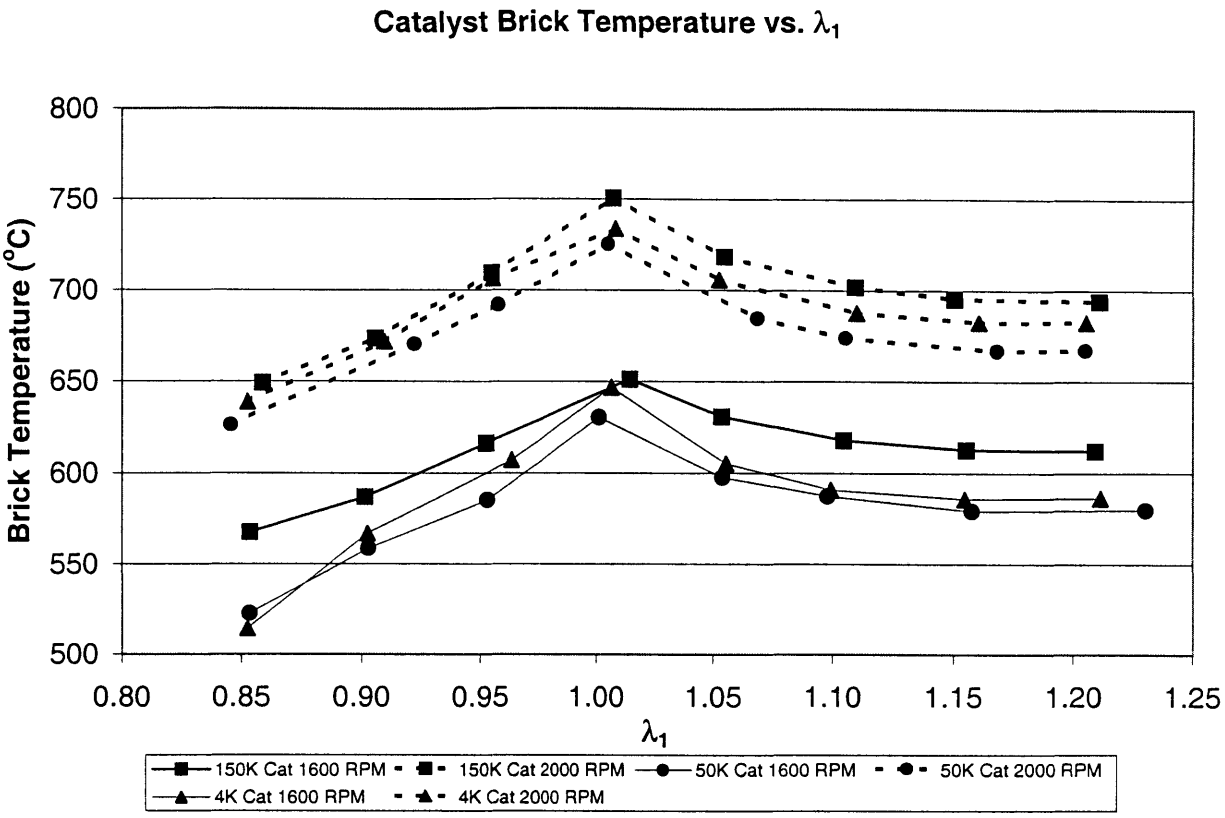

Figure 3.9: Steady State Brick Temperature vs Upstream λ, 0.5 Bar MAP

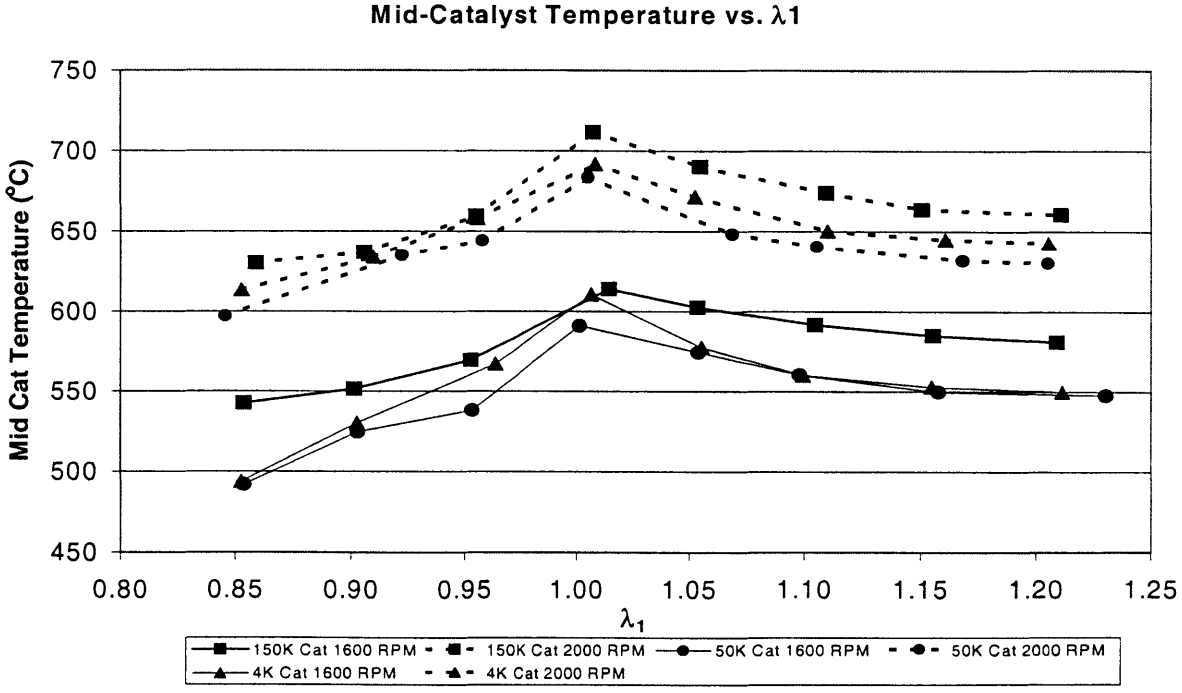

Figure 3.10: Steady State Mid-Catalyst Temperature vs Upstream λ , 0.5 Bar MAP

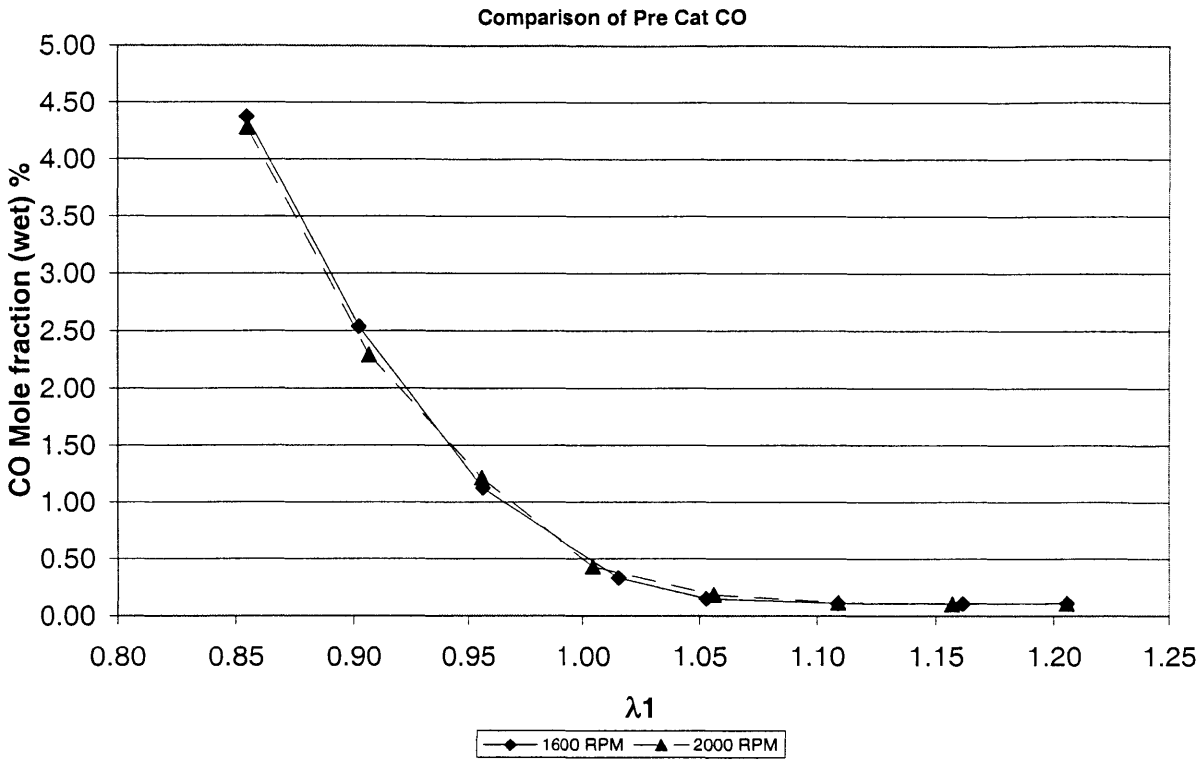

Figure 3.11: Steady State Pre-Catalyst CO vs Upstream λ, 0.5 Bar MAP

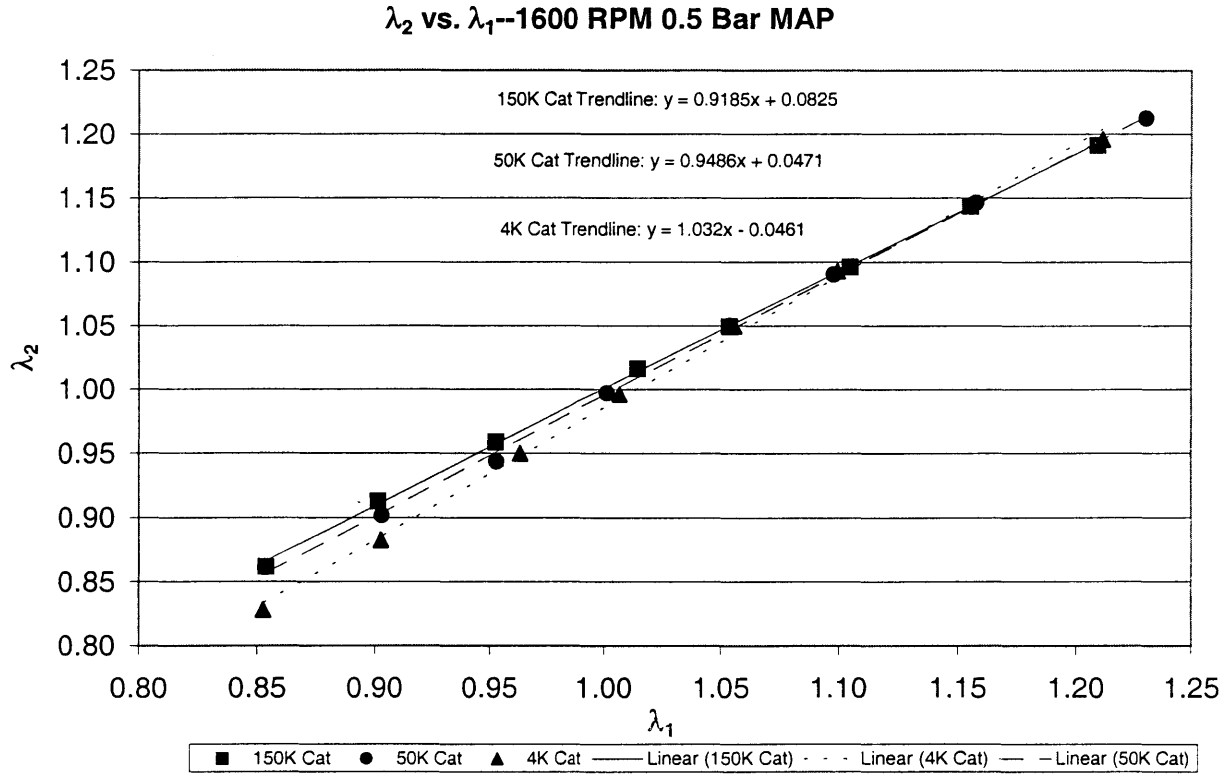

Figure 3.12: Downstream λ vs Upstream λ @ 1600 RPM, 0.5 Bar MAP

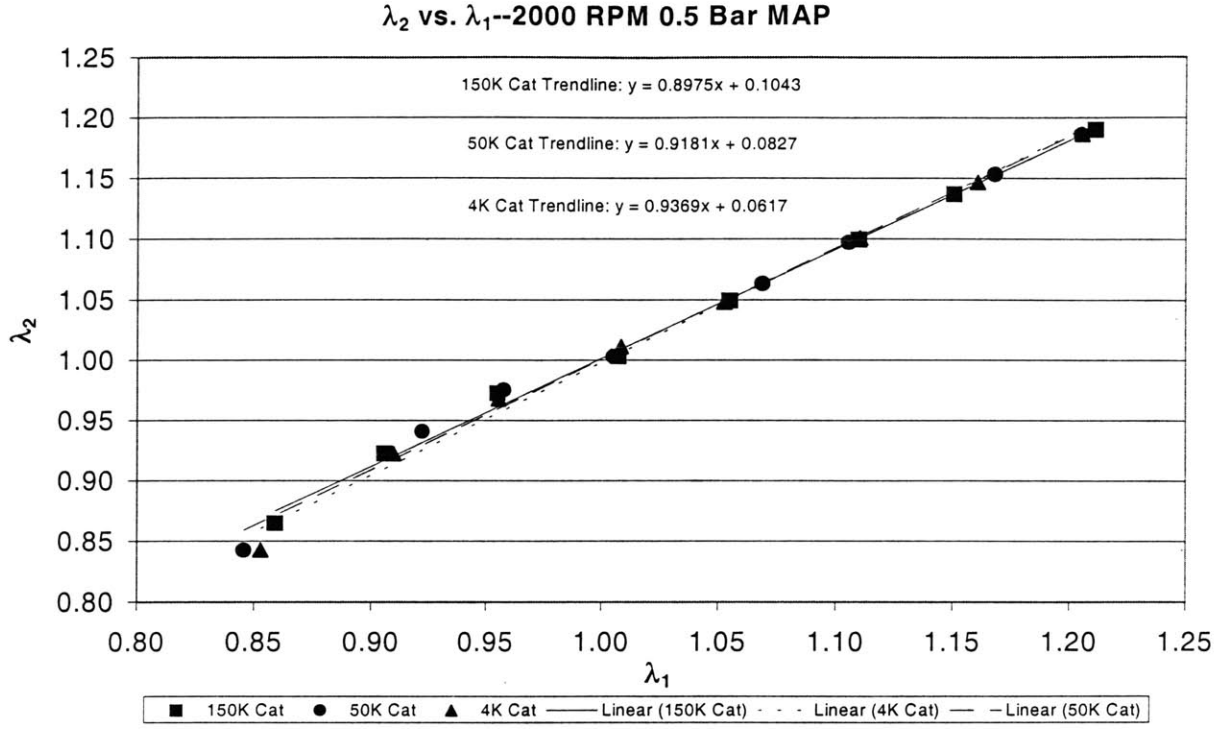

Figure 3.13: Downstream λ vs Upstream λ @ 2000 RPM, 0.5 Bar MAP

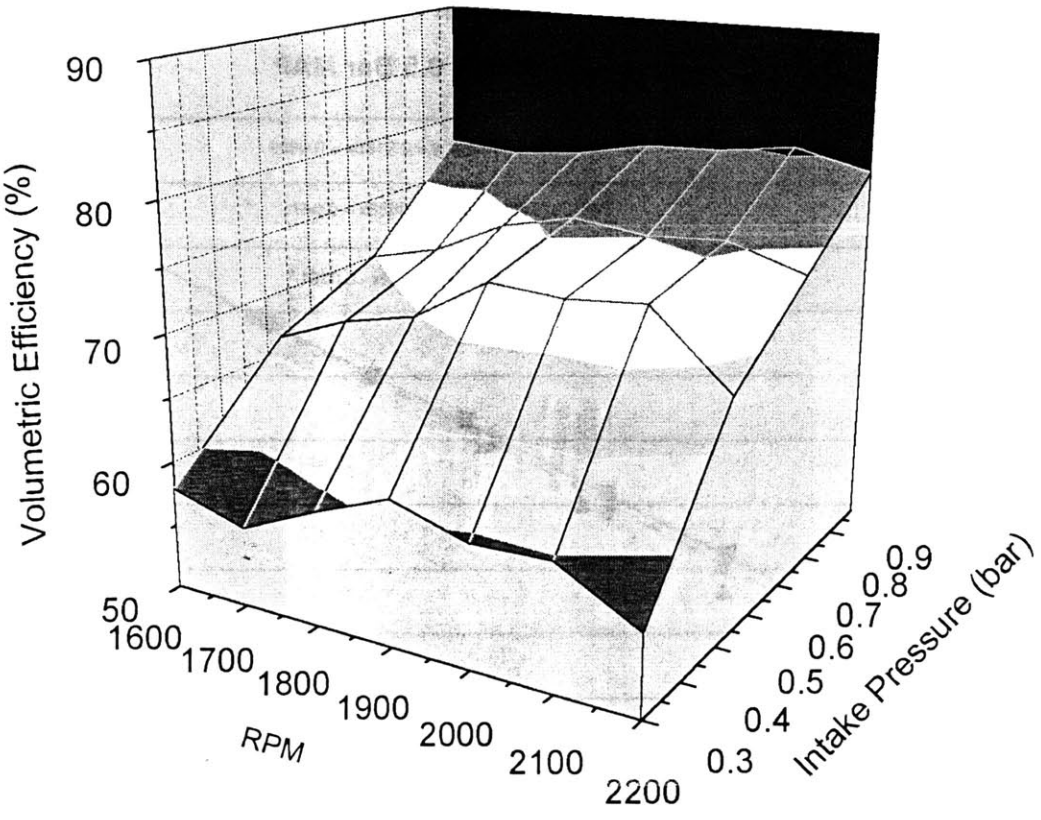

Figure 3.14: Volumetric Efficiency Map

CHAPTER 4: RAPID TRANSIENTS RESULTS AND DISCUSSION

4.1 INTRODUCTION

As seen in the previous chapter, under steady state operation near stoichiometric, even the oldest catalyst performed reasonably well. However, under real driving conditions and in the tests that must be performed for catalyst certification, there are transients. The next portion of this research is an endeavor to quantify what happens to the catalyst as these transients occur.

4.2 TRANSIENT TESTS

4.2.1 Description of Transient Tests

Transient tests were done at a constant 1900 RPM, with the load on the engine being varied by changing the intake pressure via a stepping motor controller. These tests were done closed loop, with the stock pre-catalyst oxygen sensor in communication with the engine control computer. The first set of tests was done by going from a MAP of 0.5 Bar to wide open throttle (WOT) in $7/10^{th}$ of a second, which is still approximately 3 times faster than the fastest transient in the Federal Test Procedure (FTP). The goal of these tests was to perturb the typical engine operation and observe the response of the catalytic converter, rather than just perform the minimal transient. Once at WOT, the engine was held at this high load for 40 seconds to observe the response of the catalytic converter under high mass flow rate conditions. Preliminary transient tests showed that the times shorter than 40 seconds cut short some of the physical phenomena that occurred, so 40 seconds was deemed to be the proper time period. After this period at WOT, the throttle was adjusted to return the MAP to 0.5 Bar at the same rate it was opened. In the second set of tests, the throttle was adjusted to WOT in $1/10^{th}$ of a second, making the catalytic converter see a rapid change in flow rate as well as a large lean spike. The final sets of tests to be discussed in this section are 4 step changes from a MAP of 0.5 Bar to WOT. At both WOT and 0.5, the engine was allowed to stay at that

point for 7 seconds, which was the amount of time the engine required to stabilize after the rapid throttle opening or closing. The purpose of these tests was to rapidly perturb the engine operation such that the catalyst saw a continually changing mass flow rate and exhaust gas stream composition. A summary of the different throttle opening and closing rates is shown below in Table 4.1.

All data for these tests were recorded simultaneously.

Transient Designation	Throttle Opening Time (sec)	Throttle Closing Time (sec)
Slow	0.7	0.7
Fast	0.1	0.1
Multiple Steps	0.1	0.1

Table 4.1: Programmed Throttle Opening and Closing Times for Transient Tests

4.2.2: Definition of Terminology

First, some terminology will be defined that characterizes the behavior that was quantified. Figure 4.1 shows an example of some preliminary data that was taken. The top curve is the intake pressure, and the bottom curve is the post-converter NOx. As may be seen from this example, there are two instances of breakthrough that occur: one when the throttle opens up and a smaller one that occurs when the engine is at wide-open throttle. The first peak is referred to as the "primary breakthrough", and the second peak is referred to as "secondary breakthrough." This is data from some preliminary experiments (which remained at WOT for a time period less than 40 seconds), and it may be seen that a portion of the secondary breakthrough is cut off. Of use in analyzing this breakthrough is a way to integrate the actual breakthrough and quantify the actual breakthrough. This was accomplished using the MATLAB code included in Appendix F. This code, after calibrating the data, plots the data and allows the user to select when the primary breakthrough begins and ends, and also the same for the secondary breakthrough. The selected portion of the curve is then integrated, and the area under the curve is given in units of ppm*sec. This may be easily converted to useful units such as grams of NOx by the following conversion:

$$(ppm * \sec)(10^{-6})\left(\frac{MW\ NOx}{mole\ NOx}\right)\left(\frac{mole\ exhaust}{MW\ exhaust}\right)\dot{m}_{exh} \qquad 4.1$$

This conversion is useful for comparison, and also gives a relative measure as to the severity of the breakthrough when compared to the emissions standards.

4.2.3 Transients with 4K Catalyst

4.2.3.1: Slow Transient with the 4K Catalyst

Presented in Figure 4.2 are the slow transient UEGO readings. For all of the plots to follow, the subscript "**1**" on the ordinate label refers to the pre-catalyst value, and the subscript "**2**" refers to the post-catalyst value. When the throttle is first opened, there is a lean excursion, as the engine controller did not expect the sudden throttle event. The other phenomenon to point out from this curve is that when the throttle is closed, it does not return immediately to 0.5 Bar. This is a design feature by DaimlerChrysler engineers to avoid a large rich spike when the driver lets off the throttle (accomplished by a spring damper).

Figure 4.3 shows the hydrocarbon trace for the slow transient. As may be seen, the pre-catalyst hydrocarbons increase to ~1500 ppm when the throttle is returned to 0.5 Bar from WOT. The post-catalyst hydrocarbons do not show any significant breakthrough at WOT, just some fluctuations that follow from the behavior of the pre-catalyst hydrocarbons.

Figure 4.4 is a trace of the pre- and post catalyst NOx for the slow transient event. When the throttle first opens, a slight primary breakthrough in NOx_2 is observed due to the fact that the feed gas to the catalyst is lean and the NOx cannot be completely reduced in this environment. However, the breakthrough is very small. The pre-catalyst NOx increases at WOT due to the higher combustion temperatures, and when the throttle returns to 0.5 Bar, slowly drops off. The rise and fall times of the pre-catalyst NO were related to the equilibration time of the charge heat transfer process during the load change.

The temperature record for the slow transient is included in Figure 4.5. When the throttle is opened to WOT, there is a delay in the response of the catalyst brick temperature. The mid-catalyst temperature follows this trend as well. When the throttle returns to the starting position, the brick temperature begins to decrease as catalytic

activity decreases. The mid-catalyst temperature, however, remains at a higher level due to the exhaust stream being heated as it passes through the first brick.

4.2.3.2: Fast Throttle Transient with the 4K Catalyst

Now, switching to the fast throttle opening transient, the pre- and post-catalyst λ traces may be seen in Figure 4.6. The lean excursion when the throttle is opened is much larger, peaking at $\lambda \sim 1.7$. At throttle close, the rich excursion is slightly larger, as the change in flow rate is faster with this case. The post-catalyst λ trace shows the trend of decreasing slightly as the WOT period increases, with three small "humps" observable, and then some minor fluctuations when the intake pressure is adjusted back to 0.5 Bar.

The fast throttle opening appeared to cause an engine misfire, as may be seen by the large spike in the pre-catalyst hydrocarbon level (Figure 4.7). This tracks through the catalyst and is evidenced by the spike seen in the post-catalyst HC trace. To observe the small details of the transient event, Figure 4.8 shows a zoomed plot of the HC. When the WOT events occurs, there is a slight increase in the number of pre-catalyst HC, but the largest peak occurs during the throttle down event. However, even though there is a peak (at the throttled down event) in the pre-catalyst HC, the 4K catalyst efficiently oxidizes the hydrocarbons.

During the fast transient, there is a slight amount of primary breakthrough seen in the post-catalyst NOx trace (Figure 4.9). This level of breakthrough is more then was seen in the slow throttle opening, as the engine became more fuel lean in the rapid throttle-opening event. There is no secondary breakthrough observable here in the fresh catalyst. The pre-catalyst curve shape and general magnitude is the same as observed for the slow transient, except for having the quicker jump to the higher NOx level. Also, when the engine is throttled down, the NOx drops due to the extra fuel lowering the temperature of the charge in the cylinder.

The temperature record for this event is shown in Figure 4.10, and no real differences are seen from this curve when compared to the slow throttle-opening event.

4.2.3.3: Multiple Steps Throttle Transients with the 4K Catalyst

The lambda traces for the multiple steps transient (Figure 4.11) show many interesting features. First, from the pre-catalyst lambda trace, it is observed that there is not always a lean spike when the throttle is rapidly opened. The lean spike magnitudes depend on the engine control computer detection of the air flow and the corresponding fuel metering. Since the step throttle activations were not synchronous with the reading of the air flow, the amount of fueling errors were statistical.

The hydrocarbon record shows two misfires (Figure 4.12), one on the first peak and the second on the third peak. As was the case with the fast transient, the 4K catalyst greatly lowers the magnitude of these peaks. Figure 4.13 shows the expanded view of the hydrocarbon trace. From this trace it may be seen that the hydrocarbon behavior show similar trends to the fast transients, with peaks during each of the throttle down events.

The NOx behavior (Figure 4.14) follow the same trends as seen in the rapid transient, with the NOx level increasing with the higher load, and then a sharp decrease in the level of NOx when the throttle-down event occurs. The catalyst handles the changing conditions well, showing no breakthrough for this case.

The temperature behavior for this case shows both temperature functions to be step functions, with the temperature of each time point building upon the temperature of the previous point. For the brick temperature, once the increase in catalytic activity shows up as increased temperature, the temperature stays elevated due to the heat capacities of the catalytic converter structure. This is translated into the mid-catalyst temperature as well.

4.3 TRANSIENTS WITH THE AGED CATALYSTS

The same depth of explanation will not be given for each of the plots in this section, as the same trends are seen for the 50 and 150K catalysts as observed with the 4K catalyst (Figures 4.16-4.29 show the results for the 50K catalyst, and Figures 4.30-4.43 the results for the 150K catalyst). Of note in this section are the increased levels of primary and secondary breakthrough for the NOx curves. Also of note on the 150K catalyst HC curves is how at the high flow rate experienced at WOT there are instances of some HC breakthrough. Even though the steady state tests did not show a significant

deterioration in HC conversion efficiency at stoichiometric, the deterioration of the catalyst caused some HC to break through at the high mass flow rate during the transient tests.

4.4 CONCLUSIONS FROM TRANSIENT TESTS

Drawing all of the observations together, some comments are to be made about the level of breakthrough. First, the HC breakthrough is not that significant during any of the transient events. The large HC breakthroughs occurred when there was a misfire; it is unreasonable to expect the catalyst to fully oxidize this large concentration of pollutant. The cause is best fixed by altering the engine control so the misfire does not happen. The NOx breakthroughs, on the other hand, were deemed significant enough to investigate further. The first one to be examined is the primary breakthrough. Using the MATLAB code in Appendix F and equation 4.1, all of the breakthroughs were converted to mass of NO. NO was chosen as the form of the oxide of nitrogen as NO_2 has historically been shown in spark ignition engines to occur in negligible quantities (see section 1.3.1). Looking at the primary peak breakthrough in the slow transient, Figure 4.44 shows the results that the 150K catalyst produced orders of magnitude greater breakthrough for this transient, but still a relatively small amount. Figure 4.45 shows that the 150K catalyst has more serious amounts of breakthrough, but this breakthrough does not occur at all in the 50K and 4K catalysts. The fast transients showed more primary breakthrough, as shown by Figure 4.46 (primary peak breakthrough) and Figure 4.47 (secondary peak breakthrough). The magnitude of the primary breakthrough of the fast transient is, however, on the same order as the breakthrough of the slow transients. This implies that the 150k catalysts cannot effectively handle transients of different rates without suffering breakthrough. The breakthrough numbers are more serious: if 14 of the secondary breakthrough events occur in a mile, then the car would already fail the Tier 2 emissions standards. The multiple steps transients show similar results (Figures 4.48 and 4.49). The plotted values are averaged over 4 cycles. The large spread of the step transients is due to the fact that breakthrough did not occur in each of the steps. The secondary peaks of the step transients are lower because part of the secondary peak is cut off when the

throttle position step function is followed. All of the values in tabular form may be found in Appendix G.

As for the cause of the breakthroughs, the large lean spike that makes the NOx very difficult to reduce causes the primary peak NOx breakthrough, but the conversion efficiency is still highly dependant on the catalyst age. As found in Chapter 3, the NOx efficiency decreases by ~50% between the 4K and the 150K catalyst. This explains the increasing amount of primary NOx breakthrough as the catalyst becomes older. The secondary breakthrough cause is not as obvious, as it appears to disappear after a period of ~20 seconds at WOT. However, looking at an extremely enlarged view of the UEGO traces for the 150K catalyst, it may be seen that during the period when the secondary peak occurs, the post-catalyst UEGO trace seems become "less rich", and then returns to the same level as previously (see Figure 4.50). These results suggest that the NO secondary breakthrough may be due to a deficiency of CO in the catalyst.

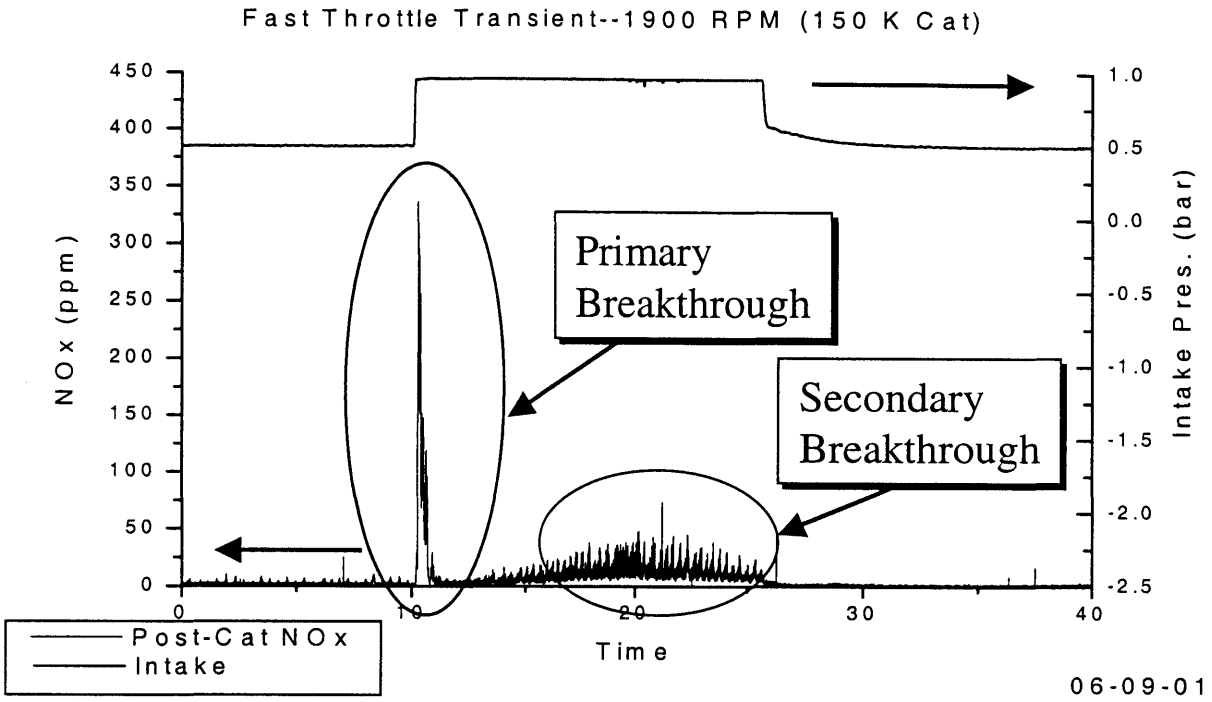

Figure 4.1: Definition of Some Chapter 4 Terminology

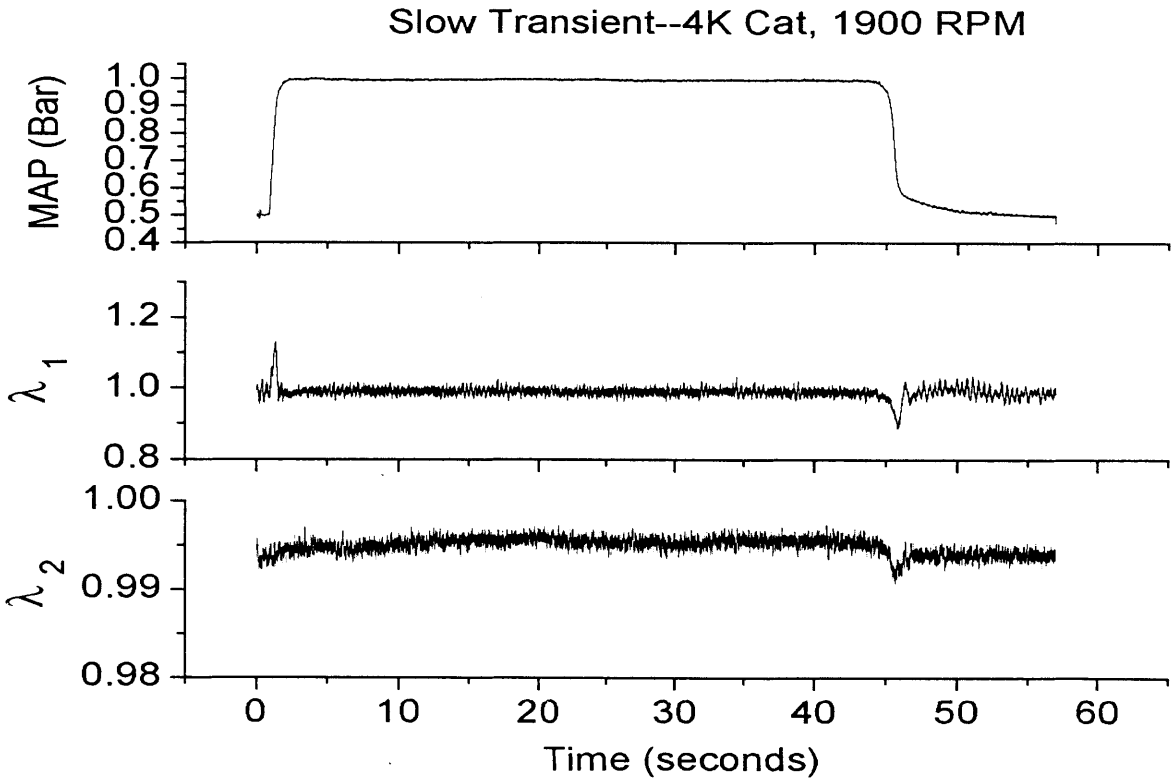

Figure 4.2: Slow Transient Pre- and Post-Catalyst (4K) λ

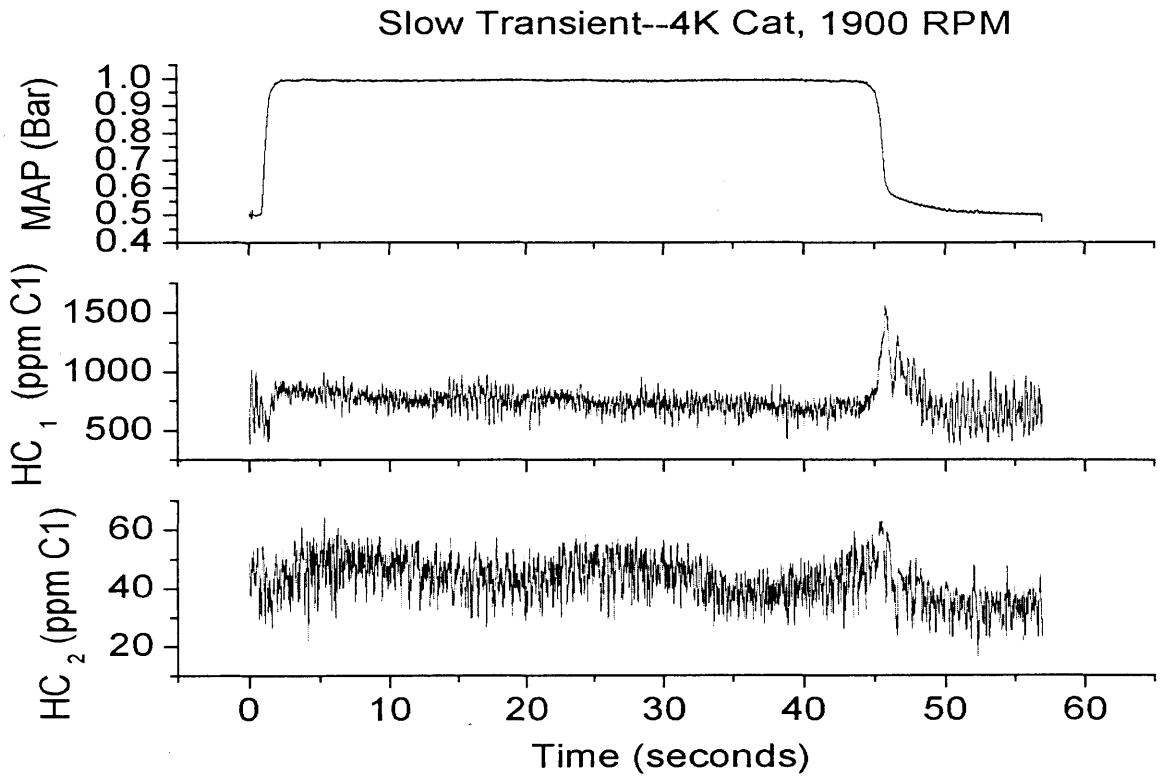

Figure 4.3: Slow Transient Pre- and Post Catalyst (4K) HC

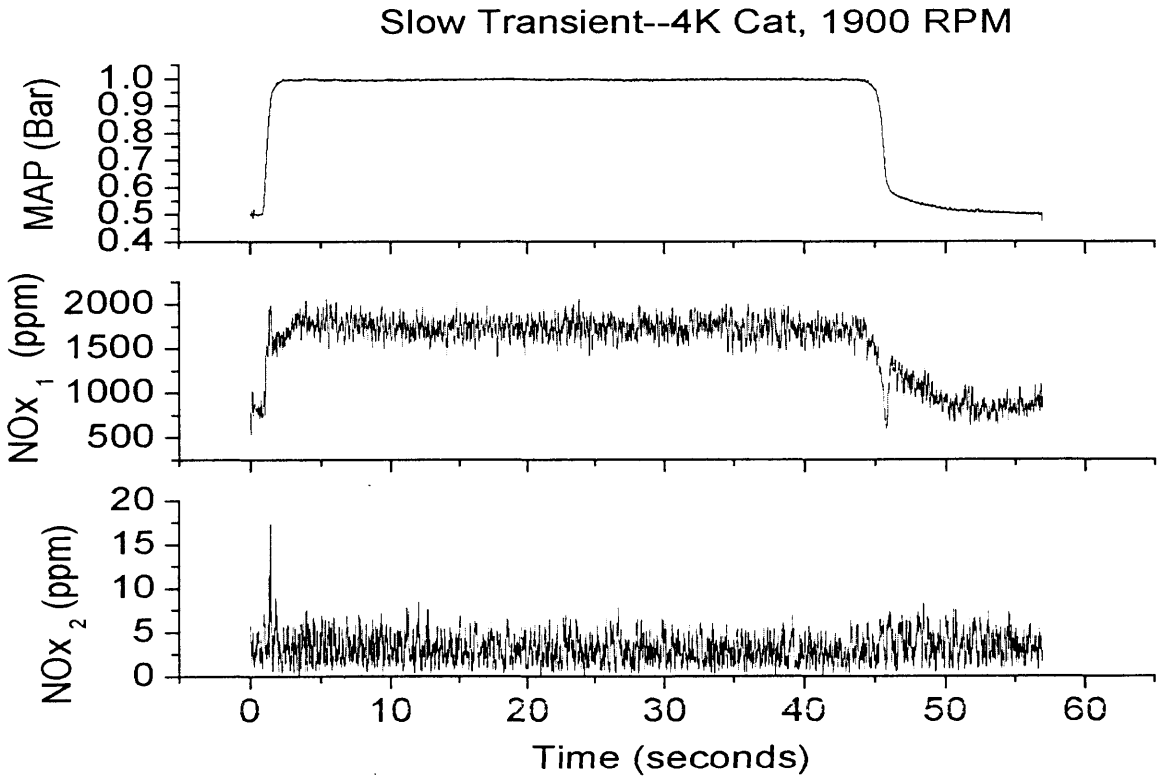

Figure 4.4: Slow Transient Pre- and Post Catalyst (4K) NOx

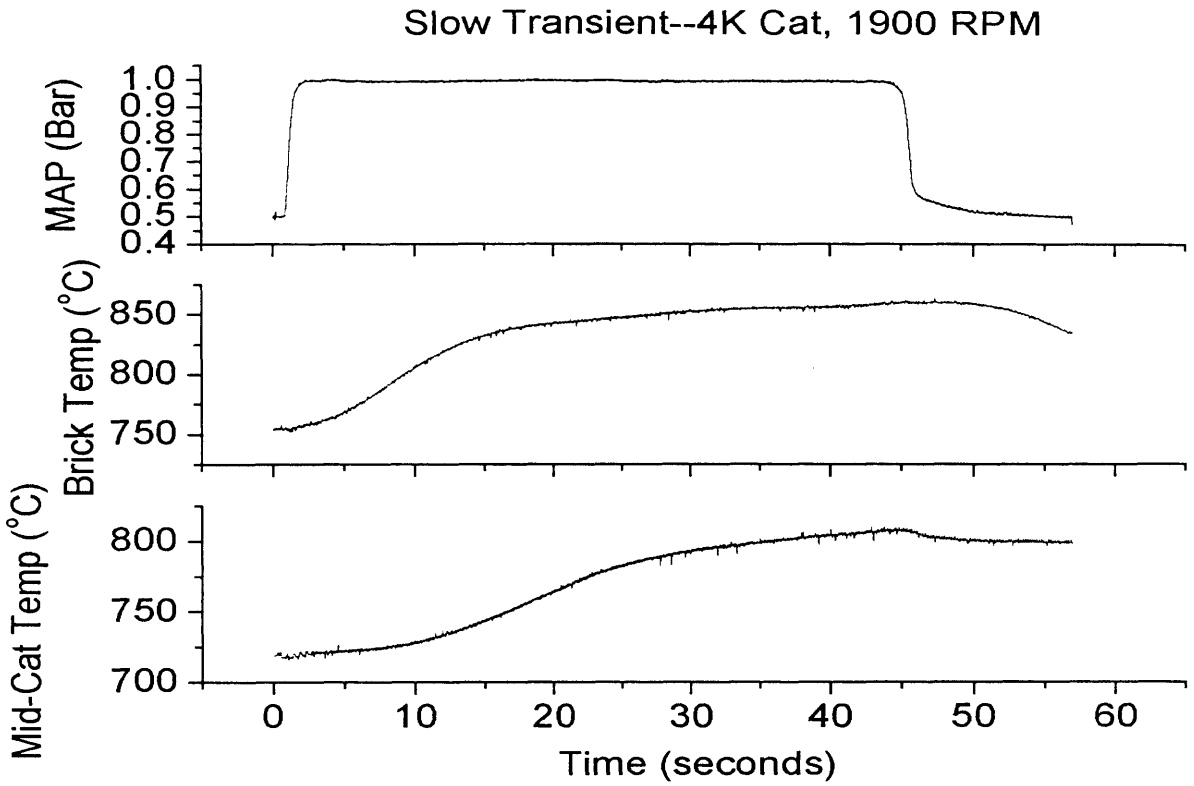

Figure 4.5: Slow Transient Catalyst Brick and Mid-Catalyst (4K) Temperature

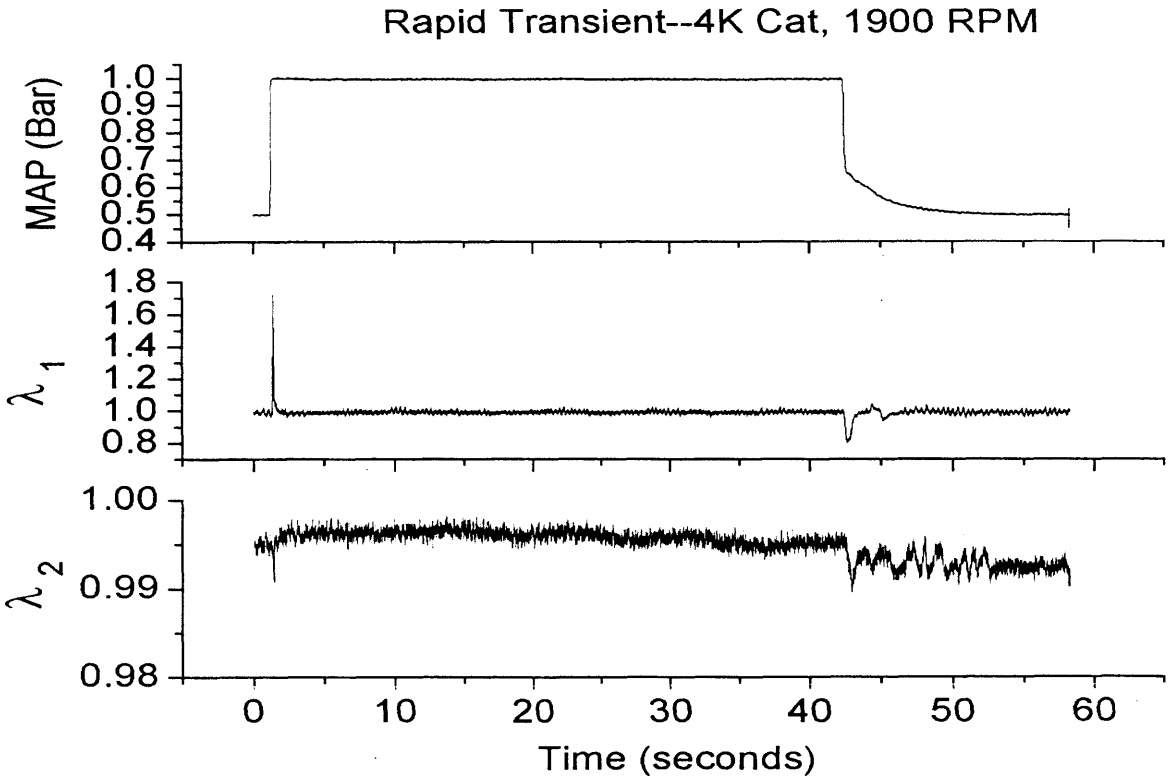

Figure 4.6: Fast Transient Pre- and Post-catalyst (4K) λ

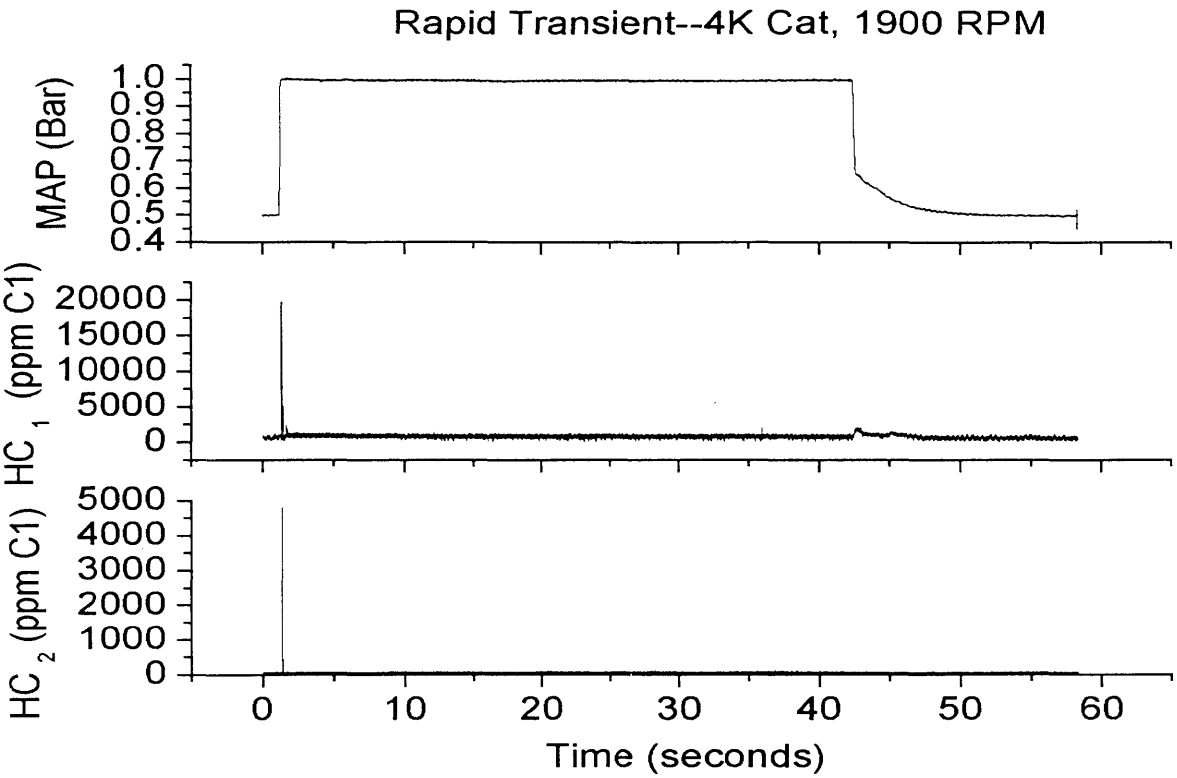

Figure 4.7: Fast Transient Pre and Post-Catalyst (4K) HC

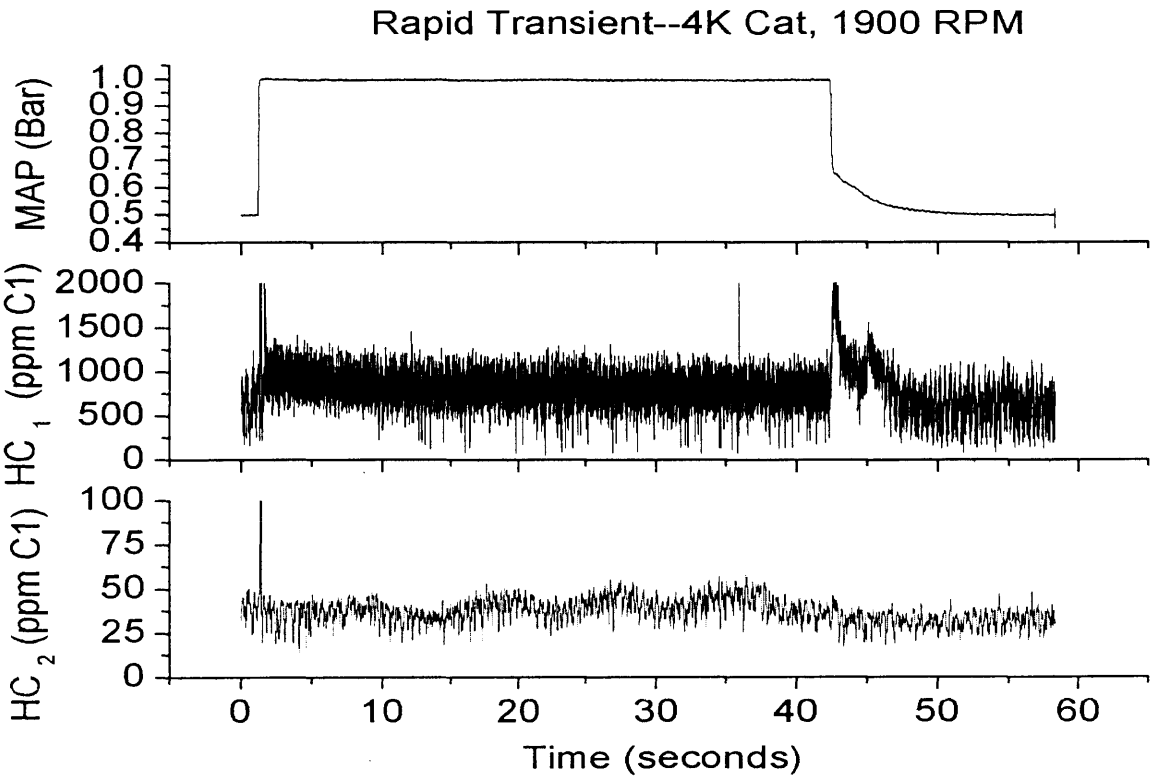

Figure 4.8: Fast Transient Expanded Pre and Post-Catalyst (4K) HC

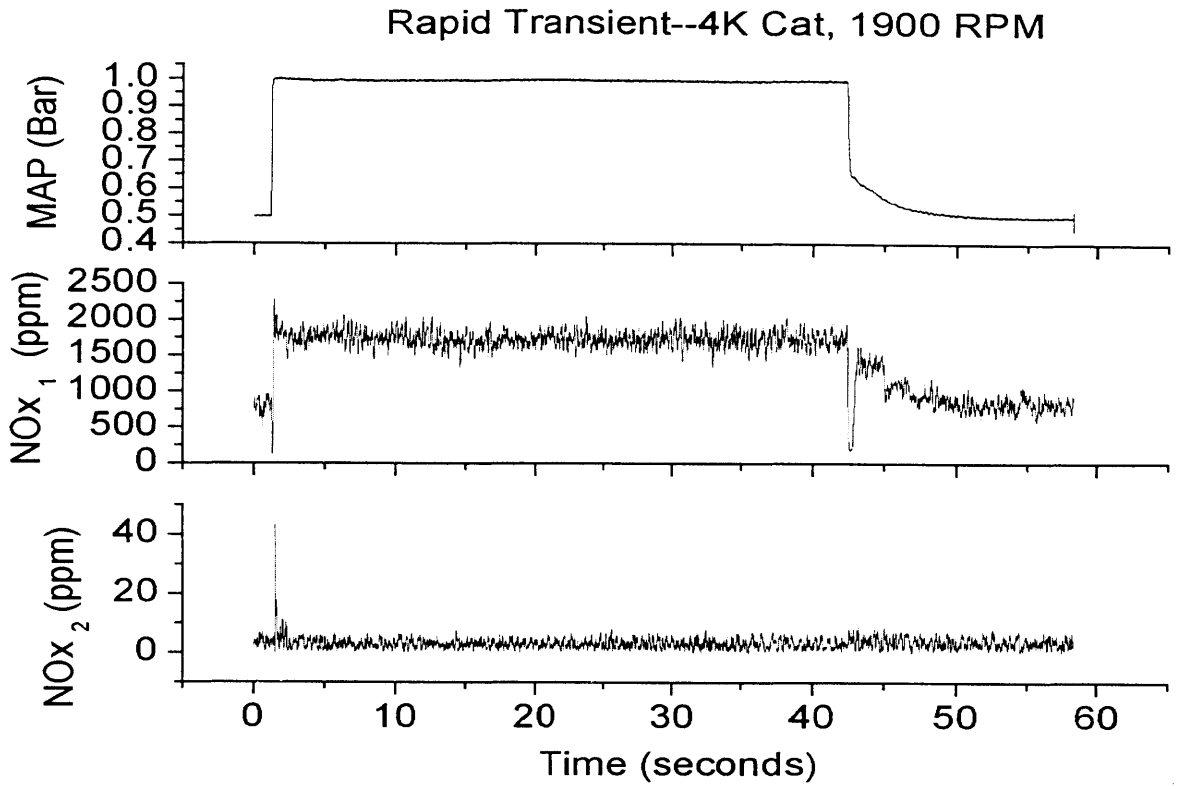

Figure 4.9: Fast Transient Pre and Post-Catalyst (4K) NOx

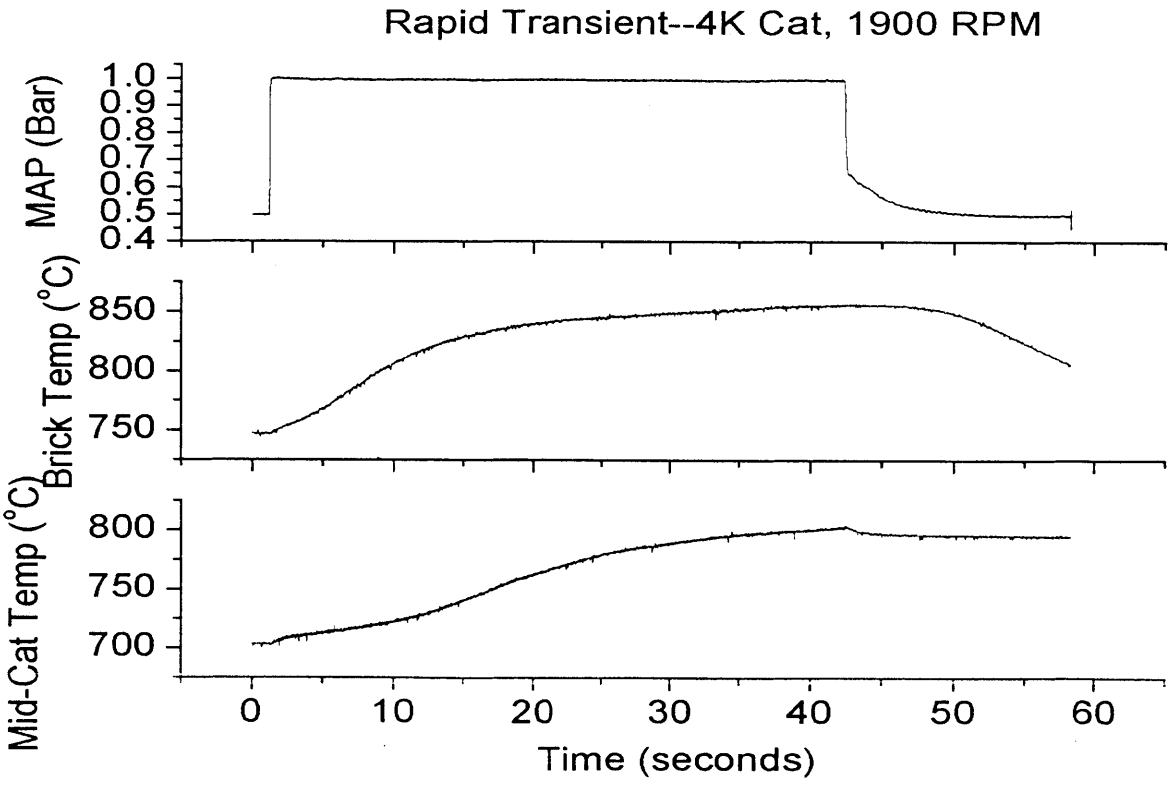

Figure 4.10: Fast Transient Catalyst Brick and Mid-Catalyst (4K) Temperature

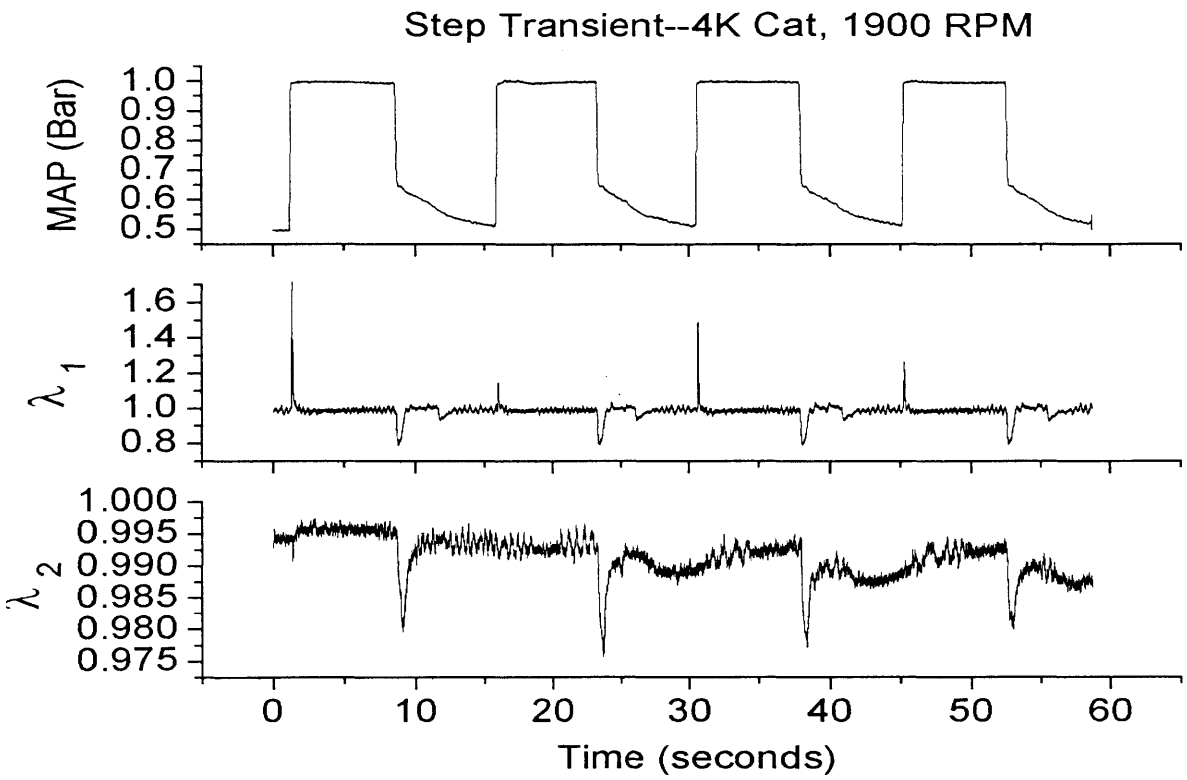

Figure 4.11: Multiple Steps Transient Pre and Post-Catalyst (4K) λ

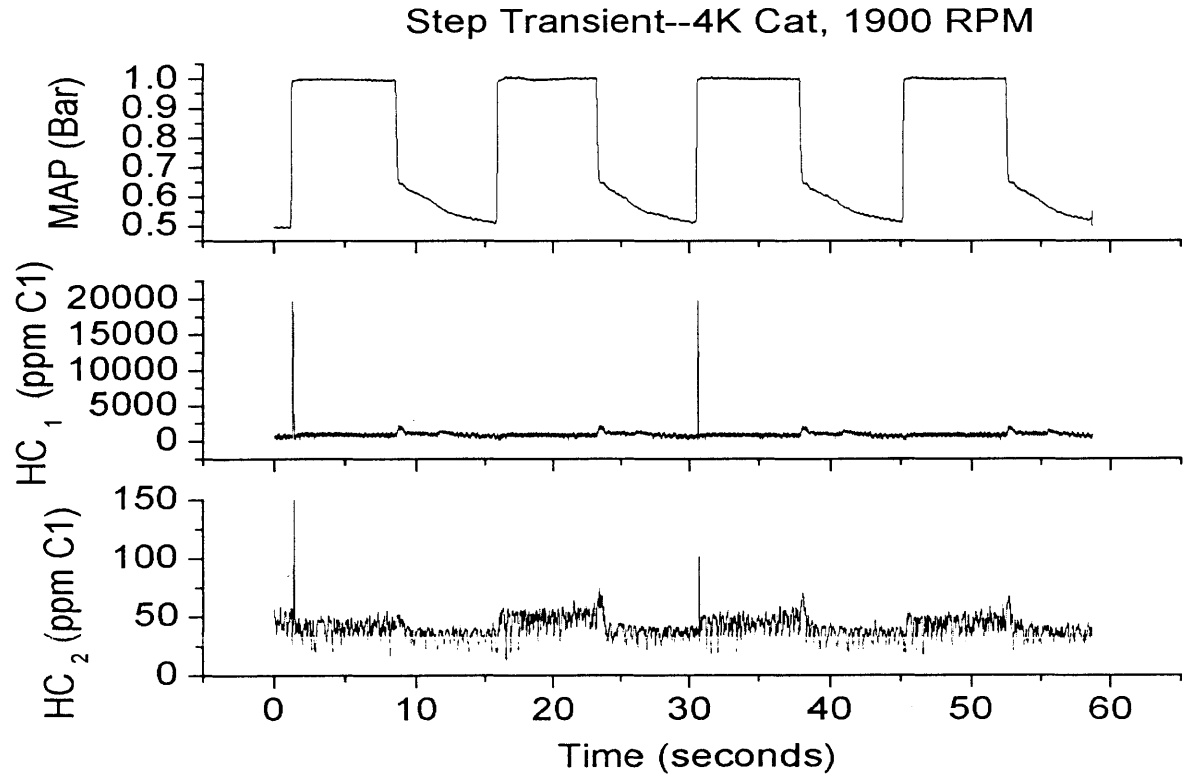

Figure 4.12: Multiple Steps Transient Pre and Post-Catalyst (4K) HC

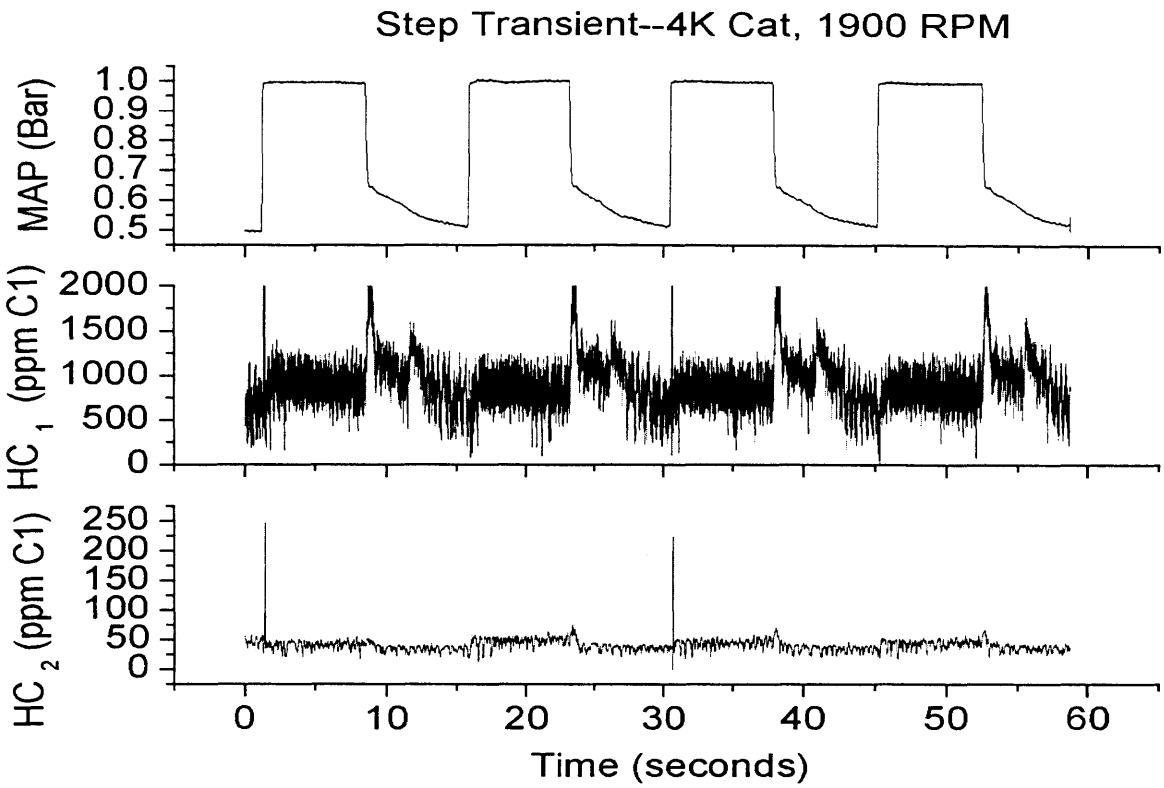

Figure 4.13: Multiple Steps Transient Expanded Pre and Post-Catalyst (4K) HC

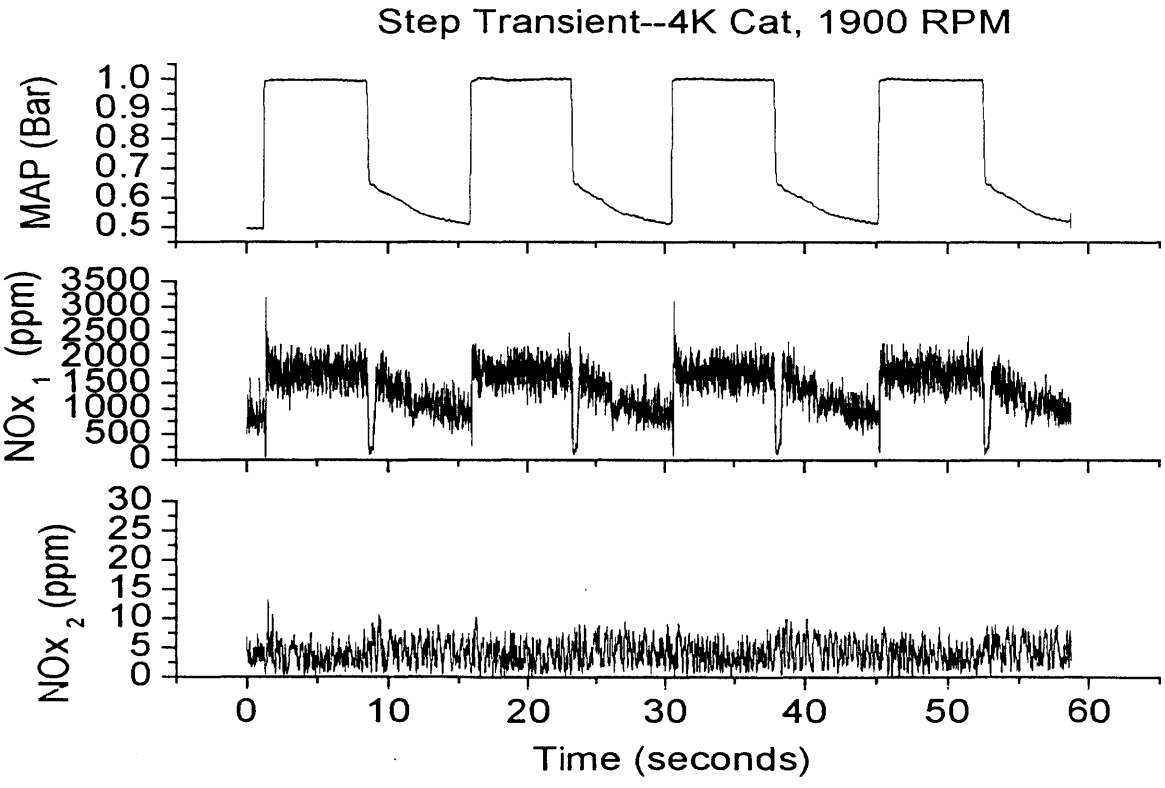

Figure 4.14: Multiple Steps Transient Pre and Post-Catalyst (4K) NOx

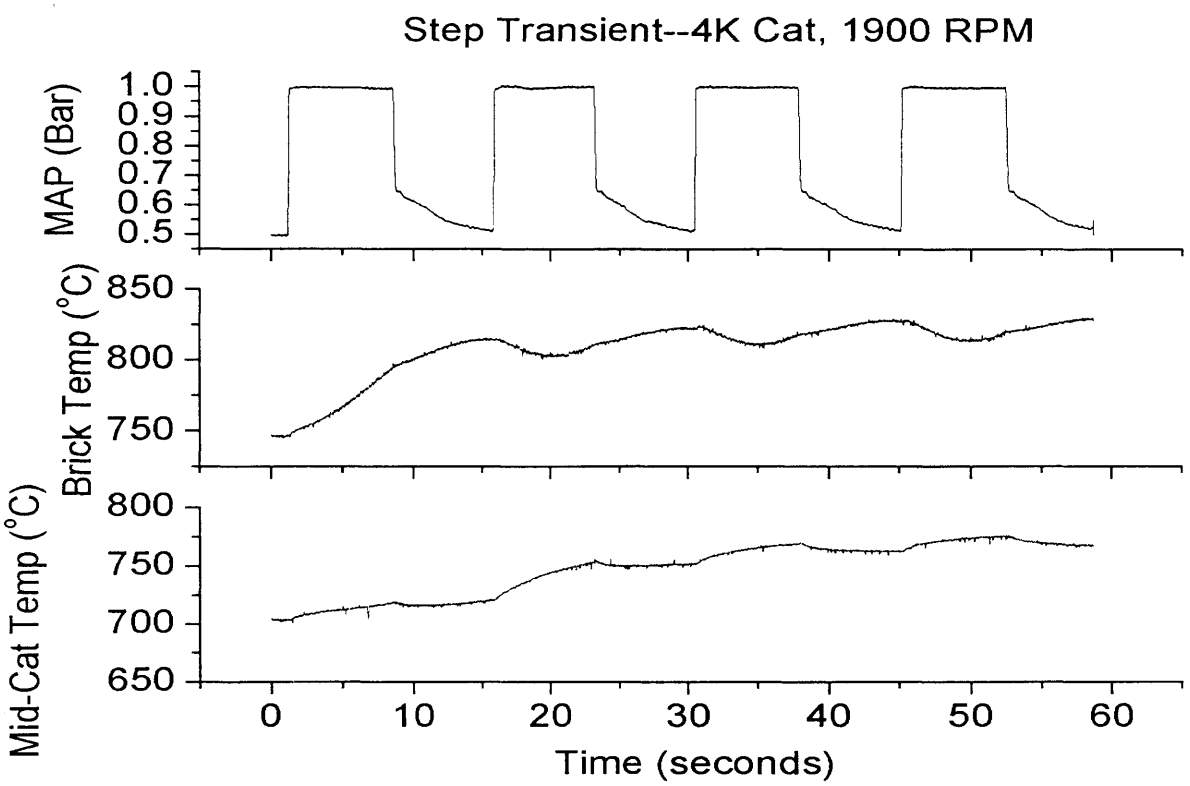

Figure 4.15: Multiple Steps Transient Catalyst Brick and Mid-Catalyst (4K) Temperature

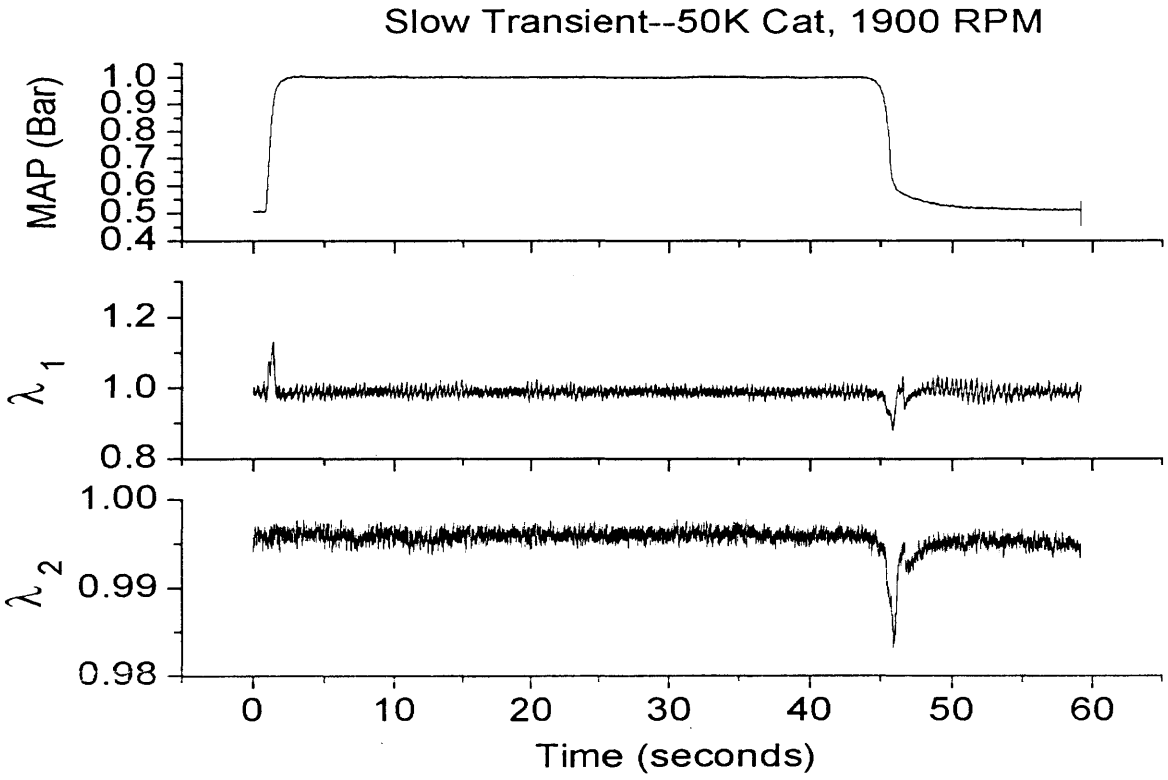

Figure 4.16: Step Transient Pre and Post-Catalyst (50K) λ

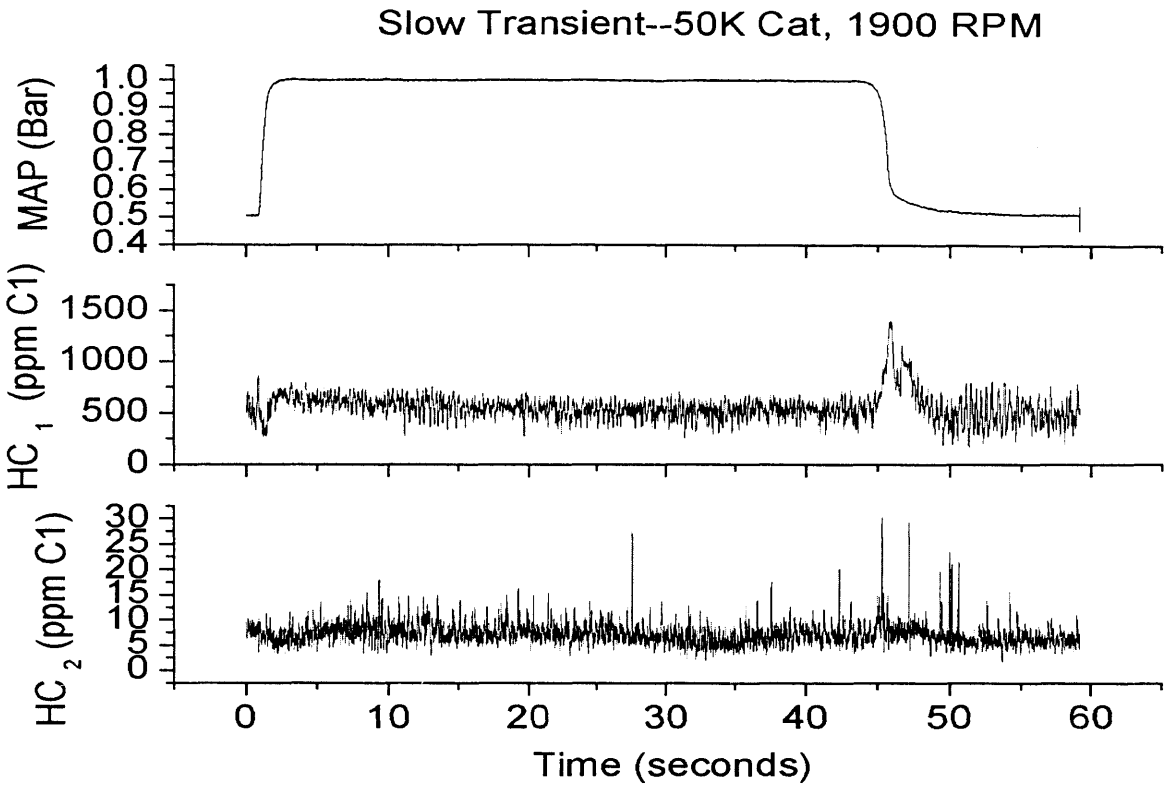

Figure 4.17: Slow Transient Pre and Post-Catalyst (50K) HC

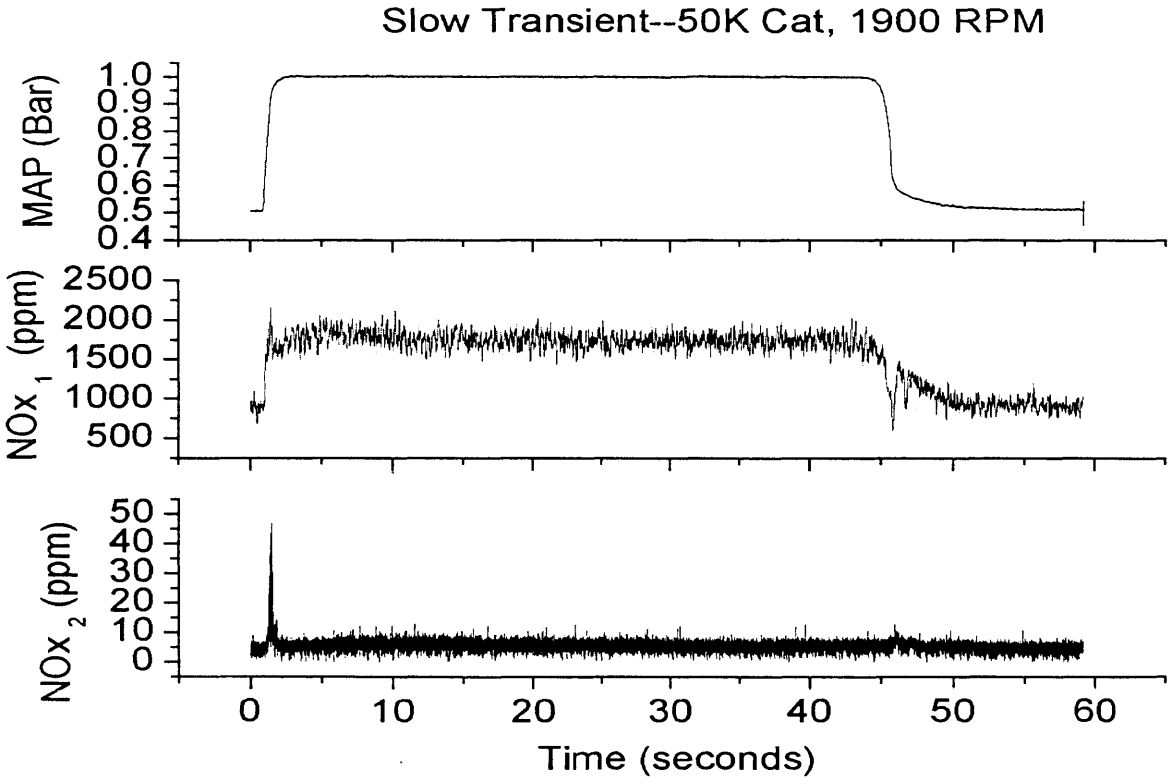

Figure 4.18: Slow Transient Pre and Post-Catalyst (50K) NOx

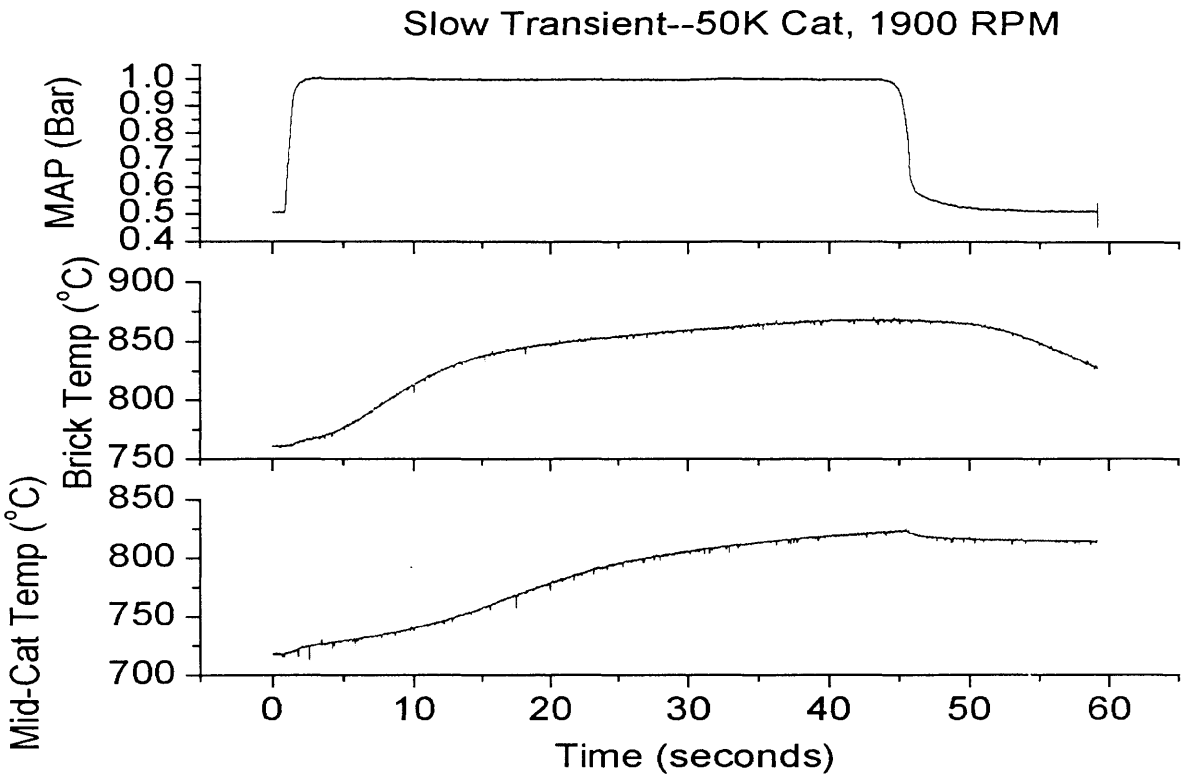

Figure 4.19: Slow Transient Catalyst Brick and Mid-Catalyst (50K) Temperature

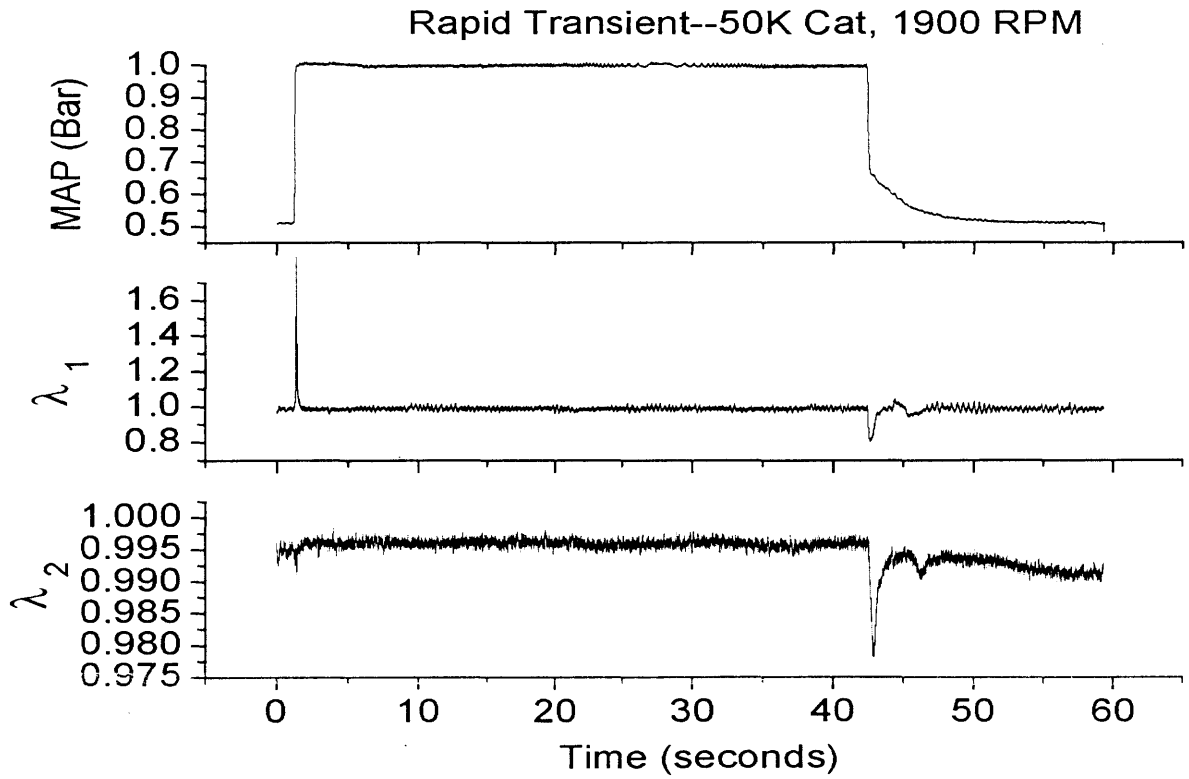

Figure 4.20: Slow Transient Pre and Post-Catalyst (50K) λ

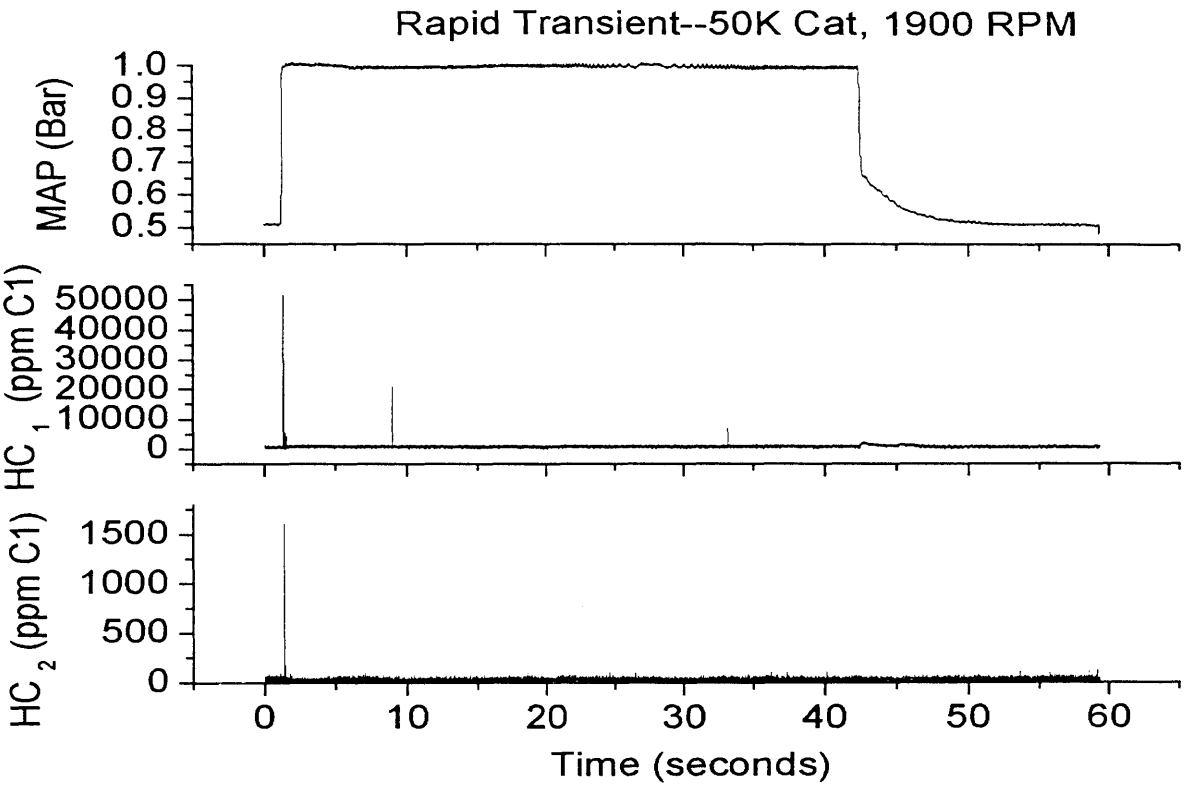

Figure 4.21: Fast Transient Pre and Post-Catalyst (50K) HC

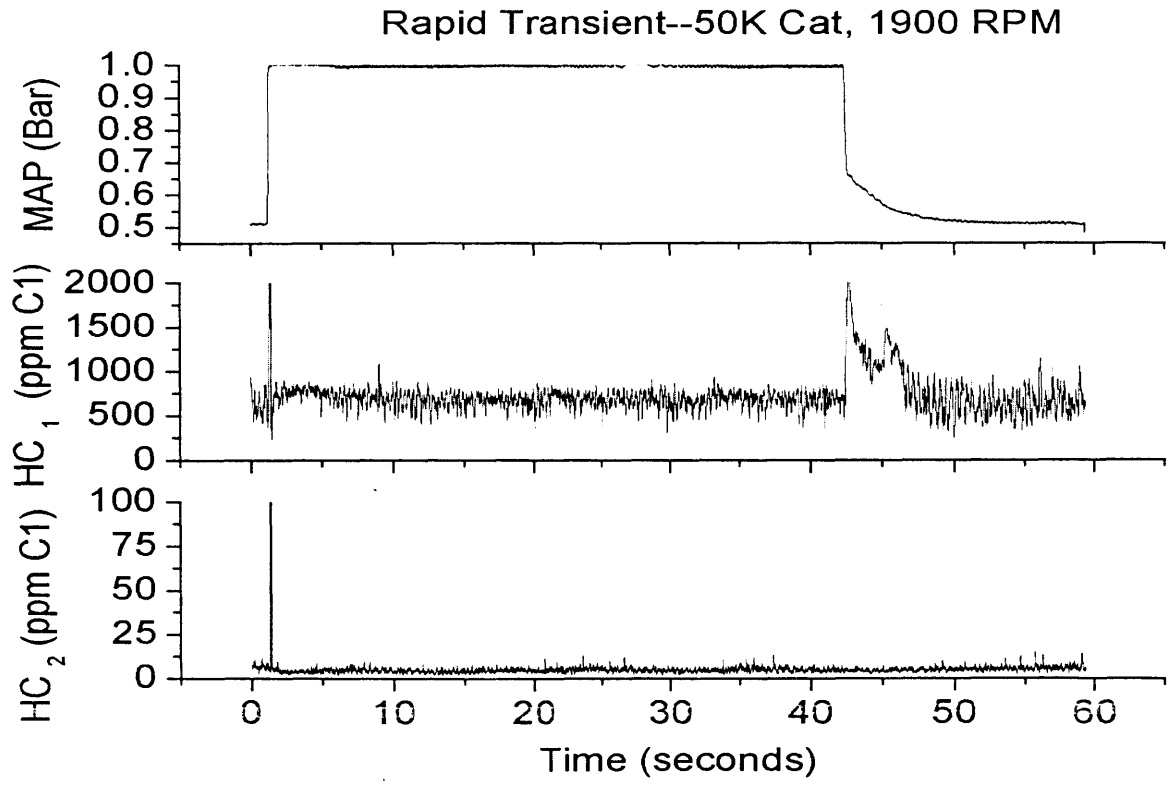

Figure 4.22: Fast Transient Expanded Pre and Post-Catalyst (50K) HC

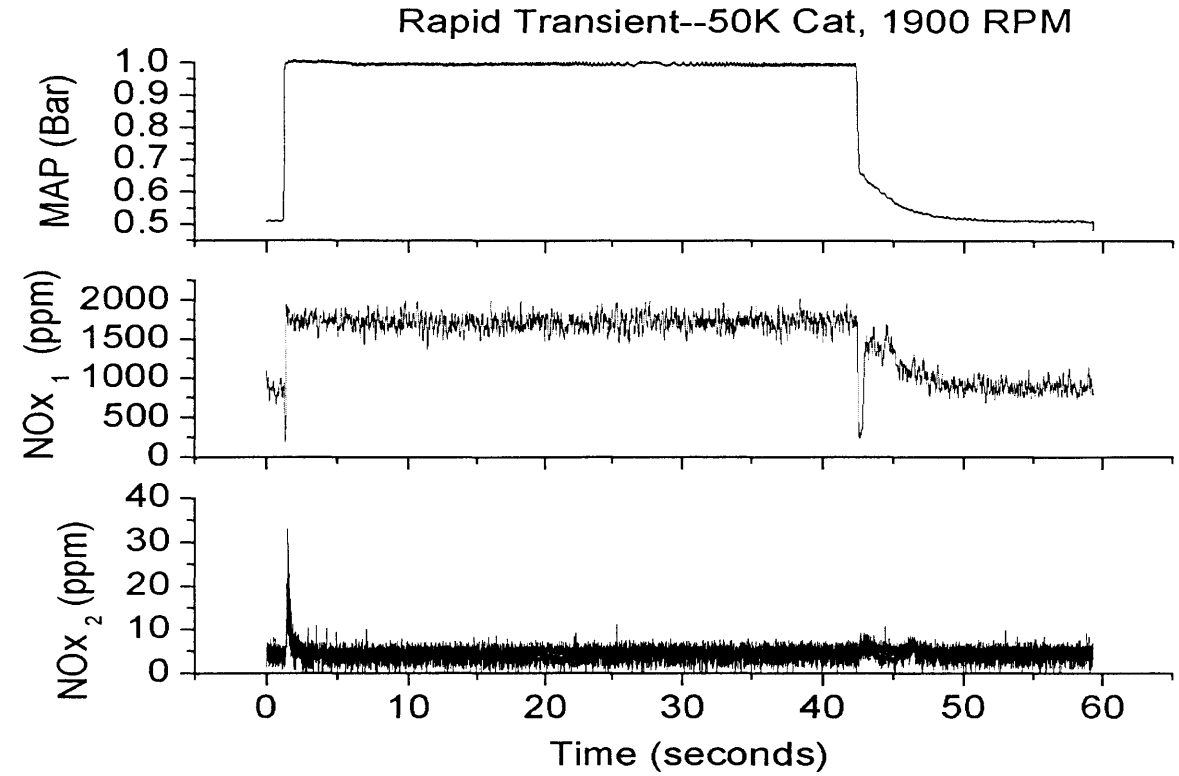

Figure 4.23: Fast Transient Pre and Post-Catalyst (50K) NOx

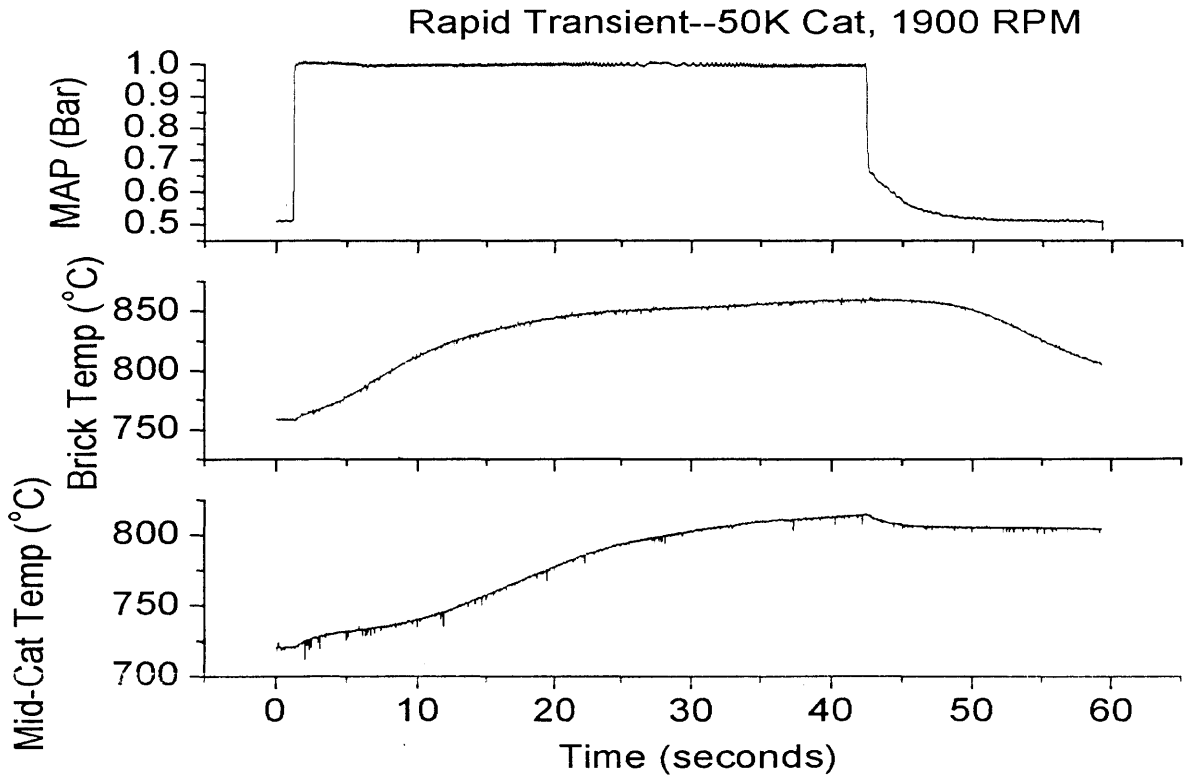

Figure 4.24: Fast Transient Catalyst Brick and Mid-Catalyst (50K) Temperature

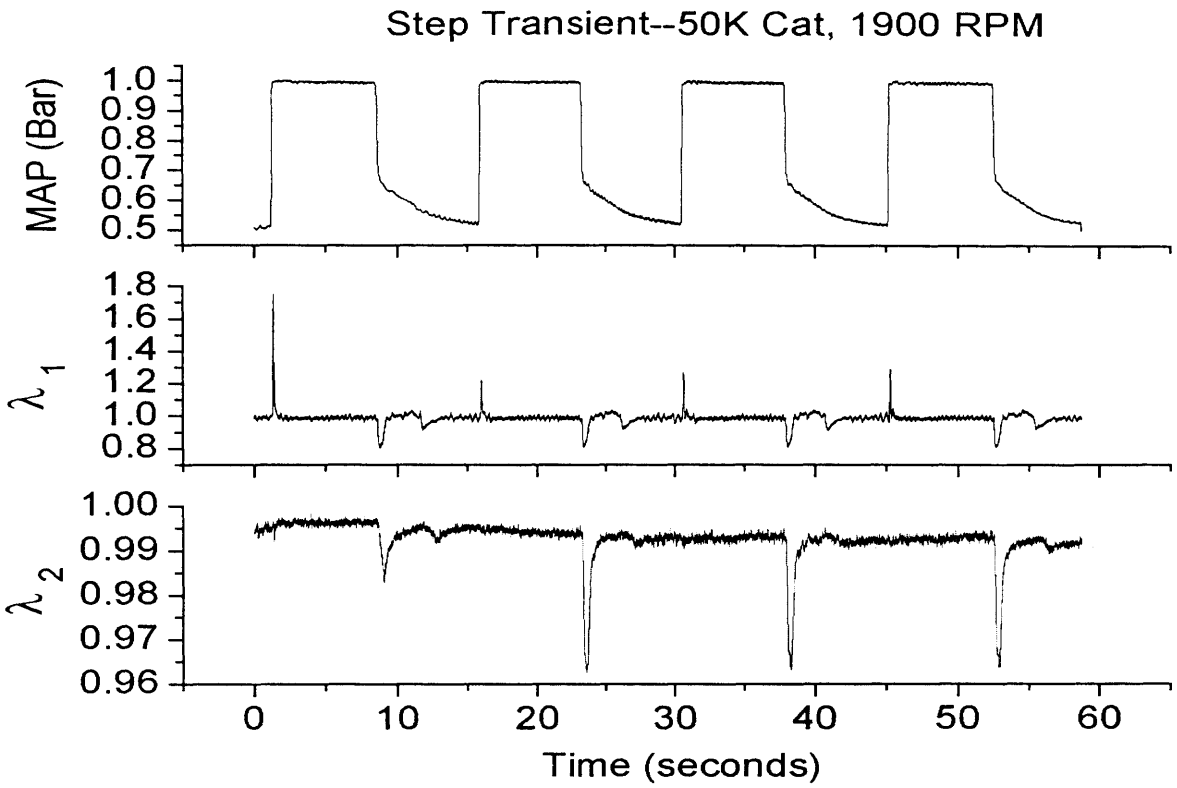

Figure 4.25: Multiple Steps Transient Pre and Post-Catalyst (50K) λ

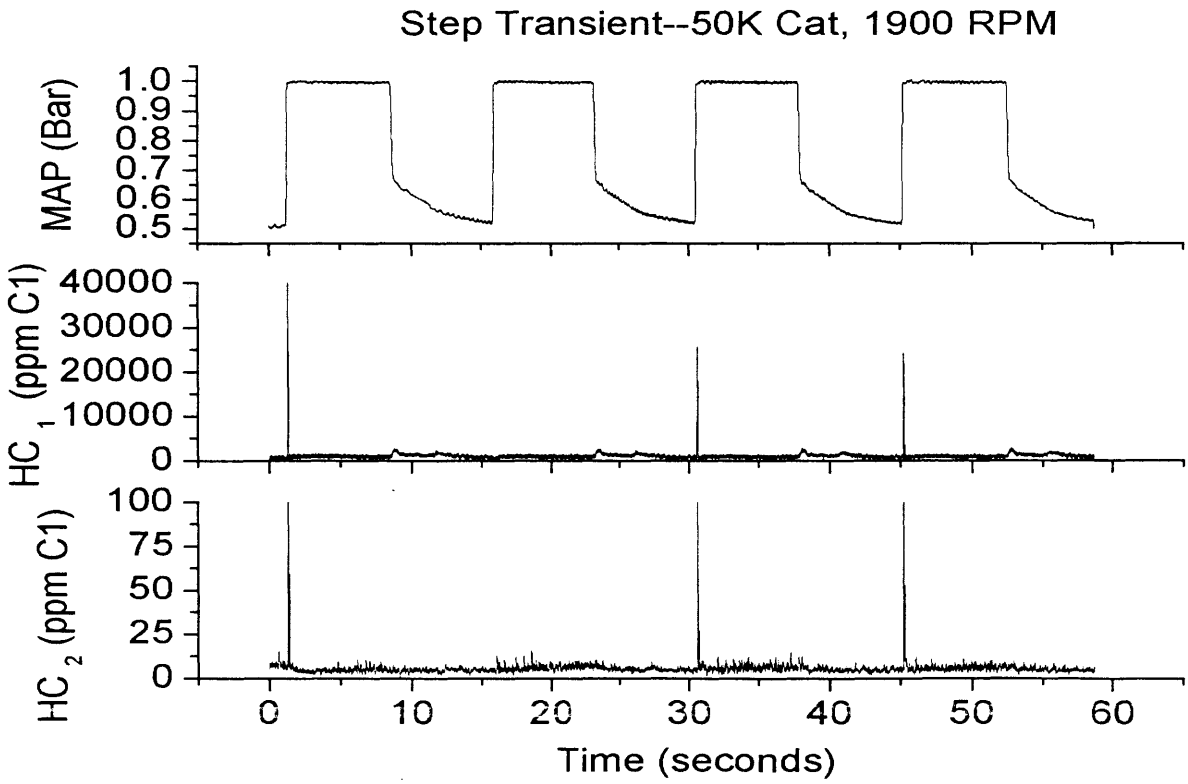

Figure 4.26: Multiple Steps Transient Pre and Post-Catalyst (50K) HC

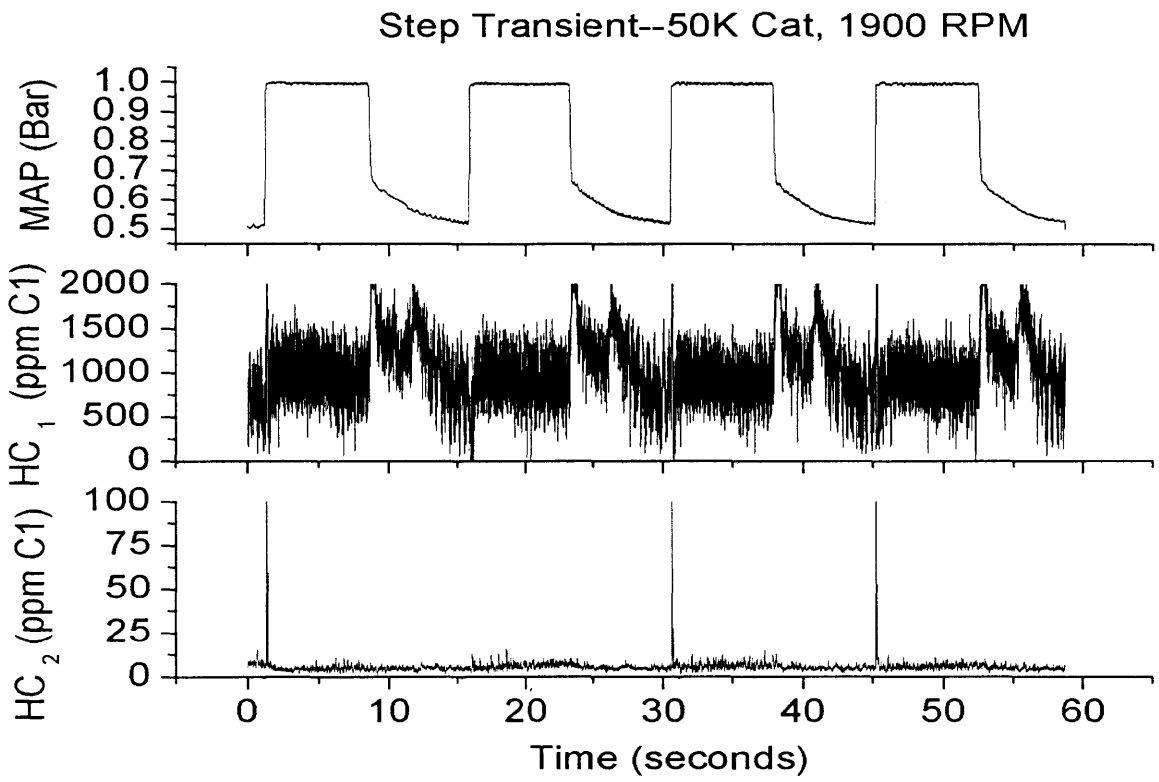

Figure 4.27: Multiple Steps Transient Expanded Pre and Post-Catalyst (50K) HC

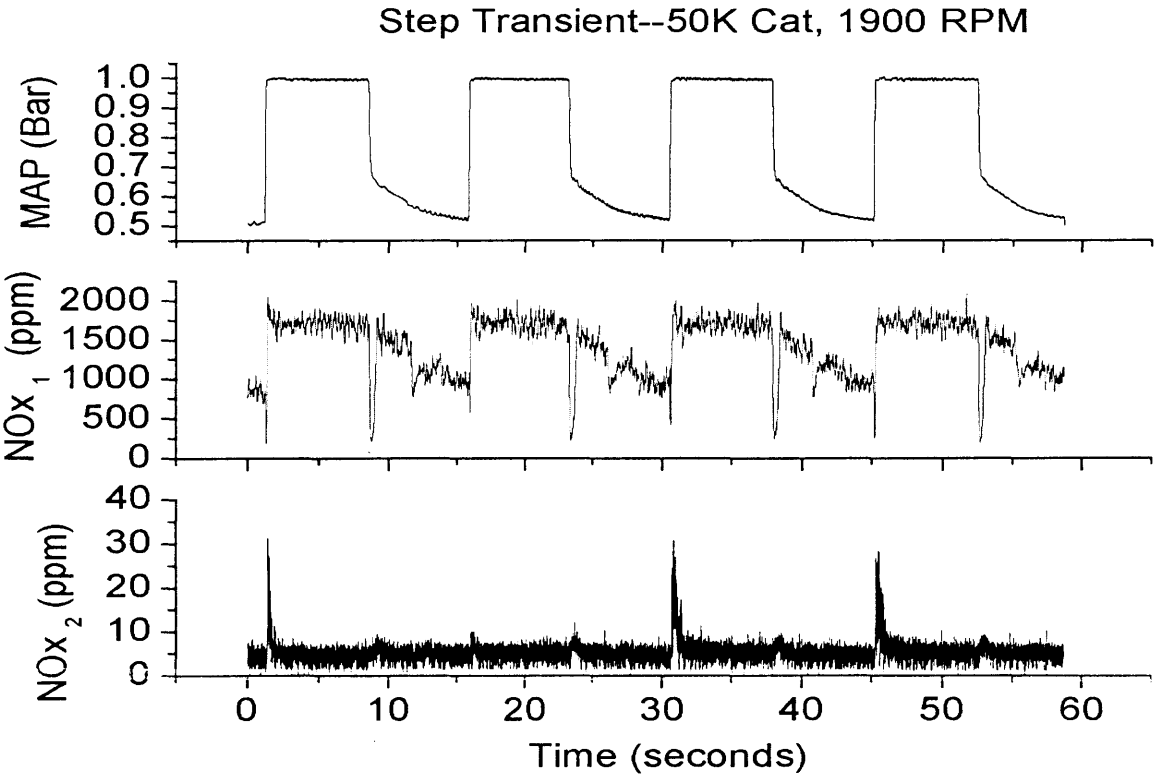

Figure 4.28: Multiple Steps Transient Pre and Post-Catalyst (50K) NOx

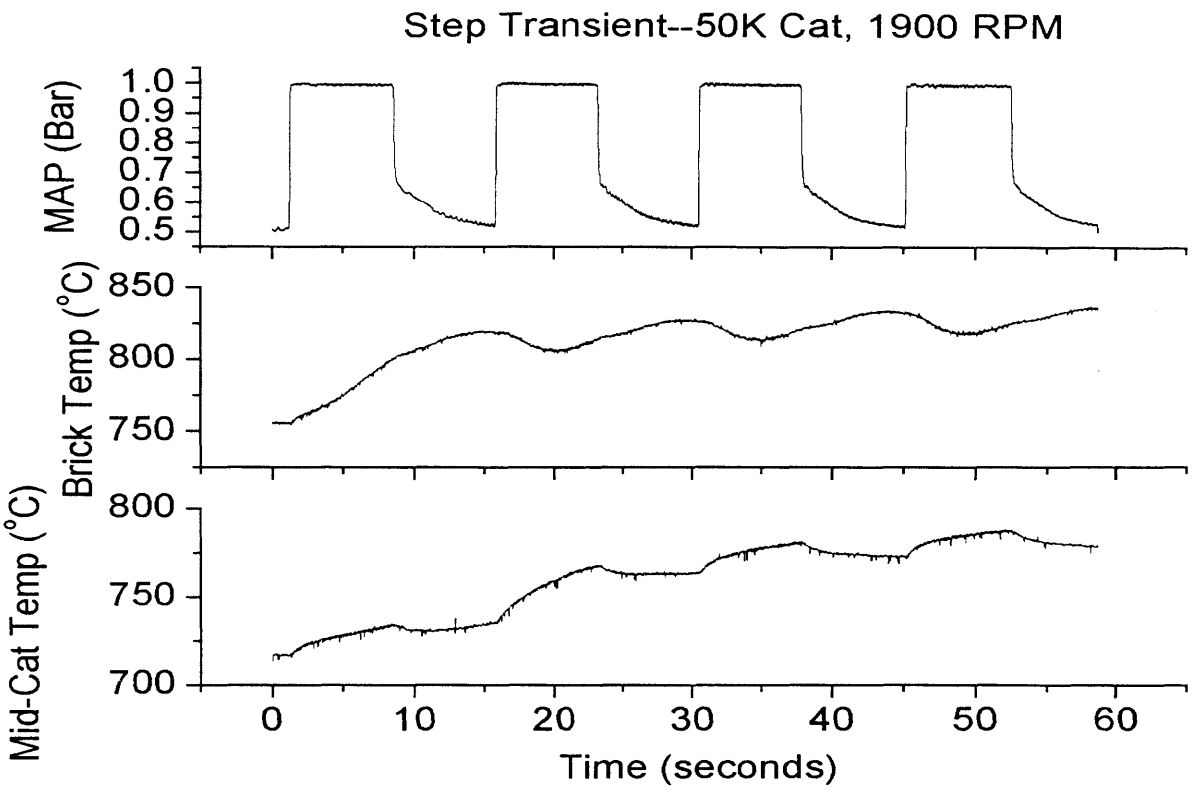

Figure 4.29: Multiple Steps Transient Catalyst Brick and Mid-Catalyst (50K) Temperature

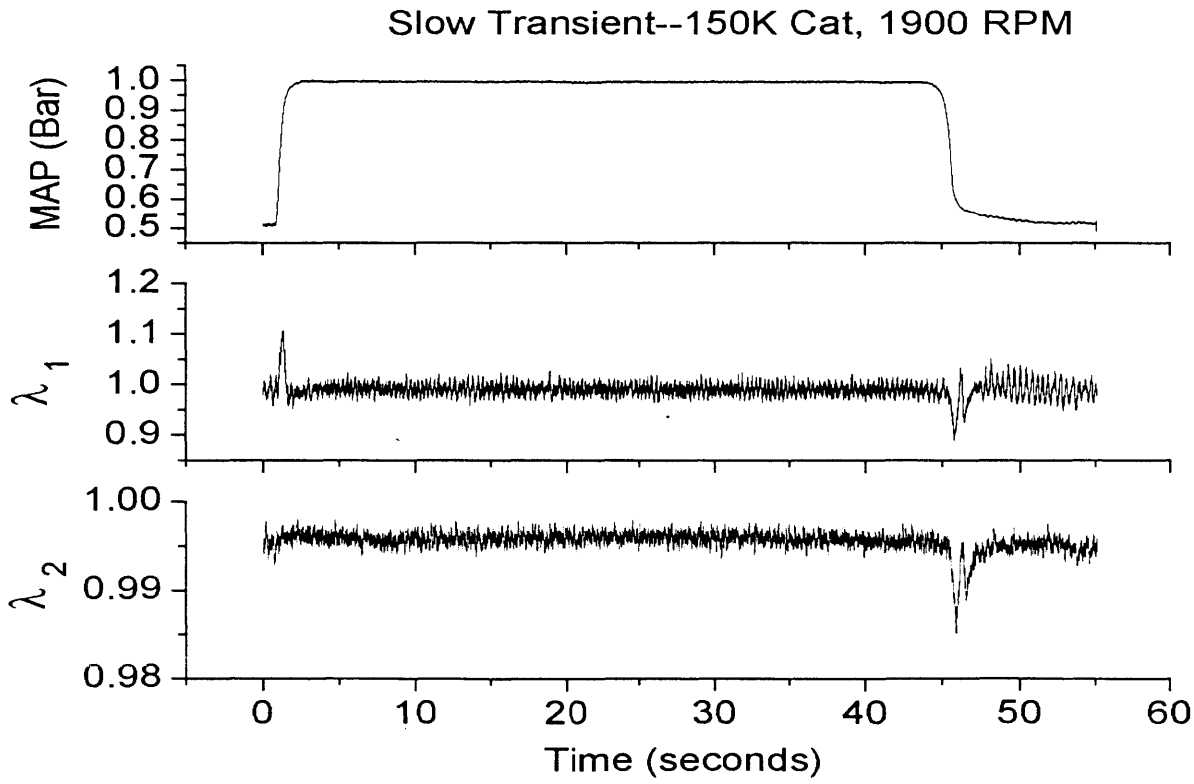

Figure 4.30: Slow Transient Pre and Post-Catalyst (150K) λ

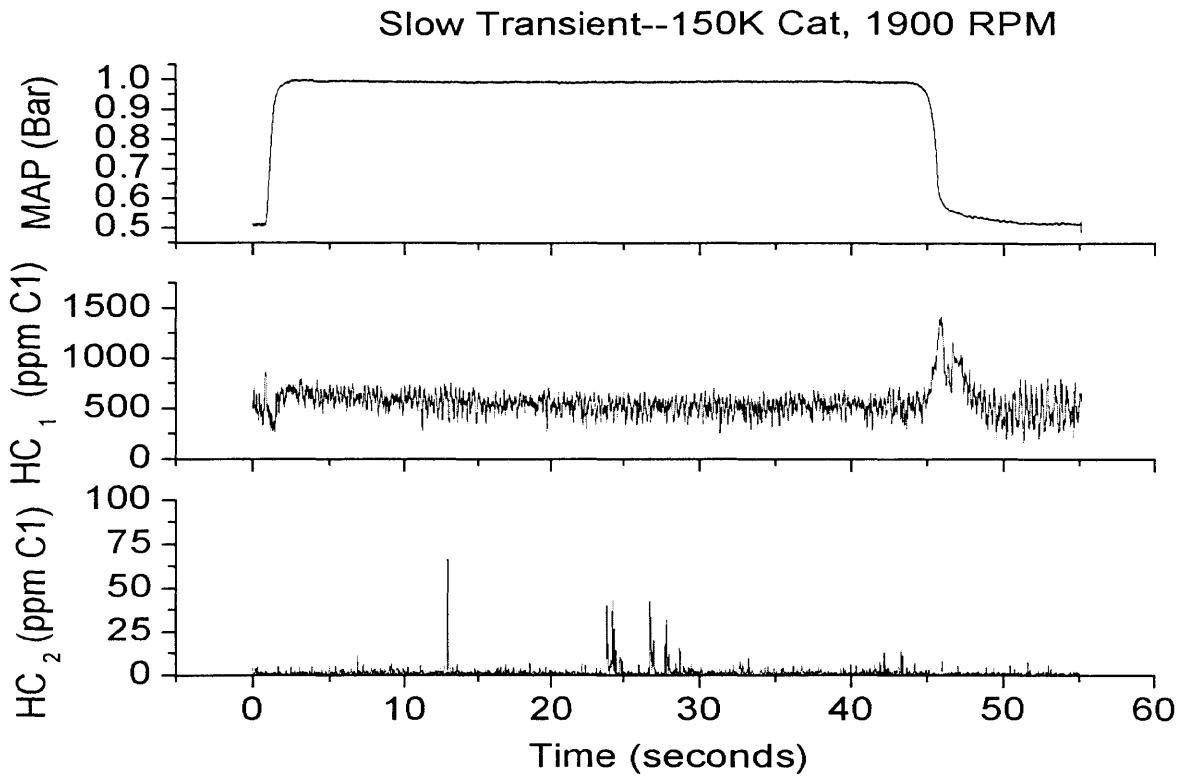

Figure 4.31: Slow Transient Pre and Post-Catalyst (150K) HC

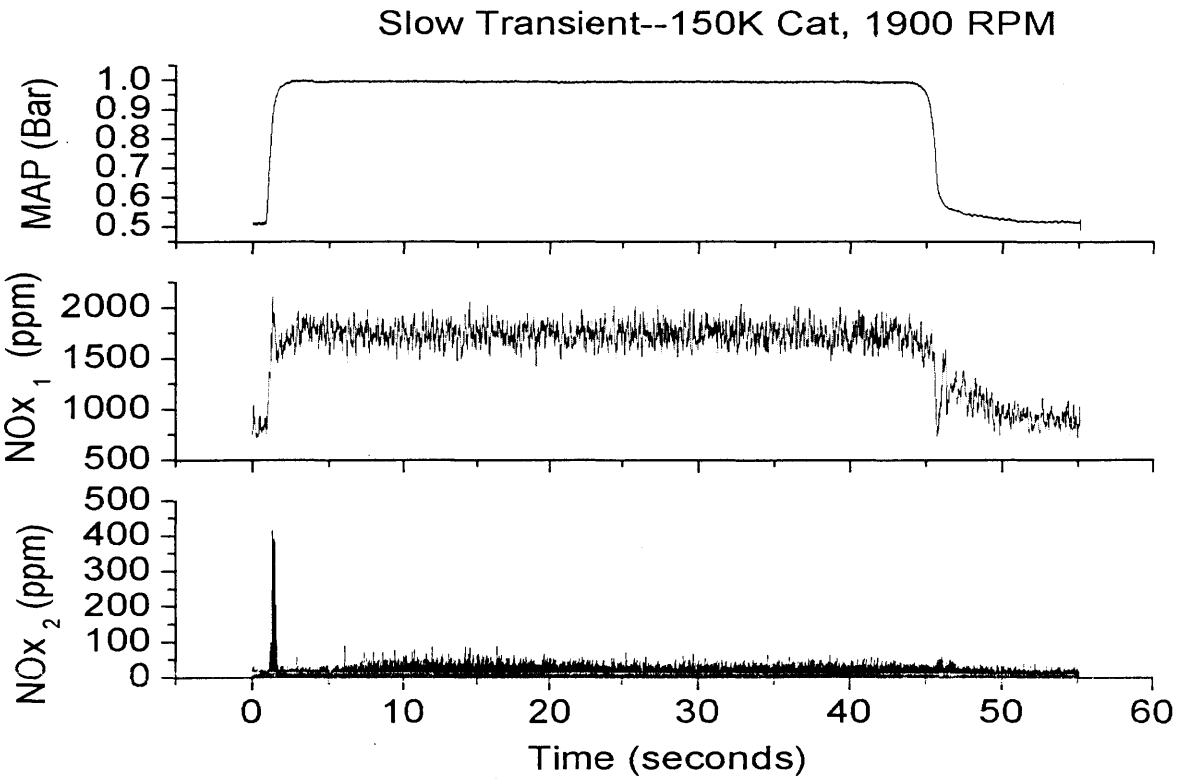

Figure 4.32: Slow Transient Pre and Post-Catalyst (150K) NOx

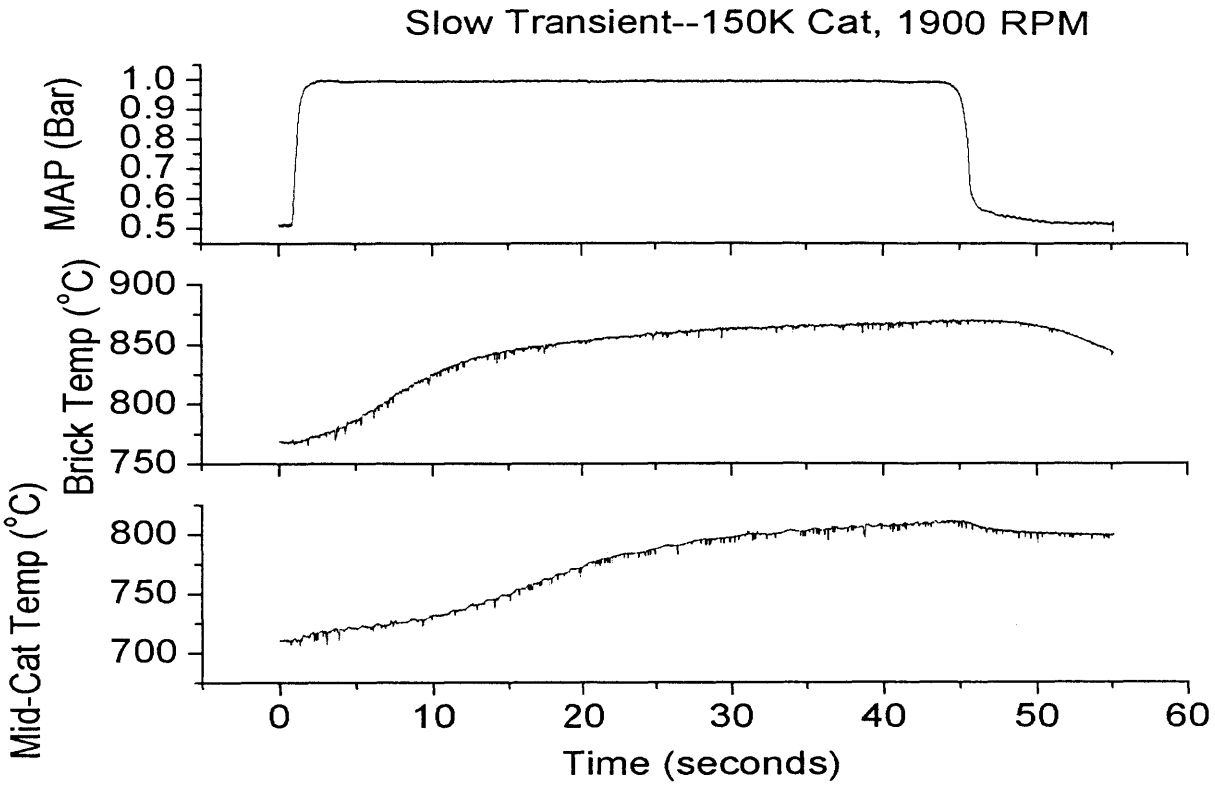

Figure 4.33: Slow Transient Catalyst Brick and Mid-Catalyst (150K) Temperature

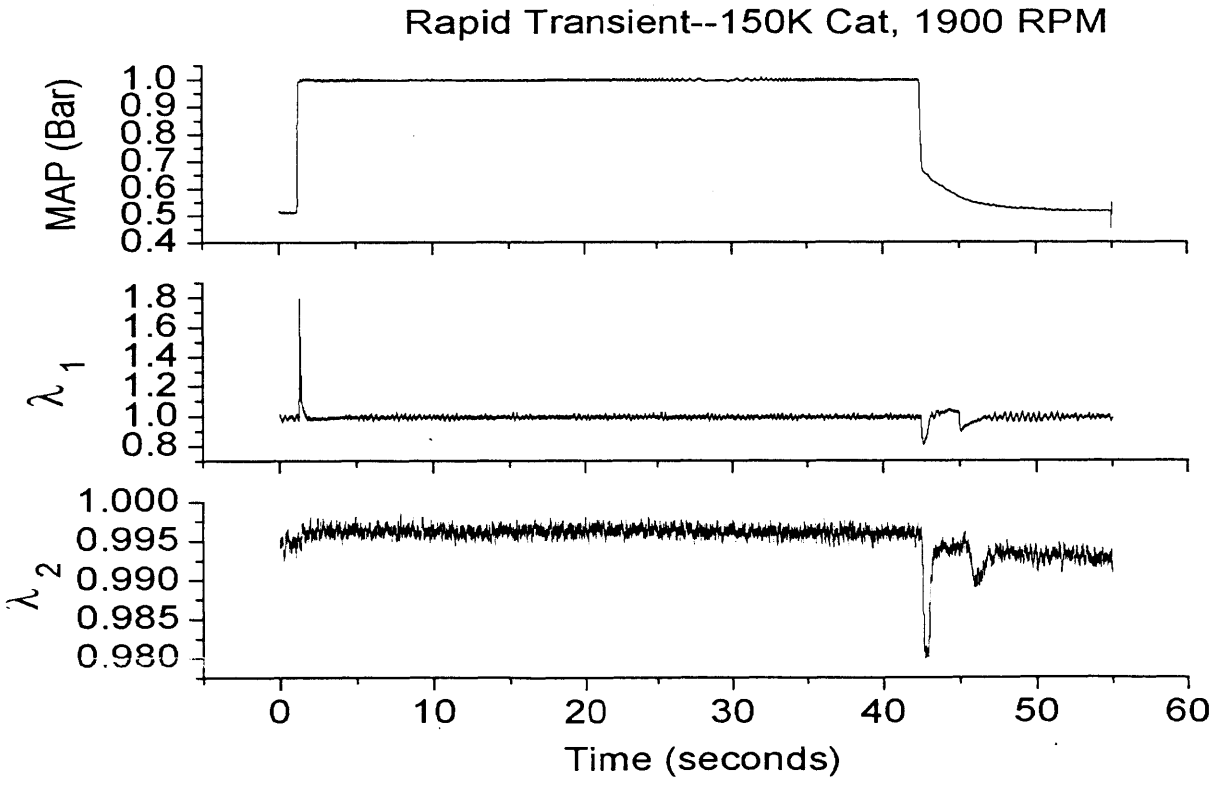

Figure 4.34: Fast Transient Pre and Post-Catalyst (150K) λ

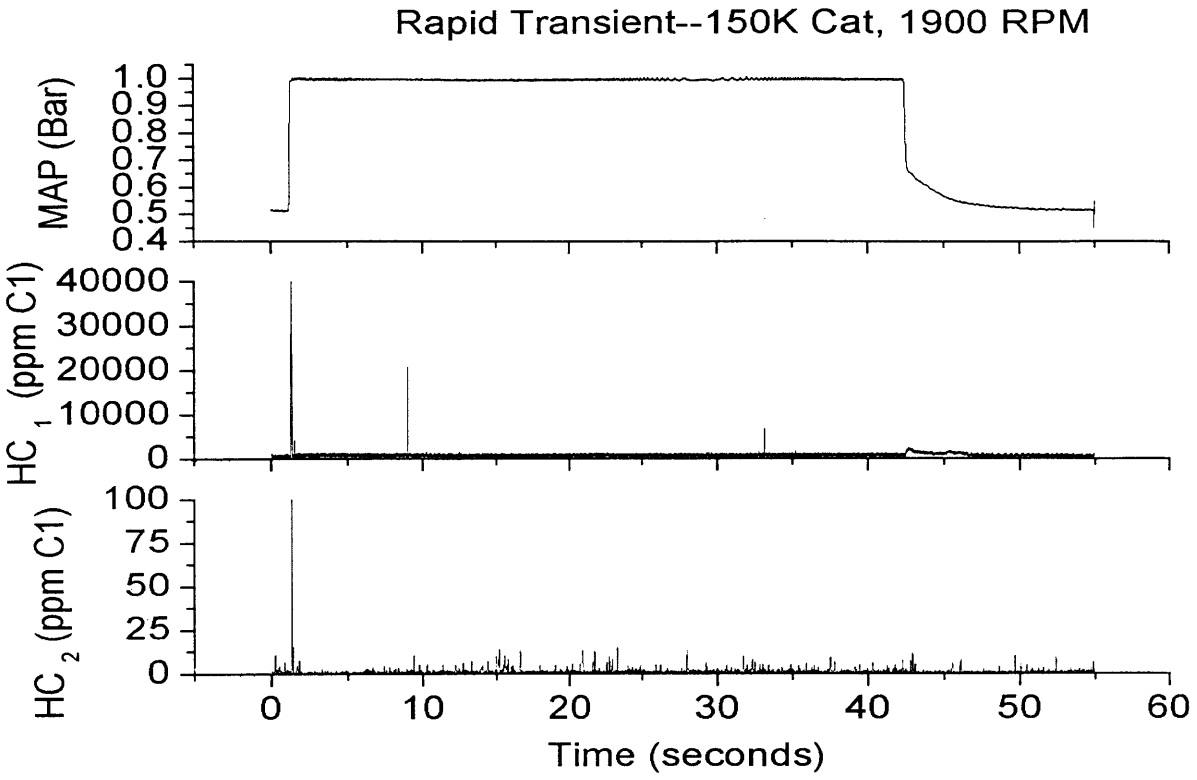

Figure 4.35: Fast Transient Pre and Post-Catalyst (150K) HC

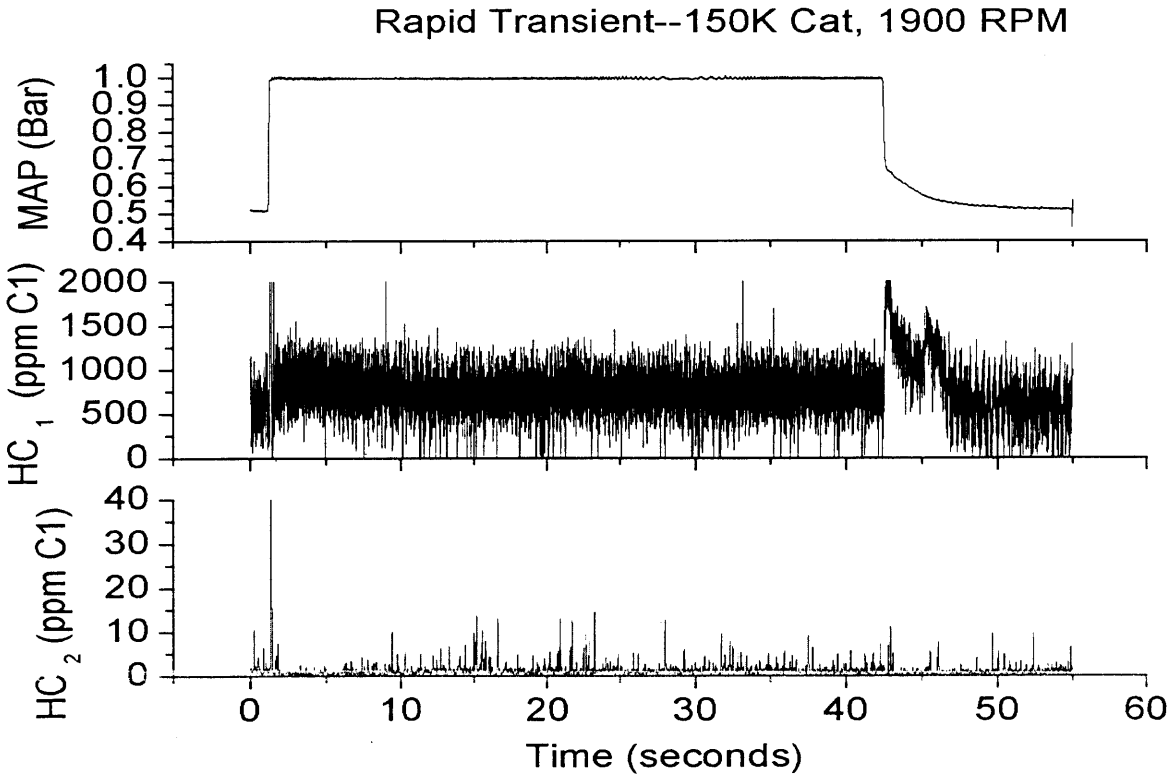

Figure 4.36: Fast Transient Expanded Pre and Post-Catalyst (150K) HC

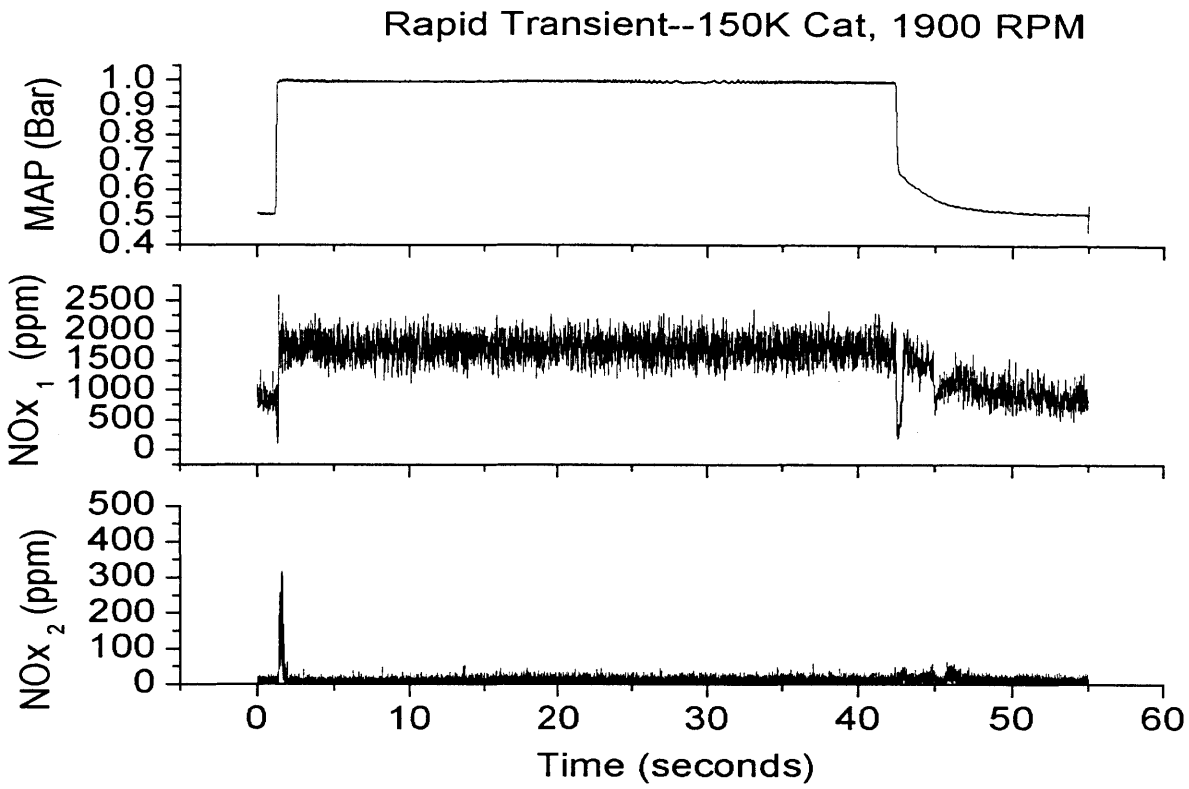

Figure 4.37: Fast Transient Pre and Post-Catalyst (150K) NOx

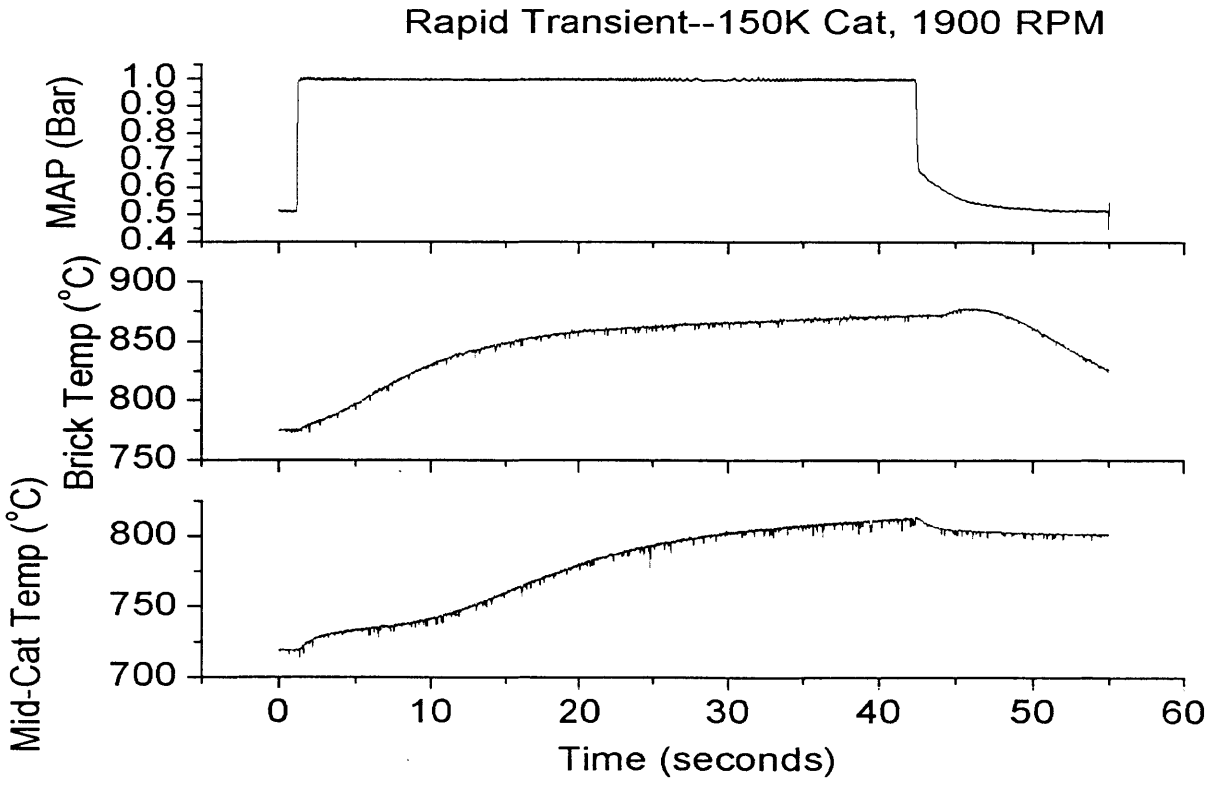

Figure 4.38: Fast Transient Catalyst Brick and Mid-Catalyst (150K) Temperature

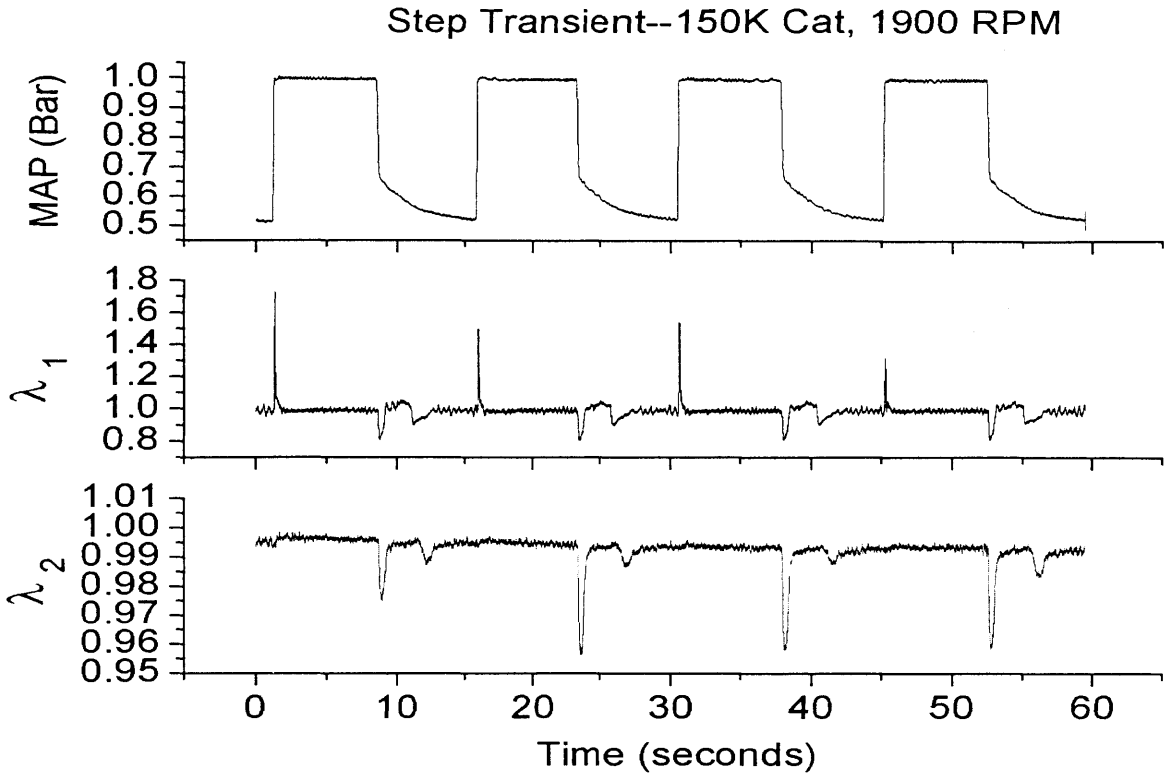

Figure 4.39: Multiple Steps Transient Pre and Post-Catalyst (150K) λ

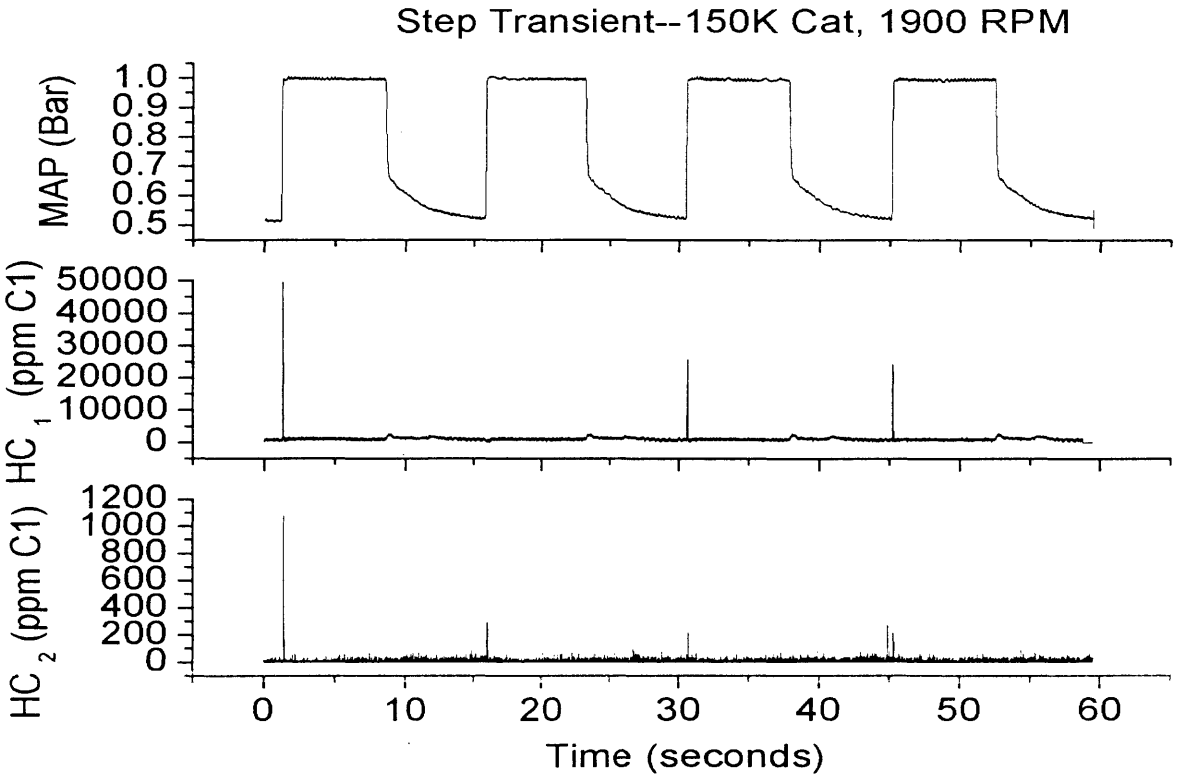

Figure 4.40: Multiple Steps Transient Pre and Post-Catalyst (150K) HC

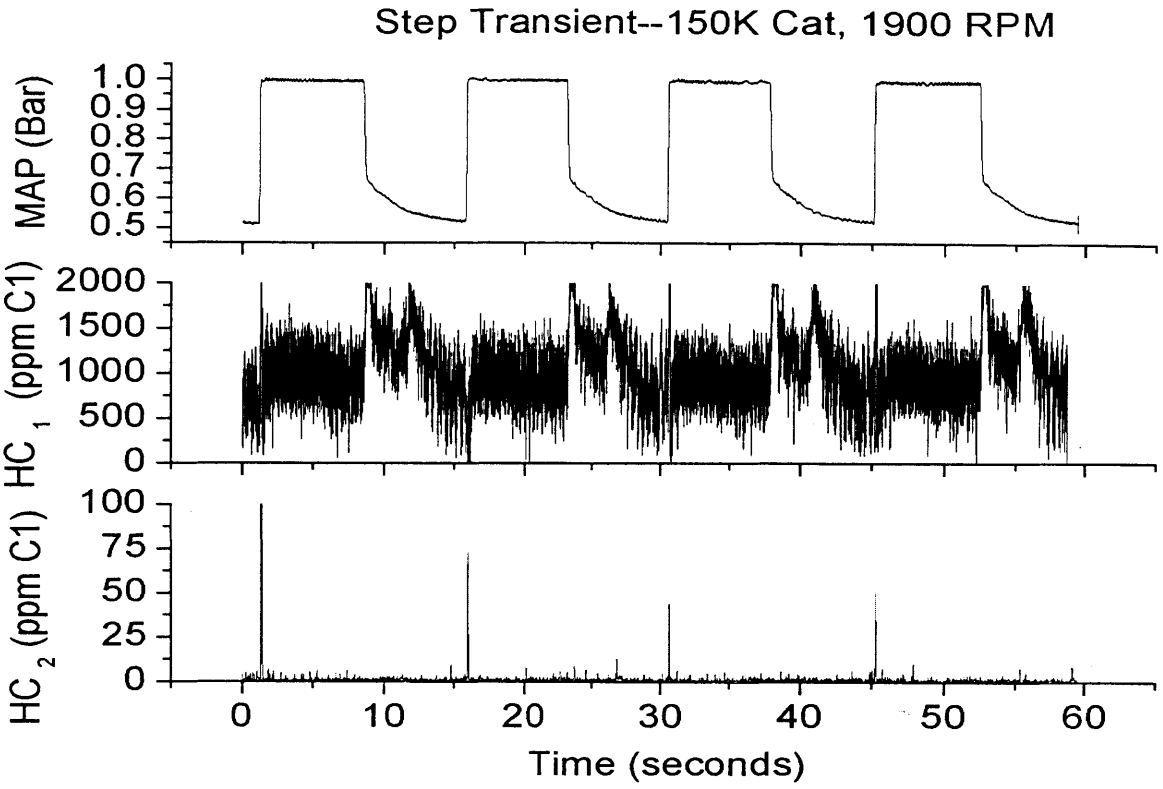

Figure 4.41: Multiple Steps Transient Expanded Pre and Post-Catalyst (150K) HC

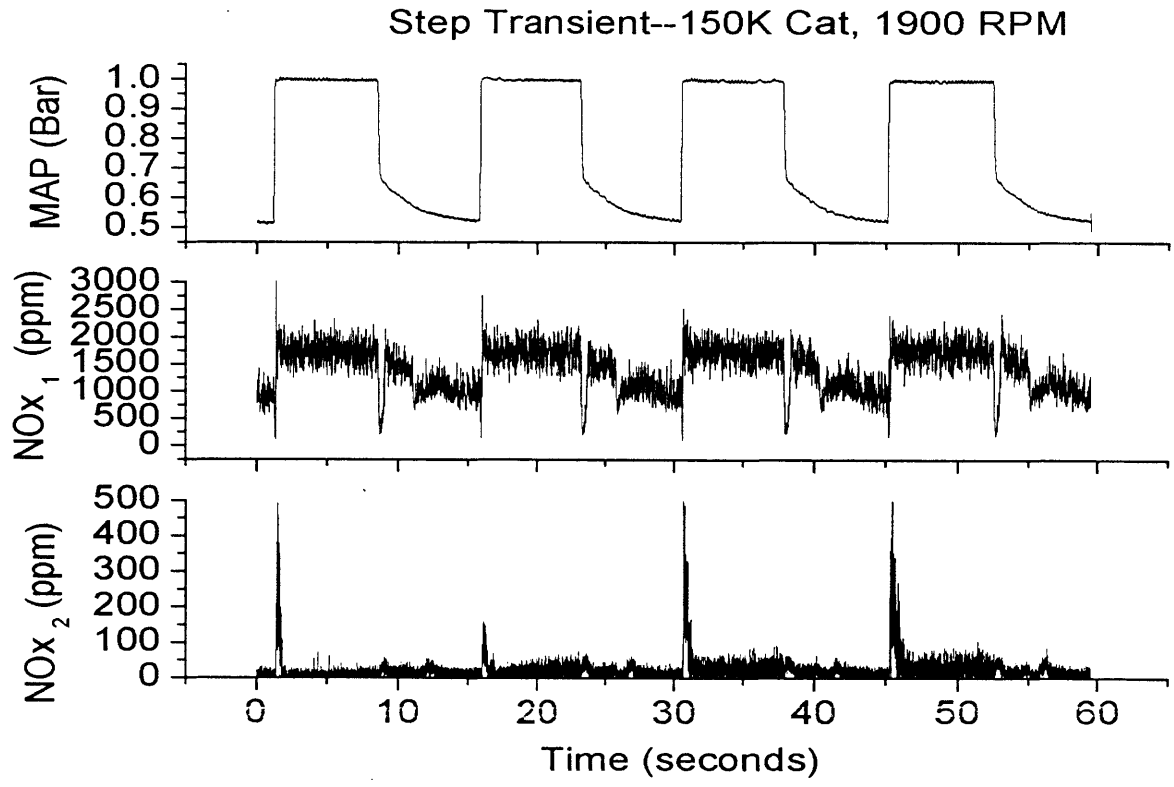

Figure 4.42: Multiple Steps Transient Pre and Post-Catalyst (150K) NOx

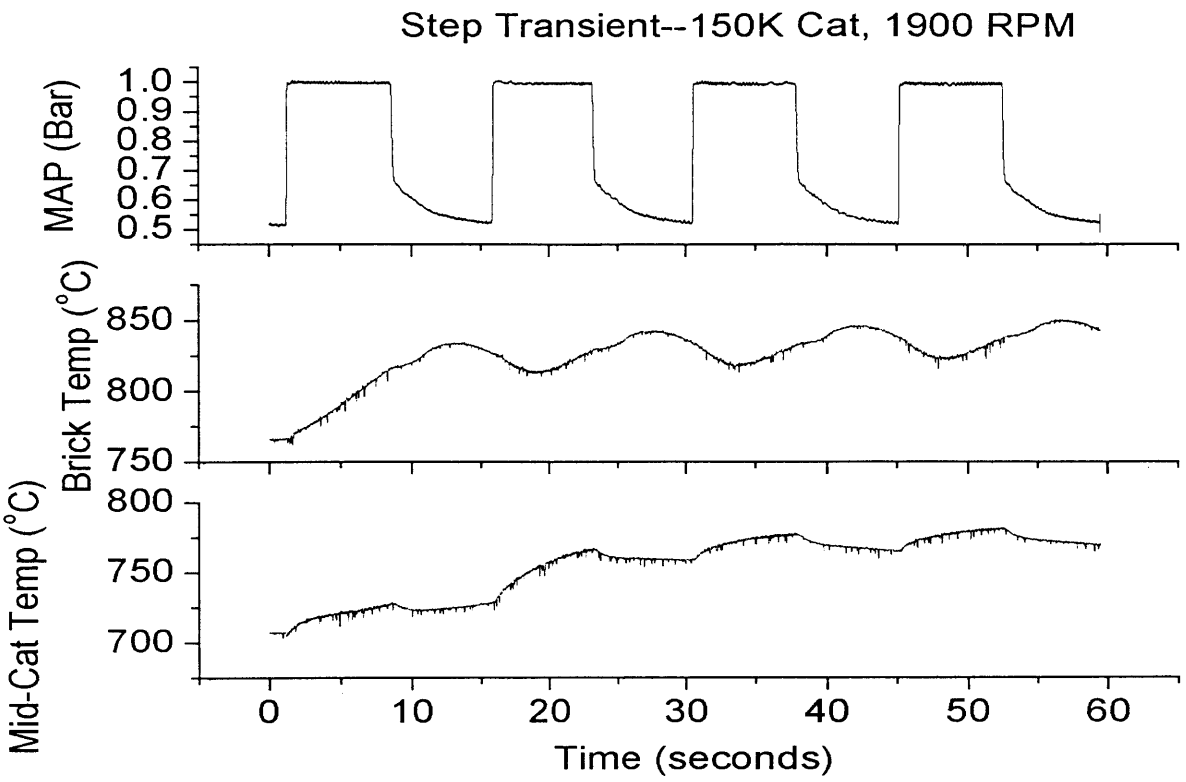

Figure 4.43: Multiple Steps Transient Catalyst Brick and Mid-Catalyst (150K) Temperature

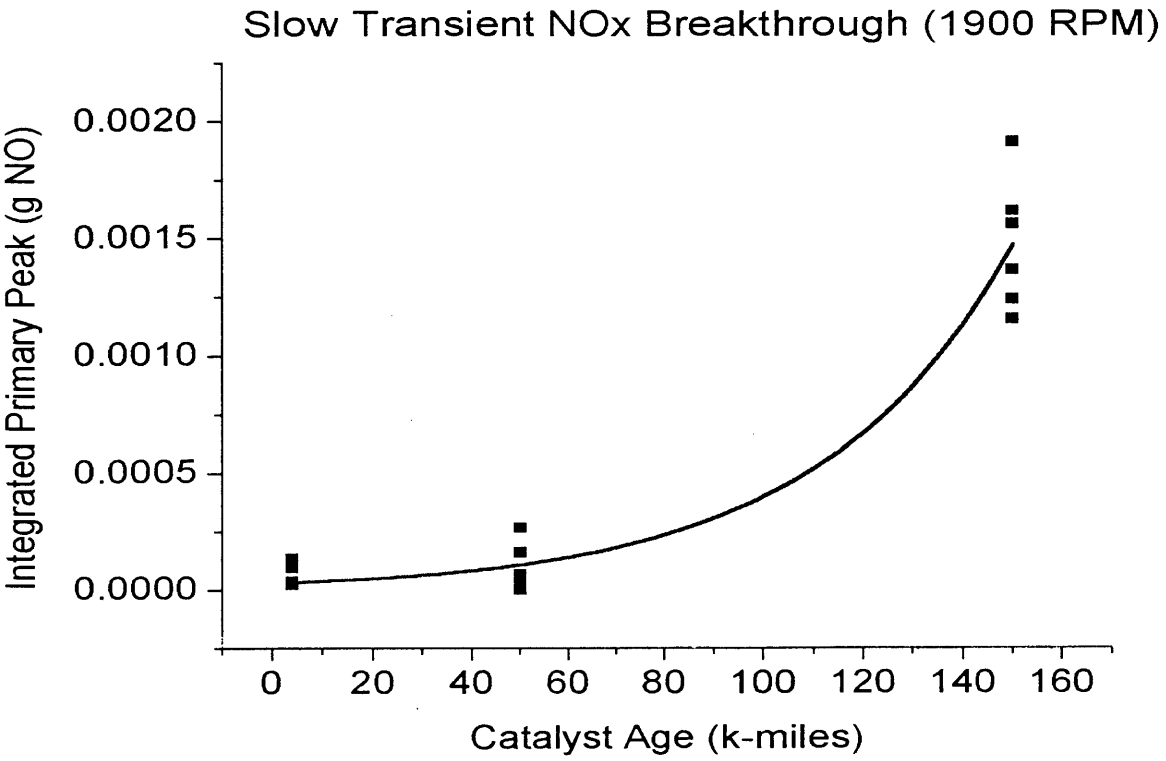

Figure 4.44: Slow Transient Primary Peak NOx Breakthrough

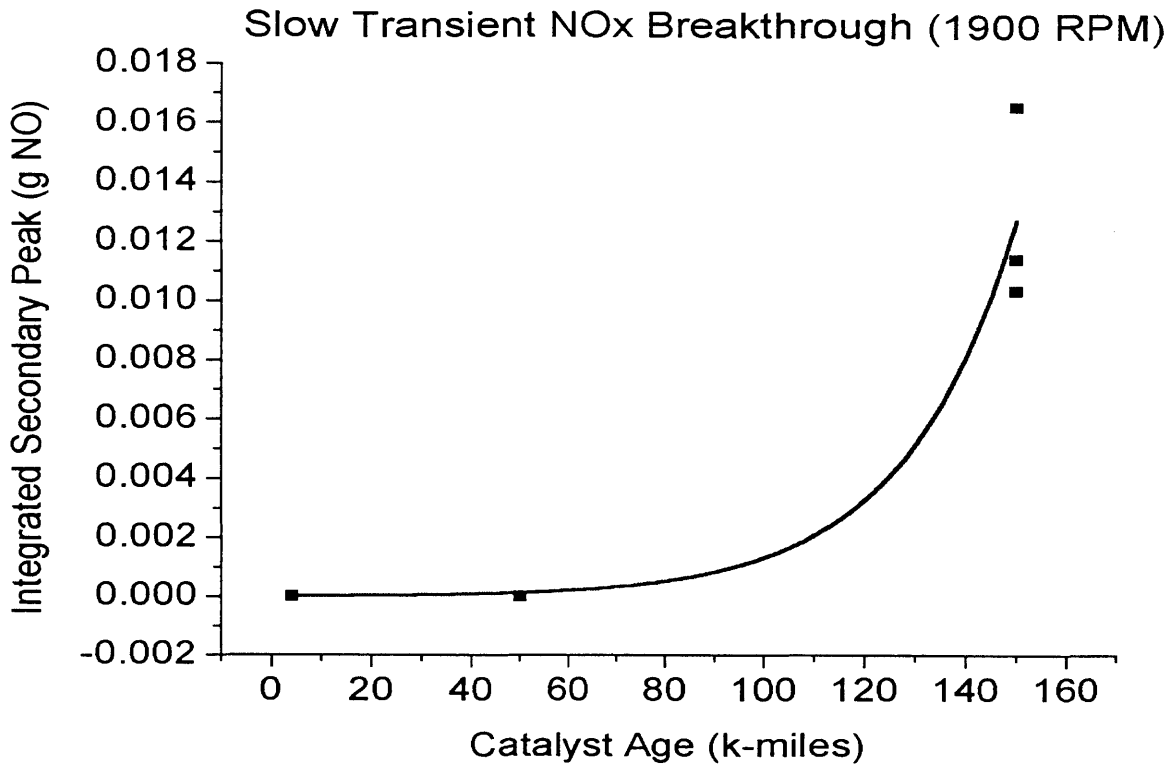

Figure 4.45: Slow Transient Secondary Peak NOx Breakthrough

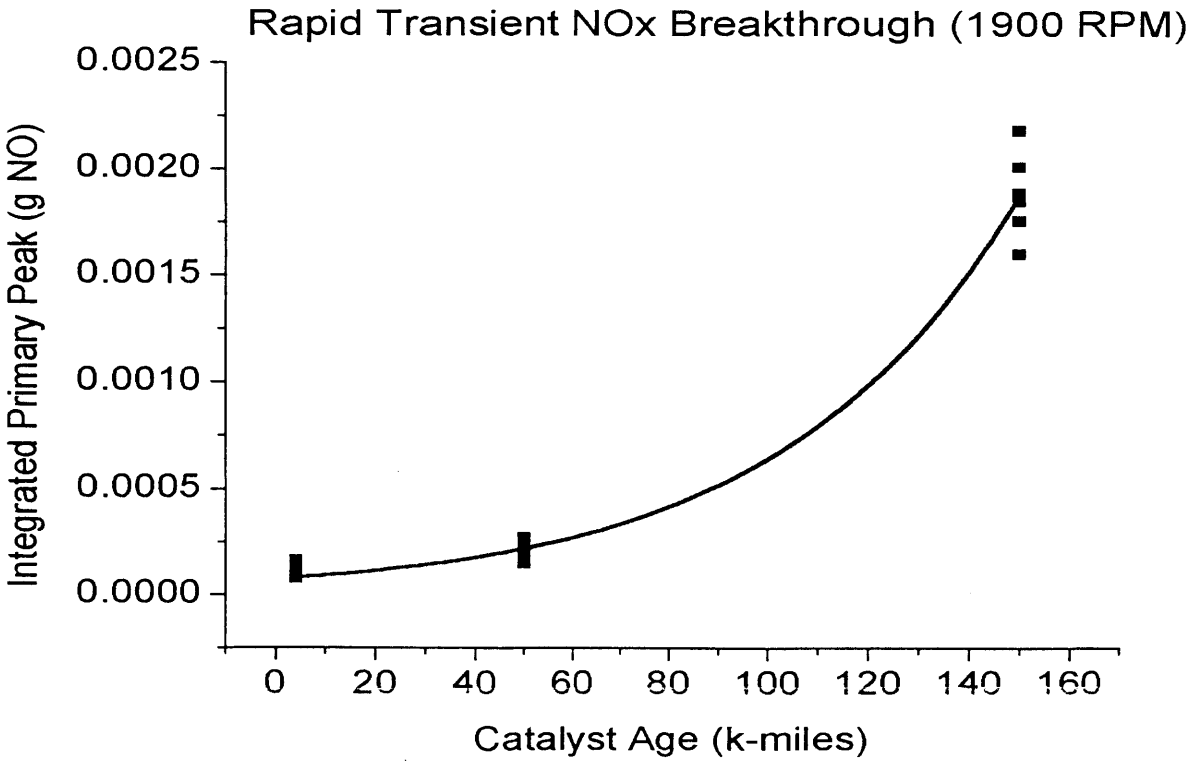

Figure 4.46: Fast Transient Primary Peak NOx Breakthrough

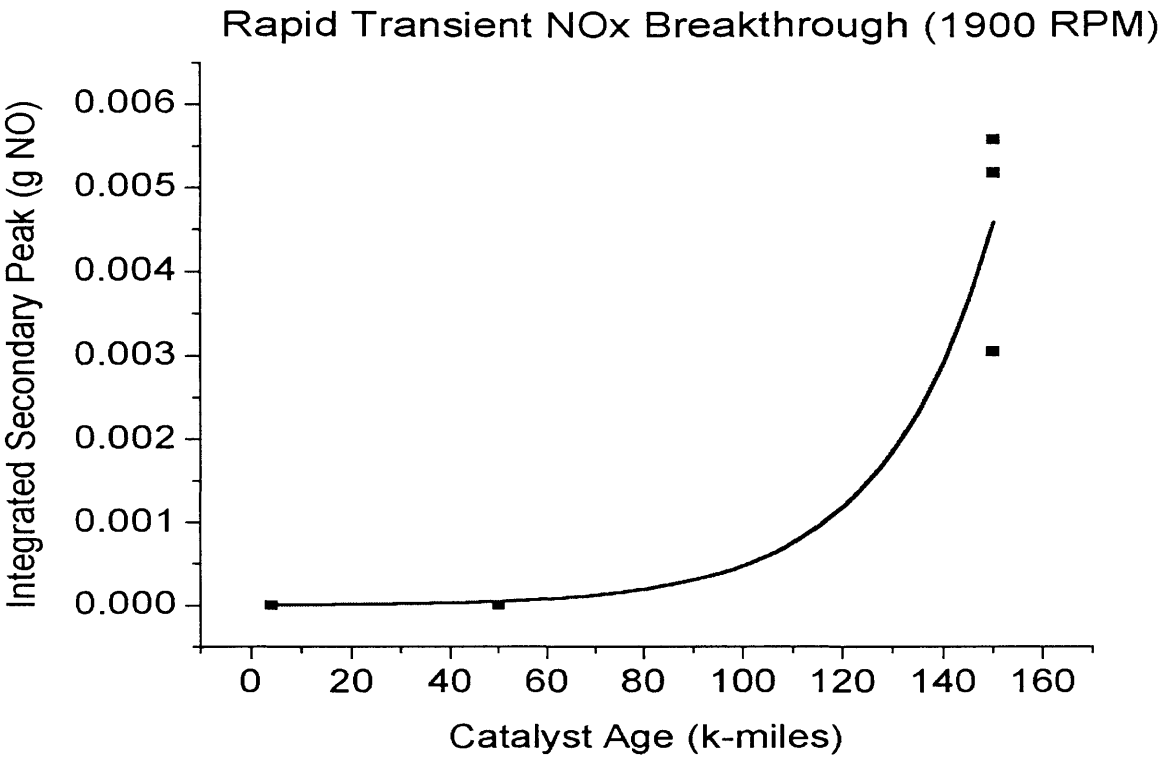

Figure 4.47: Fast Transient Secondary Peak NOx Breakthrough

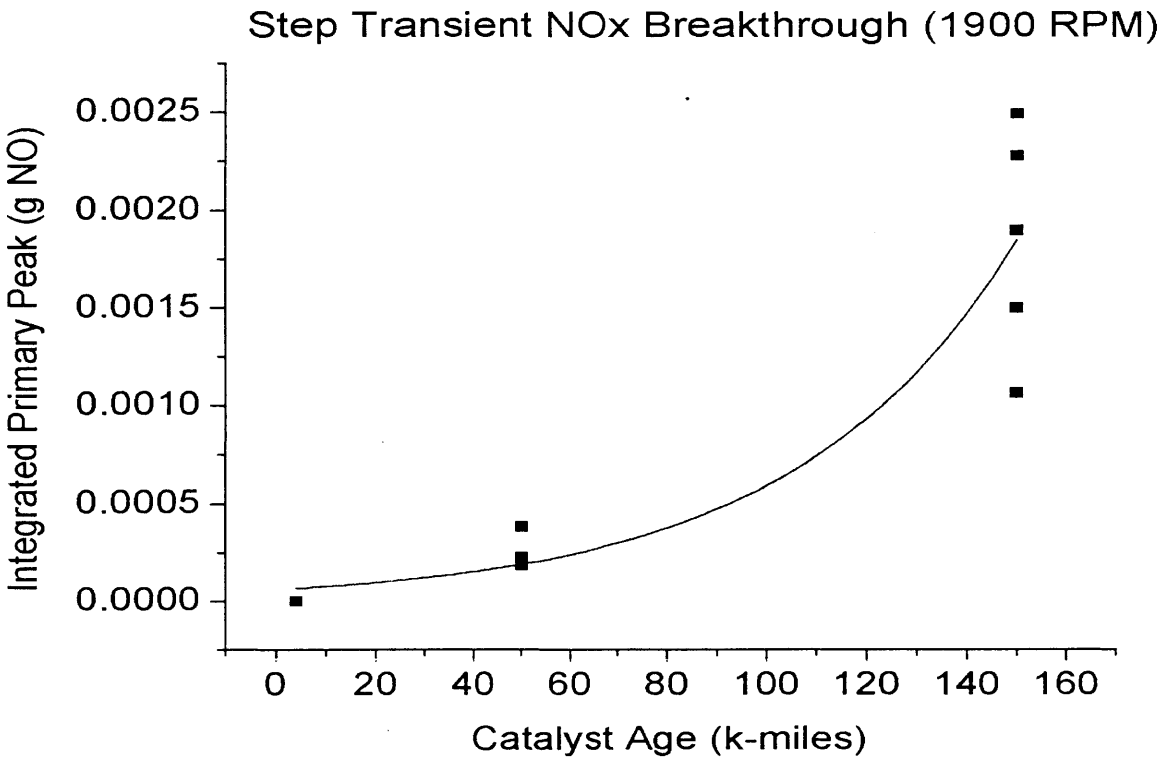

Figure 4.48: Multiple Steps Transient Primary Peak NOx Breakthrough: Values are Averaged Over 4 Cycles

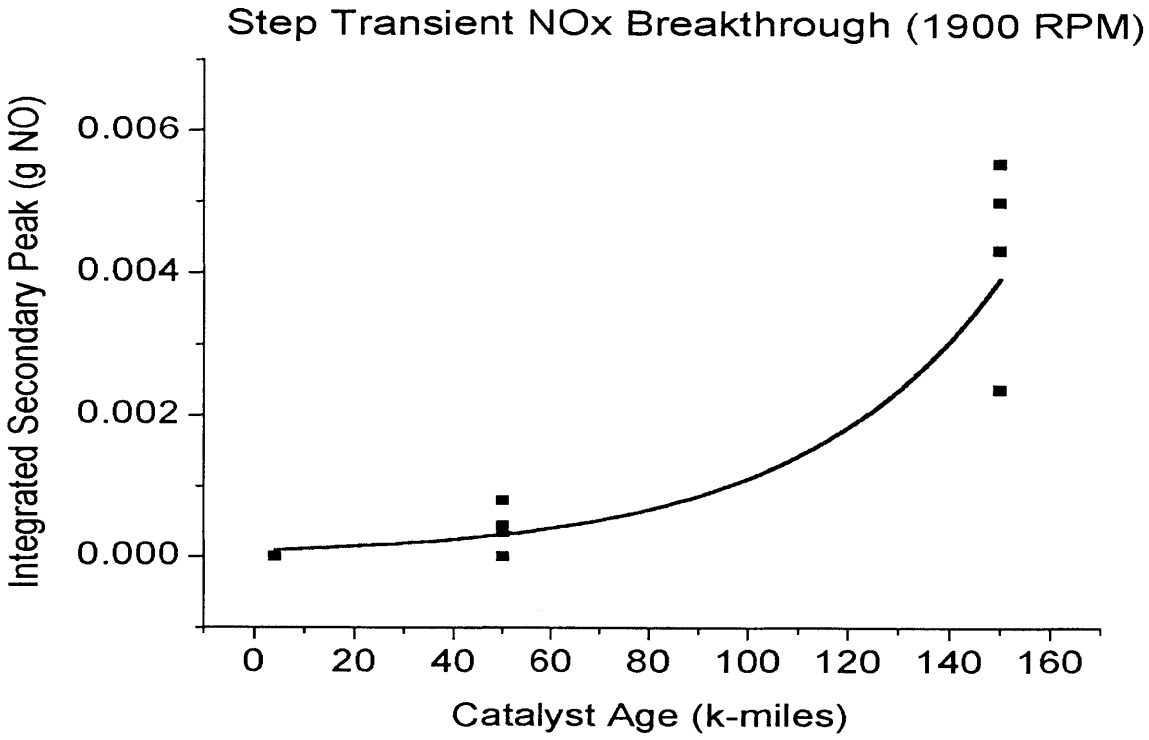

Figure 4.49: Multiple Steps Transient Secondary Peak NOx Breakthrough: Values are Averaged Over 4 Cycles

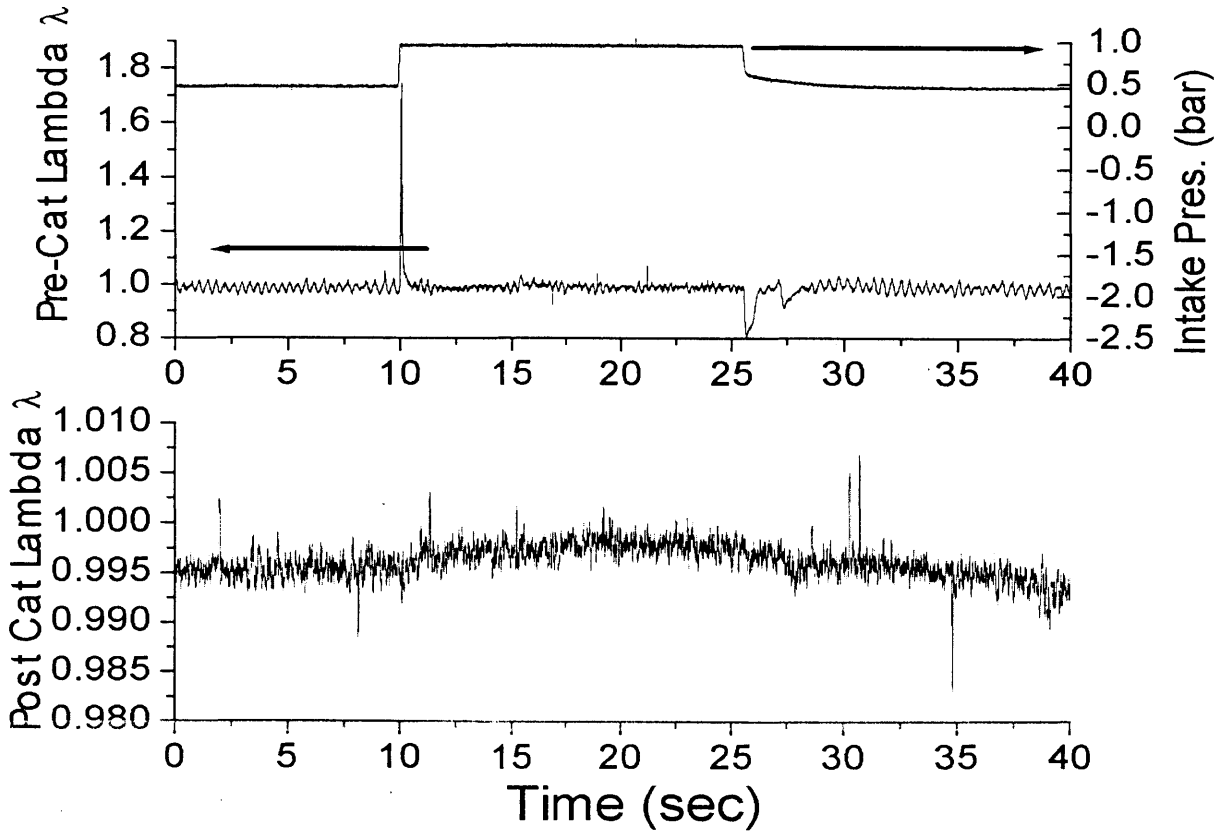

Figure 4.50: Fast Transient Expansion of Pre- and Post-Catalyst λ

CHAPTER 5: OXYGEN STORAGE TESTS

5.1: INTRODUCTION

Oxygen storage capacity is a useful measure of catalyst health. This capacity may be ascertained by comparing the pre- and post-catalyst oxygen content of the exhaust stream. The way to force the ceria (the oxygen storage mechanism—see Section 1.3.2) to release the stored oxygen is to introduce a step change in air/fuel ratio to the rich side (the converse is also true—a step change in the lean direction will result in oxygen storage). Theis, et al. used measurements of the pre- and post-catalyst emissions to calculate A/F ratio, and from the difference in the oxygen content of the exhaust stream derived the oxygen storage/release. This study found that oxygen release took on the order of 15 seconds longer than oxygen storage, so the oxygen released during step rich excursions was greater than the oxygen stored during step lean transitions [25]. Smedler, et al. performed a similar study where CO and HC measurements were used to quantify oxygen storage. Temperature was found to play a large role in oxygen storage; aged samples with higher feed gas temperature had a higher oxygen storage capacity [26]. Hepburn, et al. used pre- and post-catalyst oxygen sensors to measure oxygen content, and found that while this was a fine measure of oxygen storage capacity, its correlation to catalyst HC efficiency was weak [27].

The tests presented here were done slightly differently, as the control system was different for this engine. Also, where Theis, et al used emissions measurements to determine the oxygen storage, the UEGO output was used in the tests detailed here. Smedler, et al. used a reactor to simulate the engine exhaust and used an increase in H_2 or HC to simulate a rich step, so this is another difference with the results presented next.

5.2 OXYGEN STORAGE CALCULATION METHODOLOGY

Figure 5.1 shows some pertinent terms that must be defined to explain the oxygen storage calculation. This is an example of a typical oxygen storage test, where the air/fuel ratio is rapidly switched from a rich value to a lean value. The time periods of interest on this curve that are used in the oxygen storage calculation are marked on Figure

5.1. The first time period is marked t_0, and marks where the pre-catalyst oxygen sensor crosses the stoichiometric mark. The next point of interest is the time marked t_1, which is where the post catalyst UEGO crosses the stoichiometric point. The final time period is marked t_2, and is where the UEGO readings converge (as much as the sensor error talked about in Section 3.2.5 will allow convergence).

The following analysis uses the definition of these time periods. First, the lean burn equation is used to approximate the composition of the exhaust gas:

$$CH_{1.87} + 1.4675\lambda(O_2 + 3.773N_2) \longrightarrow CO_2 + 0.935H_2O$$
$$+1.4675(\lambda - 1)O_2 + 1.4675\lambda(3.773)N_2 \qquad 5.1$$

In the MATLAB code (shown in Appendix H), the mass fraction of oxygen is calculated from the UEGO value using the following equation:

$$y_{O2} = x_{O2}\frac{MW_{O2}}{\overline{MW}} \qquad 5.2$$

The average molecular weight is calculated assuming the lean burn equation (Equation 5.1) holds true. From the mass fraction, the oxygen mass flow rate is calculated by the following equations:

$$\dot{m}_{O2}(1) = \dot{m}_{exh}\, y_{O2}(\lambda_1) \qquad 5.3a$$

$$\dot{m}_{O2}(2) = \dot{m}_{exh}\, y_{O2}(\lambda_2) \qquad 5.3b$$

The mass flow rate of oxygen calculated from equation 5.3a is the oxygen entering the catalyst, as it is based on the upstream UEGO value. The mass flow rate leaving the catalytic converter is represented by Equation 5.3b, as that is calculated from the post-catalyst oxygen sensor. The oxygen stored will be the difference between the two values, written mathematically as:

$$M_{O2stored} = \int_{t0}^{t1} \dot{m}_{O2}(1)dt + \int_{t1}^{t2} \dot{m}_{O2}(1)dt - \int_{t0}^{t1} \dot{m}_{O2}(2)dt - \int_{t1}^{t2} \dot{m}_{O2}(2)dt \qquad 5.4$$

The limits on the integrals refer to the time periods shown on Figure 5.1. The first two terms are the oxygen mass that enters the catalyst, and the second two terms are the

oxygen mass that leaves the catalyst. The third term (the integral from t_0 to t_1) will be zero, however, as the UEGO sensor reads a rich value in this regime. From the discussion of the operation of the oxygen sensors (see Section 2.3.2), the rich reading means there is a negligible amount of oxygen present in the exhaust. Collecting terms and rewriting Equation 5.4, the final form for the amount of oxygen stored is:

$$M_{O2stored} = \dot{m}_{exh}\left[\int_{t0}^{t2} y_{O2}(1)dt - \int_{t1}^{t2} y_{O2}(2)dt\right] \qquad 5.5$$

A secondary consideration with this method of testing is whether the oxygen storage is measured or the oxygen used to oxidize hydrocarbons, CO, and H_2 is being measured. Referring back to Chapter 3 data (Figure 3.11), the amount of pre-catalyst CO is ~0.1 % wet mole fraction. From Figure 4-21 in [4], the amount of H_2 present in the pre-catalyst exhaust stream is ~0.05. The amount of oxygen required to oxidize these components is negligible compared to the amount of oxygen stored in the catalyst, so this secondary consideration may be neglected.

The first term of the RHS of equation 5.5 may be used to determine the oxygen supplied to the catalytic converter. This is interesting to look at for the closed loop modulation of the oxygen storage. Shown in Appendix I is the modulation for this engine setup and the corresponding amount of oxygen supplied to the catalytic converter.

5.2: OXYGEN STORAGE TEST RESULTS

5.2.1: Determination of Rich Starting Point

As mentioned in the above analysis, the oxygen storage tests were done from a rich starting point to a lean finishing point. They were done in this way so as to minimize the error due to the rich sensor shift. It was desired to determine the optimum point to start the rich transition from, and this was accomplished by conducting a series of tests of switching λ from 1.05 to values of 0.98, 0.97, 0.96, 0.95, and 0.90. This switch was necessary to perform before each transition from rich to lean, as the catalyst had to be depleted of its oxygen supply by a rich feed gas before the true oxygen storage could be measured. One would expect that the richer the feed gas, the shorter time period was necessary to deplete the oxygen storage. This result was observed, as may be seen from

Figure 5.2. It is interesting to note the difference in the pre- and post-catalyst oxygen sensors increasing as the feed gas becomes richer. The period of time necessary for the catalyst oxygen storage capacity to be depleted is defined as τ, and is summarized in Table 5.1 below and also graphically in Figure 5.3.

Rich Value	τ (sec)
0.90	5.39
0.95	11.66
0.96	15.77
0.97	20.61
0.98	35.62

Table 5.1: Summary of Oxygen Depletion Times

The value of 0.95 was chosen to be the optimum, as the times shown in Table 5.1 represent the time period necessary between consecutive runs, and this was desired to be minimal yet not be too rich.

5.2.2: Rich to Lean Transitions

Once the rich starting point had been determined, it was straightforward to test the different catalysts. The test matrix used in the experiments is shown below in Table 5.2:

Test Step	Engine Speed
0.95→1.05 Step	1600 RPM
0.95→1.1 Step	
0.95→1.2 Step	
0.95→1.05 Step	2000 RPM
0.95→1.1 Step	
0.95→1.2 Step	

Table 5.2: Oxygen Storage Test Matrix

Figures 5.4 through 5.30 show the tests for the 1600 RPM experiments detailed above, and the results for the 2000 RPM experiments are shown in Figures 5.31 through 5.57. For each test, the pre- and post-catalyst hydrocarbons, NOx, and the two catalyst brick temperatures were measured. The hydrocarbons follow the steady state efficiencies discussed in Section 3.2.1. The NOx emissions follow the same trends as discussed in Section 3.2.2. No rapid breakthrough was observed for either pollutant. It is interesting to note with the NOx traces that as soon as the post-catalyst UEGO reads stoichiometric, NOx begins to break through the converter. This is due to the fact that no oxygen is

being absorbed onto the catalyst, and instead is just going straight through the catalyst, producing a lean environment and making NOx reduction impossible.

5.2.2.1:Temperature Rise Phenomenon

Figure 5.58 shows a trace of the two catalyst temperatures taken for an extended period of time to observe their behavior after the test. It can be seen that after they produce the trends shown in the temperature plots in Figure 5.4-5.57, they slowly reach a new steady state temperature consistent with the temperatures presented in Figures 3.9 and 3.10.

To determine the cause of this temperature rise, a simple analysis may be applied to an open system control volume surrounding the front catalyst brick. For this control volume, the first law may be written as:

$$\dot{m}_{exh}(h_2 - h_1) = Q_{chem} \tag{5.6}$$

Expanding this expression:

$$\dot{m}_{exh}\, c_p(T_2 - T_1) = \begin{pmatrix} \chi_{CO} MW_{CO} Q_{HVCO} + \chi_{H2} MW_{H2} Q_{HVH2} \\ + x_{HC} MW_{HC} Q_{HVHC} \end{pmatrix} \frac{\dot{m}_{exh}}{MW_{exh}} \tag{5.7}$$

The terms on the right hand side of the equation are all of the components of the exhaust stream that have a potential for releasing chemical energy. The equation may be re-arranged to relate temperature rise to the exhaust stream components.

$$(T_2 - T_1) = \begin{pmatrix} \chi_{CO} MW_{CO} Q_{HVCO} + \\ x_{HC} MW_{HC} Q_{HVHC} + x_{H2} MW_{H2} Q_{HVH2} \end{pmatrix} \frac{1}{c_p MW_{exh}} \tag{5.8}$$

The change in hydrocarbons during the rich to lean transition was measured to be roughly 700 ppm, and assuming they are of the structure CH_2, would account for a 11.6 °C temperature rise (calculated using the HC portion of the RHS of equation 5.8—see Appendix J). The energy released from the hydrocarbons does not account for the entire temperature rise shown in the temperature curves. Thus, the temperature rise may be part of another physical phenomenon, because of the delay in the temperature rise does not correspond to the change in hydrocarbon supply. Further investigation is necessary to determine the cause of the temperature rise.

5.3: CONCLUSIONS FROM OXYGEN STORAGE TESTS

Some conclusions may be drawn from looking at a particular test over the range of catalyst ages. Figure 5.59 shows the 0.95→1.1 Step test (1600 RPM) and how each of the UEGO traces were different for the tests. It can be seen that the period that is required for the post-catalyst UEGO to read the same as the pre-catalyst sensor decreases with catalyst age. Also noteworthy is the fact that the slopes of the post-catalyst oxygen sensor are different. Conversations with those in industry reveal that this is a result of the ceria degradation. Catalyst manufacturers use a few forms of ceria in each catalyst formulation, which will degenerate at different rates. Each of these forms release/store the oxygen at different rates, causing different slopes to be seen [28]. The formulation is proprietary, so the author was unable to obtain the specifics in regard to the ceria formulation.

Comparing the HC breakthrough traces for the same test (Figure 5.60), no anomaly is seen. Each hydrocarbon level simply reflects the steady state HC efficiency of the catalyst.

Looking at Figure 5.61, the temperature rise in the initial portion of the curve is interesting, as there is a slight delay before the temperature starts to rise. For the brick temperature, there is a ~15-20°C rise in temperature in the 4K catalyst, a ~10-19°C rise in temperature for the 50K catalyst, and a ~10-15°C rise for the 150K catalyst. Thus, there seems to be some correlations between the reduced catalytic activity and the temperature rise.

In looking at the comparison of the NOx breakthrough (Figure 5.62), the NOx breakthrough commences when the post-catalyst UEGO reads stoichiometric. The only difference for each of the catalysts is the point where this happens. Even the fresh catalyst experiences zero efficiency for lean values.

Compiling the results for the oxygen storage calculations, there is a trend that with increasing the lean step that the catalyst sees, there is increasing oxygen stored (Figure 5.63). The 4K catalyst is well above the 50K and 150K catalyst in oxygen storage. The 50K and 150K catalyst are very close in oxygen storage capacity, but the same trend is seen of increasing storage with increasing lean step size. Figure 5.64 sums up the data for each of the catalyst, with a ~17% decrease in oxygen storage capacity

from the 4K catalyst to the 50K catalyst, and then essentially no change in the oxygen storage capacity from the 50K catalyst to the 150K catalyst.

Figure 5.65 plots the oxygen storage as a function of temperature. From the results in Chapter 3, it was known that 2000 RPM would produce higher temperature, but this seemed to have little effect on oxygen storage capacity.

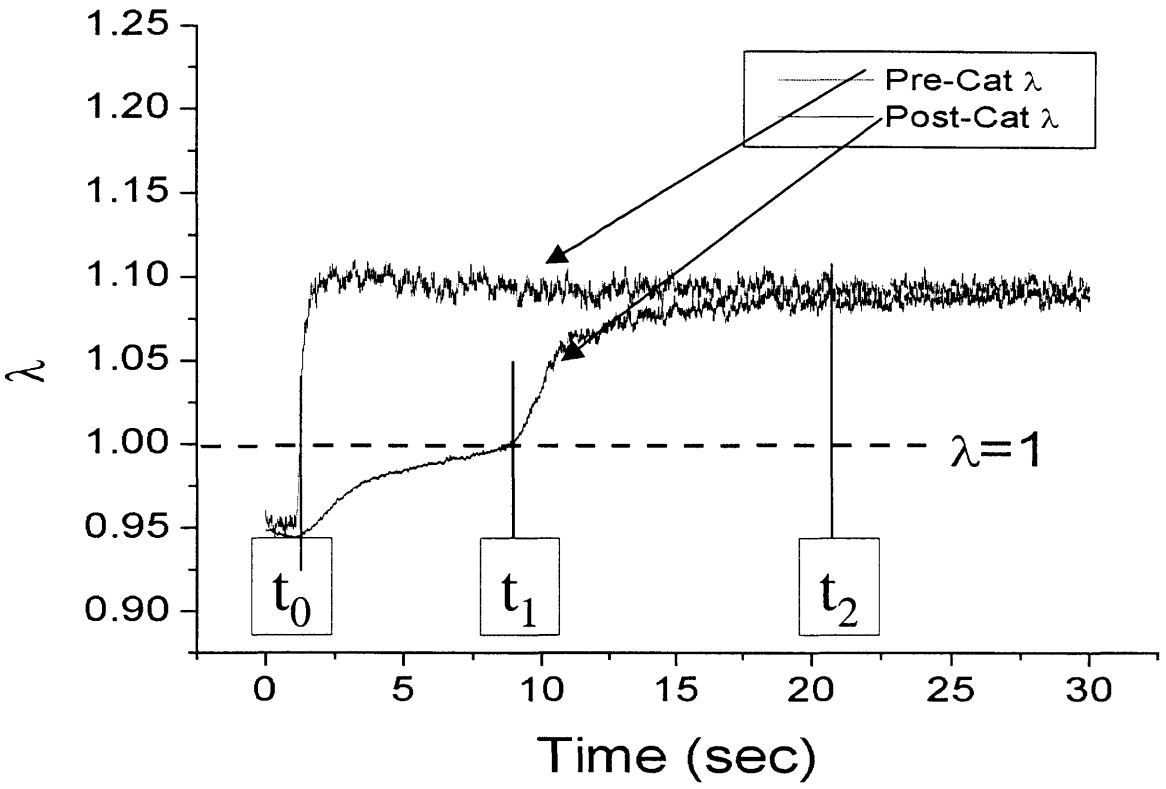

Figure 5.1: Definition of Oxygen Storage Terminology

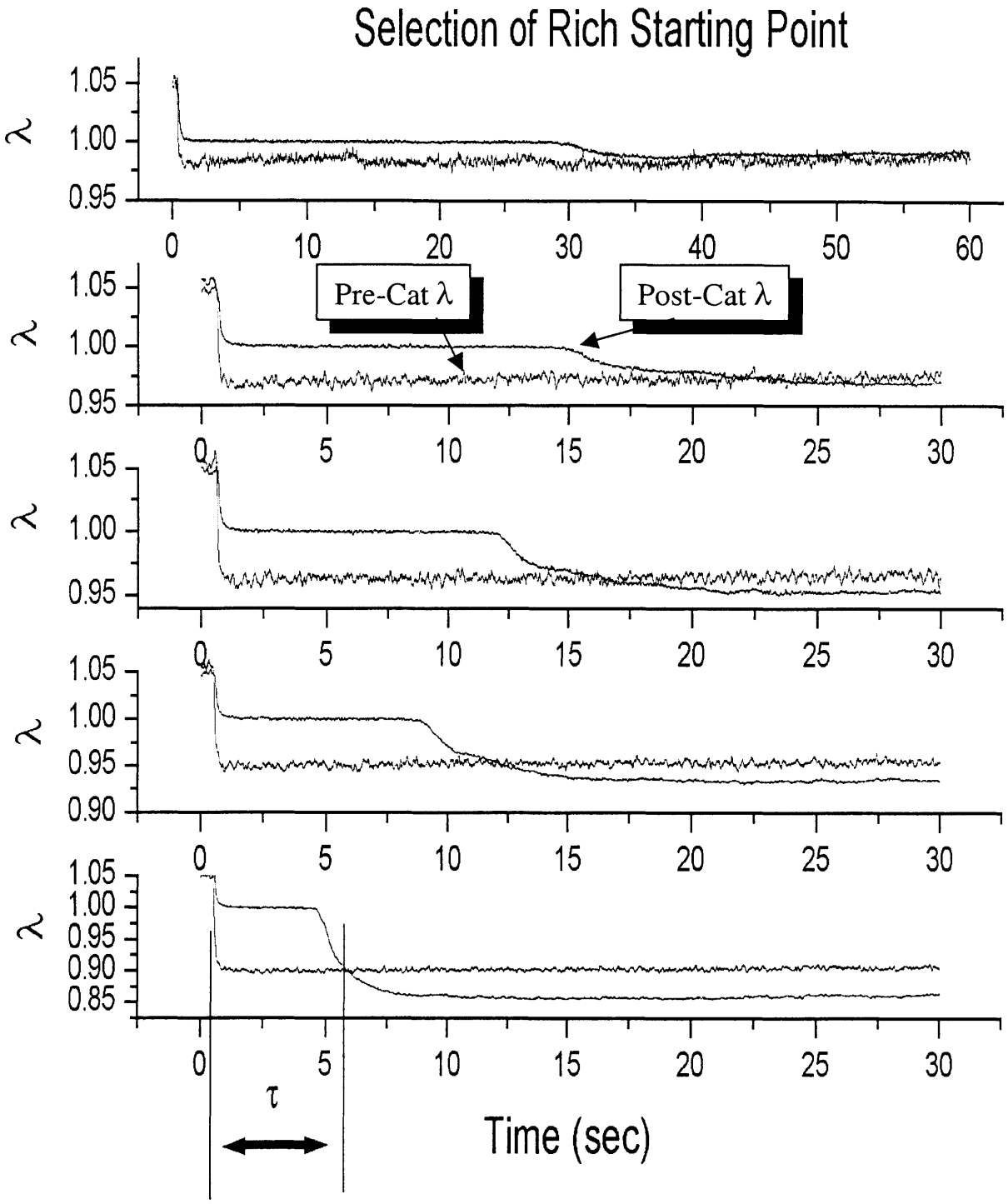

Figure 5.2: Comparison of Rich Starting Points

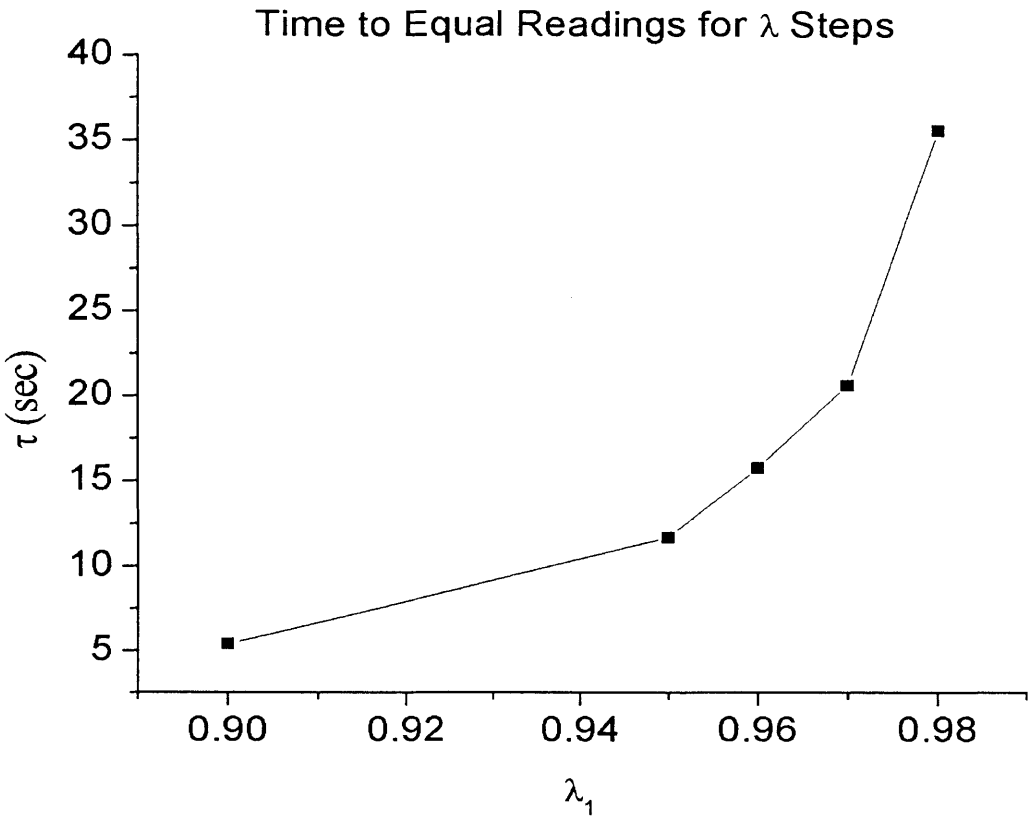

Figure 5.3: Oxygen Flush Times--1600 RPM 4K Catalyst

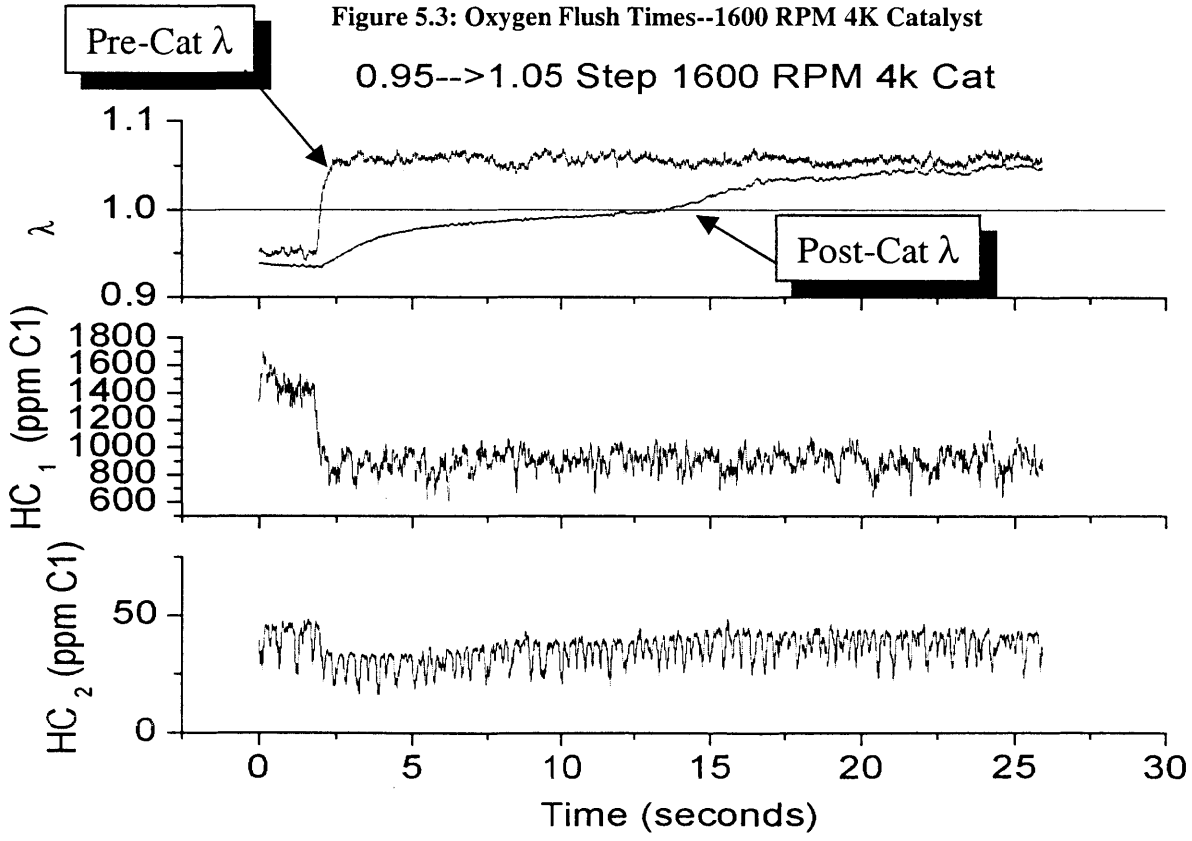

Figure 5.4: 0.95-->1.05 Step HC--1600 RPM 4K Catalyst

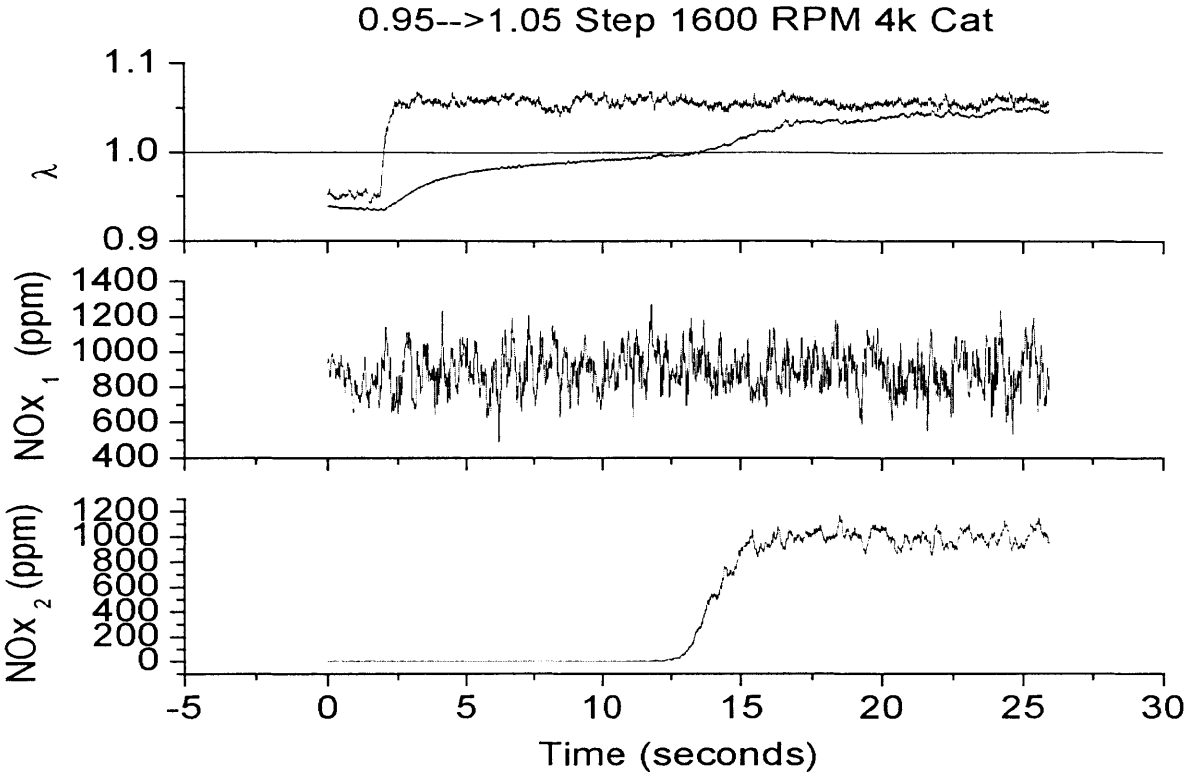

Figure 5.5: 0.95-->1.05 Step NOx--1600 RPM 4K Catalyst

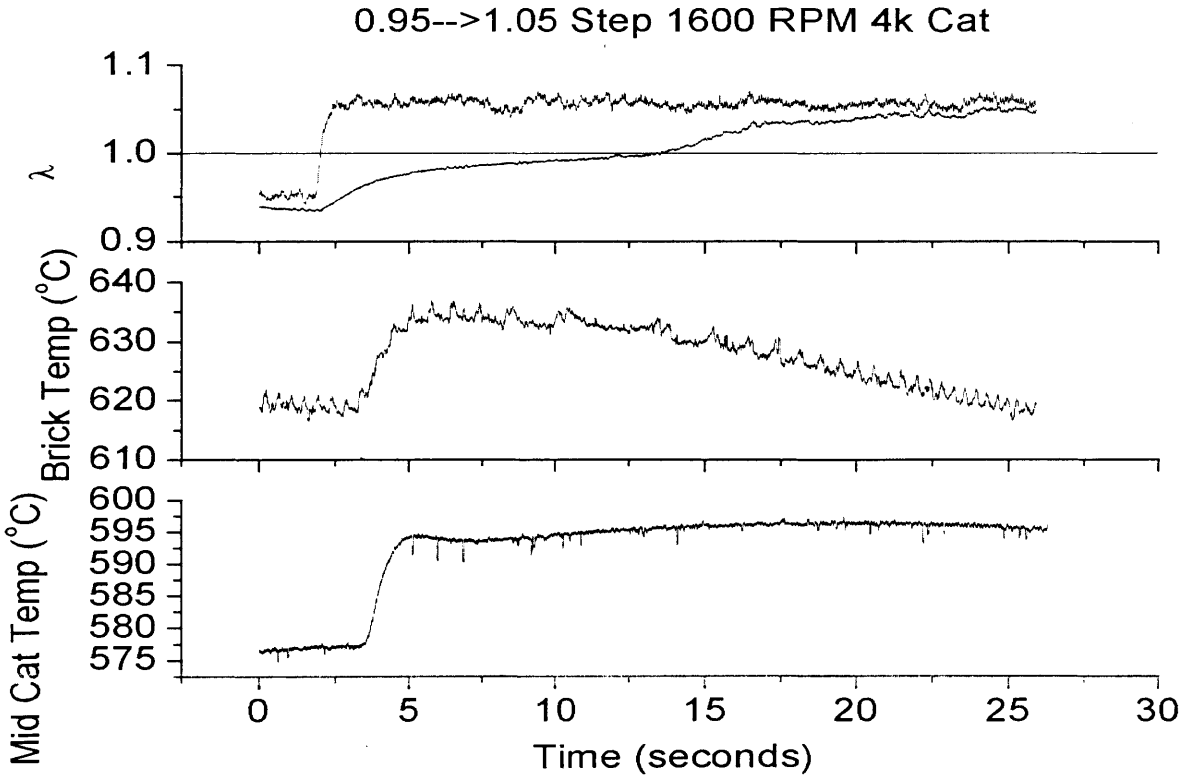

Figure 5.6: 0.95→1.05 Step Catalyst Brick and Mid-Catalyst Temperatures 1600 RPM 4K Catalyst

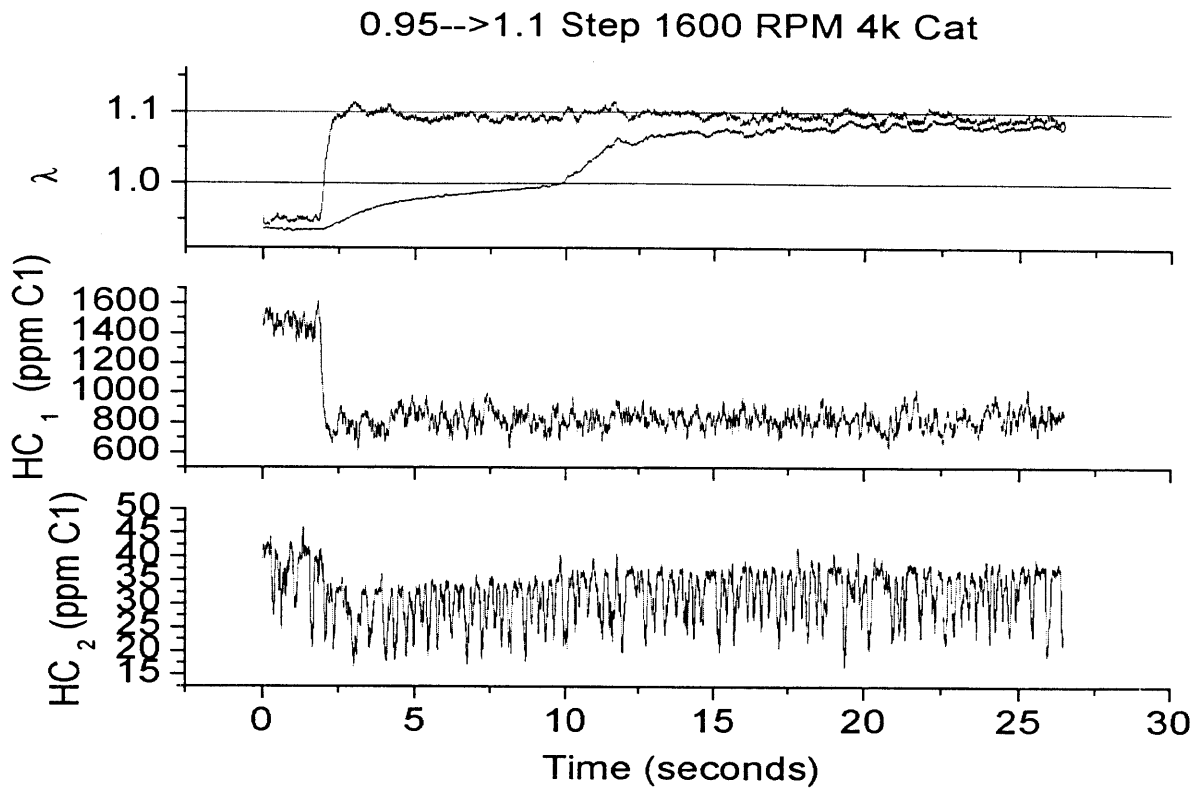

Figure 5.7: 0.95-->1.1 Step HC--1600 RPM 4K Catalyst

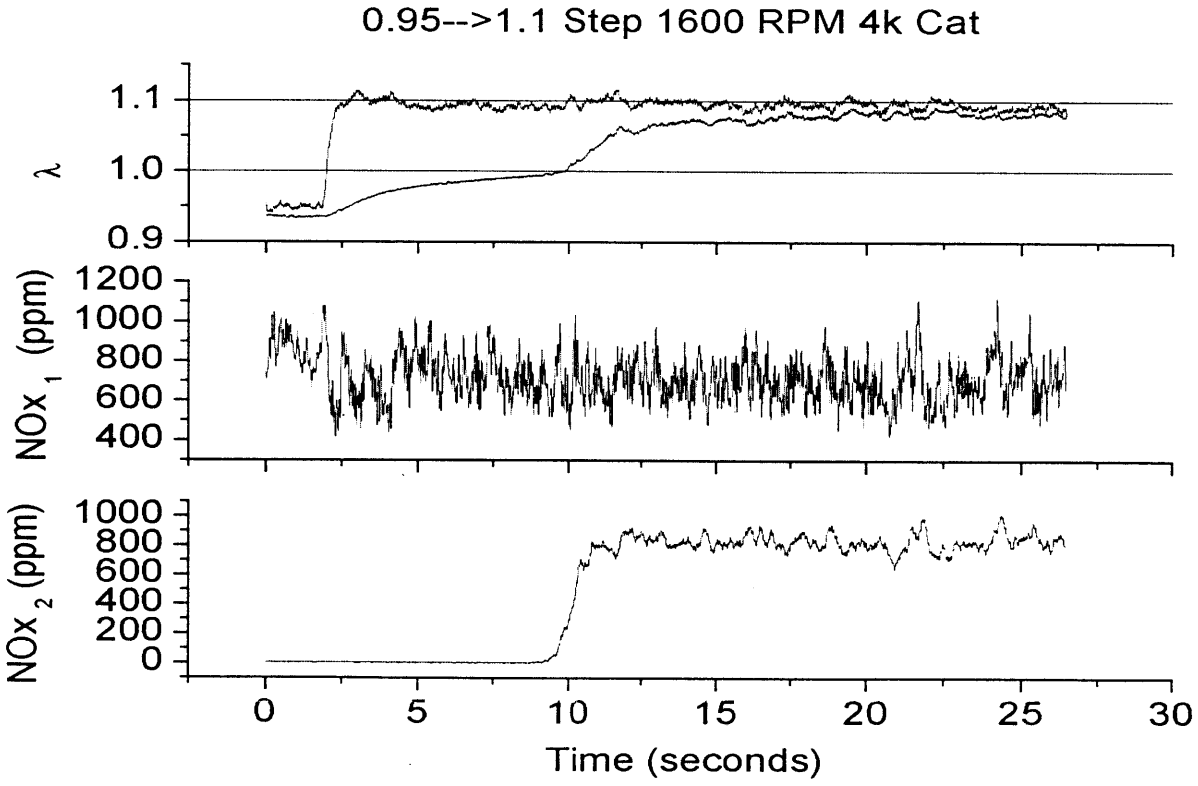

Figure 5.8: 0.95-->1.1 Step NOx--1600 RPM 4K Catalyst

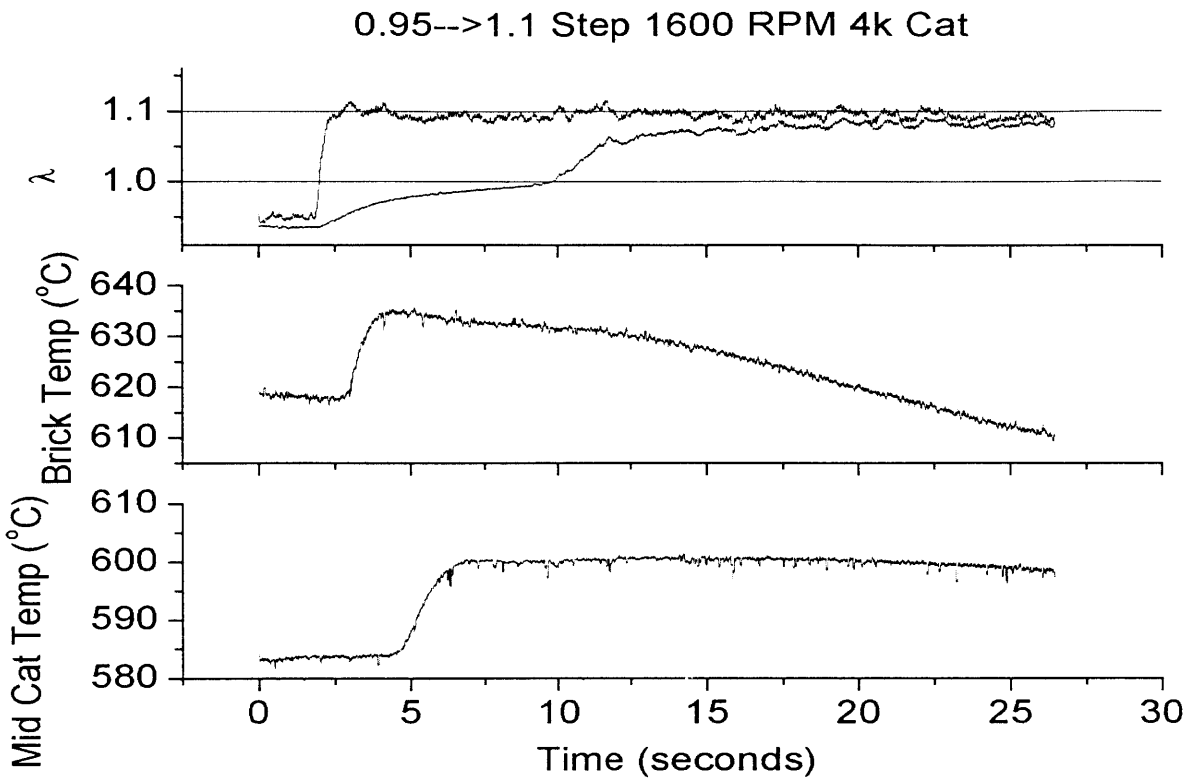

Figure 5.9: 0.95→1.1 Step Catalyst Brick and Mid-Catalyst Temperatures 1600 RPM 4K Catalyst

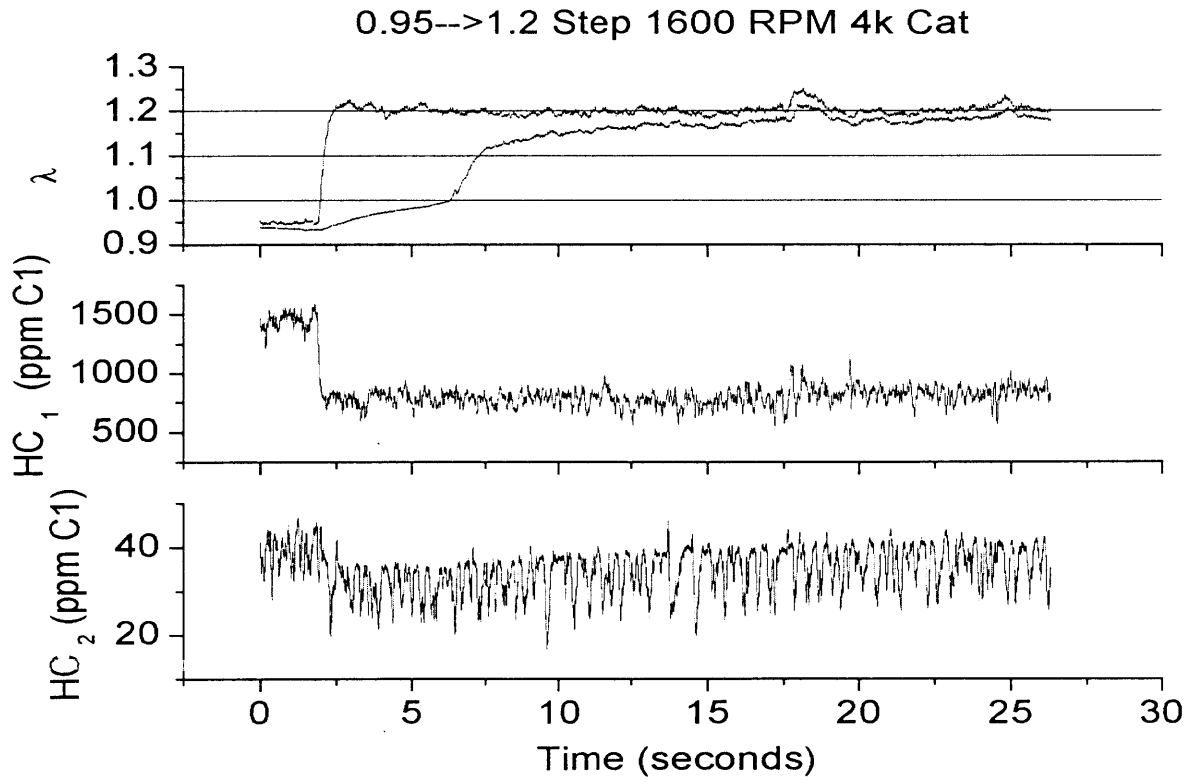

Figure 5.10: 0.95→1.2 Step HC 1600 RPM 4K Catalyst

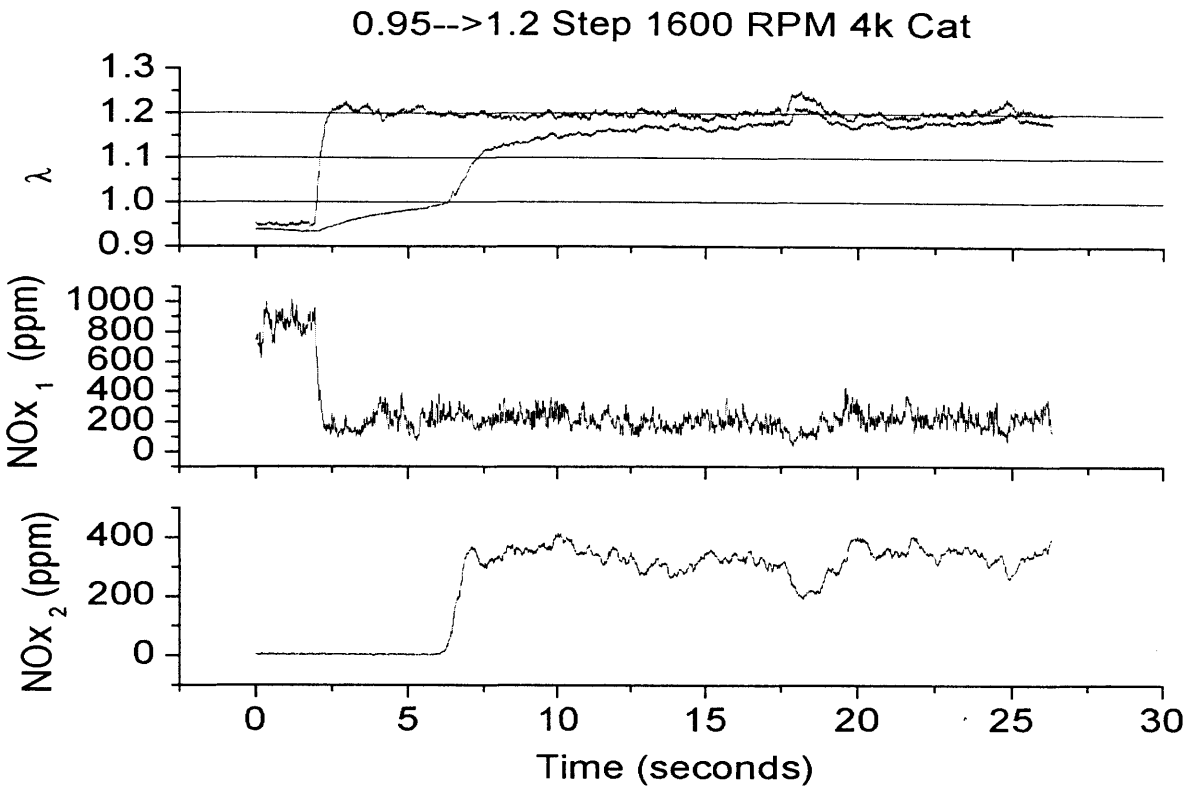

Figure 5.11: 0.95→1.1 Step NOx 1600 RPM 4K Catalyst

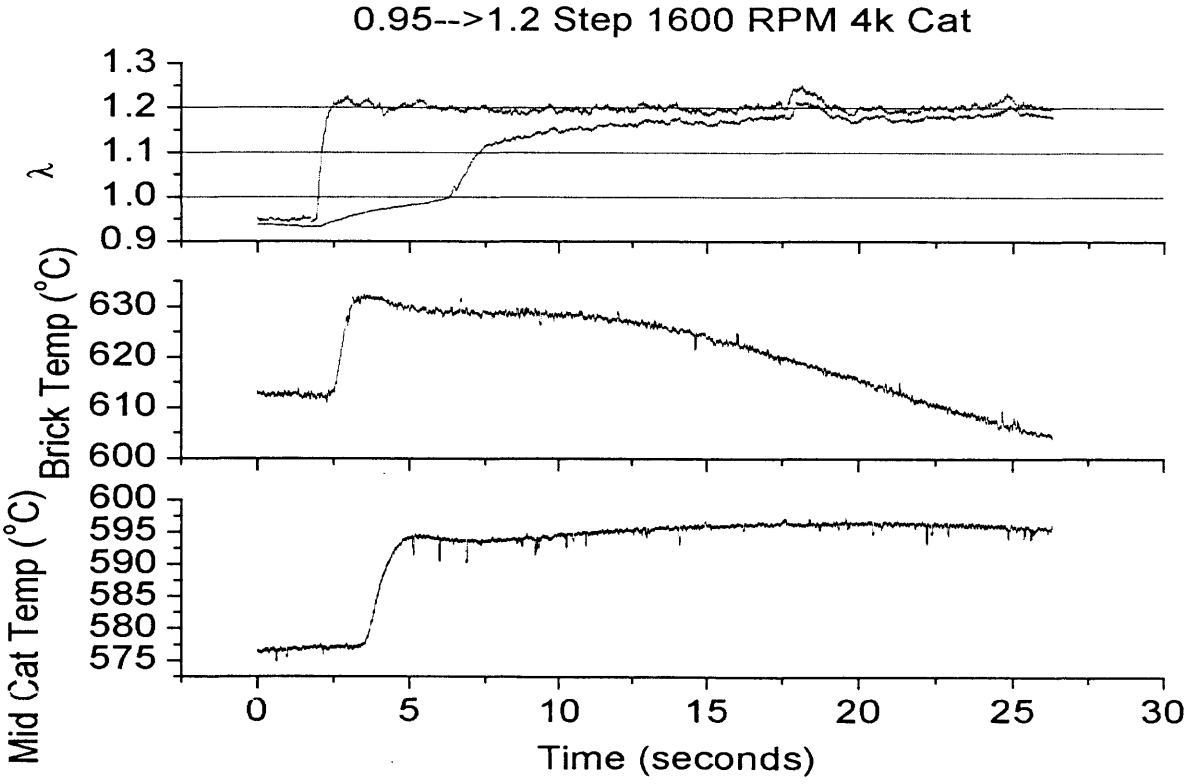

Figure 5.12: 0.95→1.2 Step Catalyst Brick and Mid-Catalyst Temperatures 1600 RPM 4K Catalyst

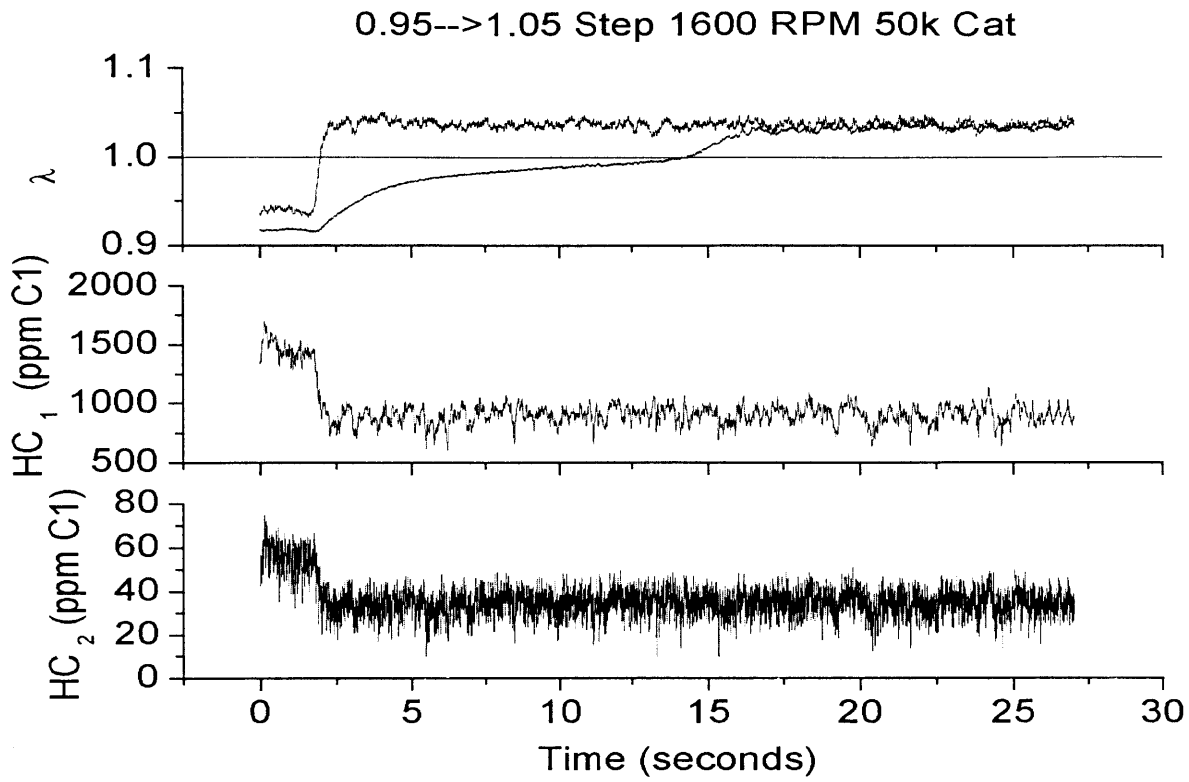

Figure 5.13: 0.95→1.05 Step HC 1600 RPM 50K Catalyst

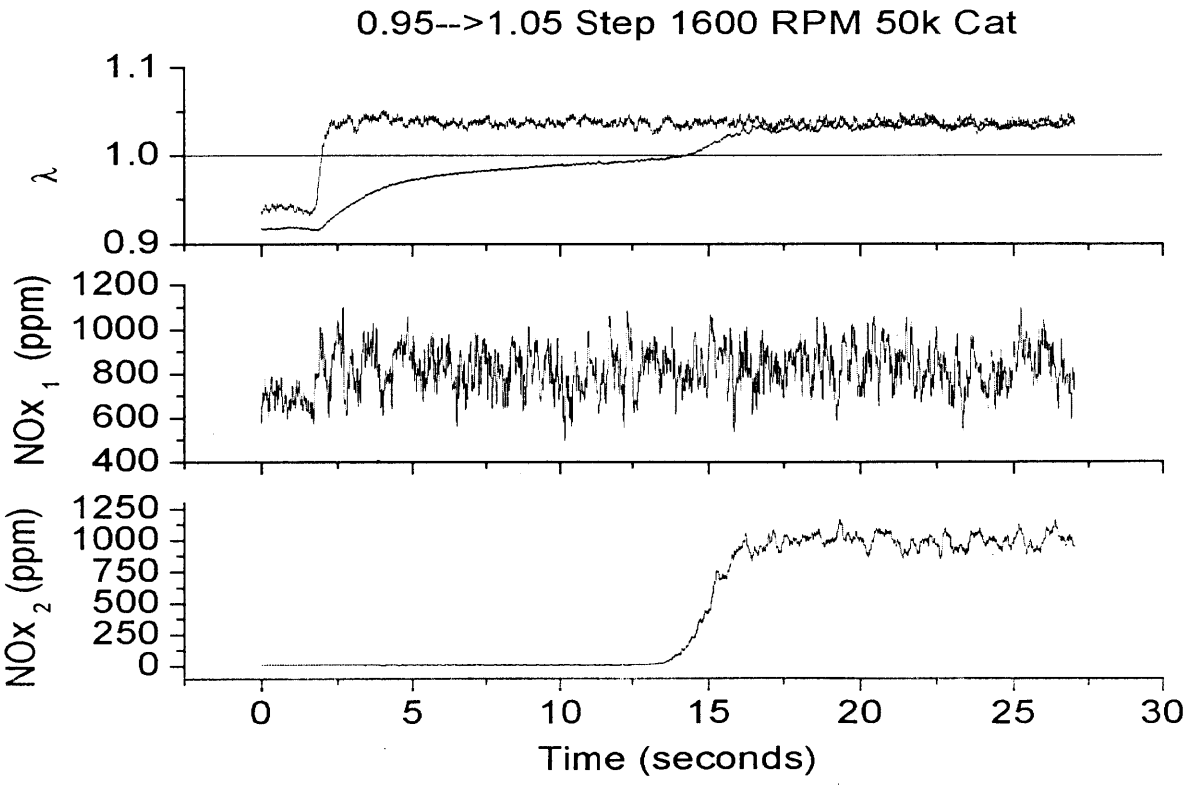

Figure 5.14: 0.95→1.05 Step NOx 1600 RPM 50K Catalyst

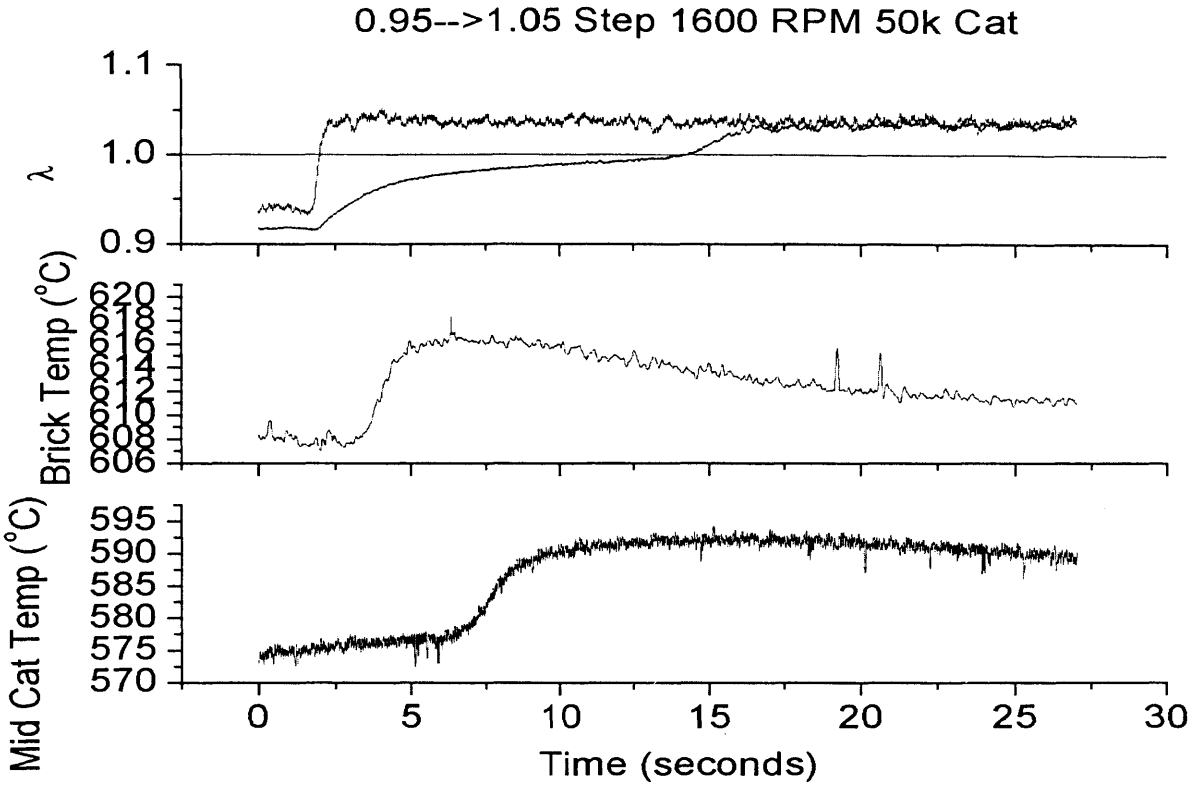

Figure 5.15: 0.95→1.05 Step Catalyst Brick and Mid-Catalyst Temperatures 1600 RPM 50K Catalyst

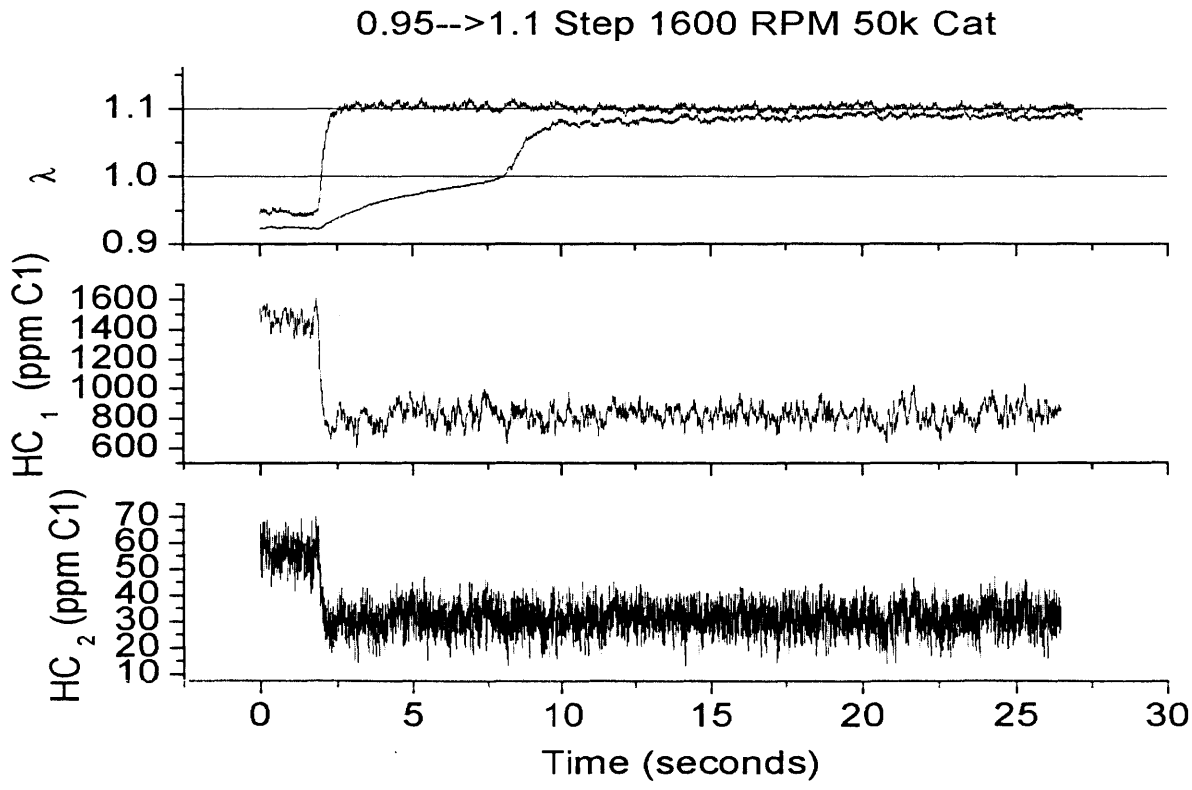

Figure 5.16: 0.95→1.1 Step HC 1600 RPM 50K Catalyst

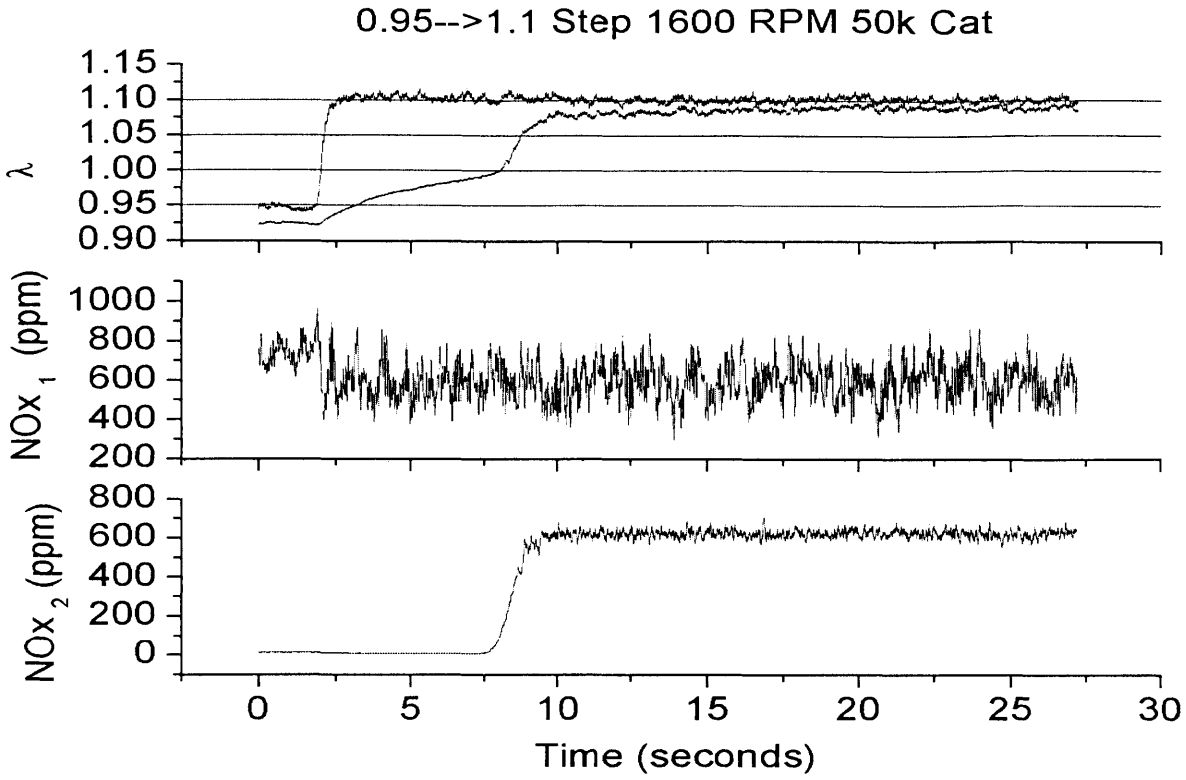

Figure 5.17: 0.95→1.1 Step NOx 1600 RPM 50K Catalyst

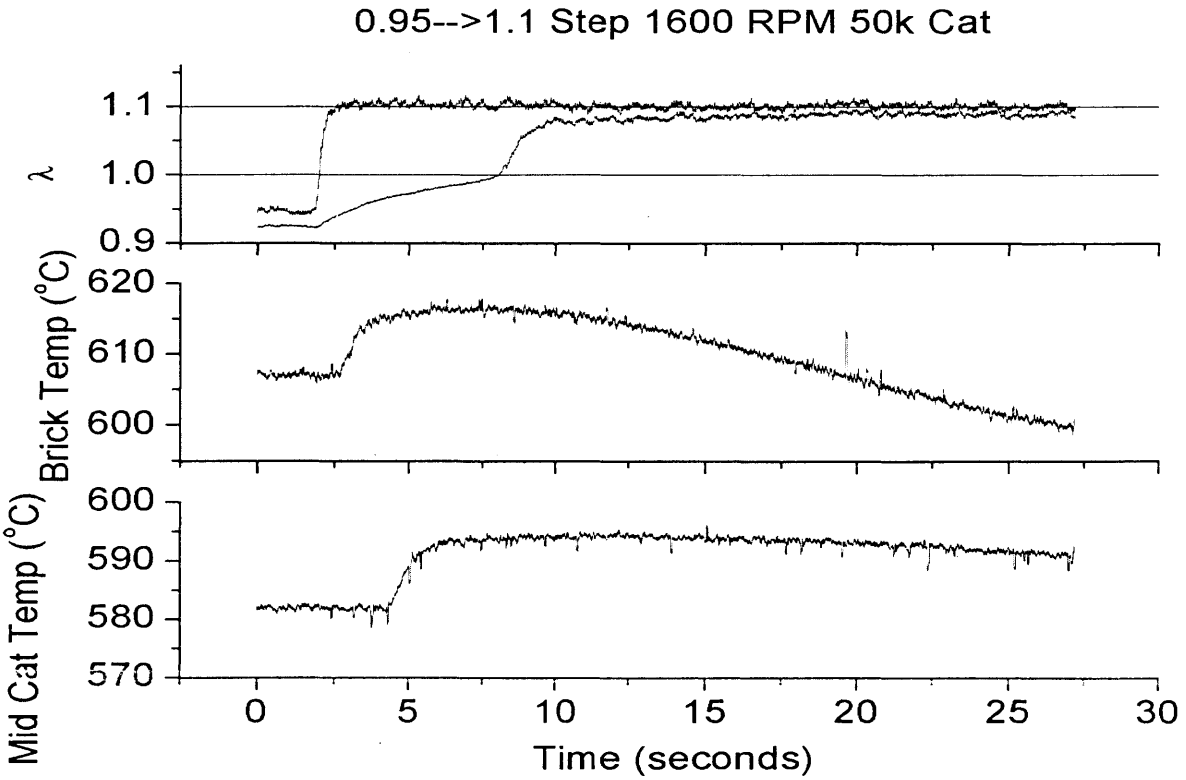

Figure 5.18: 0.95→1.1 Step Catalyst Brick and Mid-Catalyst Temperatures 1600 RPM 50K Catalyst

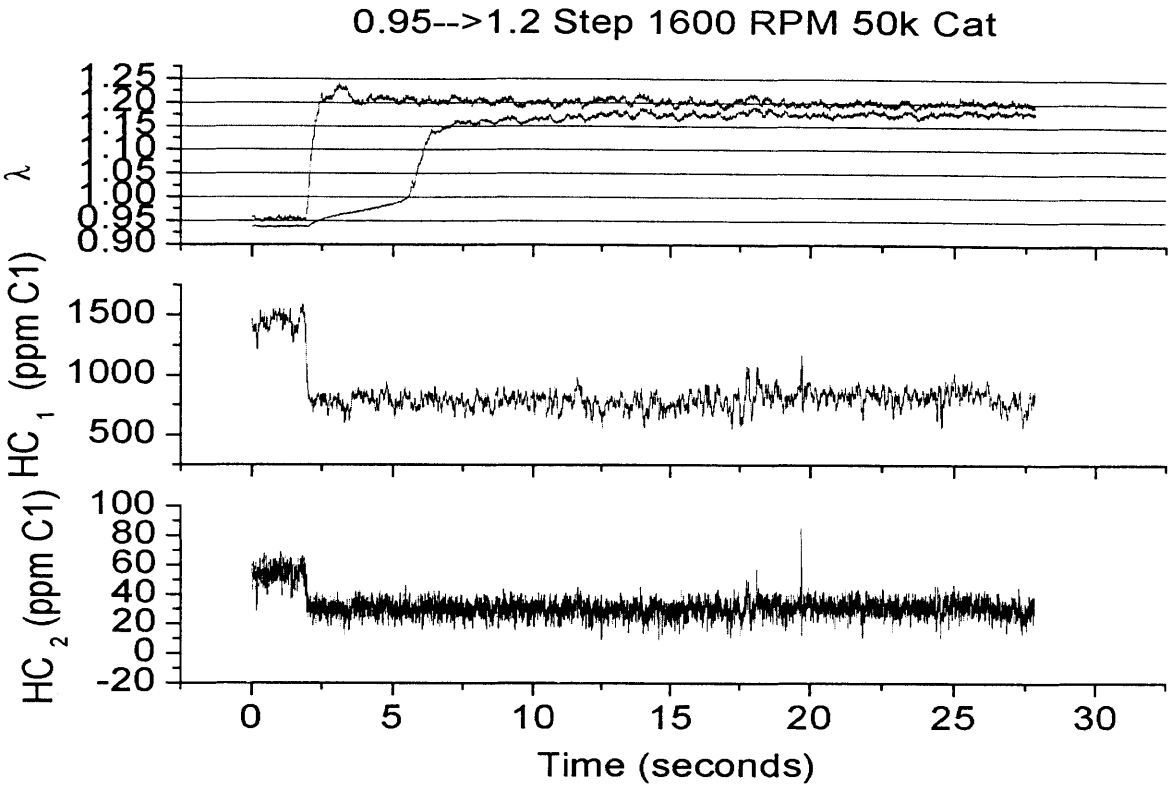

Figure 5.19: 0.95→1.2 Step HC 1600 RPM 50K Catalyst

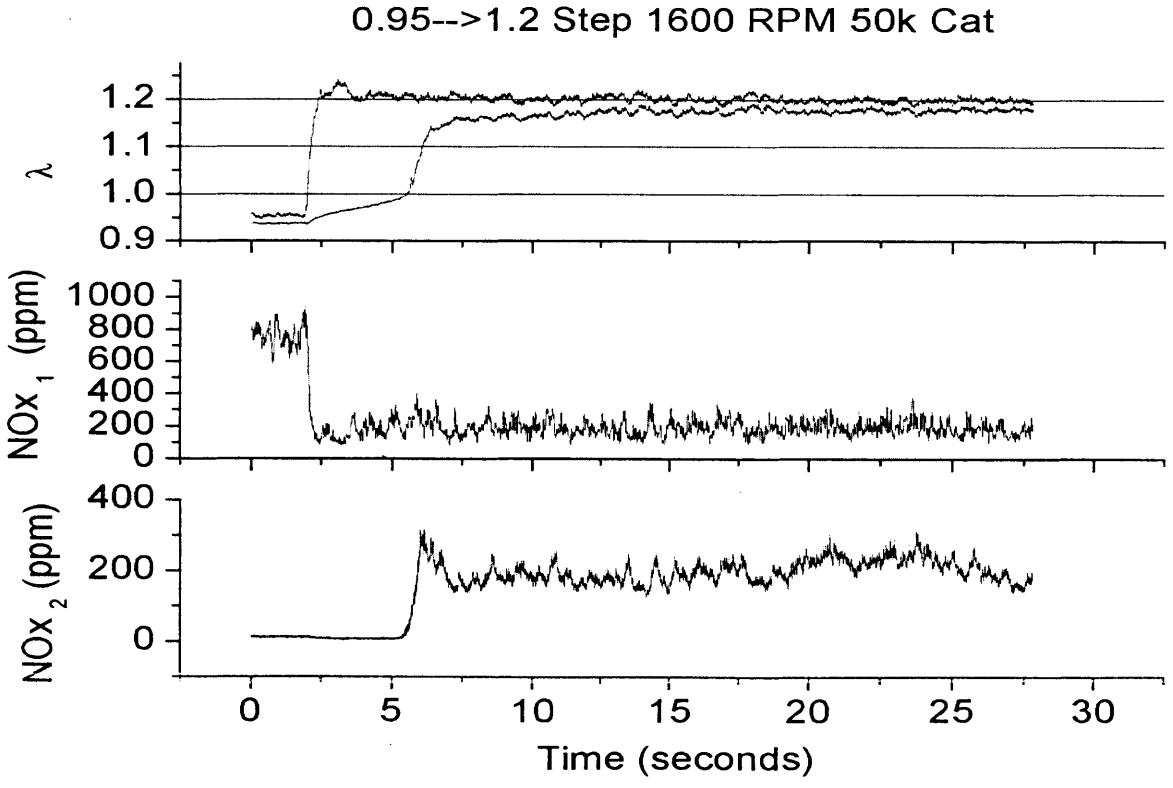

Figure 5.20: 0.95→1.2 Step NOx 1600 RPM 50K Catalyst

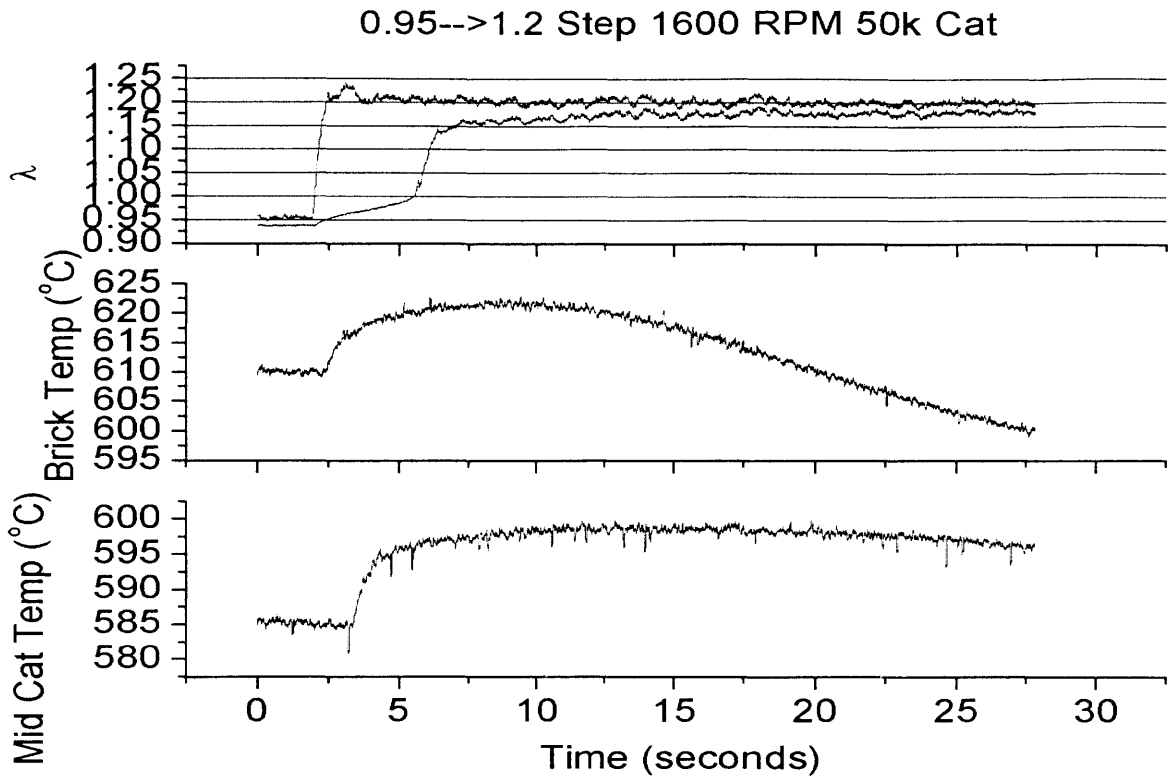

Figure 5.21: 0.95→1.1 Step Catalyst Brick and Mid-Catalyst Temperatures 1600 RPM 50K Catalyst

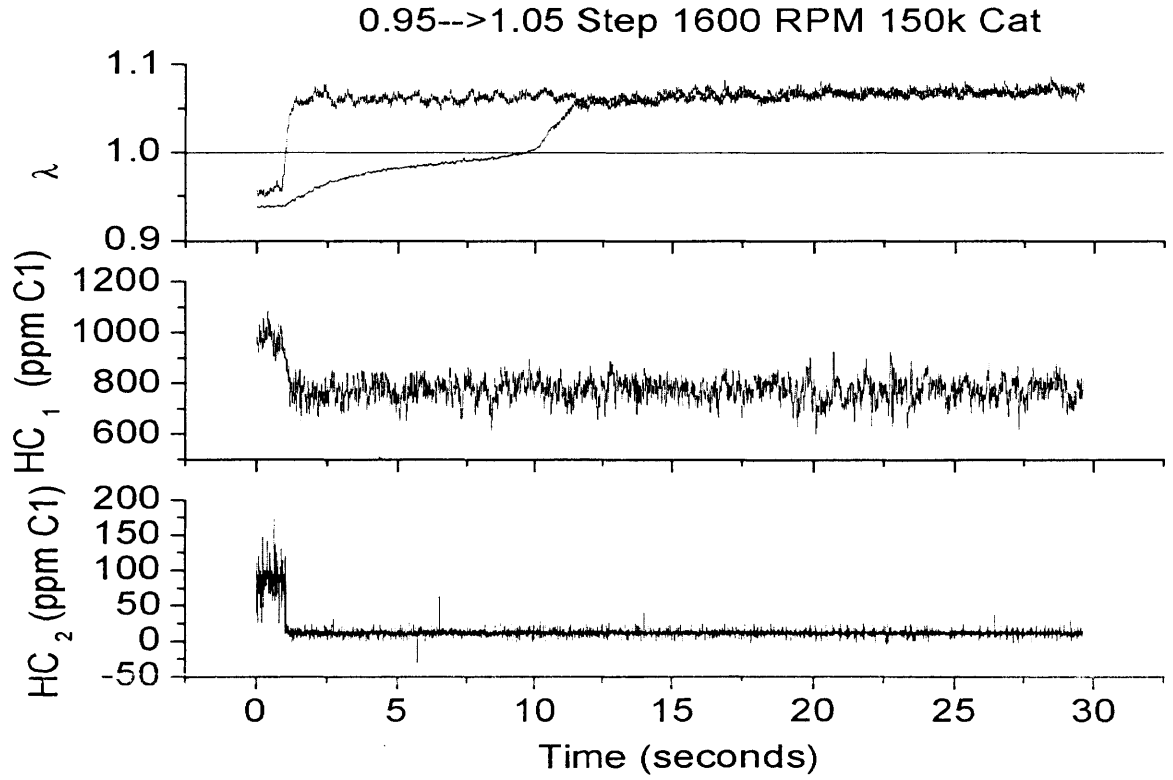

Figure 5.22: 0.95→1.05 Step HC 1600 RPM 150K Catalyst

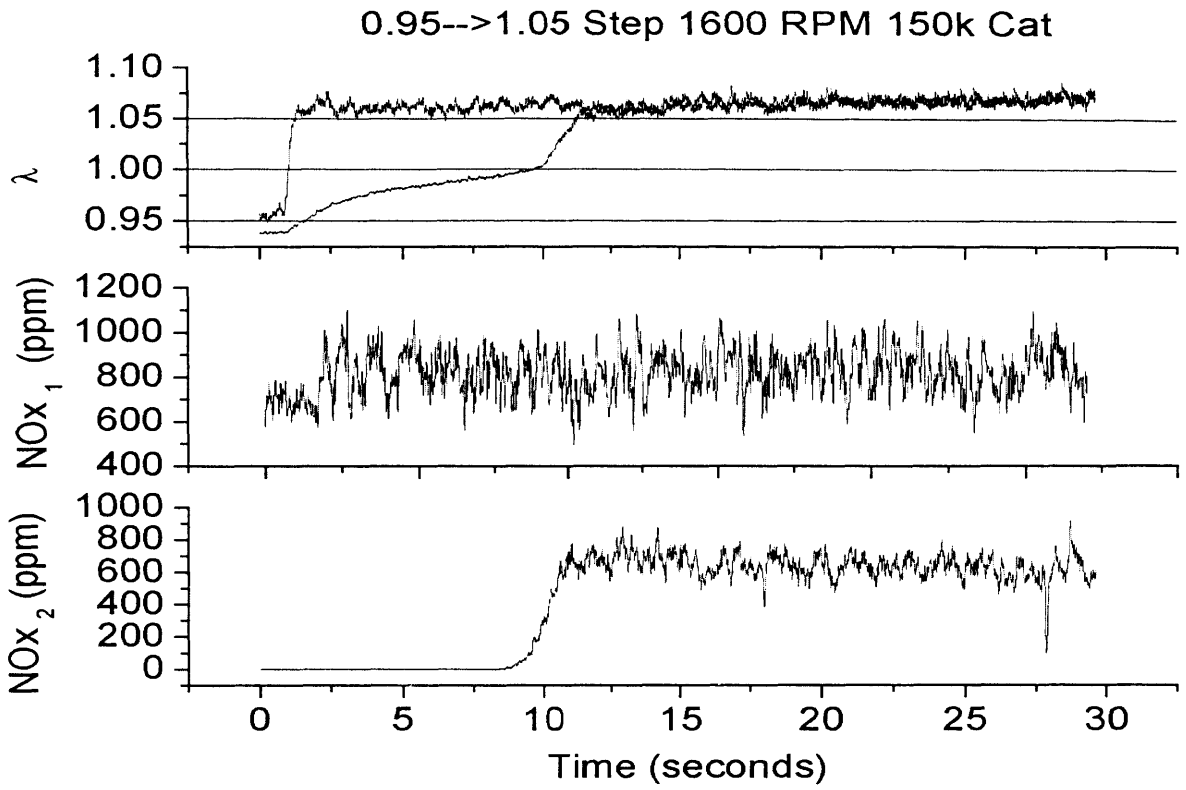

Figure 5.23: 0.95→1.05 Step NOx 1600 RPM 150K Catalyst

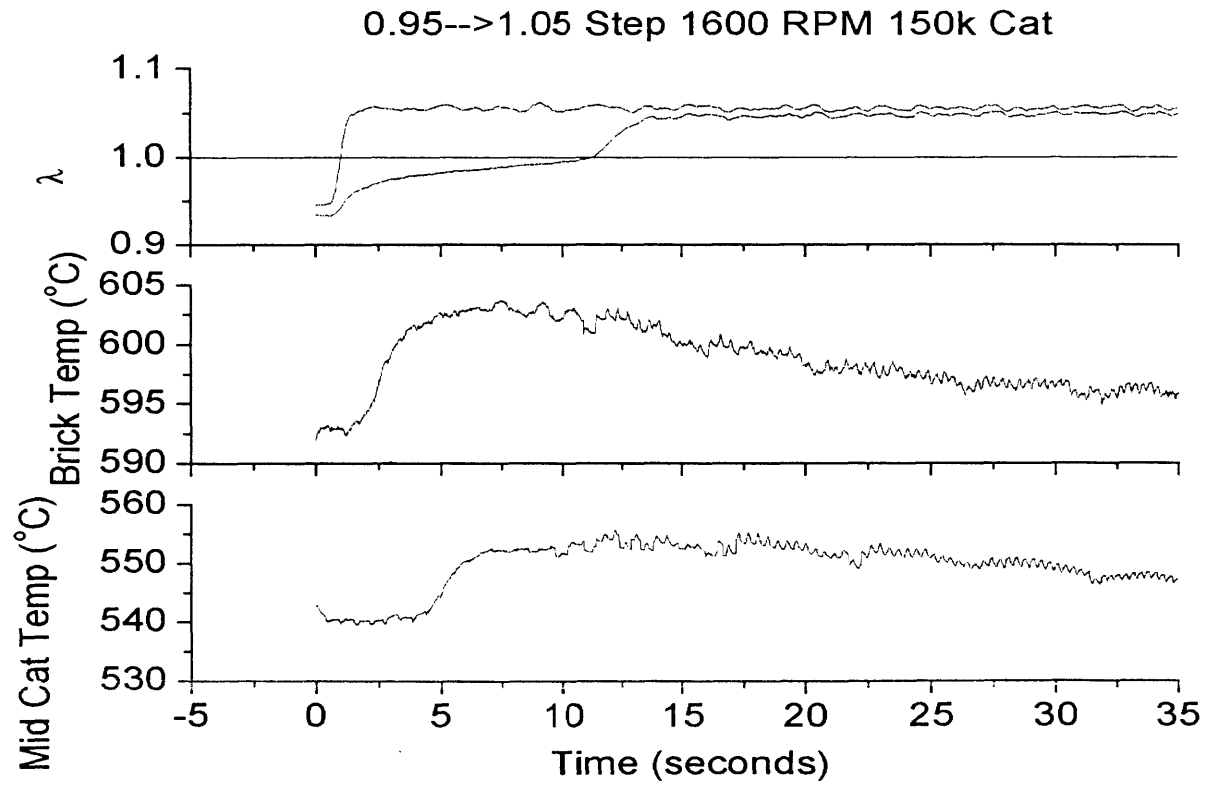

Figure 5.24: 0.95→1.05 Step Catalyst Brick and Mid-Catalyst Temperatures 1600 RPM 150K Catalyst

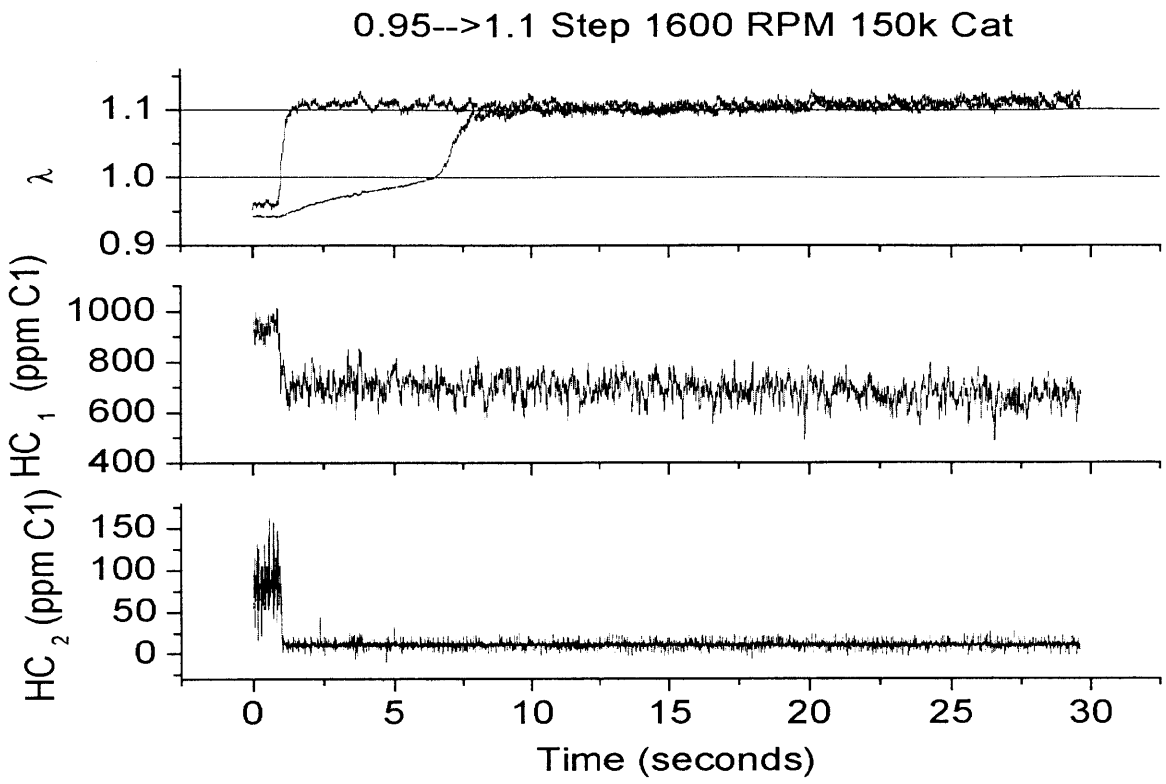

Figure 5.25: 0.95→1.1 Step HC 1600 RPM 150K Catalyst

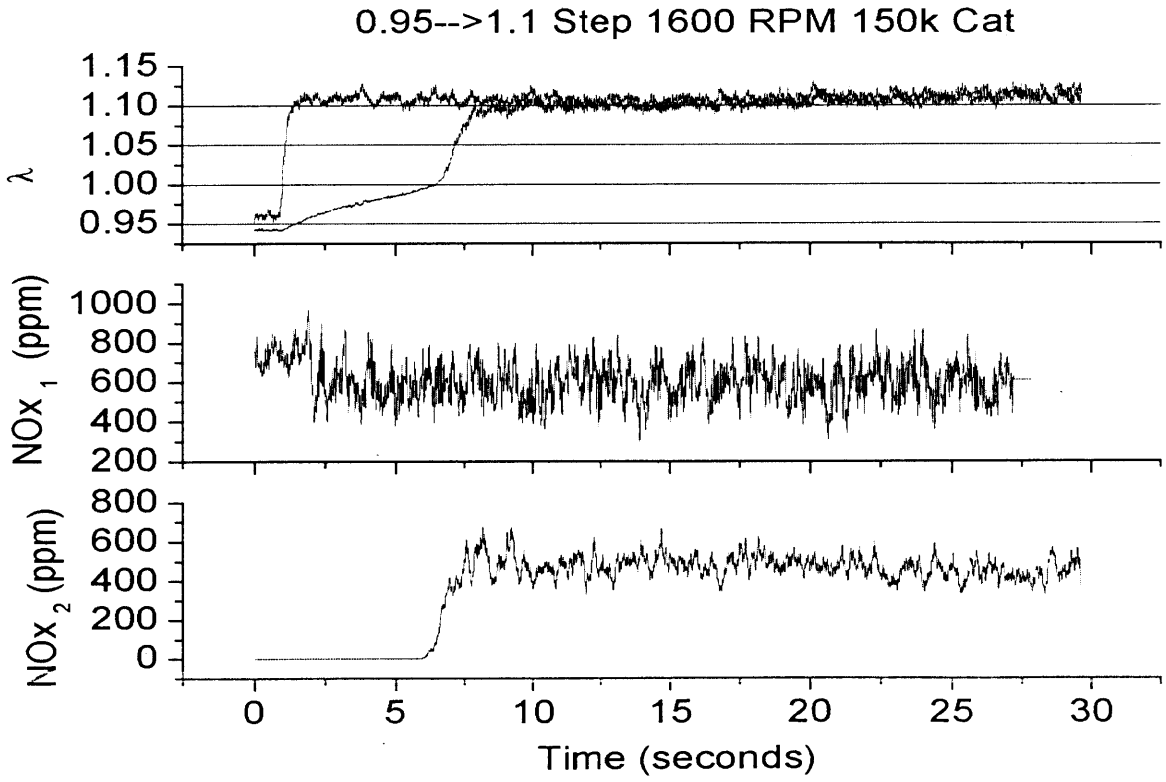

Figure 5.26: 0.95→1.1 Step NOx 1600 RPM 150K Catalyst

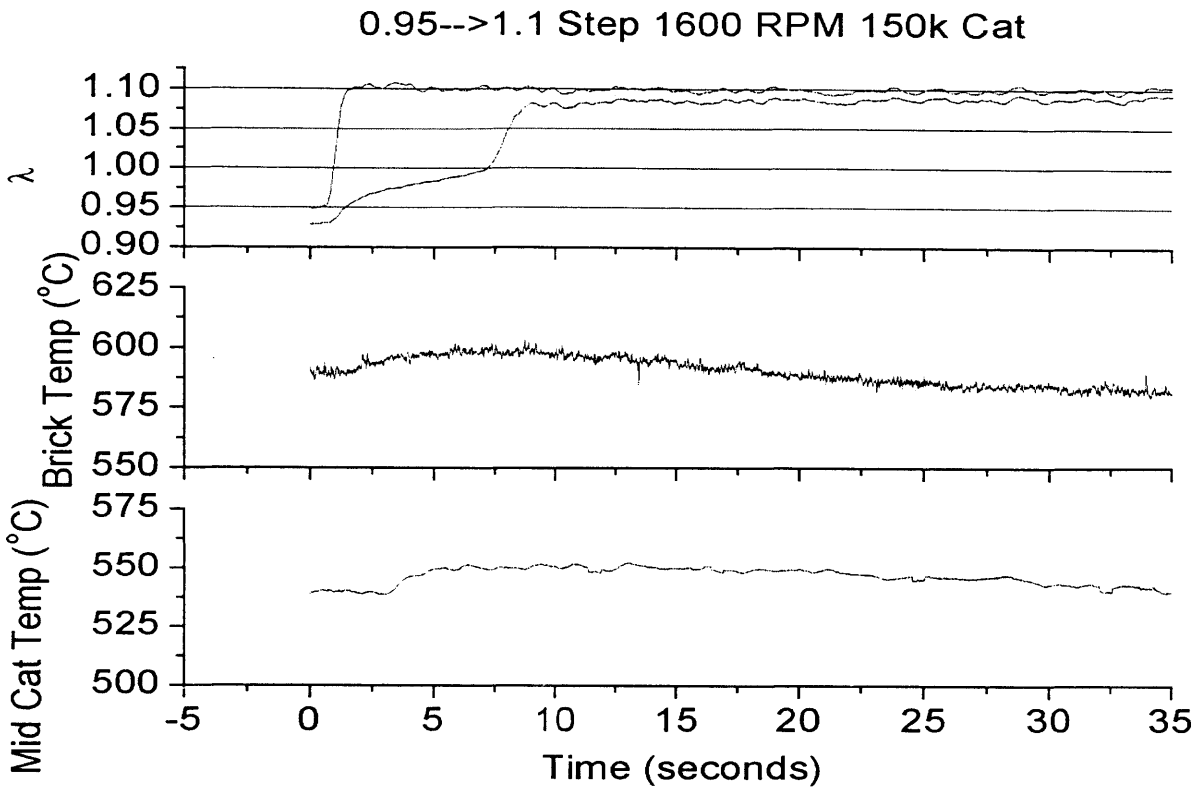

Figure 5.27: 0.95→1.1 Step Catalyst Brick and Mid-Catalyst Temperatures 1600 RPM 150K Catalyst

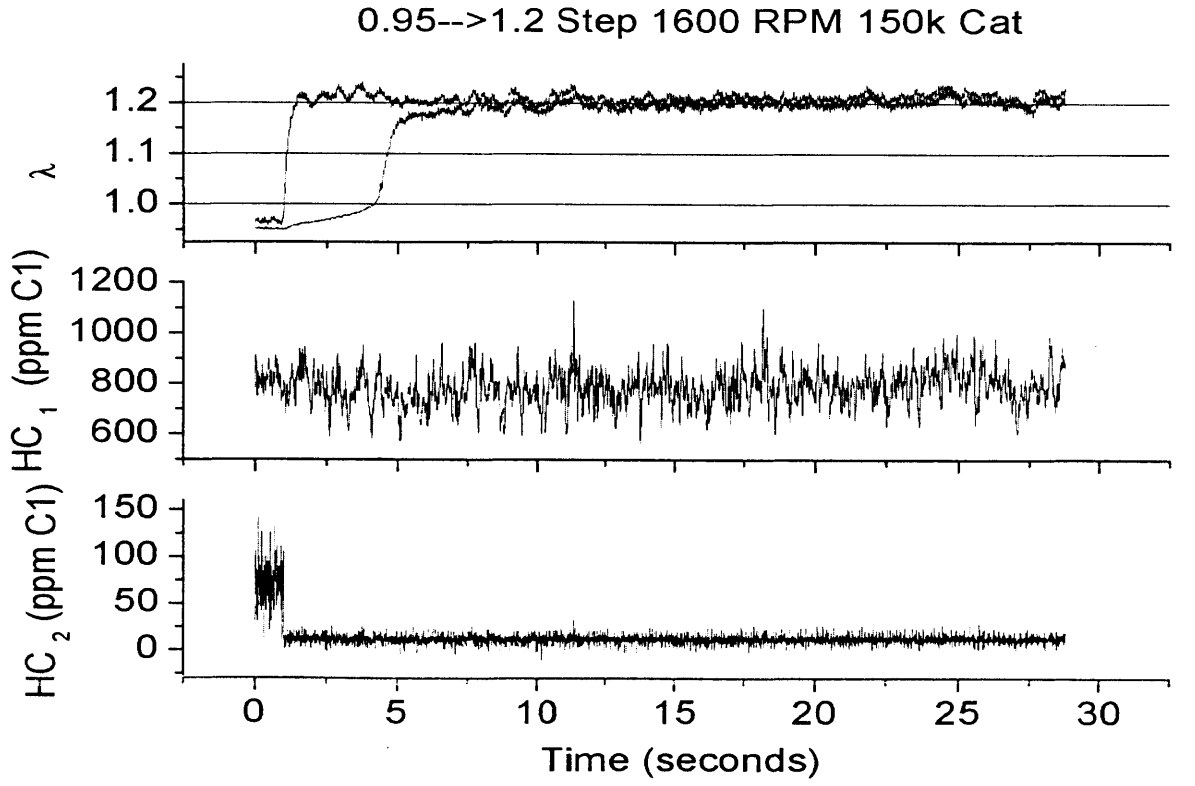

Figure 5.28: 0.95→1.2 Step HC 1600 RPM 150K Catalyst

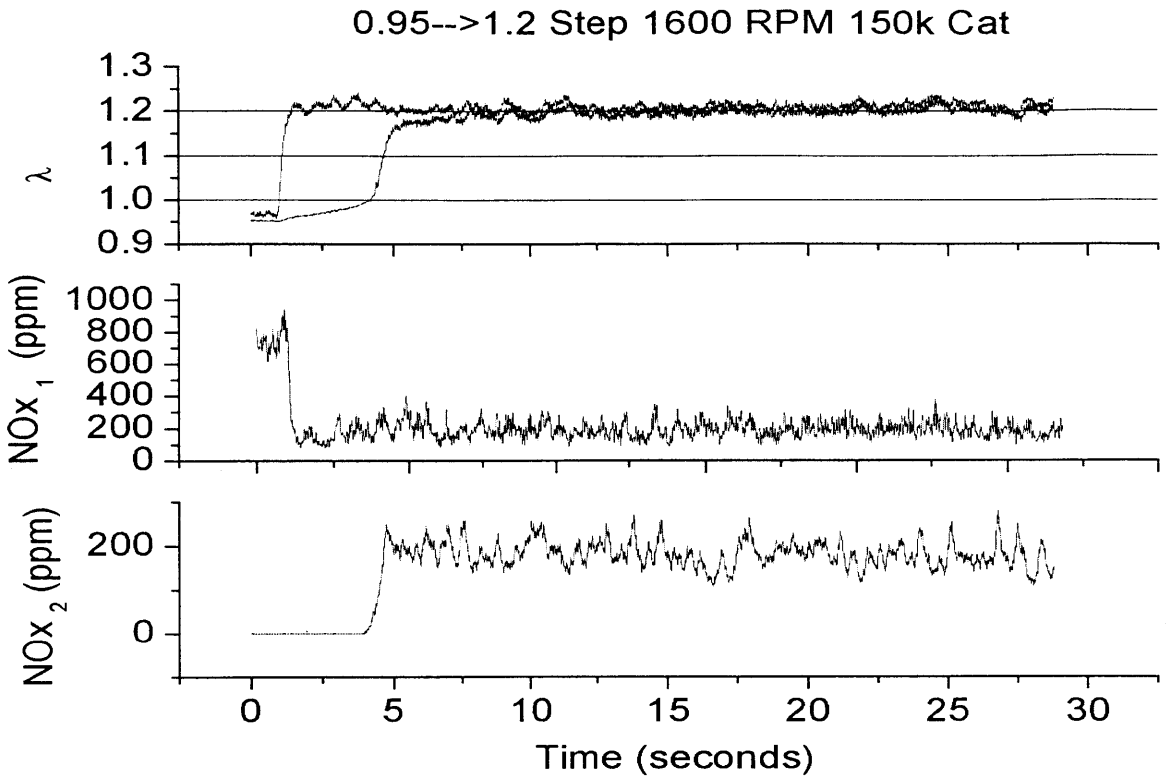

Figure 5.29: 0.95→1.2 Step NOx 1600 RPM 150K Catalyst

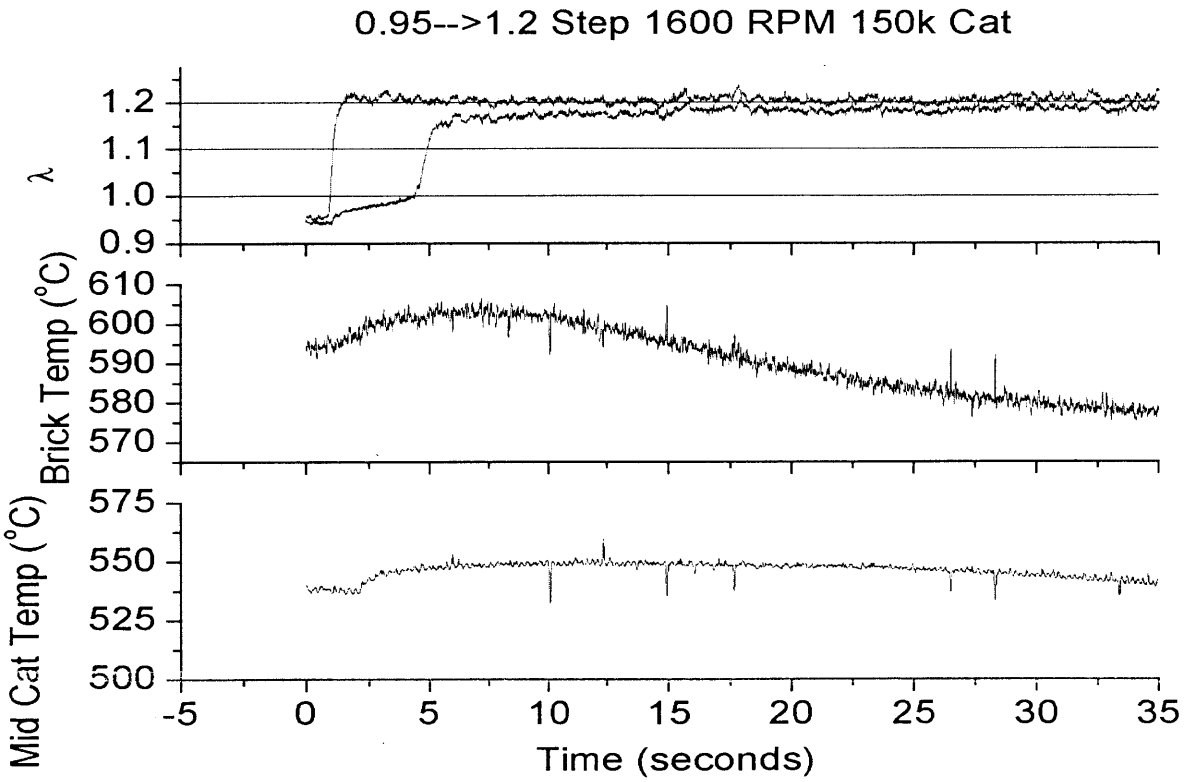

Figure 5.30: 0.95→1.2 Step Catalyst Brick and Mid-Catalyst Temperatures 1600 RPM 150K Catalyst

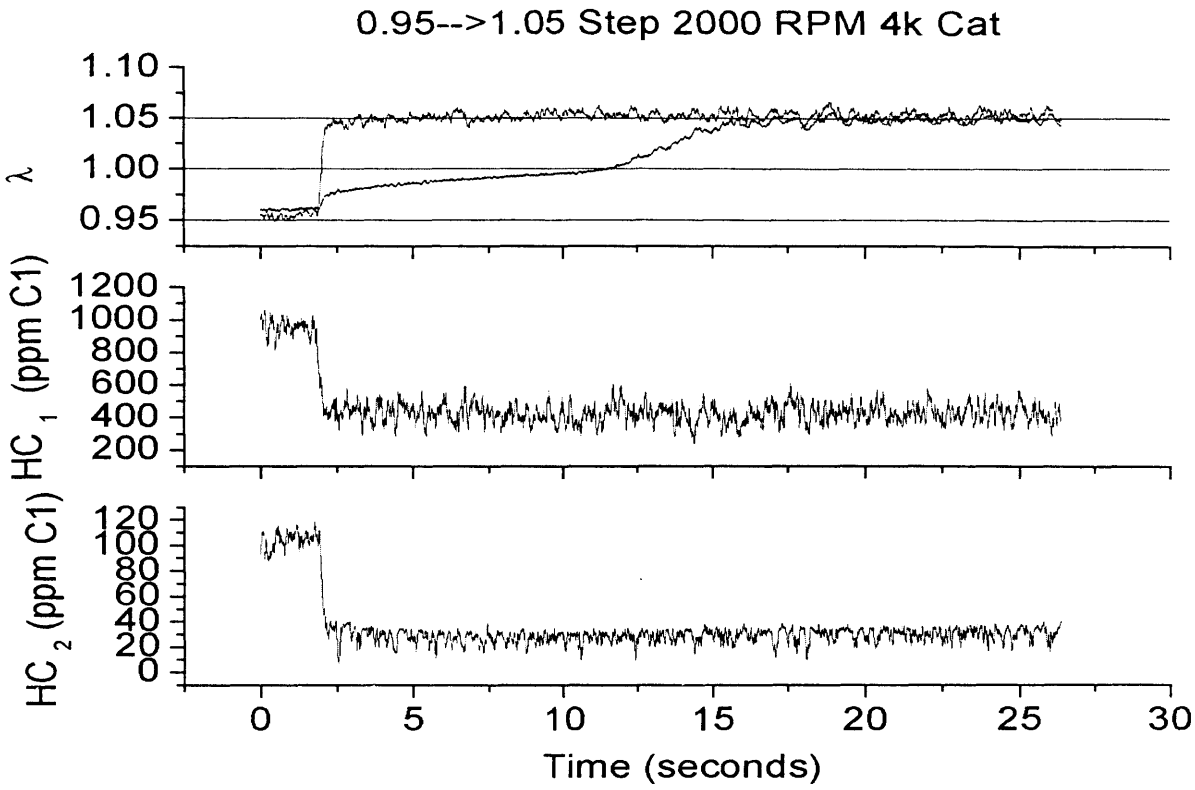

Figure 5.31: 0.95→1.05 Step HC 2000 RPM 4K Catalyst

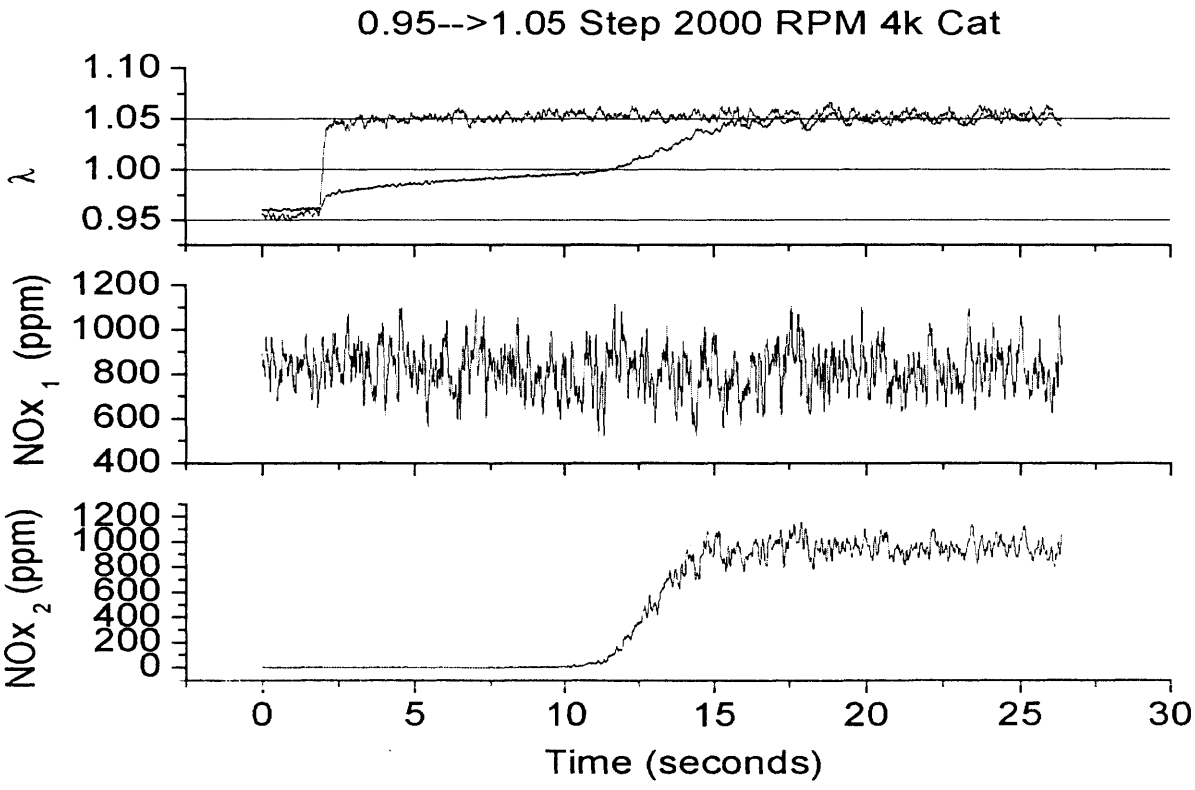

Figure 5.32: 0.95→1.05 Step NOx 2000 RPM 4K Catalyst

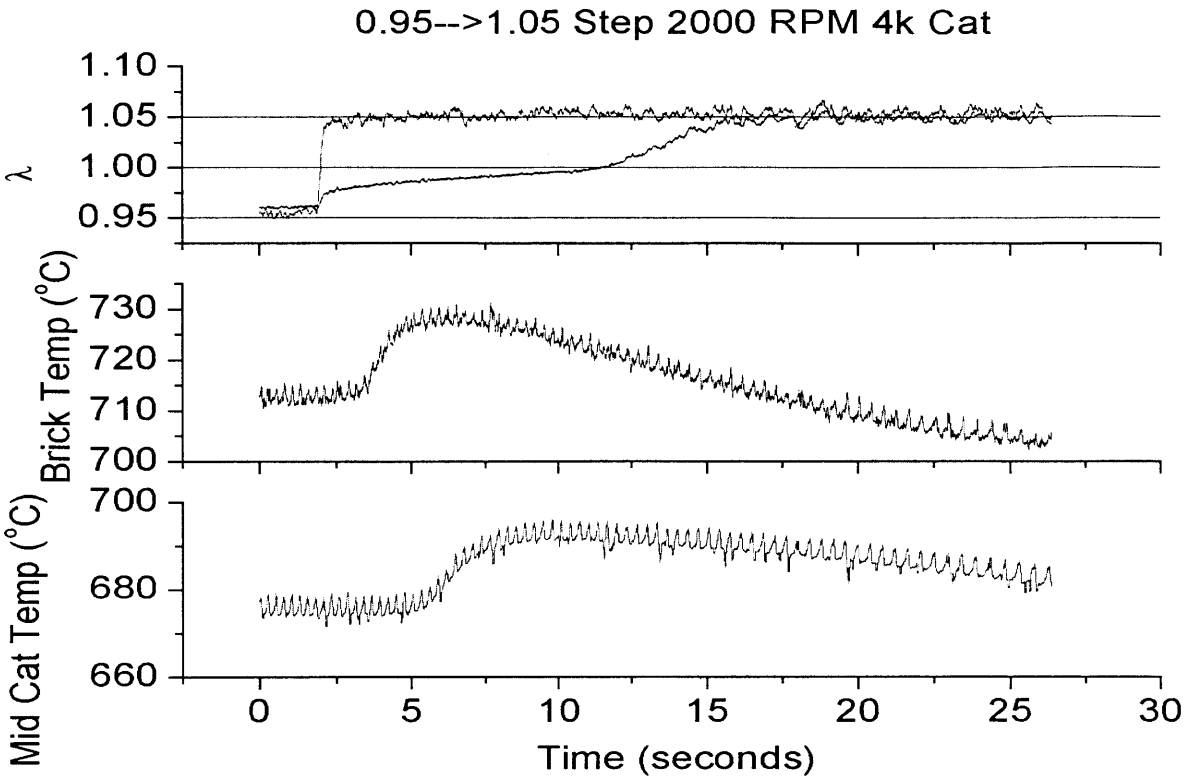

Figure 5.33: 0.95→1.05 Step Catalyst Brick and Mid-Catalyst Temperatures 2000 RPM 4K Catalyst

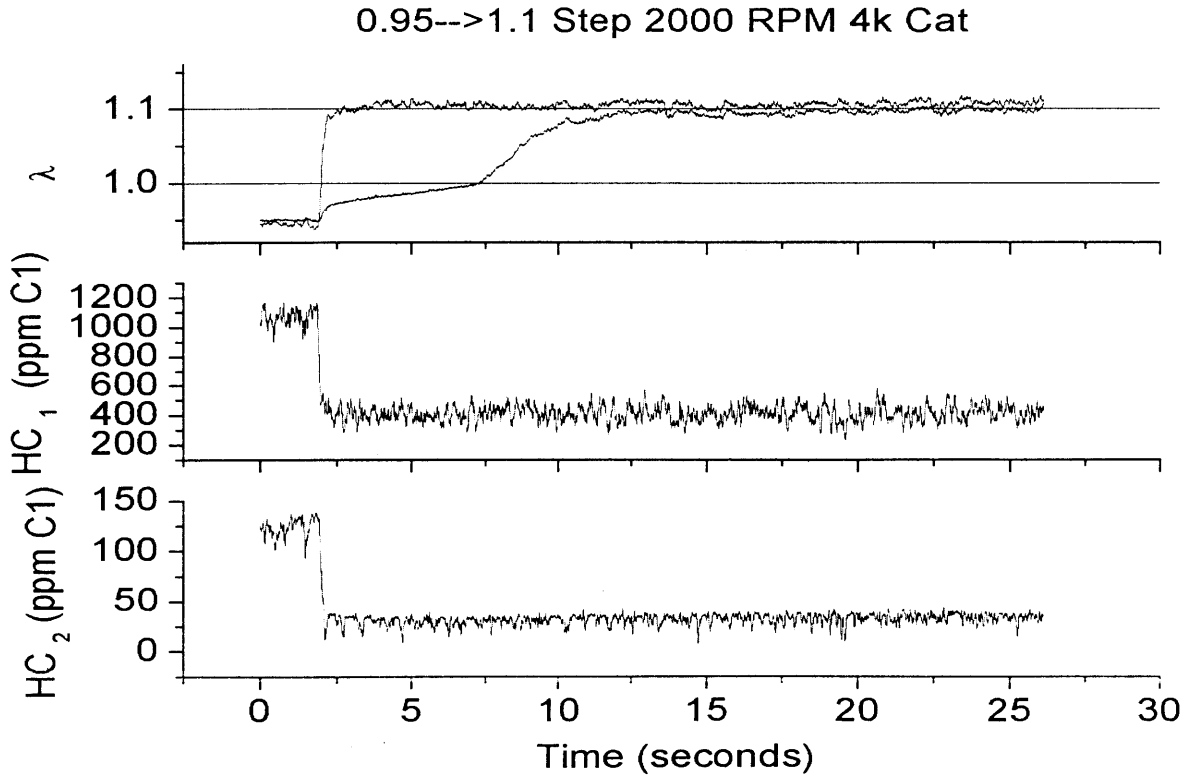

Figure 5.34: 0.95→1.1 Step HC 2000 RPM 4K Catalyst

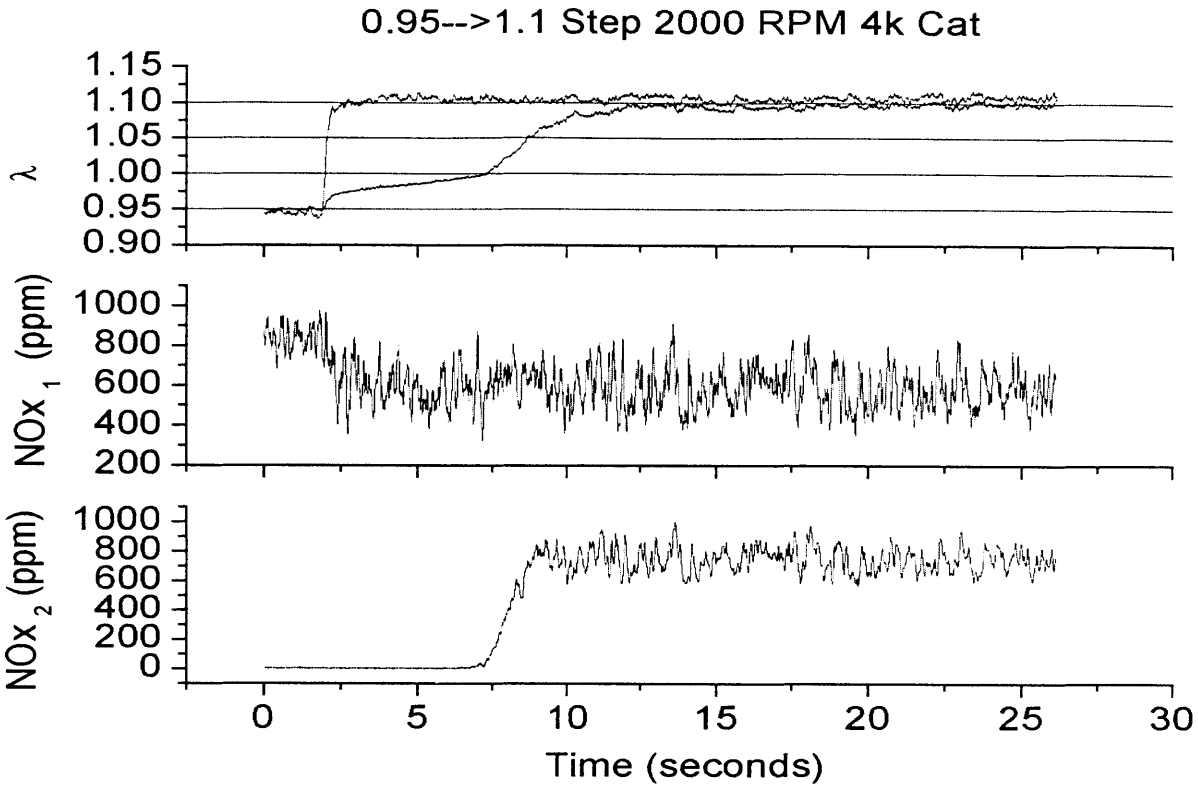

Figure 5.35: 0.95→1.1 Step NOx 2000 RPM 4K Catalyst

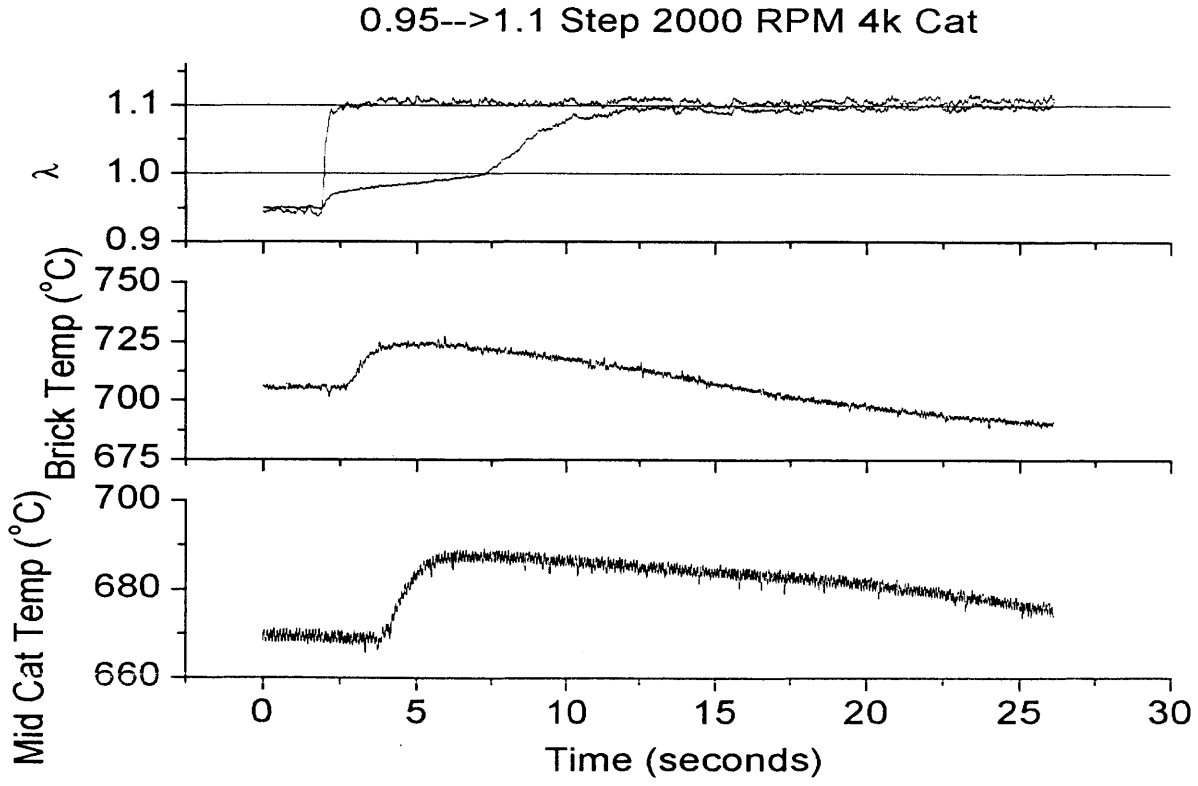

Figure 5.36: 0.95→1.1 Step Catalyst Brick and Mid-Catalyst Temperatures 2000 RPM 4K Catalyst

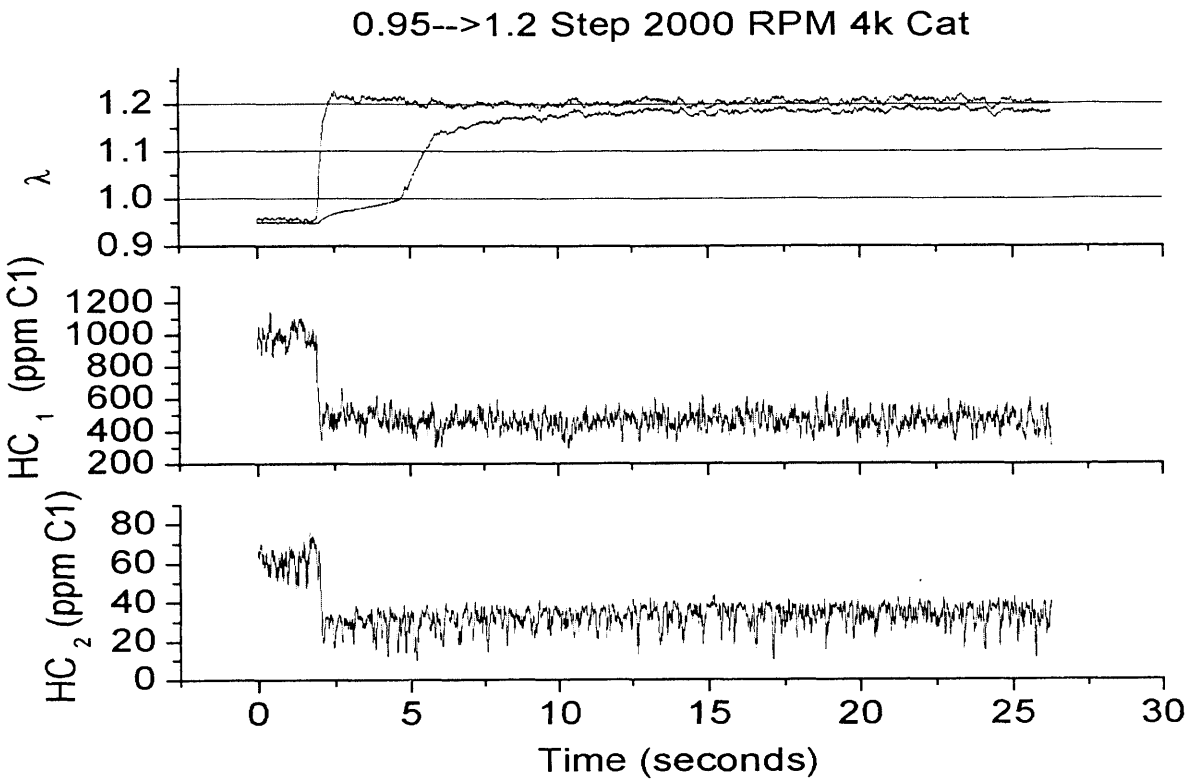

Figure 5.37: 0.95→1.2 Step HC 2000 RPM 4K Catalyst

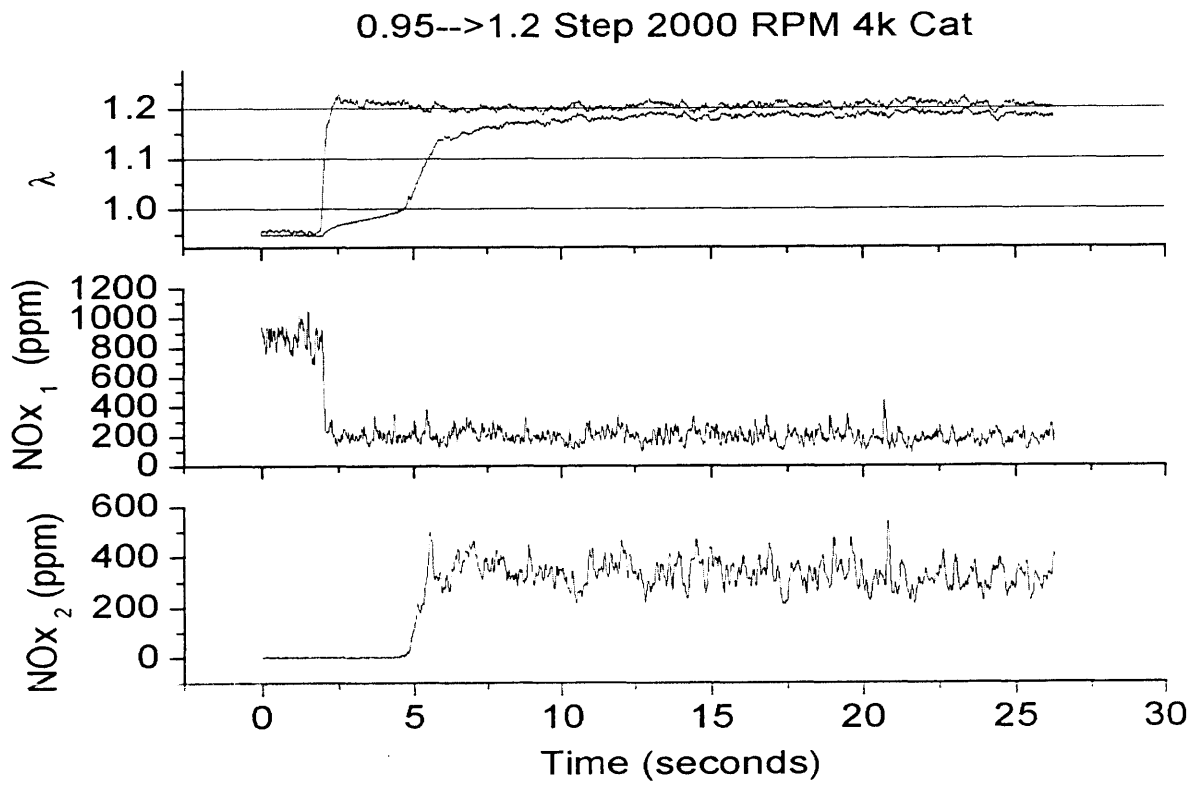

Figure 5.38: 0.95→1.2 Step NOx 2000 RPM 4K Catalyst

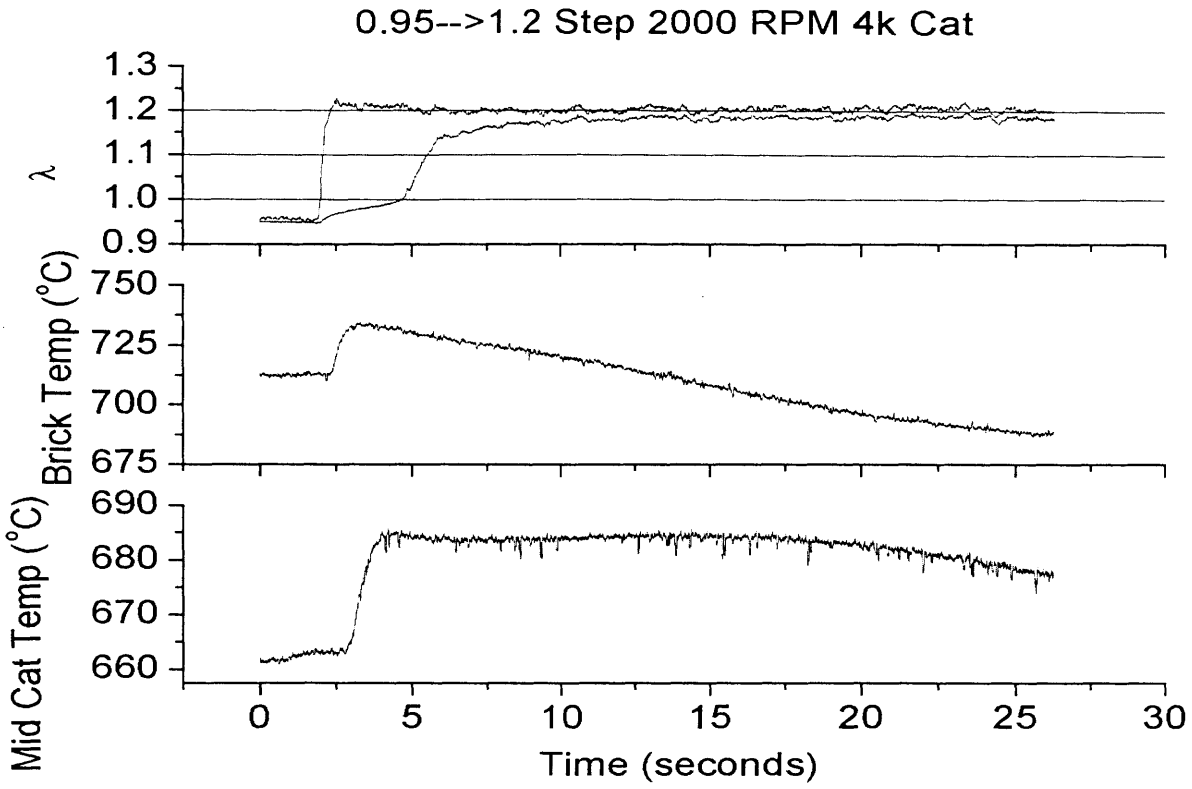

Figure 5.39: 0.95→1.2 Step Catalyst Brick and Mid-Catalyst Temperatures 2000 RPM 4K Catalyst

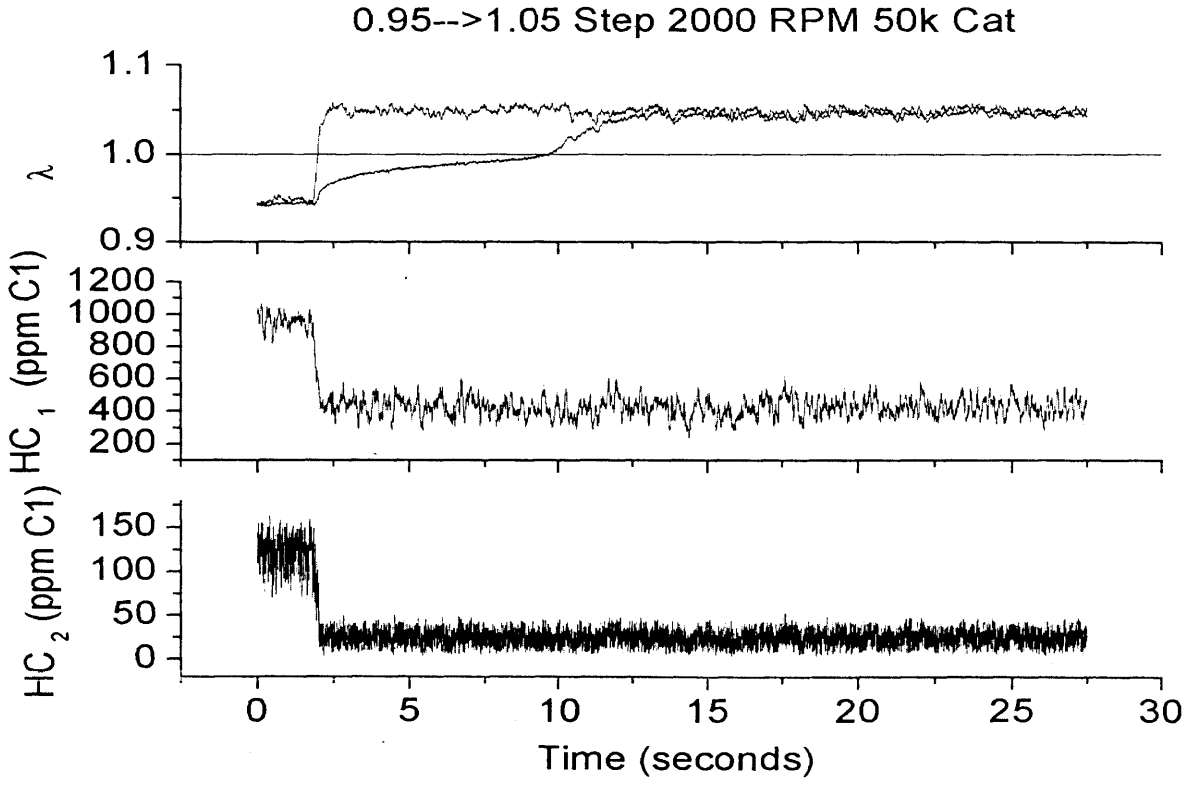

Figure 5.40: 0.95→1.05 Step HC 2000 RPM 150K Catalyst

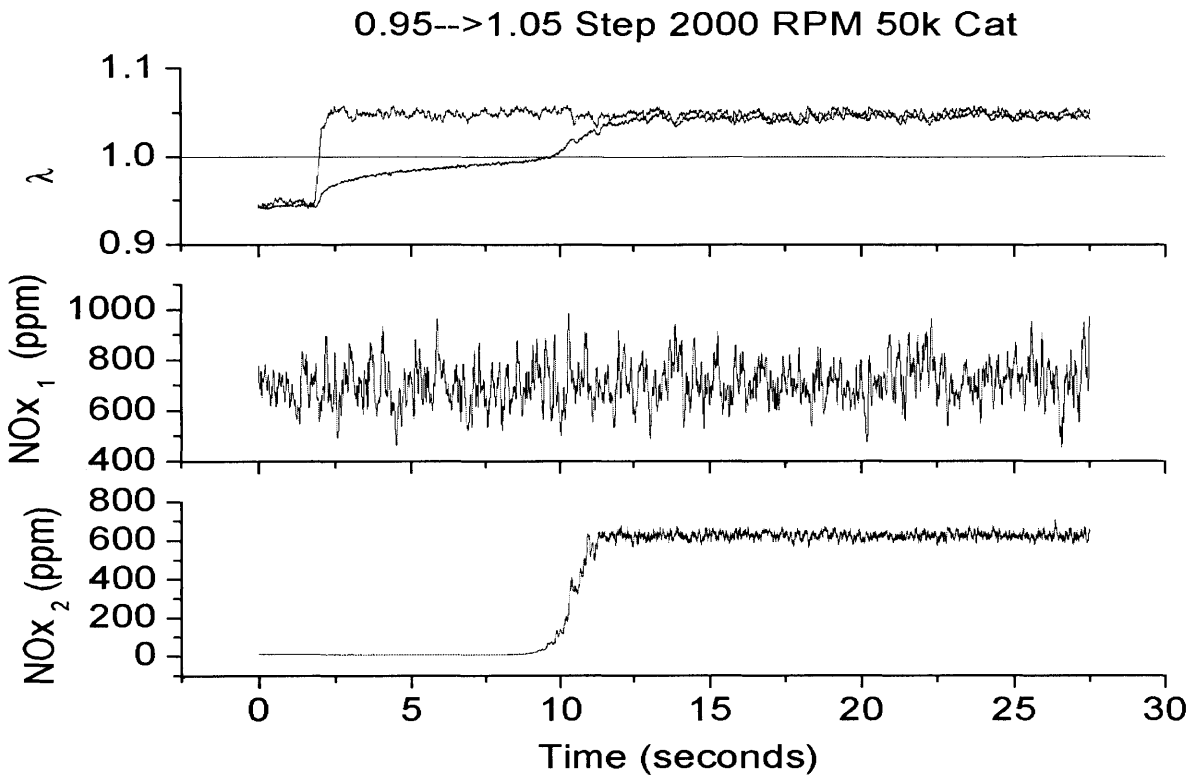

Figure 5.41: 0.95→1.05 Step NOx 2000 RPM 50K Catalyst

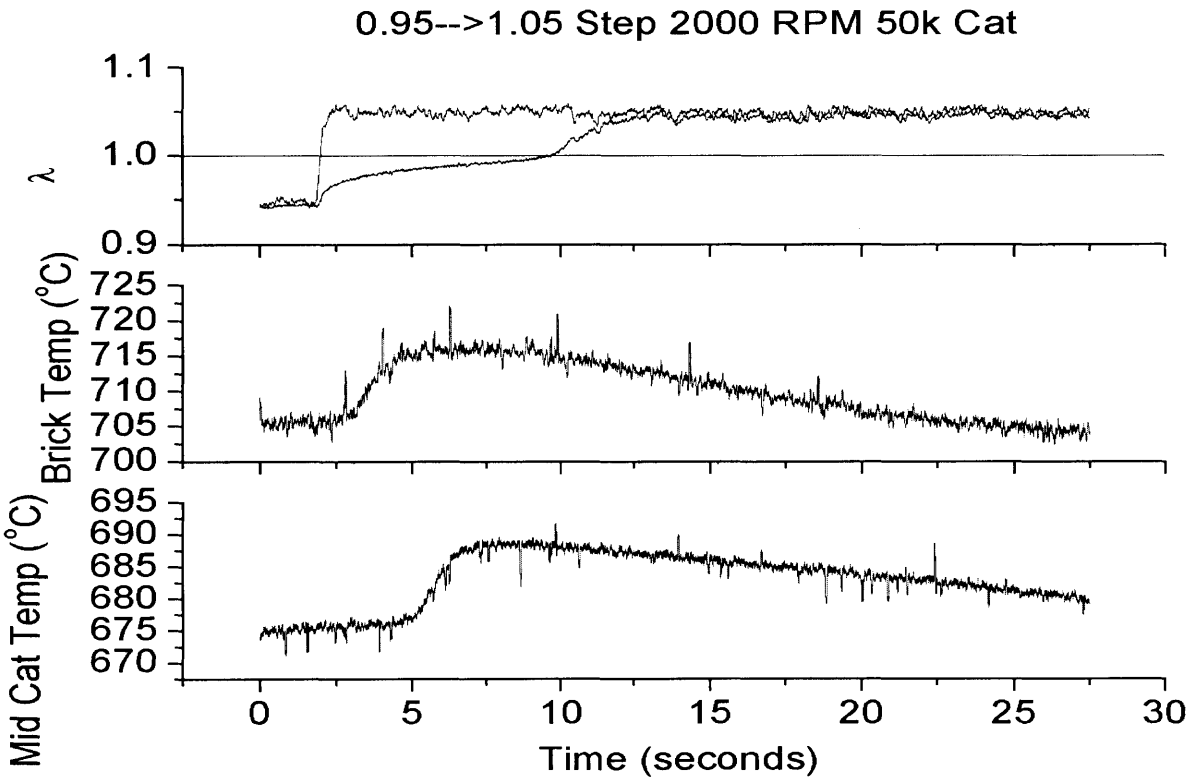

Figure 5.42: 0.95→1.05 Step Catalyst Brick and Mid-Catalyst Temperatures 2000 RPM 50K Catalyst

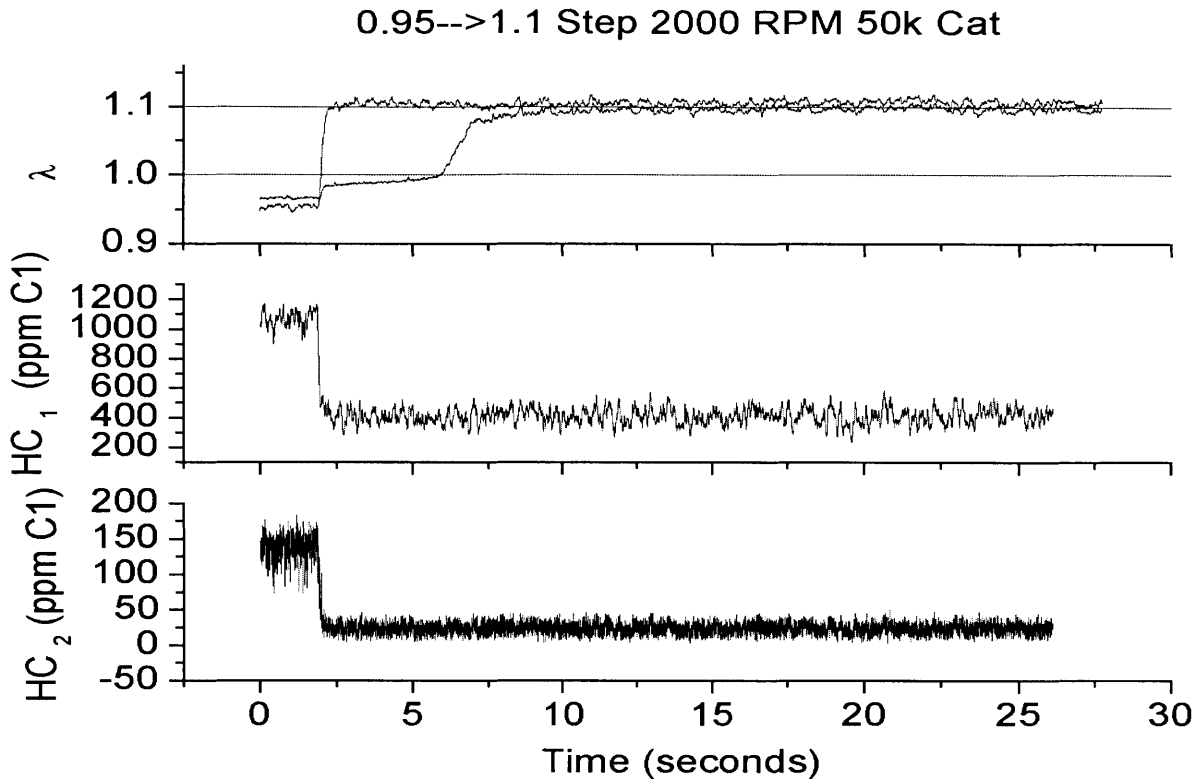

Figure 5.43: 0.95→1.1 Step HC 2000 RPM 50K Catalyst

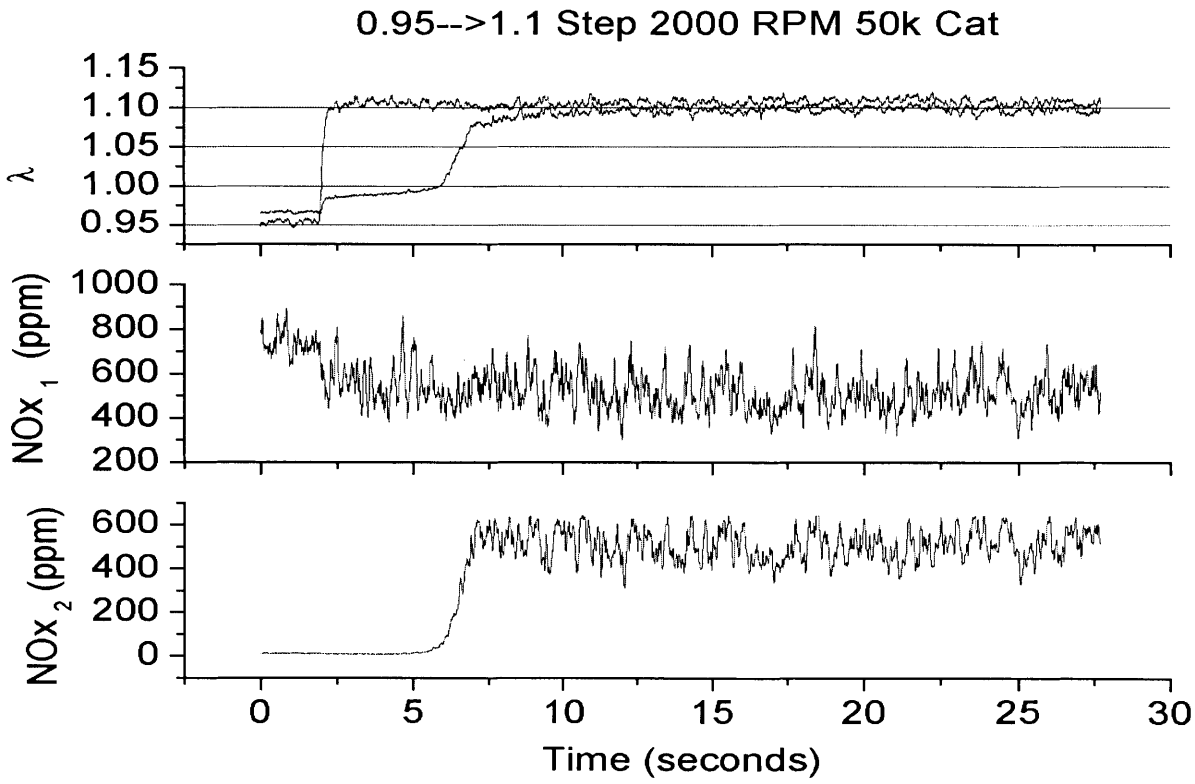

Figure 5.44: 0.95→1.1 Step NOx 2000 RPM 50K Catalyst

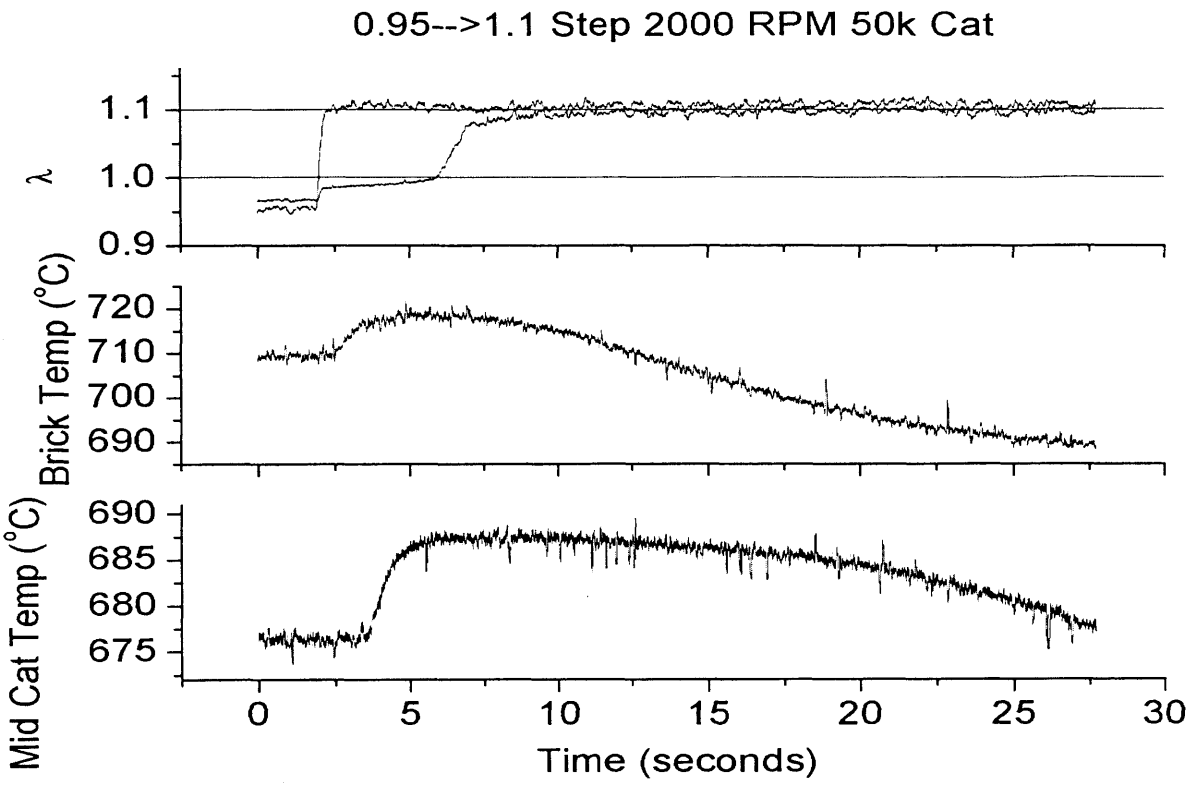

Figure 5.45: 0.95→1.1 Step Catalyst Brick and Mid-Catalyst Temperatures 2000 RPM 50K Catalyst

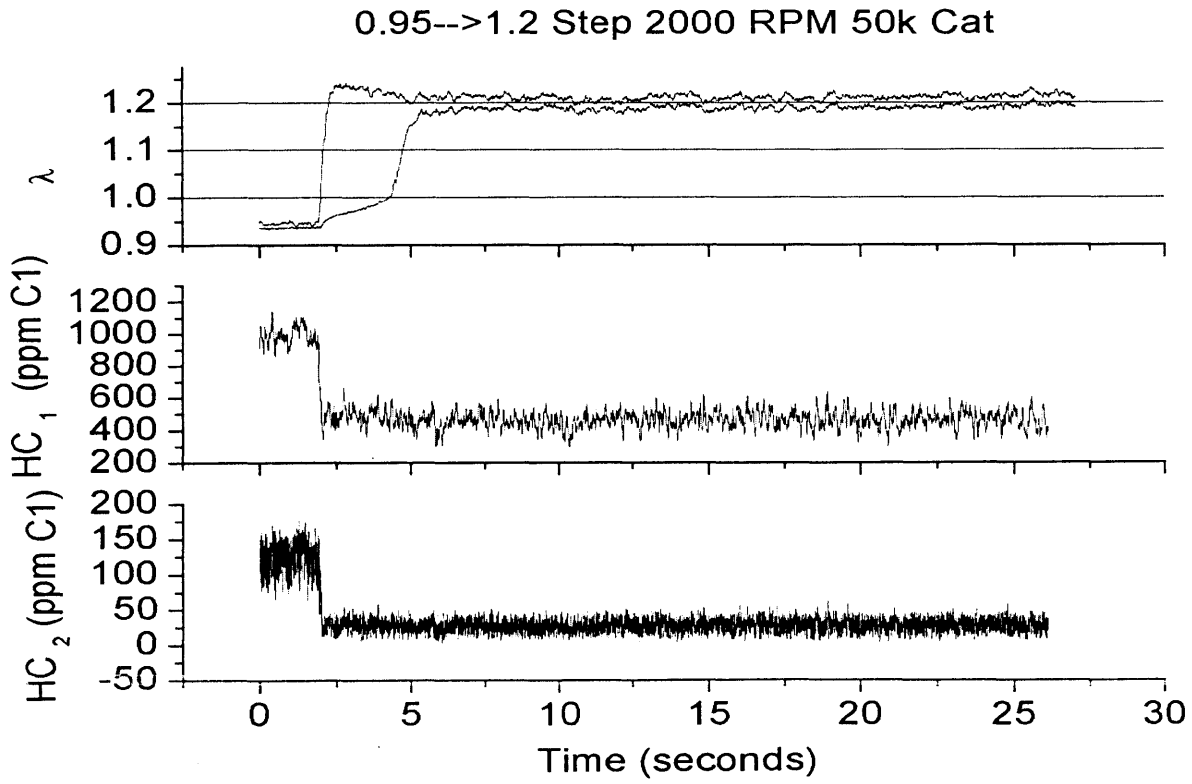

Figure 5.46: 0.95→1.2 Step HC 2000 RPM 50K Catalyst

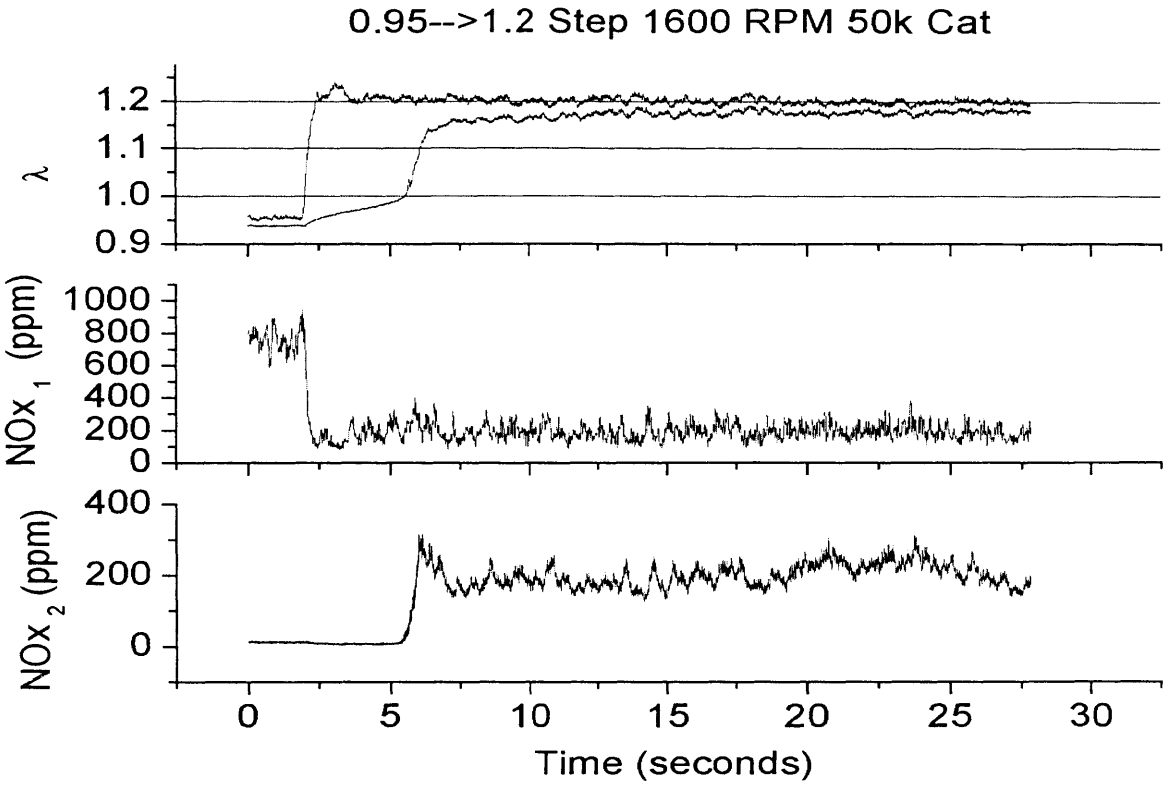

Figure 5.47: 0.95→1.2 Step NOx 2000 RPM 150K Catalyst

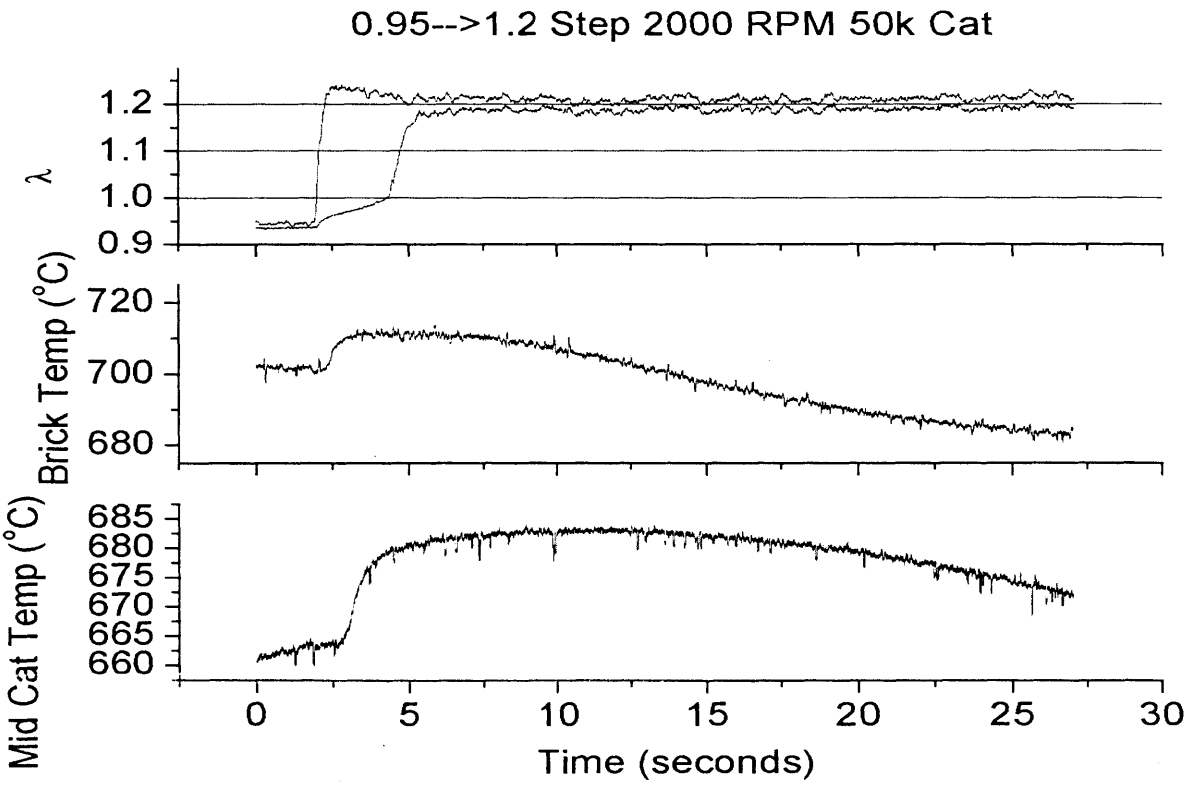

Figure 5.48: 0.95→1.2 Step Catalyst Brick and Mid-Catalyst Temperatures 2000 RPM 50K Catalyst

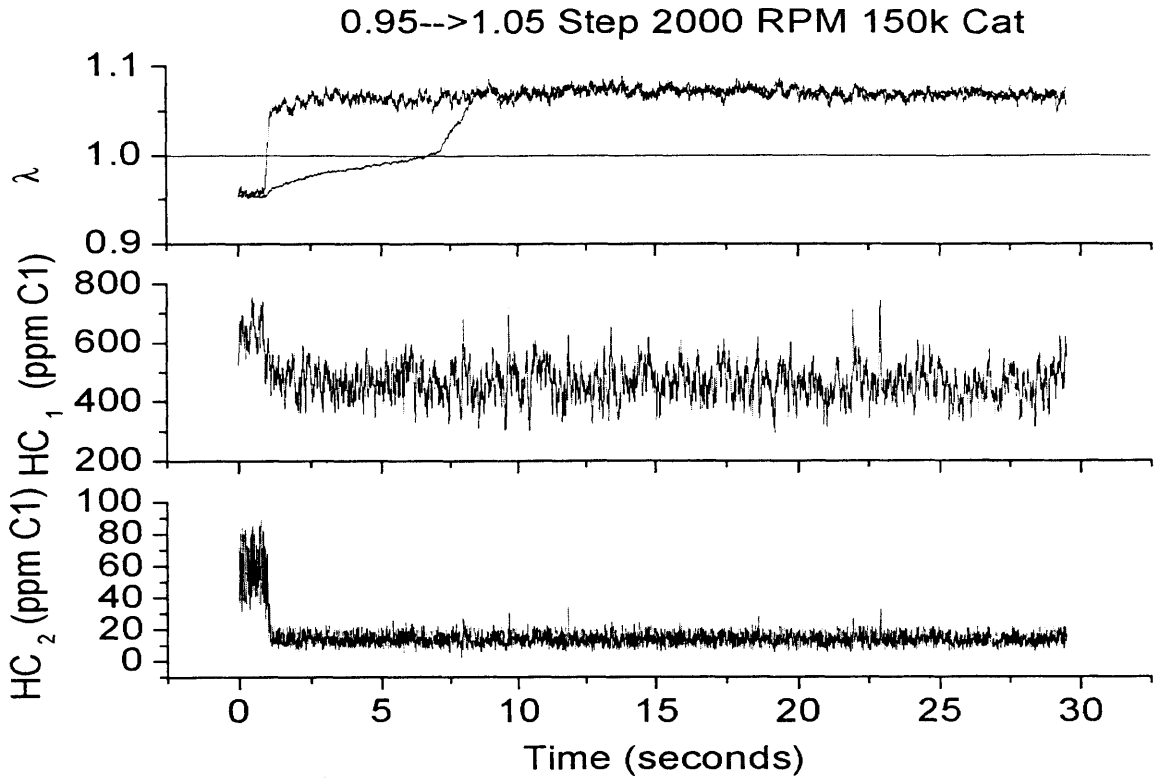

Figure 5.49: 0.95→1.05 Step HC 2000 RPM 150K Catalyst

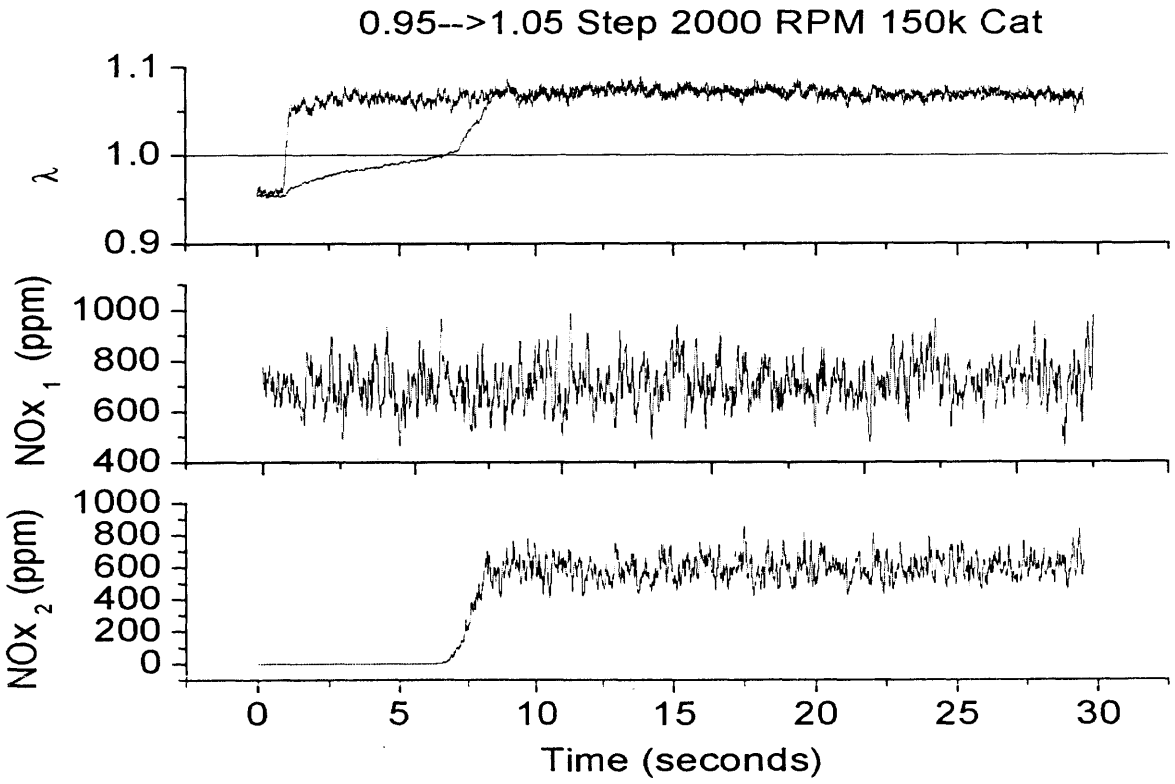

Figure 5.50: 0.95→1.05 Step NOx 2000 RPM 150K Catalyst

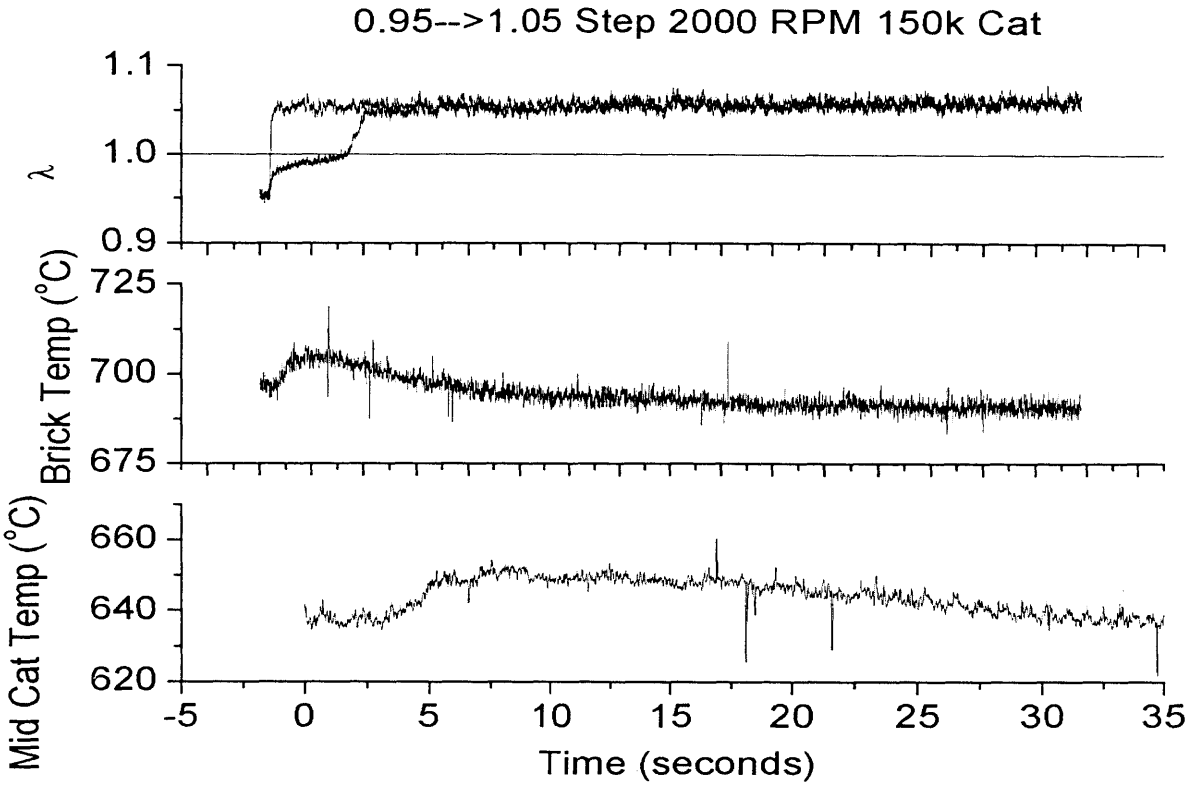

Figure 5.51: 0.95→1.05 Step Catalyst Brick and Mid-Catalyst Temperatures 2000 RPM 150K Catalyst

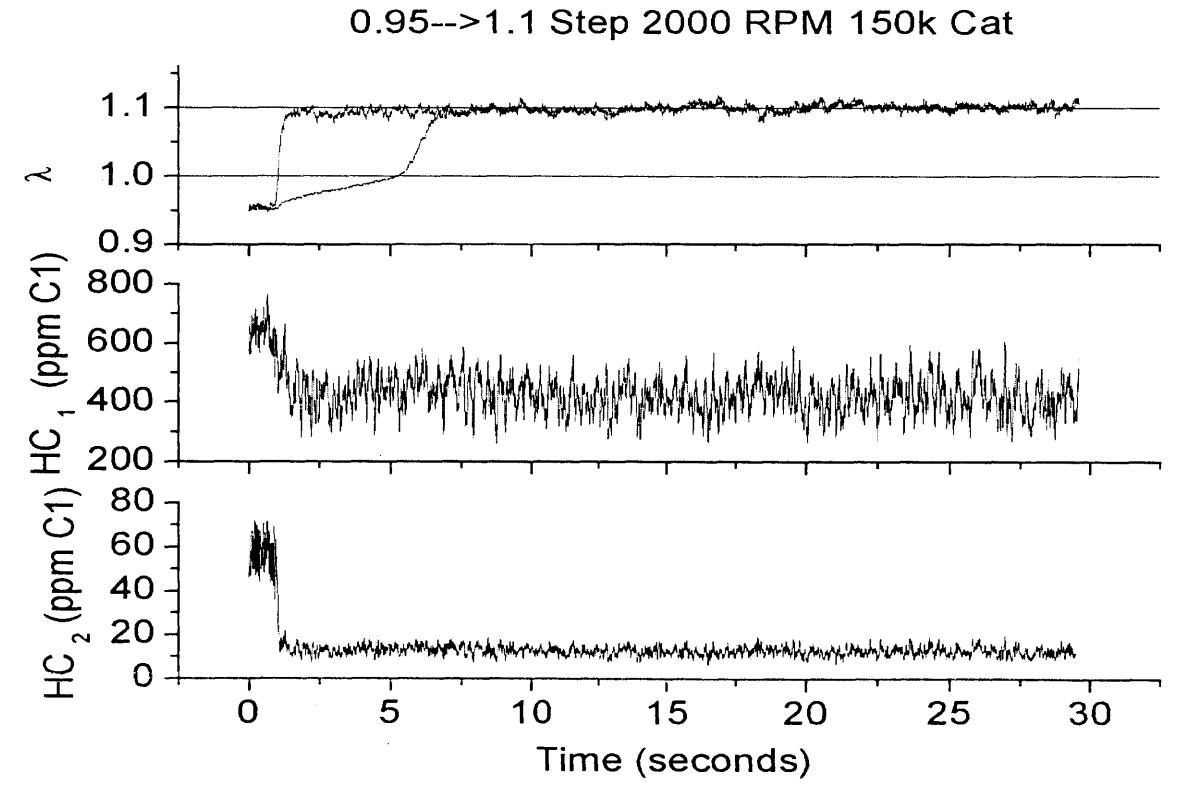

Figure 5.52: 0.95→1.1 Step HC 2000 RPM 150K Catalyst

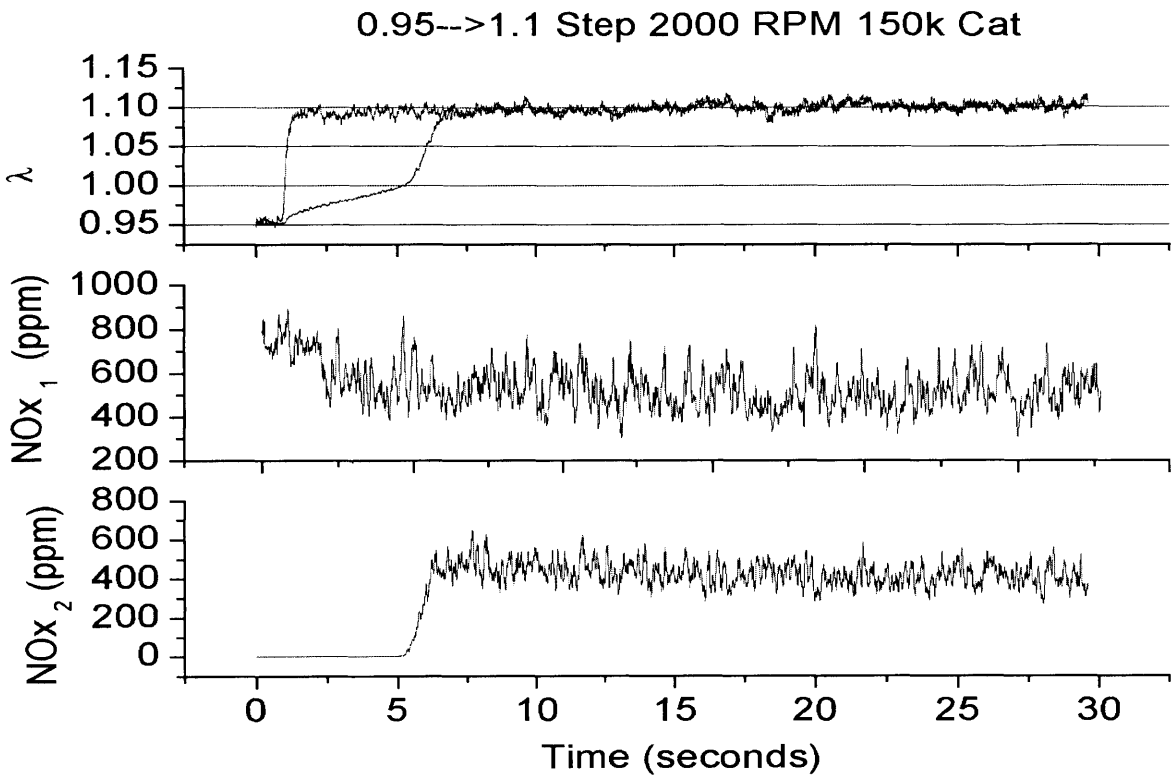

Figure 5.53: 0.95→1.1 Step NOx 2000 RPM 150K Catalyst

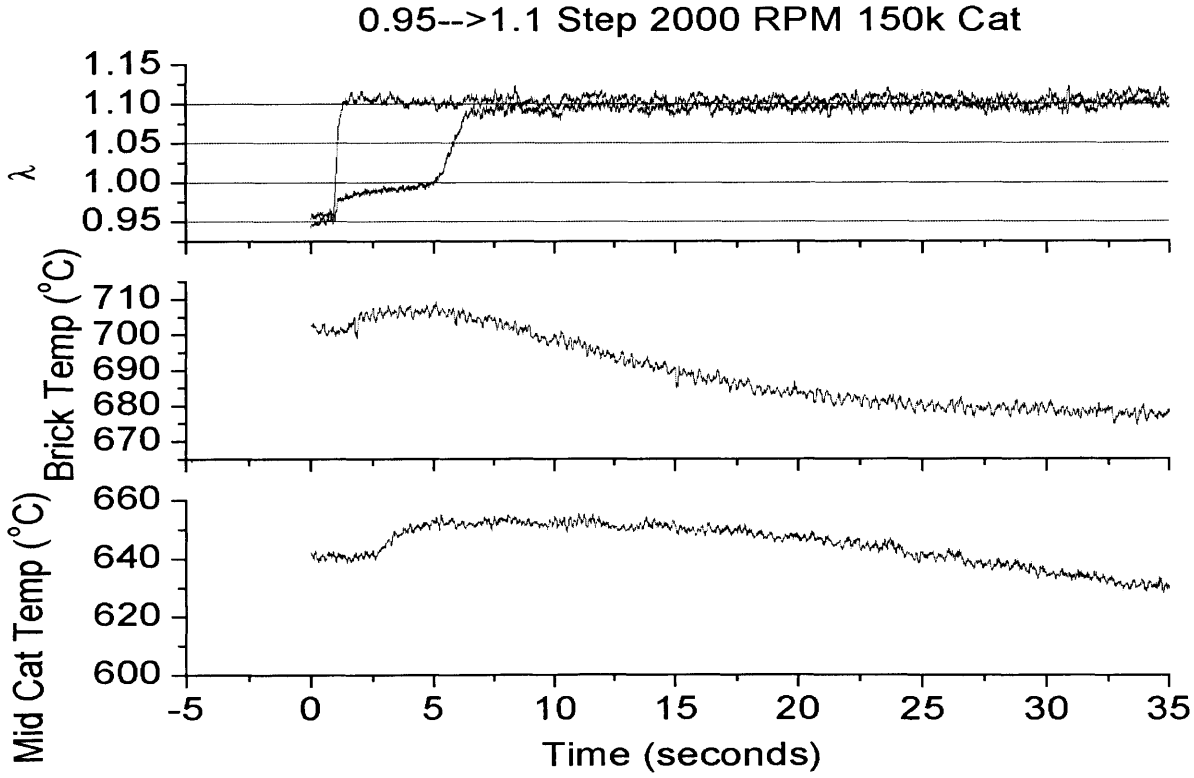

Figure 5.54: 0.95→1.1 Step Catalyst Brick and Mid-Catalyst Temperatures 2000 RPM 150K Catalyst

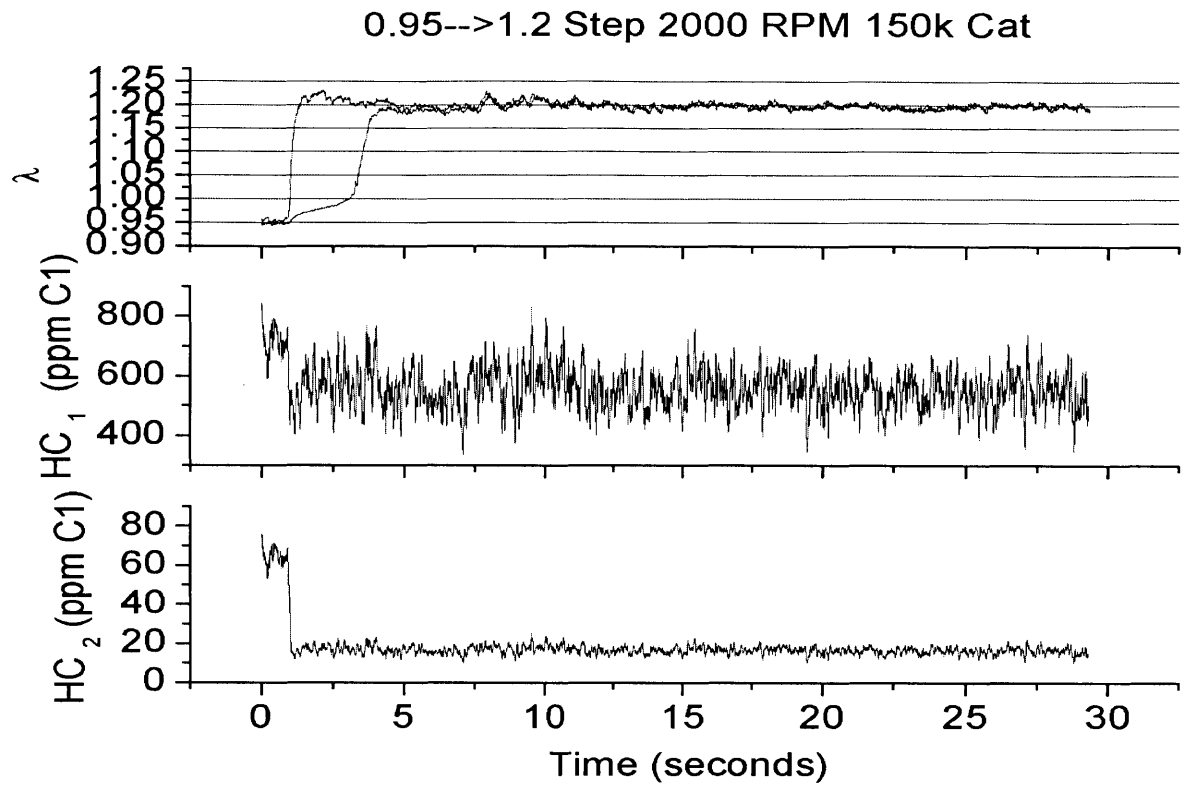

Figure 5.55: 0.95→1.2 Step HC 2000 RPM 150K Catalyst

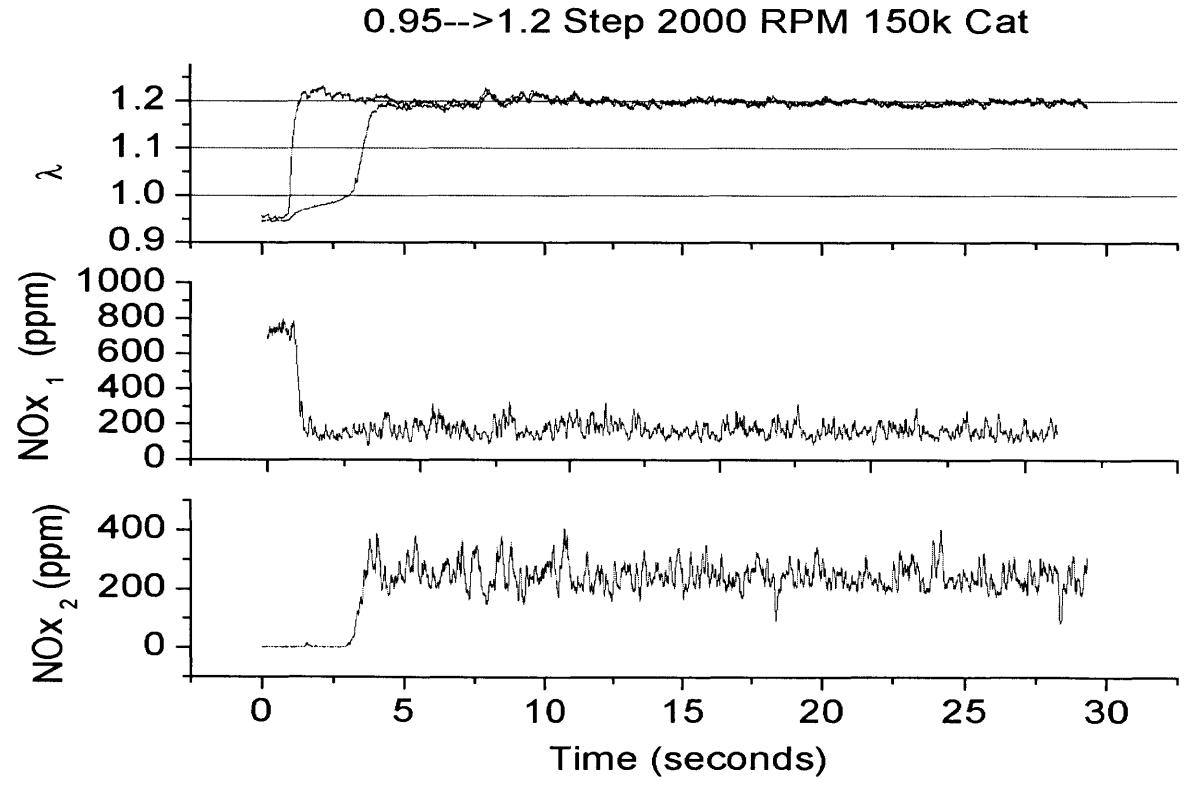

Figure 5.56: 0.95→1.2 Step NOx 2000 RPM 150K Catalyst

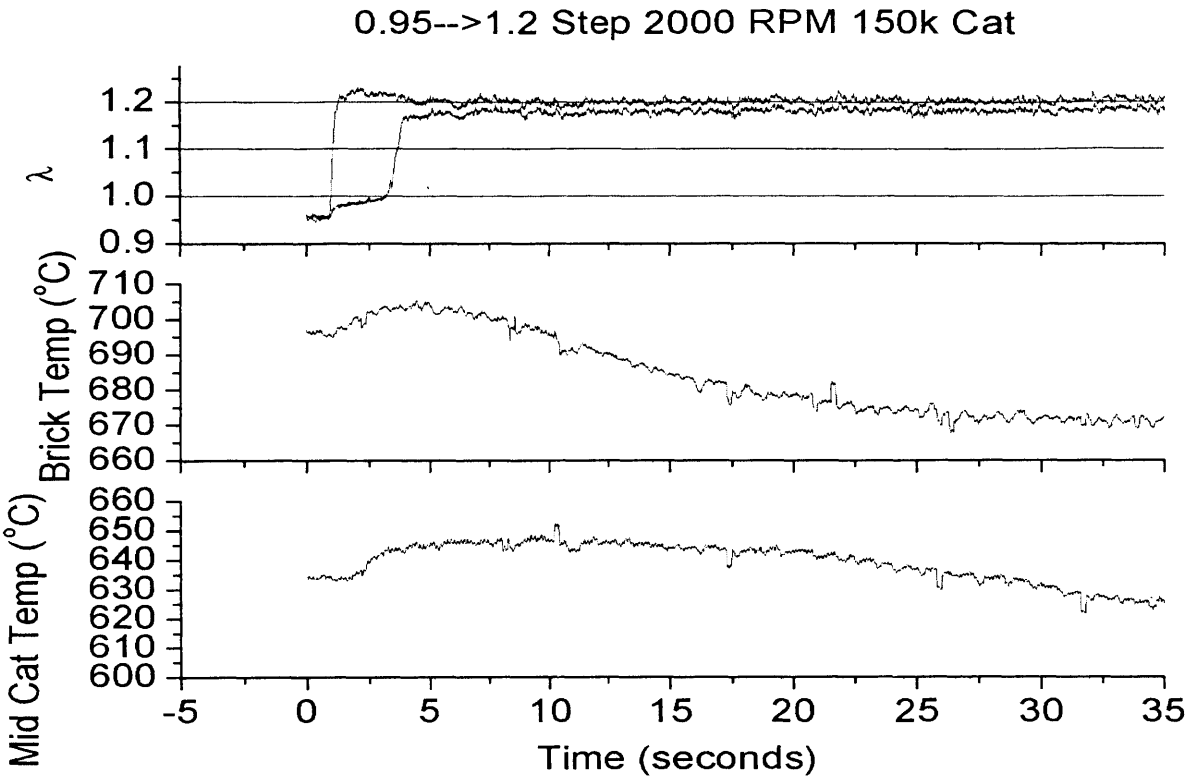

Figure 5.57: 0.95→1.2 Step Catalyst Brick and Mid-Catalyst Temperatures 2000 RPM 150K Catalyst

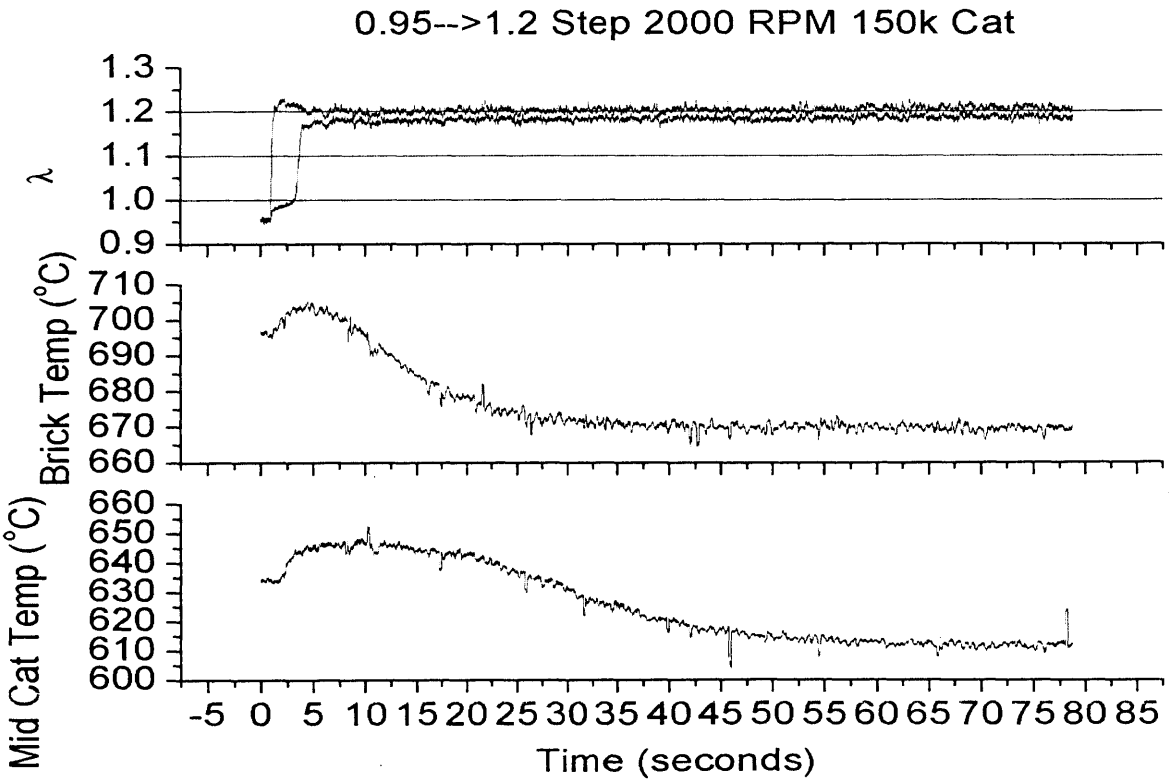

Figure 5.58: 0.95→1.2 Step Extended Catalyst Brick and Mid-Catalyst Temperatures 2000 RPM 150K Catalyst

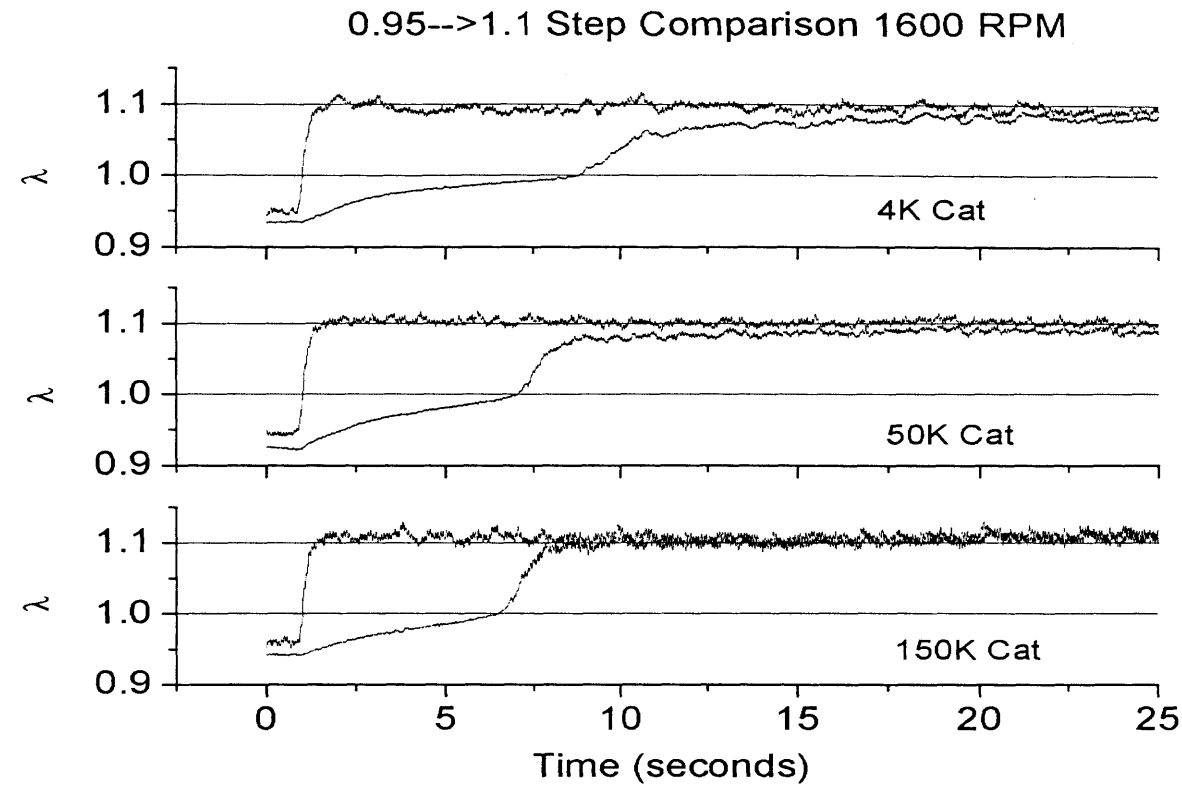

Figure 5.59: 0.95→1.1 Step λ Comparison of 4K, 50K, 150K Catalyst

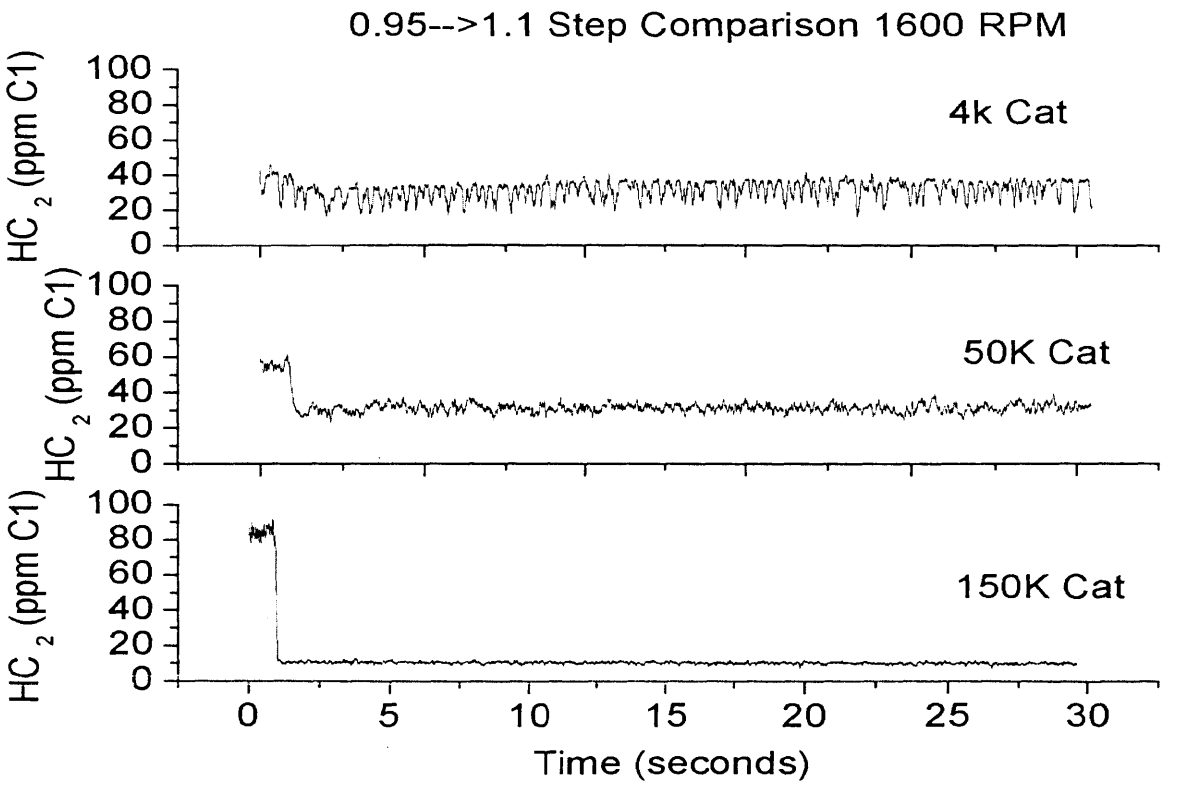

Figure 5.60: 0.95→1.1 Step HC Breakthrough Comparison of 4K, 50K, 150K Catalyst

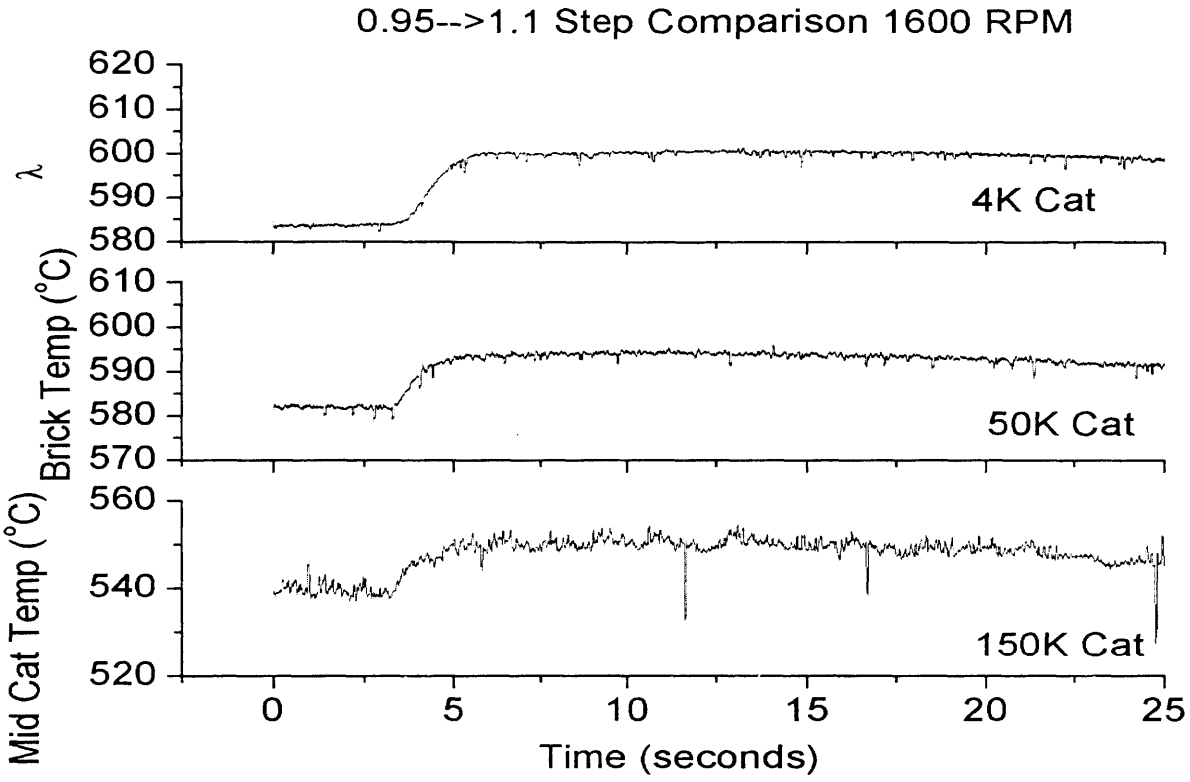

Figure 5.61: 0.95→1.1 Step Mid-Catalyst Temperature Comparison of 4K, 50K, 150K Catalyst

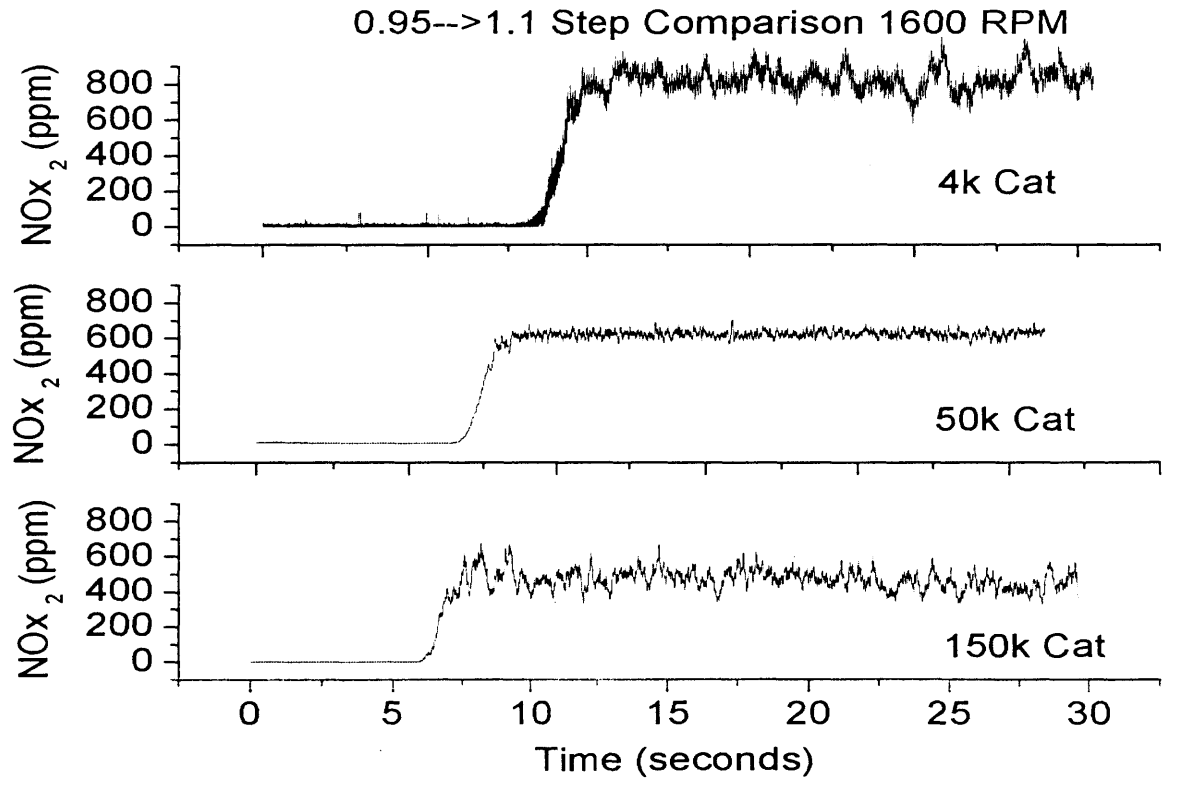

Figure 5.62: 0.95→1.1 Step NOx Breakthrough Comparison of 4K, 50K, 150K Catalyst

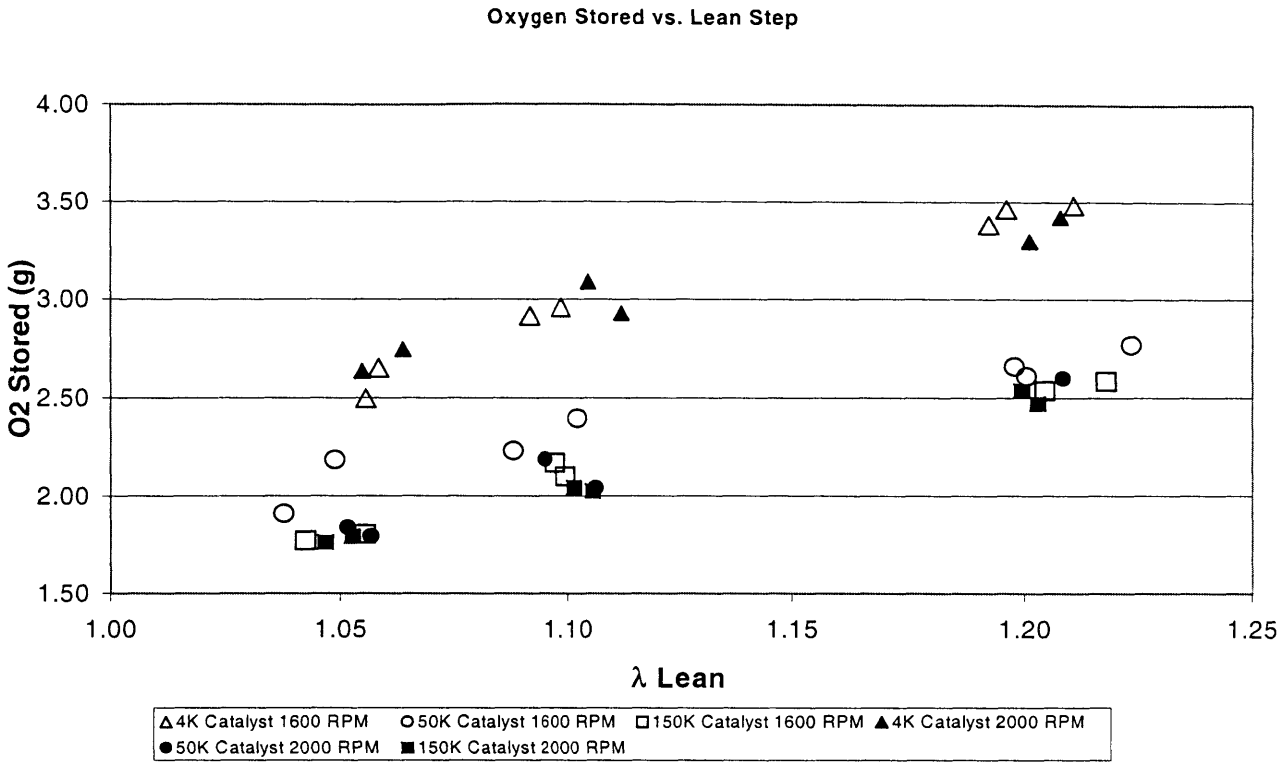

Figure 5.63: Oxygen Storage of 4K, 50K, 150K Catalyst as a Function of the Lean Step

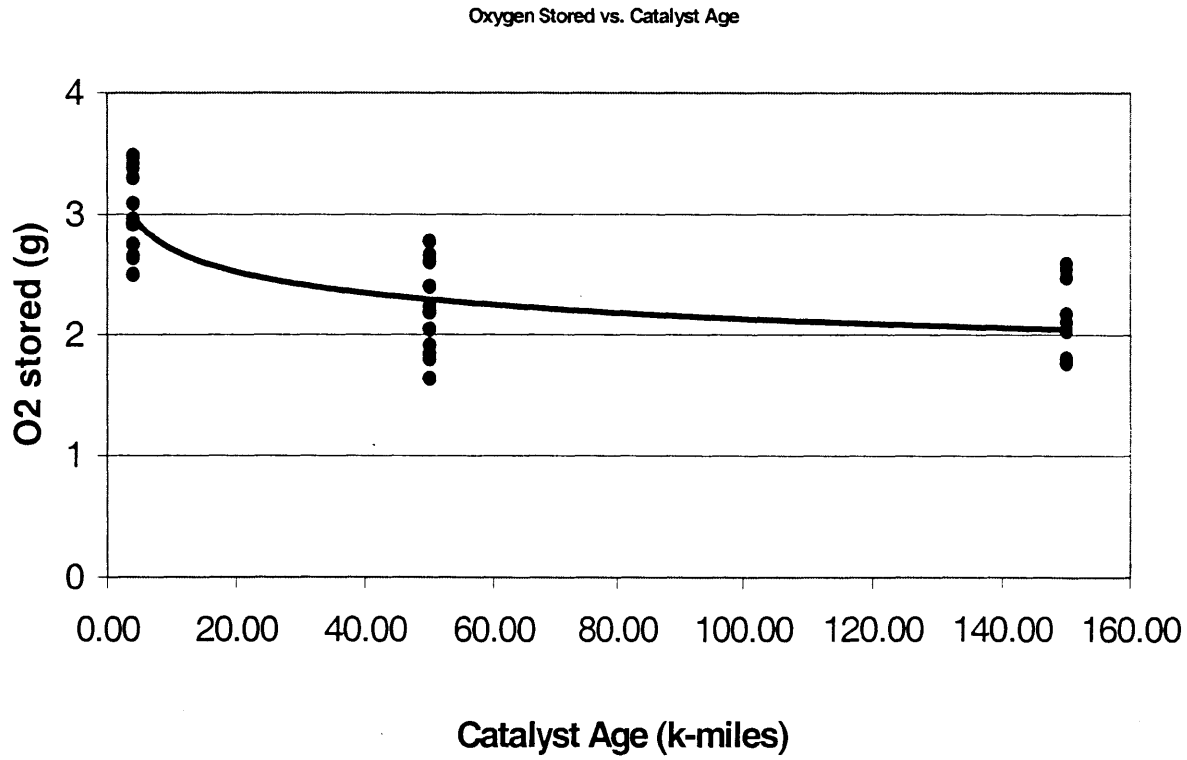

Figure 5.64: Oxygen Storage of 4K, 50K, 150K Catalyst as a Function of the Catalyst Age

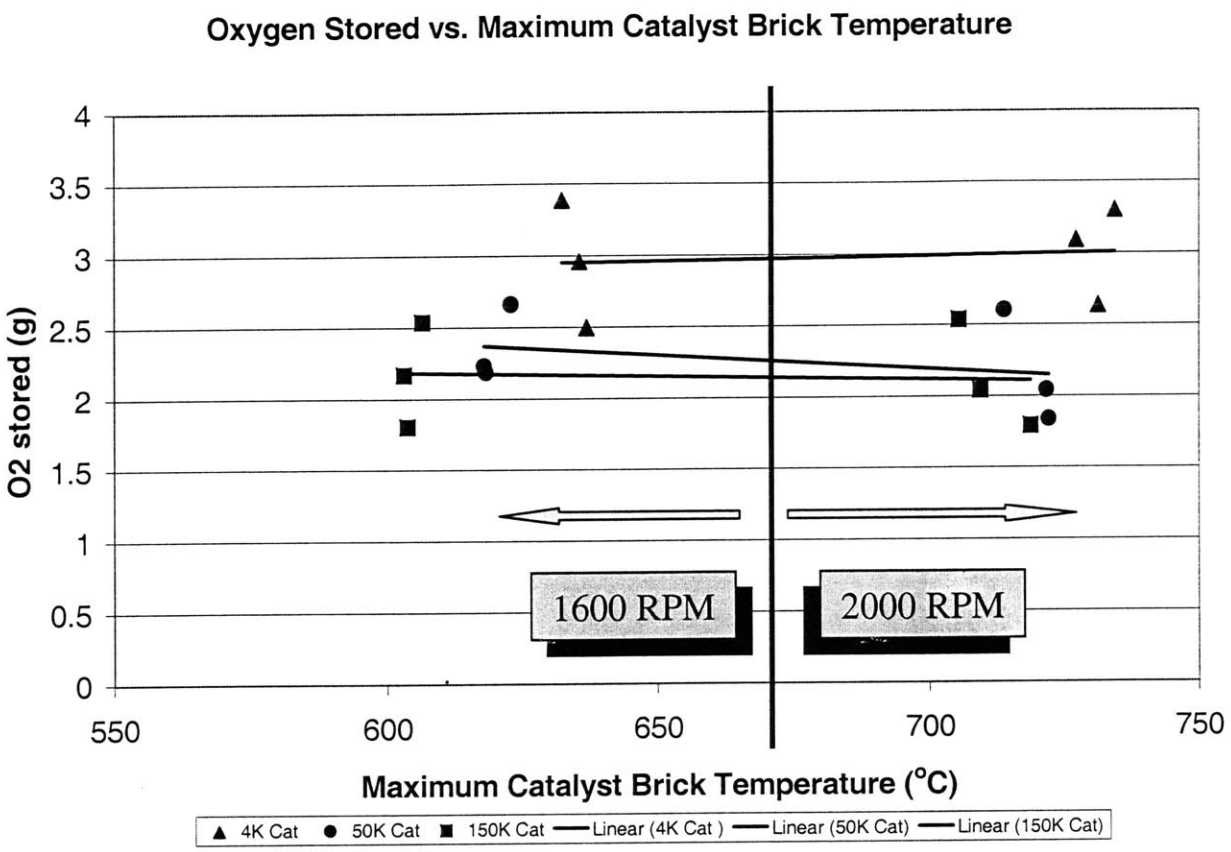

Figure 5.65: Oxygen Storage of 4K, 50K, 150K Catalyst as a Function of the Maximum Catalyst Brick Temperature

CHAPTER 6: CONCLUSIONS AND FURTHER RESEARCH DIRECTIONS

6.1: CONCLUSIONS

From this body of research, several conclusions may be made:

1. There is a bias in the oxygen sensor readings that causes the post-catalyst sensor to read "richer" than the upstream oxygen sensor, even though fundamentally the air/fuel ratio does not change across the catalyst. This error is greater as the exhaust stream becomes richer, but the error decreases as the catalyst ages due to the older catalyst affecting the exhaust stream gas composition less. This is supported by previous work.
2. At a stoichiometric operating point, the hydrocarbon efficiency of the catalyst does not change dramatically, going from 99% for a 4K catalyst to ~96% when aged to 150K miles. The NOx efficiency, on the other hand, drops from 99% to ~50% for this operating point.
3. Throttle transients show that as the throttle is opened to wide-open throttle, a NOx breakthrough occurs which rapidly increases with catalyst age (from 0.1 mg NO for the 4K catalyst to 2 mg NO for the 150K catalyst). Some of the cause for the breakthrough is the chemistry of the exhaust stream (namely the reducing of NOx in a lean environment), but the increasing breakthrough with age shows that the catalyst deterioration is the primary reason. A secondary NOx breakthrough occurs when the engine is at wide-open throttle. This breakthrough is a function of catalyst age, as it only appears significantly on the older catalysts. The post catalyst λ reading becoming less rich when this secondary NOx breakthrough occurs suggests that this breakthrough may be due to the catalytic converter temporarily running out of carbon monoxide.
4. The primary and secondary breakthroughs may become an issue under strict emissions standards if the driver is extremely aggressive. For example, with the oldest catalyst, the primary breakthrough on the fast transient was the same order of magnitude as the slow transient primary breakthrough. This suggests a catalyst

indifference to transient severity (at least with the two transients detailed here), which may be an issue during catalytic converter certification testing.

5. The decrease of oxygen storage capacity from the 4K catalyst (~ 3 g O_2 storage capacity) to 50K (~2.3 g O_2 storage capacity) is large compared to the decrease from 50K to 150K (~2 g O_2 storage capacity). This implies that the loss in NOx efficiency from the 50K to 150K catalyst is a result of the loss of catalytic activity, not loss of oxygen storage.
6. Oxygen storage was found to be a function of step size; the leaner the engine was run during the oxygen storage tests, the more oxygen was stored. Maximum brick temperature (the increase in maximum brick temperature was produced by an increase in flow rate) was found not to play a role in the amount of oxygen stored. The freshest catalyst stored the most oxygen and showed the highest maximum brick temperature of the three catalysts, but the oxygen storage capacity did not change with an increase in maximum brick temperature for this or any of the catalysts.

6.2: FURTHER RESEARCH DIRECTIONS

This research of looking at the engine and catalyst from a system perspective has yielded interesting results. Continuing this research to further explore this interaction will be beneficial. Measuring the CO efficiency of the catalysts will provide further insight into the results given here. A fast-response CO meter would yield important information about catalyst behavior during the transient, and support or refute the postulate for the secondary breakthrough presented here. Also, modeling of the catalyst during these transients would aid in the understanding of the chemical behavior of the catalyst as well as provide insight into the temperature rise. Also of interest may be to disassemble the catalysts and measure the active material present, providing a more concrete correlation for the loss of oxygen storage/loss of material separation.

APPENDIX A: STEP MOTOR PROGRAM CODE

For a transient of 40 second duration, as shown below:

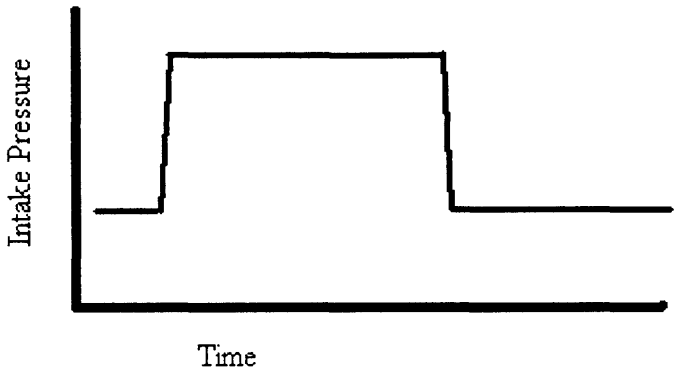

The code which produces the profile shown above is shown below:

```
ENN
+190
W 15000
-190
END
```

For the slow transient, the velocity of the step motor was set to 100 steps/second. For the fast transient operation, the velocity was set to 10,000 steps/second.

A step change profile was also implemented, shown below:

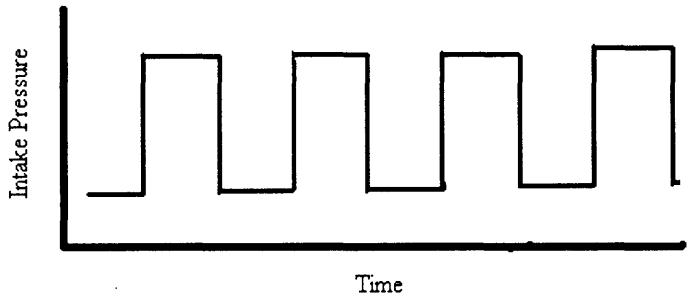

The indexer code that produces the step transient profile is given below:

```
ENN
+190
W 7000
-190
W 7000
+190
W 7000
```

```
-190
W 7000
+190
W 7000
-190
+190
W 7000
-190
END
```

This code specifies a 7 second dwelling time for wide open throttle as well as a 7 second dwelling time for the starting intake pressure (0.5 bar for the tests run).

APPENDIX B: FUEL PROPERTIES [15]

Tests	Results
Specific Gravity, 60/60 F	0.7283
API Gravity	62.79
Corrosion 50C	1A
Phosphorous (grams/gallon)	0.001
Sulfur (ppm)	28.2
Multi-Substituted Alkyl Aromatics	13.4
MTBE (LV%)	11.1
Oxidation Stability (min)	1440+
Existent Gums (mg/ 100 ml) (washed)	0.0
Reid Vapor Pressure	10.85
Benzene Content (LV%)	1.23
Distillation (°F)	
IBP	84.2
5%	102.7
10%	113.7
20%	133.9
30%	154.8
40%	175.3
50%	195.4
60%	217.4
70%	237.6
80%	258.6
90%	289.9
95%	316.9
EP	370.8
Loss	0.9
Residue	1.2
Hydrocarbon Type (Vol %)	Uncorrected
Aromatics	23
Olefins	4.3
Saturates	72.7
Research Octane Number	96.5
Motor Octane Number	87.8
Antiknock Index	92.2
Sensitivity	8.7

APPENDIX C: STEADY STATE MATLAB CODE

Code for the HC and NOx efficiencies

```
clear all
close all
file=input('File name: ', 's');


test=load(file);


l1=test(:,1);
l2=test(:,2);
f1=test(:,3);
f2=test(:,4);
n1=test(:,5);
n2=test(:,6);
bricktemp=test(:,7);
midcat=test(:,8);

%calibrate FFID, NO meters
f1=xx.*f1;
f2=xx.*f2;
n1=xx.*n1;
n2=xx.*n2;

avel1=mean(l1)
avel2=mean(l2)
avef1=mean(f1)
avef2=mean(f2)
aven1=mean(n1)
aven2=mean(n2)
avebricktemp=mean(bricktemp)
avemidcat=mean(midcat)
```

APPENDIX D: WATER CONTENT IN SPARK IGNITION EXHAUST [4]

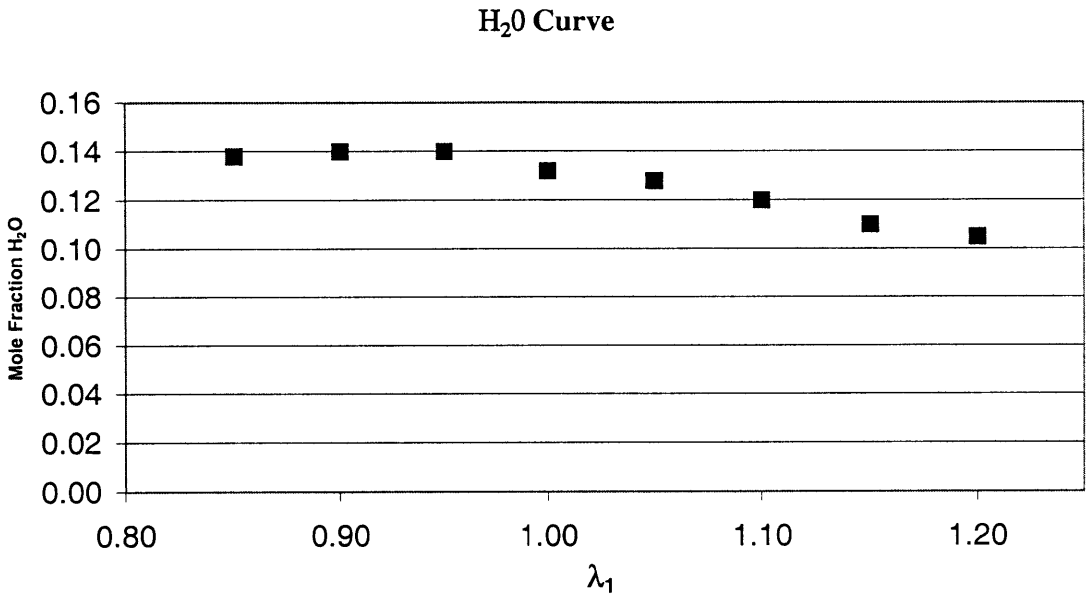

APPENDIX E: TABLES OF STEADY STATE EMISSIONS MEASUREMENTS AND EFFICIENCY

4k Catalyst Efficiency

Speed (RPM)	λ_1	λ_2	η_{HC}	η_{NOx}
1600	0.852	0.828	90.65%	99.64%
	0.902	0.883	95.00%	99.82%
	0.963	0.950	97.68%	99.90%
	1.006	0.996	99.99%	99.93%
	1.055	1.050	99.98%	0.00%
	1.099	1.093	99.99%	0.00%
	1.155	1.145	99.99%	0.00%
	1.211	1.196	99.99%	0.00%
2000	0.853	0.843	83.41%	99.37%
	0.910	0.922	91.00%	99.68%
	0.955	0.968	96.00%	99.78%
	1.008	1.011	99.92%	99.92%
	1.053	1.048	99.64%	0.00%
	1.110	1.101	99.29%	0.00%
	1.161	1.147	99.14%	0.00%
	1.205	1.186	99.08%	0.00%

50K Catalyst Efficiency

Speed (RPM)	λ_1	λ_2	η_{HC}	η_{NOx}
1600	0.853	0.861	67.09%	98.84%
	0.903	0.902	79.73%	99.35%
	0.953	0.944	96.16%	99.55%
	1.001	0.997	99.69%	76.08%
	1.054	1.050	99.60%	0.00%
	1.098	1.090	99.60%	0.00%
	1.158	1.146	99.77%	0.00%
	1.230	1.212	99.89%	0.00%
2000	0.845	0.842	75.23%	97.89%
	0.922	0.941	84.67%	98.25%
	0.958	0.975	95.53%	97.25%
	1.005	1.003	99.98%	71.32%
	1.069	1.063	99.54%	0.00%
	1.105	1.097	99.82%	0.00%
	1.168	1.153	99.95%	0.00%
	1.205	1.186	99.94%	0.00%

150k Catalyst Efficiency

Speed (RPM)	λ_1	λ_2	η_{HC}	η_{NOx}
1600	0.854	0.862	60.91%	97.03%
	0.901	0.913	69.11%	98.31%
	0.952	0.959	91.11%	98.68%
	1.014	1.017	98.84%	57.32%
	1.054	1.050	99.31%	0.00%
	1.105	1.096	99.88%	0.00%
	1.155	1.144	99.95%	0.00%
	1.209	1.192	99.96%	0.00%
2000	0.859	0.865	70.21%	94.89%
	0.906	0.923	77.91%	94.81%
	0.955	0.973	94.34%	93.52%
	1.007	1.003	99.98%	51.65%
	1.055	1.049	99.96%	0.00%
	1.109	1.099	99.95%	0.00%
	1.150	1.137	99.95%	0.00%
	1.211	1.190	99.94%	0.00%

CO Emissions

RPM	λ1	Pre-Catalyst CO (% wet mol frac.)
1600	0.8543	4.37%
	0.9021	2.54%
	0.9561	1.12%
	1.0153	0.33%
	1.0528	0.15%
	1.1086	0.11%
	1.1612	0.11%
	1.2055	0.11%
2000	0.8545	4.28%
	0.9065	2.29%
	0.9557	1.22%
	1.0042	0.43%
	1.056	0.18%
	1.109	0.12%
	1.1567	0.11%
	1.2056	0.11%

APPENDIX F: MATLAB CODE USED TO EVALUATE TRANSIENTS

```
clear all
close all
file=input('File name: ', 's');


test=load(file);


pres=test(:,1);
l1=test(:,2);
l2=test(:,3);
f1=test(:,4);
f2=test(:,5);
n1=test(:,6);
n2=test(:,7);
bricktemp=test(:,8);
midcat=test(:,9);

n=length(pres);


%delete negative values
disp('Deleting negative values.....');
for i=1:n
   if n2(i)<0
      n2(i)=0;
      f2(i)<0
      f2(i)=0;
   end
end


t=[0:n-1]'/1000; %time in sec

pres=mov_avg(pres,51);

%slope change detection

subplot(2,1,1), plot(t,pres);
ylabel('Intake Pres. (bar)');

i=1000*input('Slope change= ');

while i<16000
   fslope=abs((pres(i+250)-pres(i-250))./500);
   if (fslope) > .0006;
      slopeindex=i;
      break
      break
```

```
   end
   i=i+1;
end


%shifts the matrices so they all have the same starting point
compindex=slopeindex-2000;

newpres=pres(compindex:n);
newl1=l1(compindex:n);
newl2=l2(compindex:n);
newn1=n1(compindex:n);
newn2=n2(compindex:n);
newf1=f1(compindex:n);
newf2=f2(compindex:n);
newbricktemp=bricktemp(compindex:n);
newmidcat=midcat(compindex:n);


nnew=length(newpres);

tnew=[0:nnew-1]'/1000;

%calibrate pres, l1, l2, NOx
newpres=0.2*newpres-0.2;
newn1=newn1*XXX;
newn2=newn2*XXX;
newf1=newf1*XXX;
newn2=newf2*XXX;

subplot(2,1,1), plot(tnew,newpres);
ylabel('Intake Pres. (bar)');

subplot(2,1,2),semilogy(tnew,newn2);
ylabel('Post Cat NOx (ppm)');
xlabel('Time (sec)');



%NOx peaks
numppeaks=input('Number of Primary NOx peaks: ');
numspeaks=input('Number of Secondary NOx peaks: ');


if numppeaks>0
   for i=1:numppeaks
      pintstart=1000*input('Start of primary peak: ');
      pintend=1000*input('End of primary peak: ');
      selection=newn2(pintstart:pintend);
      ppeaks(i,1)=sum(selection);  %gives culmulative NOx ppm
      intppeaks(i,1)=0.001*trapz(selection);  %gives integral of NOx
ppm*sec
   end
   disp('Sum of ppeaks=')
   disp(ppeaks)
   disp('Integral of ppeaks=')
```

```
   disp(intppeaks)
end



if numspeaks>0
   for i=1:numspeaks
      sintstart=1000*input('Start of secondary peak: ');
      sintend=1000*input('End of primary peak: ');
      selection=newn2(sintstart:sintend);
      speaks(i,1)=sum(selection);  %gives culmulative NOx ppm
      intspeaks(i,1)=0.001*trapz(selection);  %gives integral of NOx
ppm*sec
   end
      disp('Sum of speaks=')
      disp(speaks)
      disp('Integral of speaks=')
      disp(intspeaks)
end




Output(:,1)=tnew;
Output(:,2)=newpres;
Output(:,3)=newl1;
Output(:,4)=newl2;
Output(:,5)=newn1;
Output(:,6)=newn1;
Output(:,7)=newf1;
Output(:,8)=newf2;
Output(:,9)=newbricktemp;
Output(:,10)=newmidcat;

save xxx.dat Output -ascii -tabs
```

APPENDIX G: INTEGRATED VALUES OF TRANSIENT NOX BREAKTHROUGH

Catalyst Age (K-miles)	Transient Designation	Primary NO Breakthrough (g NOx * 10^5)	Secondary NO Breakthrough (g NOx * 10^5)
4	Fast	7.61	0.00
4	fast	16.22	0.00
4	fast	11.92	0.00
50	fast	23.19	0.00
50	fast	19.31	0.00
50	fast	24.38	0.00
50	fast	26.83	0.00
50	fast	16.66	0.00
50	fast	14.81	0.00
150	fast	201.26	0.00
150	fast	218.22	0.00
150	fast	189.01	0.00
150	fast	175.77	305.02
150	fast	160.00	558.76
150	fast	185.02	518.76
4	slow	9.43	0.00
4	slow	13.38	0.00
4	slow	3.69	0.00
4	slow	2.86	0.00
4	slow	2.13	0.00
50	slow	6.60	0.00
50	slow	3.88	0.00
50	slow	5.07	0.00
50	slow	0.00	0.00
50	slow	26.71	0.00
50	slow	16.15	0.00
150	slow	161.84	0.00
150	slow	123.95	0.00
150	slow	136.56	0.00
150	slow	156.23	1141.30
150	slow	191.15	1657.00
150	slow	115.45	1033.75
4	step	5.79	0.00
4	step	19.17	0.00
4	step	6.61	0.00
4	step	20.53	0.00

Catalyst Age (K-miles)	Transient Designation	Primary NO Breakthrough (g NOx * 10^5)	Secondary NO Breakthrough (g NOx * 10^5)
4	step	4.34	0.00
4	step	17.46	0.00
4	step	4.96	0.00
50	step	90.81	0.00
50	step	23.02	79.62
50	step	22.51	0.00
50	step	16.59	56.04
50	step	17.03	0.00
50	step	8.93	174.55
50	step	21.11	0.00
50	step	34.45	0.00
50	step	26.49	0.00
50	step	12.35	0.00
50	step	12.75	0.00
50	step	21.96	0.00
50	step	32.77	0.00
50	step	19.72	68.44
50	step	12.50	75.62
50	step	24.60	173.09
50	step	21.94	194.18
150	step	206.52	82.87
150	step	36.69	337.04
150	step	78.75	274.79
150	step	103.20	258.58
150	step	134.31	147.68
150	step	66.12	262.15
150	step	271.01	62.58
150	step	127.72	476.19
150	step	317.34	795.57
150	step	320.69	544.10
150	step	195.24	51.24
150	step	77.88	617.38
150	step	313.82	604.46
150	step	190.22	432.71
150	step	190.35	45.79
150	step	63.52	651.35
150	step	273.82	552.71
150	step	224.36	559.28

APPENDIX H: MATLAB CODE USED TO EVALUATE OXYGEN STORAGE

```
clear all
close all
file=input('File name: ', 's');
rpm=input('Enter engine speed (rpm): ');

test=load(file);
%****************
if rpm < 1700;
   %air flow (g/s) calculation using volumetric efficiency=66.17%
@1600, 0.5 Bar
   %air flow (g/s) calculation using volumetric eff=73.22% @2000, 0.5
bar
   air=12.3;
else
   air=17.01;
end


%****************


l1=test(:,1);
l2=test(:,2);
n1=test(:,3);
n2=test(:,4);
f1=test(:,5);
f2=test(:,6);
bricktemp=test(:,7);
midcat=test(:,8);

%calibrate FFID, NOx meters

n1=495.5*n1;
n2=495.5*n2;
f1=1731.6*f1;
f2=206.18*f2;

n=length(l1);

%finds the point where the transition occurs
while i<16000
   fslope=abs((l1(i+250)-l1(i-250))./500);
   if (fslope) > .0006;
      slopeindex=i;
      break
      break
   end
   i=i+1;
end
```

```
%shifts the matrices so they all have the same starting point
compindex=slopeindex-2000;

newn1=n1(compindex:n);
newl1=l1(compindex:n);
newl2=l2(compindex:n);
newn2=n2(compindex:n);
newf1=f1(compindex:n);
newf2=f2(compindex:n);
newbricktemp=bricktemp(compindex:n);
newmidcat=midcat(compindex:n);
nnew=length(newn1);
tnew=[0:nnew-1]'/1000;


%find where integration should begin for l1
for i=1:10000;
   if l1new(i)>1;
      l1_lean=i;
      break
      break
   end
end


%this is for lambda1
%molecular weight of exhaust based on lean burn equation
wex1=60.85+1.4675*(l1new-1)*32+1.4675*l1new*28.16*3.773;
%average molecular weight of exhaust
w1=wex1./(1+.935+1.4675*(l1new-1)+1.4675*l1new*3.773);
%mole fraction of O2 based on lean burn equation
xO21=(1.4675*(l1new-1))./(1+.935+1.4775*(l1new-1)+1.4675*l1new*3.773);
%mass fraction of O2
yO21=xO21.*32.1./w1;

%exhaust mass flow rate--air is the measured air flow rate
me=air.*(1+(1./l1new(l1_lean+2000))* .0685);

%this is for lambda2
%average molecular weight of exhaust based on lean burn equation
wex2=60.85+1.4675*(l2new-1)*32+1.4675*l2new*28.16*3.773;
%average molecular weight of exhaust
w2=wex2./(1+.935+1.4675*(l2new-1)+1.4675*l2new*3.773);
%mole fraction of O2 based on lean burn equation
xO22=(1.4675*(l2new-1))./(1+.935+1.4775*(l2new-1)+1.4675*l2new*3.773);
%mass fraction of O2
yO22=xO22.*32.1./w2;



%lambda plots
figure('PaperOrientation', 'landscape','PaperPosition',[.1,.1,11,8.5])
subplot(3,1,1),plot(t,l1new);
axis([0,30,0.8,1.2]);
hold on;
plot(t,l2,'-r');
```

```
ylabel('\lambda');
legend('Pre-Cat \lambda','Post-Cat \lambda', 4)
hold off
text(15,0.95,'Brick residence time (s) = ','Fontsize', 10);
text(15,0.85,restime,'Fontsize', 10);


l2_lean=input('Where does lambda 2 go lean?: ');
%multiply this x 1000 to match sampling rate
l2_lean=l2_lean*1000;

%select the oxygen storage portions from the data
intyO21=yO21(l1_lean:l1_lean+10000);
intyO22=yO22(l2_lean:l1_lean+10000);

%integrate the mass fractions of L1 and L2
oxy=num2str(me*(0.001*trapz(intyO21)-0.001*trapz(intyO22)));

t1=t(l1_lean:l1_lean+2000);
t2=t(l2_lean:l1_lean+2000);
subplot(3,1,2), plot(t1,intyO21);
text(20,0.15,'O_2 stored (g) =','Fontsize', 10);
text(20,0.1,oxy,'Fontsize', 10);
axis([0,30,0,0.2]);
ylabel('Mass Fraction of O_2 from \lambda_1');

subplot(3,1,3),plot(t2,intyO22);
mes=num2str(me);
text(20,0.15,'m_e_x_h (g/s)= ','Fontsize', 10);
text(20,0.1,mes,'Fontsize',10);
axis([0,30,0,0.2]);
xlabel('Time (sec)');
ylabel('Mass Fraction of O_2 from \lambda_2');

newbricktemp=mov_avg(newbricktemp,25);
newmidcat=mov_avg(newmidcat,25);

%average lambda to get accurate value of step
avelambda=mean(l1new(l1_lean+4000:l1_lean+6000))
me
oxy
maxbrick=max(newbricktemp)
maxmidcat=max(newmidcat)
Output(:,1)=tnew;
Output(:,2)=newl1;
Output(:,3)=newl2;
Output(:,4)=newn1;
Output(:,5)=newn1;
Output(:,6)=newf1;
Output(:,7)=newf2;
Output(:,8)=newbricktemp;
Output(:,9)=newmidcat;
save xxx.dat Output -ascii -tabs
```

APPENDIX I: AIR/FUEL MODULATION AND OXYGEN SUPPLIED TO THE CATALYST

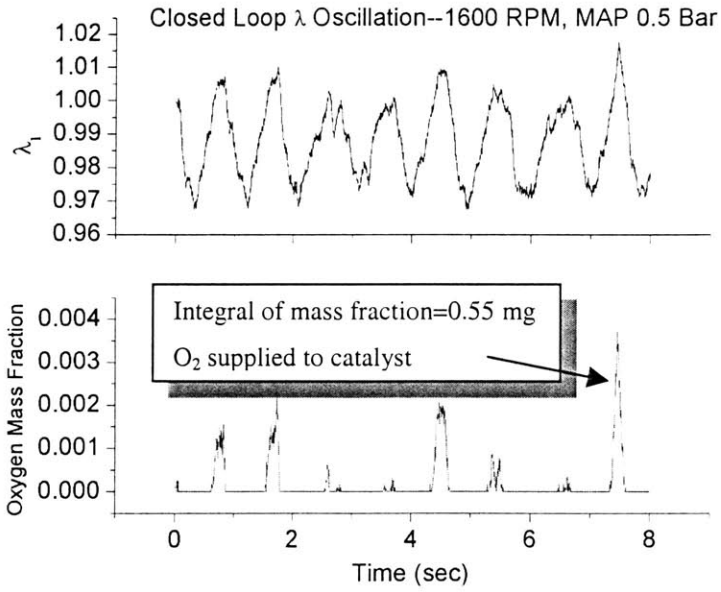

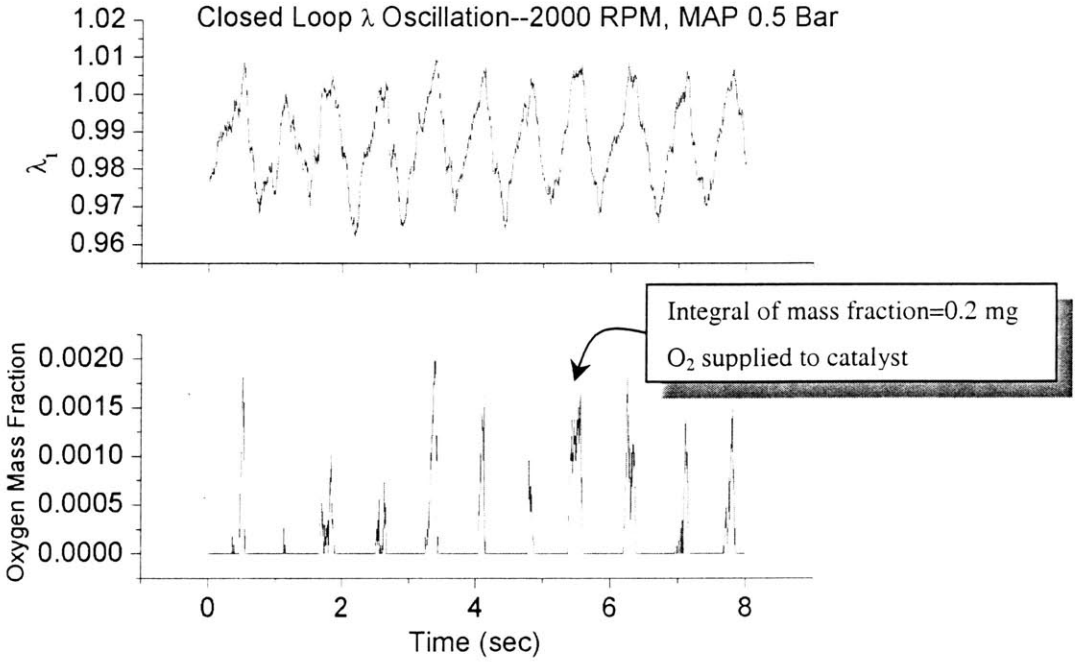

APPENDIX J: CALCULATION OF HC CONTRIBUTION TO TEMPERATURE RISE

From HC portion of equation 5.8:

$$(T_2 - T_1) = (x_{HC} MW_{HC} Q_{HVHC}) \frac{1}{c_p MW_{exh}}$$

with MW_{HC}=0.014 kg/mol (assuming a structure of CH_2), xHC=700/10^6, Q_{HVHC}=44,000,000 J/kg (the heating value of fuel, from [4]), c_p=1280 J/(kg-K) (this is the value for air, which is a valid approximation as the exhaust stream is over 70% nitrogen), and MW_{exh}=0.029 kg/mol.

Plugging these values into the equation:

$$(T_2 - T_1) = \left(\left(\frac{700}{10^6} \ ppm \right) (0.014\, kg/mol)(44{,}000{,}000\, J/kg) \right) \frac{1}{(1280\, J/(kg-K))(0.029\, kg/mol)}$$

or

$\underline{\Delta T_{21}=11.6\ K=11.6\ ^{\circ}C}$

REFERENCES

1. Tier 2/Sulfur Regulatory Impact Analysis. Environmental Protection Agency. Chapter II: Health and Welfare Concerns. December 1999.
2. "Control of Air Pollution From New Motor Vehicles: Tier 2 Motor Vehicle Emissions and Gasoline Sulfur Control Requirements; Final Rule." Environmental Protection Agency. Federal Register, February 10, 2000.
3. "The History of Reducing Tailpipe Emissions." Environmental Protection Agency. EPA420-F-99-017. May 1999.
4. Heywood, John B. Internal Combustion Engine Fundamentals. McGraw-Hill, Inc. New York, 1988.
5. Heck, Ronald M., and. Farrauto, Robert J. Catalytic Air Pollution Control—Commercial Technology. John Wiley & Sons, Inc. New York, 1995.
6. Fisher, Galen B., Theis, Joseph R., Casarella, Mark V., and. Mahan, Stephen T. "The Role of Ceria in Automotive Exhaust Catalysis and OBD-II Catalyst Monitoring". SAE paper # 931034 (1993).
7. Falk, C.D., and Mooney, J.J. "Three-Way Conversion Catalysts: Effect of Closed-Loop Feed-Back Control and Other Parameters on Catalyst Efficiency." SAE paper # 800462 (1980).
8. Adomaitis, J.R., and Heck, R.M. "Vehicle Control Strategies Effect on Catalyst Performance." SAE paper # 881597. (1988).
9. Smedler, G., Lundgren, S, Romare, A., Wirmark, G., Jobson, E., Hogberg, E., and Weber, K.H. "Spatially Resolved Effects of Deactivation on Field-Aged Automotive Catalysts." SAE paper # 910173. (1991).
10. Truex, T.J. "Interaction of Sulfur with Automotive Catalysts and the Impact on Vehicle Emissions-A Review." SAE paper # 1999-01-1543. (1999).
11. Schleyer, C.H., Eckstrom, J., Eng, K.D., Freel, J., Gorse, R.A., Natarajan, M., Gunst, R.F., and Schlenker, A.M. "Reversibility of Sulfur Effects on Emissions of California Low Emission Vehicles." SAE paper 1999-01-1544. (1999).
12. "Service Manual-1998 Town & Country, Caravan, and Voyager." Chrysler Corporation, 1997.
13. "Series 1000A Dynamometer Controller-Revision A" Digalog Corp, 1984.
14. "Federal Certification Exhaust Emissions Standards for Light Duty Vehicle (Passenger Cars) and Light-Duty Trucks: FTP, Cold CO, and Highway & Idle Tests." U.S. Environmental Protection Agency Office of Transportatino and Air Quality. EPA420-B-00-001. February 2000.
15. 11# RVP Gasoline Specifications. Chevron Phillips Chemical Company LP, 2001.
16. Yamada, T., Hayakawa, N., Kami, Y., and Kawai, T. "Universal Air-Fuel Ratio Heated Exhaust Gas Oxygen Sensor and Further Applications." SAE paper # 920234 (1992).
17. Cheng, W.K., Summers, T., Collings, N. "The Fast-Response Flame Ionization Detector." Prog. Energy Combustion Science, Vol. 24, pp. 89-124. Pergamon, 1998.
18. "HFR 400 Fast Fid User Manual and Specifications TH 91.6." Cambustion Ltd.

19. McKerny, T.A., Moser, W. "Use of a Heated Sample-Inlet, 2-Reaction Chamber NOx Analyzer for Combustion Optimization."
20. "fNOx400 Fast Response Nitric Oxide Measurement System User Manual version 1.10. Cambustion Ltd.
21. Conversation with Prof. W.K. Cheng. December 5, 2001.
22. "Rosemount Analytical Model 880A Non-Dispersive Infrared Analyzer Instruction Manual." Rosemount Analytical, Inc.
23. Buglass, J.G, Morgan, T.D.B., and Graupner, J.O. "Interactions Between Exhaust Gas Composition and Oxygen Sensor Performance". SAE Paper 982646. 1998.
24. Germann, H., Taglaiferri, S, and Geering, H.P. "Differences in Pre- and Post-Converter Lambda Sensor Characteristics." SAE Paper 960335.
25. Theis, J. R. "An Engine Test to Measure the Oxygen Storage Capacity of a Catalyst." SAE paper # 961900 (1996).
26. Smedler, G., Eriksson, S., Lindblad M., Bernier H., Lundgren S., and Jobson E. "Deterioration of Three-Way Automotive Catalysts, Part II—Oxygen Storage Capacity at Exhaust Conditions." SAE paper # 930944. (1993).
27. Hepburn, J.S., Dobson, D.A., Hubbard, C.P., Guldberg, S.O., Thanasiu, E., Watkins, W.L., Burns, B.D., and Gandi, H.S. "A Review of the Dual EGO Sensor Method for OBD-II Catalyst Efficiency Monitoring." SAE paper # 942057. (1994).
28. Conversation with Rudy Smaling. November 2001.